Target Site Pharmacokinetics of Antiinfectives in the Treatment of Serious Gram-positive Infections

Dissertation

zur Erlangung des akademischen Grades
doctor rerum naturalium (Dr.rer.nat.)

Vorgelegt der
Naturwissenschaftlichen Fakultät I / Biowissenschaften
der Martin-Luther-Universität Halle-Wittenberg

von Nele Plock
geb. am 17.08.1978 in Oldenburg (Oldb)

Gutachter:
1. Prof. Dr. Charlotte Kloft
2. Prof. Dr. Hans-Hubert Borchert
3. Prof. Dr. Andreas Langner

Halle (Saale), 22. Februar 2007

Für Paps.

Abstract

This thesis aimed at investigating the pharmacokinetics (PK) of antiinfectives at the site of infection. This objective was pursued in three different projects. In the first project, vancomycin and linezolid were studied in *in vitro* experiments to enable the conduction of clinical trials investigating their PK by using the microdialysis approach. A rapid and reliable HPLC assay capable of measuring vancomycin concentrations in microdialysate and plasma was developed. Moreover, a previously existing analytical assay for linezolid was extended to the matrices urine, bone marrow, bone biopsy samples and bone microdialysate. Microdialysis investigations were able to show that vancomycin is suitable for microdialysis experiments on the condition that Ringer's solution is replaced by phosphate buffer in microdialysis perfusate. In the second project, microdialysis was applied to corticancellous bone tissue of healthy sows after single intravenous linezolid infusion. The *in vivo* study was able to demonstrate the feasibility and validity of the microdialysis technique in bone tissue. PK investigations revealed that linezolid did not penetrate into bone tissue to the extent that might have been expected from measuring plasma and homogenated tissue samples. AUC and C_{max} values stayed considerably below those of all other matrices. By relating the results to pharmacokinetic indices such as AUC/MIC it was concluded that the standard linezolid dose might not be sufficient for the treatment of bone infections in both animals and humans. Finally, in the third project a clinical trial was conducted in order to assess the PK of linezolid in healthy volunteers and septic patients after single and multiple dosing. Unbound linezolid concentrations were determined in plasma as well as the interstitium (ISF) of subcutaneous adipose tissue and skeletal muscle applying the microdialysis technique. Using the population PK approach unbound linezolid plasma concentrations were characterised by a two-compartment model. The observed PK nonlinearity was attributed to a change in clearance, which presumably might be due to an inhibition of the respiratory chain enzyme activity in the course of linezolid treatment. It was accounted for by introducing an empirical inhibition compartment. ISF concentrations were implemented by the use of two additional compartments that were coded using monodirectional rate constants and partition coefficients. Overall, linezolid displayed good penetration abilities into both subcutaneous and muscular ISF. However, large variability was observed. Creatinine clearance, body weight and thrombocytes were able to explain some of the observed variability in clearance, peripheral volume of distribution, rate into the muscular compartment and on the partition coefficient into muscular ISF. These relations should be confirmed in subsequent trials that might profit from the developed optimised study design, which is characterised by a reduction of total samples from 120 to 14 per individual without any loss of information. Afterwards, they might be used to guide linezolid dose selection and might therefore help to improve individual therapy and outcome of serious infections in the critically ill.

Zusammenfassung

Im Rahmen dieser Arbeit wurde innerhalb von drei Projekten die Pharmakokinetik (PK) von Antiinfektiva am Infektionsort untersucht. Zur Vorbereitung der Durchführung von Klinischen PK Studien mit Vancomycin und Linezolid mit Hilfe der Mikrodialysetechnik wurden diese Substanzen im ersten Projekt in *in-vitro* Experimenten untersucht. Hierfür wurde eine schnelle und zuverlässige HPLC Methode für Vancomycin in Plasma und Mikrodialysat entwickelt. Zusätzlich wurde eine bestehende Analytik für Linezolid auf die Matrizes Urin, Knochenmark, Knochenbiopsie und Knochenmikrodialysat ausgeweitet. Vancomycin erwies sich als geeignet für Mikrodialyseexperimente unter der Voraussetzung, dass Ringerlösung im Perfusat durch Phosphatpuffer ersetzt wurde. Im Rahmen des zweiten Projekts wurde nach Linezolid-iv-Einmalapplikation die Mikrodialysetechnik im Knochengewebe gesunder Schweine angewendet. Die Studie zeigte, dass Mikrodialyse im Knochengewebe durchfürbar ist und valide Ergebnisse liefert. PK-Untersuchungen zeigten, dass Linezolid nicht in dem Ausmaß in das Knochengewebe penetrierte wie durch Messung von Plasma- und Knochenbiopsieproben zu erwarten gewesen wäre. Sowohl die AUC als auch C_{max}-Werte lagen deutlich unterhalb der Werte der anderen Matrizes. Unter Einbeziehung von PK Indices wie AUC/MIC wurde geschlussfolgert, dass die momentane Linezolid-Standarddosierung für die Behandlung von Knocheninfektionen bei Tieren und Menschen nicht ausreichend sein könnte. Im dritten Projekt wurde im Rahmen einer klinischen Studie die PK von ungebundenem Linezolid im Plasma und Interstitium (ISF) des Unterhautfettgewebes (sc) und Skelettmuskels (im) bei gesunden Probanden und septischen Patienten nach Einfach- und Mehrfachdosis mit Hilfe der Mikrodialysetechnik untersucht. Unter Verwendung eines populationspharmakokinetischen Ansatzes konnten ungebundene Plasmakonzentrationen durch ein Zweikompartimentmodell beschrieben werden. Die beobachtete Nichtlinearität wurde einer Clearance-Änderung zugeschrieben, die wahrscheinlich durch eine Hemmung der Atmungskette im Behandlungverlauf erklärt werden kann. Diese Hemmung wurde mit Hilfe eines Inhibitionskompartiments in das Modell inkorporiert. ISF-Konzentrationen wurden durch zwei weitere Kompartimente, monodirektionale Geschwindigkeitskonstanten und Partitionskoeffizienten (PC) beschrieben. Insgesamt penetrierte Linezolid gut in sc und im ISF, jedoch mit hoher Variabilität. Ein Teil der Variabilität der Parameter Clearance, peripheres Verteilungsvolumen sowie Geschwindigkeitskonstante und PC in das im-Kompartiment konnte duch Kreatinin-Clearance, Körpergewicht und Thrombozytenzahl erklärt werden. Dies sollte in weiteren klinischen Untersuchungen bestätigt werden, die unter der Verwendung des optimierten Studiendesigns durchgeführt werden könnten. Dies zeichnet sich durch eine Reduktion der Probenanzahl von 120 auf 14 aus. Anschließend könnten die gefundenen Beziehungen einen Beitrag dazu leisten, die Linezolidtherapie zu individualisieren und so die Therapie schwerwiegender Infektionen bei kritisch Kranken zu verbessern.

Contents

Abbreviations

ADMA	administration matrix
AGE	age of subject at the day of inclusion into the study (years)
AIC	Akaike information criterion
ALT	alanine aminotransferase (U/L; same as GPT)
AMT	amount of drug administered (mg)
ANOVA	analysis of variance
APCH	APACHE score (acute physiology and chronic health evaluation)
AST	aspartate aminotransferase (U/L; same as GOT)
ATP	adenosine triphosphate
AU	absorption units
AUC	area under the concentration-time curve
$AUC_{ss,\tau}$	area under the curve during one dosing interval at steady state
BP	blood pressure (mm Hg)
$C_{bone,ISF}$	concentration in bone interstitium (µg/mL)
$C_{dialysate}$	concentration in microdialysate (µg/mL)
CDP-1	vancomycin crystalline degradation product 1
CID	identification number of study centre where subject was included
CL	clearance (L/h)
C_{max}	maximum concentration (µg/mL)
C_{min}	minimum concentration (µg/mL)
CMT	number of compartment in model
C_{nom}	nominal concentration (µg/mL)
CNS	central nervous system
$C_{perfusate}$	concentration in the microdialysis perfusate (µg/mL)
CPU	central processing unit
CLCR	creatinine clearance (mL/min)
CRP	C-reactive protein (mg/dL)
CV	coefficient of variation in percent
Da	dalton – unified atomic mass unit defined to be 1/12 of the mass of one atom of carbon-12
DAY	study day
df	degree of freedom
DSA	dataset A
DV	dependent variable
EVID	identification number of event

FDA	Food and Drug Administration
FLMA	flag for matrix (plasma, s.c., i.m.)
FO	first-order
FOCE	first-order conditional estimation
FPIA	fluorescence polarisation immunoassay
g	acceleration due to gravity (1 g = 9.80665 m/s^2)
GAM	generalised additive model
GGT	gamma glutamyl transferase (U/L)
HCl	hydrochloric acid
HPLC	high performance liquid chromatography
HT	height (cm)
i.m.	intramuscular
IBW	ideal body weight (kg)
IC50	concentration yielding 50% of maximal inhibition (mg/L)
ICH	International Conference on Harmonisation
ICU	intensive care unit
ID	individual subject record number
IIV	interindividual variability
IOV	interoccasion variability
ISF	interstitial space fluid
K30	monodirectional rate-constant into and from compartment 3 (h^{-1})
K40	monodirectional rate-constant into and from compartment 4 (h^{-1})
KA	first-order absorption rate-constant (h^{-1})
KIC	first-order rate-constant into inhibition compartment (h^{-1})
k_m	Michaelis Menten constant (mg/L)
lc	lateral microdialysis catheter
LDH	lactate dehydrogenase (U/L)
LEUC	leucocytes (nL^{-1})
LLOQ	lower limit of quantification (µg/mL)
log	decadic logarithm
m	mass
MAO	monoamine oxidase
mc	medial microdialysis catheter
MeOH	methanol
MIC$_{90}$	concentration of an antibiotic in a given culture medium at which 90% of bacterial growth is inhibited
min	minutes

mM	milli molar
mRNA	messenger ribonucleic acid
MRSA	methicillin-resistant *staphylococcus aureus*
NADP	nicotinamide adenine dinucleotide phosphate, oxidised
NADPH	nicotinamide adenine dinucleotide phosphate, reduced
NLME	nonlinear mixed effect(s)
NONMEM	nonlinear mixed effects modelling software program
OCC	occasion (number of dose)
O_{ELS}	extended least squares objective function
OFV	objective function value
PBS	phosphate-buffered saline
PC	partition coefficient
PC23	partition coefficient between plasma and subcutaneous ISF
PC24	partition coefficient between plasma and muscle ISF
PD	pharmacodynamic(s)
PF	tissue penetration factor
pH	reverse logarithmic representation of hydrogen ion (H^+) concentration in a solution (measure of acidity or alkalinity)
PK	pharmacokinetic(s)
pk_a	acid dissociation constant
Q	intercompartmental clearance (L/h)
QC	quality control
R	range
RATE	(amount/infusion duration) normalised to 1 h
RE	relative error in percent
RP	reversed phase
RR	relative recovery in percent
rRNA	ribosomal ribonucleic acid
RSE	relative standard error in percent
s	standard deviation
s^2	variance
s.c.	subcutaneous
SA	*staphylococcus aureus*
SCRE	serum creatinine concentration (mg/dL)
SD	standard deviation
SE	standard error
SEX	sex of subject

T_0	starting time point of first infusion
$t_{1/2}$	terminal elimination half-life (h)
THRO	thrombocytes (nL^{-1})
TILD	relative time after start of last drug administration (h)
TIME	relative time after start of first drug administration (h)
t_{max}	time of maximum concentration (h)
t_R	retention time
tRNA	transfer ribonucleic acid
TYPE	type of study subject (healthy, sepsis or septic shock)
UV	ultra violet
US	United States
V	volume of distribution (L)
VAR	fractional value of clearance which cannot be inhibited
VIST	study visit
V_{max}	maximum elimination rate (mg/h)
V_{SS}	apparent volume of distribution at steady state (L)
WT	body weight (kg)
$\tilde{x}$	median
$\bar{x}$	arithmetic mean
ε	random deviation between the individual prediction and the observed measurement ('random effects')
η	difference between the individual prediction and the population parameter estimate ('random effects')
θ	typical value of a population parameter ('fixed effects')
κ	intraindividual parameter difference of different study occasions ('random effects')
λ_z	slope of terminal elimination rate-constant (h^{-1})
ξ	any additional model parameter
π^2	variance of κ
σ^2	variance of ε
υ	variance function
ϕ	vector of model parameters
ω	standard deviation of η
ω^2	variance of η
Θ	vector of all fixed-effects parameters
Σ	variance-covariance matrix of ε
Ω	variance-covariance matrix of η and κ

1   Introduction

1.1   Gram-positive infections

In the last decades, the number and severity of gram-positive infections has significantly increased [1, 2]. The rate of gram-positive infections such as single-organism bacteraemias in cancer patients increased from 29% of in 1973 to 69% in 1993 [3, 4]. These changes seem to result mainly from the continual evolution of antibiotic use, antibiotic resistance and changes in clinical practice, e.g. the long-term use of indwelling catheters [5], rather than from some intrinsic change in susceptibility of the host or from the virulence of the organisms [6]. In addition, bactaeremia due to gram-negative organisms becomes less prevalent because of the use of prophylactic antimicrobial regimens [6]. A special risk is placed by nosocomial infections, i.e. infections as a result of hospitalisation, which are especially threatening for intensive care (ICU) patients [7]. Particularly, infections due to bacteria resistant to some of the available antimicrobials result in an increased morbidity and mortality as well as in augmented health care costs [8-10]. In Germany, the rate of nosocomially acquired methicillin-resistant *staphylococcus aureus* (MRSA) increased from 8% in 1997 to 26.9% in 2002 [11]. In the United States (US), 60% of all nosocomial infections acquired are caused by resistant bacteria [12]. The risk factors for nosocomial infections are manifold: underlying disease severity [13] (especially in patients who receive enteral nutrition [14, 15] or who are mechanically ventilated [15, 16]), time of hospital stay [17] or the prevalence of pathogens with increased levels of resistance [18]. Overall, the prevalence of nosocomial infections in ICUs was reported to be 15% in Germany [19] whereas in countries such as Italy and Turkey it ranged between 30% and 50% [20, 21]. Of all patients admitted to the ICU 14% already suffer from an infection. Most of these patients are treated with antibiotics. In addition, many patients receive antibiotic treatment because of suspected infection or as infection prophylaxis [22]. As a result, the development of drug-resistant bacteria is promoted [23].

Gram-positive bacteria such as staphylococci and enterococci are among the most common ICU pathogens [24]. As *staphylococcus aureus* (SA) is the leading cause of bacterial infections worldwide [25] the rise and spread of MRSA is of special concern [26]. The MRSA prevalence in Germany and the United Kingdom was reported to be 9% – 19% and 31% – 45%, respectively [27]. In the US, 55.3% of all SA isolates were methicillin resistant in the year 2000, an increase of 29% over the previous five years [28]. In the SENTRY antimicrobial surveillance program SA was responsible for 22% of bloodstream infections, 23% of pneumonias and 39% of skin and soft tissue infections [25]. In Europe, SA was reported with a freuquency of 30% in ICU infections, 60% of which were resistant to methicillin [29]. In a comparison of MRSA with methicillin-susceptible SA

the resistant strain was identified as a risk factor for outcome, also because patients infected with MRSA were likely to be older, had experienced prolonged hospitalisation or previous antibiotic therapy [30]. Thus, special attention has to be directed to the eradication of these problematic pathogens. As most strains of MRSA are cross-resistant to multiple antibiotic classes [25], for a long time vancomycin (see 1.1.1) has been the drug of choice for MRSA treatment [31]. However, as the use of vancomycin increased pathogens with decreased susceptibility have emerged. The first MRSA not fully susceptible to vancomycin was isolated in Japan in 1997 [32]. Since then, even vancomycin resistant strains have been reported [33-35]. Although vancomycin is still one of the most important antimicrobial agents for the treatment of MRSA, the increasing resistance necessitates the introduction of new compounds for the eradication of those multiple-resistant strains. Most of the recently approved antibiotics have been developed based on previously established antibiotics. One of them is telithromycin, which was developed for the treatment of upper and lower respiratory tract infections [36] but which does not display any activity against MRSA [37]. Furthermore, tigecycline with activity against both gram-negative organisms as well as MRSA [38, 39] and quinupristin/dalfopristin, a streptogramin for parenteral administration with activity against MRSA [40], were introduced. An interesting option for the treatment of gram-positive infections is daptomycin, which belongs to the class of lipopeptide antibiotics. Originally developed in the early 1990s and then neglected for a few years interest in the drug was renewed in 1997. It was finally approved in the US in September 2003 [41]. Linezolid (see 1.1.2) is the first member of a structurally unique class of antibiotics (oxazolidinones) used for the treatment of MRSA infections and has been the first real innovation over a period of 35 years [42].

1.1.1 Vancomycin

1.1.1.1 Physicochemical properties

Vancomycin hydrochloride is the hydrochloride of a mixture of related glycopeptides produced by the growth of certain strains of *Amycolatopsis orientalis* or by any other means [43]. The main component of the mixture is Vancomycin B [(S_a) – (3S,6R,7R,22R,23S,26S,aS,36R,38aR) – 44 – {[2 – O – (3-amino - 2,3,6 – trideoxy – 3 – C – methyl – α – L – *lyxo* - hexopyranosyl) – β – D – glucopyranosyl]oxy} – 3 – (carbamoylmethyl) – 10,19 – dichloro – 2,3,4,5,6,7,23,24,25,26,36,37, 38,38a – tetradecahydro – 7,22,28,30,32 – pentahydroxy – 6 – [(2R) – 4 – methyl – 2 – (methyl-amino)valeramido] – 2,5,24,38,39 – pentaoxo – 22*H* – 8,11:18,21 – dietheno – 23,36 – (iminome-thano) – 13,16:31,35 – dimetheno – 1*H*,16*H* – [1,6,9]oxadiazacyclohexadecino – [4,5-*m*][10,2,16] – benzoxadiazacyclotetracosine – 26 – carboxylic acid, monohydrochloride] with a molecular weight of 1486 Da [44]. The chemical structure of vancomycin is given in figure 1.1 and can be described as a seven-member peptide chain with two sugar moieties, vancosamine and glucose [45]. It is a white to almost white hygroscopic powder that is freely soluble in water and slightly
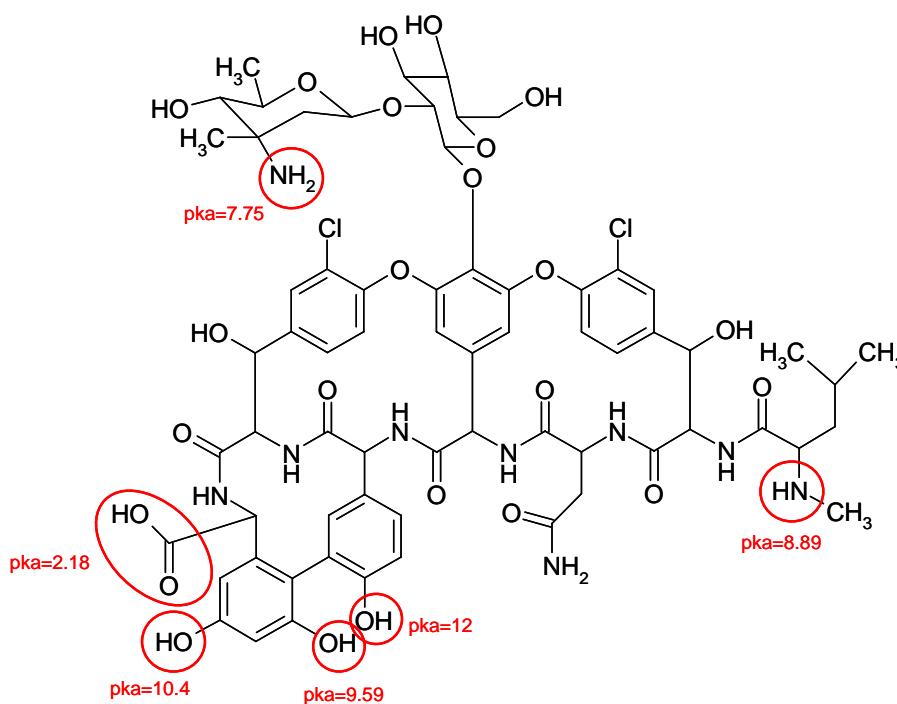
Figure 1.1: Chemical structure of vancomycin including pk$_a$ values

soluble in alcohol [43]. Vancomycin hydrochloride is an acidic compound. A 5% solution in water has a pH value of 2.5 to 4.5 [46].

1.1.1.2   Pharmacokinetic properties

Vancomycin is not absorbed from the gastrointestinal tract. Thus, if systemic treatment is intended it has to be administered intravenously. After intravenous administration vancomycin penetrates into almost all tissues [47-52]. It has a volume of distribution of approximately 50 L [53], displays a protein binding of approximately 55% [54] and is excreted almost unchanged in urine [47], having a terminal plasma elimination half-life of 7 h and 12 h for young and elderly healthy volunteers, respectively [55]. The recommened dose is 500 mg every 6 hours or 1 g every 12 hours and should be reduced in patients with impaired renal function as clearance is linearly correlated with creatinine clearance [56].

Vancomycin has been subject to population pharmacokinetic analyses (see section 1.5). Its pharmacokinetic properties have been described by using one- [57] and two-compartment models [56] (see section 2.4.2).

1.1.1.3   Pharmacodynamic properties

Vancomycin is a glycopeptide antibiotic that acts as an inhibitor of the biosynthesis of the major structural cell wall polymer peptidoglycan [58]. It forms a complex with the D-alanyl-D-alanine peptidoglycan termini that are present in various phases of polymer synthesis [59] and by this prevents the action of peptidoglycan polymerase and transpeptidase that would otherwise crosslink

peptidoglycan intermediates by displacement of the terminal D-alanine [60]. Thus, it displays bactericidal activity on bacteria in their growth phase [61-64].

Vancomycin is active against gram-positive aerobic and anaerobic pathogens with the exception of *bacteroides* [47]. It does not exhibit any activity against gram-negative or *mycobacteria* [65]. Vancomycin is approved for reserve treatment of serious infections, i.e. endocarditis, osteomyelitis, pneumonia, sepsis or soft tissue infections, due to pathogens such as s*taphylococcus* and s*treptococcus spp.* [66] or for the treatment of patients with significant allergy to β-lactams [49].

The minimum inhibitory concentration (MIC_{90}) is the lowest antibiotic concentration that inhibits 90% of bacterial growth in an *in vitro* setting. It is a measure for the sensitivity of a pathogen against an antimicrobial agent. For *staphylococci* susceptibility is defined by a MIC_{90} value below 4 µg/mL while pathogens with a value larger than 8 µg/mL are classified as resistant [67].

1.1.1.4   Adverse events/Drug interactions

Adverse events that have been reported during the treatment with vancomycin include anemia, diarrhoea, headache, nausea and vomiting, pruritus, rash, fever and red man syndrome [68, 69]. Reversible neutropenia, eosinophilia and occasionally thrombocytopenia have been reported. In addition, nephrotoxicity as well as ototoxicity are associated with vancomycin administration [44]. Because this risk is thought to be increased at high plasma concentrations it is recommended that dosage should be adjusted to avoid maximum plasma concentrations above 20 to 40 µg/mL and minimum concentrations exceeding 10 µg/mL [70].

Nephrotoxicity as well as ototoxicity might be aggravated when other oto- or nephrotoxic drugs are given simultaneously. Especially patients who are given aminoglycosides should be monitored closely [47]. However, not all antibiotics increase vancomycin toxicity. It has been reported that some drugs such as cilastatin sodium, flomoxef sodium and fosfomycin sodium have the ability to reduce or eliminate the nephrotoxic effects in a dose-dependent manner by inhibiting vancomycin uptake into the kidney [71-73].

Other drug interactions include the increased effect of some muscle relaxants like succinylcholine by increasing and prolonging its neuromuscular blockade [47].

1.1.2   Linezolid

1.1.2.1   Physicochemical properties

Linezolid [(S) – N – [[3 – [3 – Fluoro – 4 – (4 – morpholinyl)phenyl] – 2 – oxo – 5 – oxazolidinyl]-methyl] – acetamide] has a molecular weight of 337.35 Da [74]. Its chemical structure is shown in figure 1.2. It is a white to yellow crystalline powder with a melting point of 179°C [75]. Linezolid has an n-octanol-water partition coefficient of 0.55. It has weak basic properties (pk_a 1.8) and is slightly soluble in water at pH values between 5 and 9. Solubility increases at a pH value below 3 and at higher temperatures [75].
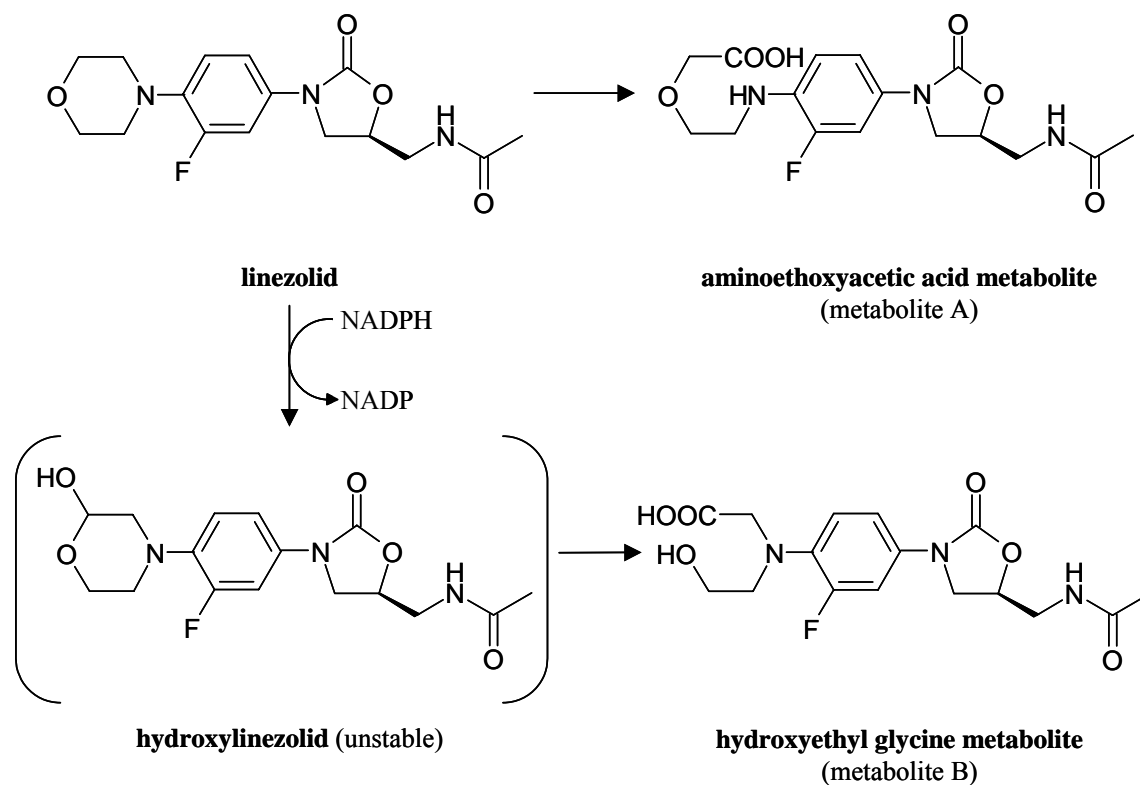
Figure 1.2: Major metabolic pathways of linezolid (modified from [76, 77])

1.1.2.2 Pharmacokinetic properties

Linezolid can be administered both orally and intravenously. As it has a bioavailability of 100% that is not affected by food intake [78] dose adjustment is not necessary when switching from one route of administration to the other [79, 80]. The recommended linezolid dose is 600 mg every 12 hours [81].

In vitro, linezolid displays a plasma protein binding of 31% independent of concentration [82, 83]. At steady state it has a volume of distribution of 40 to 50 L which approximates total body water [84]. It has a total clearance of 7 L/h and a terminal elimination half-life of approximately 5 h [85]. In patients with severely impaired renal function no significant changes in total clearance were observed. Thus, a dose adjustment was reported to be not necessary in this patient population [86].

Of the total amount of linezolid in the body only 30% are eliminated unchanged via the kidneys [87] while a major part of the administered linezolid is metabolised by oxidation of its morpholino ring (see figure 1.2), resulting in two metabolites: an aminoethoxyacetic acid metabolite (metabolite A) and a hydroxyethyl glycine metabolite (metabolite B) that is formed by nonenzymatic oxidation in an *in vitro* setting [74]. In urine, 40% of the dose appear as metabolite B and 10% as metabolite A while 6% and 3% are eliminated via faeces as metabolite B and A, respectively [74]. Linezolid does not have any effect on any known cytochrome P450 or vice versa [87, 88]. However, metabolite formation was found to be optimal under basic (pH 9.0) conditions which suggests the potential involvement of either an uncharacterised P450 enzyme or an

alternative microsomal-mediated oxidative pathway [77]. In addition, the formation of metabolite B is dependent on NADPH *in vitro* [77]. Linezolid penetrates well into tissues. Its distribution into lung tissue was studied in 25 healthy volunteers. Concentrations in epithelial lining fluid by far exceeded those in plasma [89, 90]. Good penetration abilities were also reported for skin [91], subcutaneous [92] and muscle tissue [92-94], bone [93-95] and cerebrospinal fluid [96].

The pharmacokinetics of linezolid have been studied using a population pharmacokinetic approach (see section 1.5). Its pharmacokinetic properties have been described by using one- or two-compartment models (see section 2.4.2) with either linear [97] or parallel linear and saturable Michaelis Menten elimination [98-100]. Nonlinearity has been described for linezolid elimination. It has so far been attributed to a saturable elimination pathway [81].

1.1.2.3   Pharmacodynamic properties

Linezolid acts through inhibition of an early phase of protein synthesis. Discussions about the exact mode of action are ongoing. Linezolid presumably binds with the 23S rRNA of the ribosomal 50S subunit and by this inhibits the formation of the N-formylmethionyl-tRNA-ribosome-mRNA ternary initiation complex in bacterial translation systems [101, 102]. This theory is supported by the fact that the development of bacterial resistance is associated with 23S rRNA alterations during treatment [103]. In addition, linezolid might have other binding sites at the ribosomal subunits [101, 104]. Based on the mechanism of action linezolid displays bacteriostatic properties [105].

Linezolid is active against gram-positive aerobic and anaerobic pathogens [81]. The activity is most notable against *staphylococci* and *enterococci* [106-108] In addition, bactericidal activity has been reported for linezolid against *Streptococcus pneumoniae* and *Streptococcus pyogenes* [106, 107]. While some studies reported activity against *mycobacteria* [109-112] it is not active against most gram-negative bacteria [85]. Linezolid is approved for reserve treatment of serious infections such as pneumonia or severe skin and soft tissue infections. Therapy should not exceed a duration of 28 days [81].

The susceptibility breakpoint (MIC_{90}) for linezolid lies between 2 and 4 µg/mL depending on the type of bacteria [81, 113]. Bacteria with a MIC_{90} higher than 8 µg/mL are classified as resistant [114].

1.1.2.4   Adverse events/Drug interactions

Clinical trials have shown that linezolid is generally well tolerated for up to 28 days [115]. Frequent adverse events include headache, nausea, dizziness, vomiting and an increase in transaminases [81, 116]. Especially prolonged treatment can lead to myelosuppression (anemia, leukopenia, pancytopenia, thrombocytopenia) which is reversible after discontinuation of therapy [117-119]. Complete blood counts should be monitored weekly in patients who receive linezolid,

particularly in those who receive linezolid for longer than two weeks [74]. Moreover, optical neuropathy has been observed after long-term treatment [81].

Linezolid is a weak and reversible monoamine oxidase (MAO) inhibitor. Although an increased frequency of adrenergic or serotonergic adverse events has not been reported it is recommended that linezolid is used with caution in patients treated with other MAO inhibitors [120]. However, although an interaction with tyramine has been reported it is not recommended to restrict normal dietary intake of tyramine-containing foods when taking linezolid as an oral dose of at least 100 mg of tyramine is necessary to raise the systolic blood pressure by more than 30 mm Hg. This dose of tyramine is an order of magnitude larger than that encountered even in exceptionally tyramine-rich meals [79, 121]. Decreased linezolid plasma concentrations have been reported for simultaneous administration of linezolid and rifampin [122] that might be due to an up-regulation of linezolid intestinal secretion.

1.2   Individualisation of drug therapy

Up to today many drugs are still administered using the same dosing regimen for all patients. However, some drug examples have shown that this approach towards equalisation may lead to a loss in therapeutic quality. One therapeutic area where individualised therapy is widely accepted is cancer treatment [123]. Although disagreement still exists about the way dose individualisation should be performed drug amounts are mostly calculated based on the body size [124-126].

An improved approach is the use of maximum a posteriori probability Bayesian fitting [127, 128]. Numerous studies have found a clear relation between systemic exposure and the toxicity of e.g. anticancer agents. Moreover, the clearance of most of these drugs differs widely between patients. These findings, combined with the narrow therapeutic index of anticancer drugs, suggest that patient outcome would be improved if doses were individualised to achieve a target systemic exposure [129-131].

However, not only cancer treatment should be considered for individualised therapy. The same is true for all other drugs which exhibit any toxicity in the concentration range that could possibly be attained by standard dosing regimen. One example is aminoglycoside therapy [132]. However, although one aim of therapy should certainly be the restraint of toxicity, another one should always be the attainment of a certain drug effect. For this, therapeutically active drug concentrations have to be reached at the site of action [133]. The calculation of pharmacokinetic parameters is mostly based on drug concentrations in plasma. Most drugs, however, do not exert their effect in the plasma compartment [134]. In antimicrobial therapy, most drug dosing regimens have largely ignored the fact that the antibiotic first has to penetrate into the target tissue in order to exert its action [135]. It has commonly been believed that most antibiotics achieve equilibrium between plasma and tissue [136-138]. Recent studies, however, have demonstrated that target site drug

concentrations may substantially differ from corresponding plasma concentrations [139-145]. In addition, it has been shown that only the unbound fraction of a drug is able to penetrate into target tissues [134] and that it is only this unbound fraction that is pharmacologically active [146-148], whereas in most cases total drug concentrations are measured. A further misconception is the declaration that tissue is a uniform matrix and that antibiotic concentrations measured in biopsy samples reflect the active compound at the site of action [134]. This, however, is not true. Most anti-infective agents exert their action in the interstitium as this is the space where most relevant bacteria reside [149]. Consequently, if concentrations at the site of infection remain below the MIC_{90} this might have a severe impact on the outcome of therapy [133] and the promotion of drug resistance [150, 151]. Following this reasoning one should rather aim at directly measuring unbound concentrations in the interstitial space fluid (ISF) [152]. This approach has been recommended by the Food and Drug Administration in their draft guidance for developing antimicrobial drugs, stating that the relation between unbound concentrations at the site of infection and the *in vitro* susceptibility of the target pathogen should be determined before applying for drug approval [153]. A technique suitable for measuring unbound concentrations directly at the site of infection is microdialysis [154].

1.3   Microdialysis

The microdialysis sampling technique emerged from the neurosciences where it was originally used for measuring concentrations of neurotransmitters in rat brain [155]. From this experimental field it gradually spread to other research areas and it has now gained an important role for both *in vitro* experiments and the investigation of unbound *in vivo* tissue concentrations of both endogenous and exogenous compounds.

A microdialysis system consists of the microdialysis pump, the microdialysis catheter, also called probe, and a microvial in which the sample is collected [156]. During the process of microdialysis the catheter is inserted into the ISF of various tissues. Usually it is designed as a concentric probe that consists of a thin dialysis tube with an inner diameter in the range of approximately 0.15 – 0.3 mm and a semipermeable membrane at the tip of the probe. Each membrane has its own specific molecular weight cut-off determined by its pore size that usually ranges from 6 – 100 kDa. Therefore, in many cases the probe is impermeable to large molecules, e.g. proteins. A perfusion fluid enters the probe through the inlet tubing at a constant flow rate (generally 0.5 – 5 µL/min [157]), passes the membrane and is then transported through the outlet tubing and collected in a microvial (dialysate). While the perfusion fluid passes the membrane, molecules up to a certain molar mass diffuse into (recovery) or out of (delivery) the perfusion fluid. The direction of the diffusion process is dependent on the concentration gradient. Thus, microdialysis can be used for both collecting a substance in the dialysate as well as delivering it into the ISF (figure 1.3) [158].

The method of microdialysis sampling is characterised by many different features. Compared to biopsy sampling, microdialysis allows for the continuous monitoring of drug concentrations in the tissue over long time periods. It is a minimally invasive technique and can, therefore, be applied without placing any additional burden on patients. As microdialysis collects a drug at the site of action [159] while providing protein-free samples it is able to directly measure the pharmacologically active drug fraction.
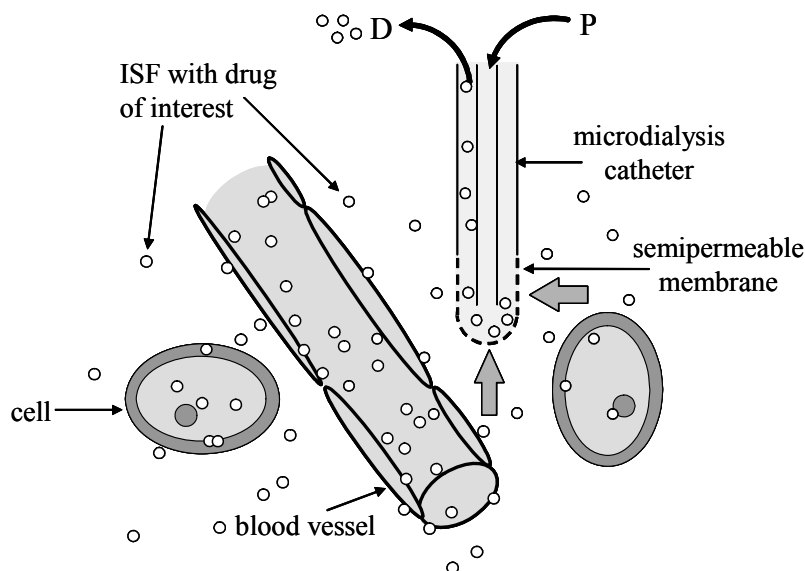
Figure 1.3: Principle of microdialysis (not drawn to scale for illustrational purposes): molecules up to a certain molar mass diffuse into (recovery) or out of (delivery) the perfusion fluid and can be measured in the dialysate; D: dialysate; P: perfusate.

1.3.1   Relative recovery

In order to quantify drugs in the ISF, the dialysate fraction obtained from microdialysis experiments is measured. However, as the microdialysis catheter is constantly perfused, diffusion equilibrium between the perfusate and the ISF will never be complete. Thus, only a fraction of the actual drug amount in the ISF can be detected in the dialysate. The ratio between the concentration of a substance in the dialysate to that in the ISF is termed relative recovery (RR). The RR is dependent on the velocity of the diffusion process across the membrane which is influenced by:

- temperature
- weight cut-off and membrane area
- concentration gradient
- composition of perfusate
- flow rate and
- tortuosity of the sample matrix.

As RR will never reach 100% (except in the No-net-flux situation, see below) a microdialysis probe has to be calibrated before drawing any conclusions about concentrations in the ISF.

1.3.2 Calibration procedures

There are many different methods for calibration and thus, for determination of RR that yield results of diverse quality.

- Method of flow rate variation [158, 160, 161]
- Method of No-net-flux [158, 161, 162]
- Dynamic No-net-flux [158, 163]
- Retrodialysis [158, 161, 164, 165]
- Endogenous reference substance [158, 166-169]

In all experiments conducted in this thesis calibration was performed by the retrodialysis method. Therefore, this method will be commented on in more detail.

Retrodialysis is a technique that allows probe calibration *in situ* and will not expose patients to avoidable stress [164]. The retrodialysis process is illustrated in figure 1.4. It operates by using a perfusate spiked with the analyte in a known concentration. The diffusion process is assumed to be quantitatively equal in both directions (an assumption that should always be confirmed in *in vitro* experiments). Therefore, the substance loss through the membrane is the same as its *in vivo* recovery. The RR can be calculated by the following equation:

$$RR,\% = \left(1 - \frac{C_{dialysate}}{C_{perfusate}}\right) \cdot 100 \tag{1.1}$$

where $C_{dialysate}$ and $C_{perfusate}$ correspond to the concentrations measured in microdialysis dialysate and perfusate, respectively. Essential for obtaining correct results is the following consideration: The diffusion process will only be equal if the ISF does not yet contain any analyte before the actual calibration process. If retrodialysis is used for measuring drug concentrations, the determination of RR should be carried out before the first administration of the drug. However, measurements during steady state conditions will be possible if the concentration of the drug in the
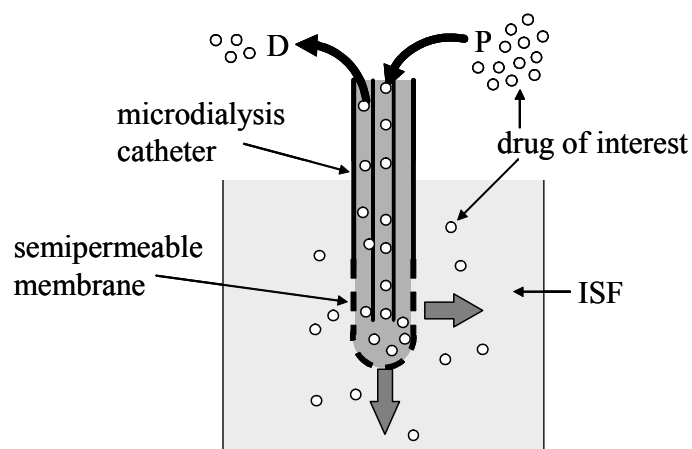
Figure 1.4: Microdialysis calibration: Method of retrodialysis. Recovery is calculated from the ratio of drug concentration in the dialysate to that in the perfusate; D: dialysate; P: perfusate

perfusate is equal to or exceeds the tenfold of that in the ISF. For steady state conditions, the required analyte concentration in the perfusate has to be determined in advance during *in vitro* experiments. In this case, an absolutely accurate determination of RR is impossible as the drug is already present in the ISF. However, a close approximation is sufficient for clinical application as intraindividual coefficients of variation for ISF concentration measurements by microdialysis were shown to range between 10% and 20% depending on the analyte [133].

1.4   Tissue distribution in septic patients: Pathophysiological characteristics

Diffusion is the most important mechanism by which tissue distribution is accomplished. This process can be described by Fick's first law of diffusion. It states that diffusion is dependent on the concentration gradient, the area of diffusion and the diffusion coefficient [170]. Thus, equilibration will be enhanced when the concentration gradient is higher and the available diffusion area and diffusion coefficient are increased. The diffusion coefficient is directly proportional to temperature and inversely related to the particle's radius and the viscosity of the surrounding medium [171]. In addition, the diffusivity will be reduced if distance increases [172]. These physical principles can easily be carried forward to drugs and their distribution in the body. Highly protein-bound compounds are only fractionally available for diffusion as their free concentration is decreased. In addition, diffusion is impeded by the presence of physiological membranes. High inter- and intratissue variability in diffusibility is present *in vivo* due to differences in blood flow and the permeability and diffusion area of membranes, respectively [173-177]. Furthermore, the rate and extent of drug distribution are determined by cardiac output and the relative distribution between blood and tissue that is determined by the tissue mass, the lipophily of the drug and, for ionisable drugs, their pk_a and the environmental pH [178]. This given variability in diffusibility can be increased in pathophysiological conditions during sepsis (figure 1.5). Sepsis is a term for the systemic response to infection [179]. An aggravated condition of this is septic shock. It is characterised by a hyperdynamic stage which consists of high cardiac output combined with low peripheral vascular resistance [180, 181]. Septic shock is the most common cause of death in ICUs [182]. Several conditions during sepsis can be responsible for lower tissue drug concentrations in the critically ill as compared to healthy volunteers. One of the major reasons for changes in tissue distribution in septic patients is the so-called 'third spacing' that mostly affects drugs with a small extracellular volume of distribution [183]. It is characterised by increased capillary permeability leading to the development of interstitial oedema [184-186]. This, in turn, leads to increased volumes of distribution of antiinfectives distributing in the ISF. Consequently, concentrations of these antiinfectives at the target site can be significantly lower than those in healthy volunteers. At worst, if the drug concentration stayed below the MIC_{90} of the relevant pathogen over long time
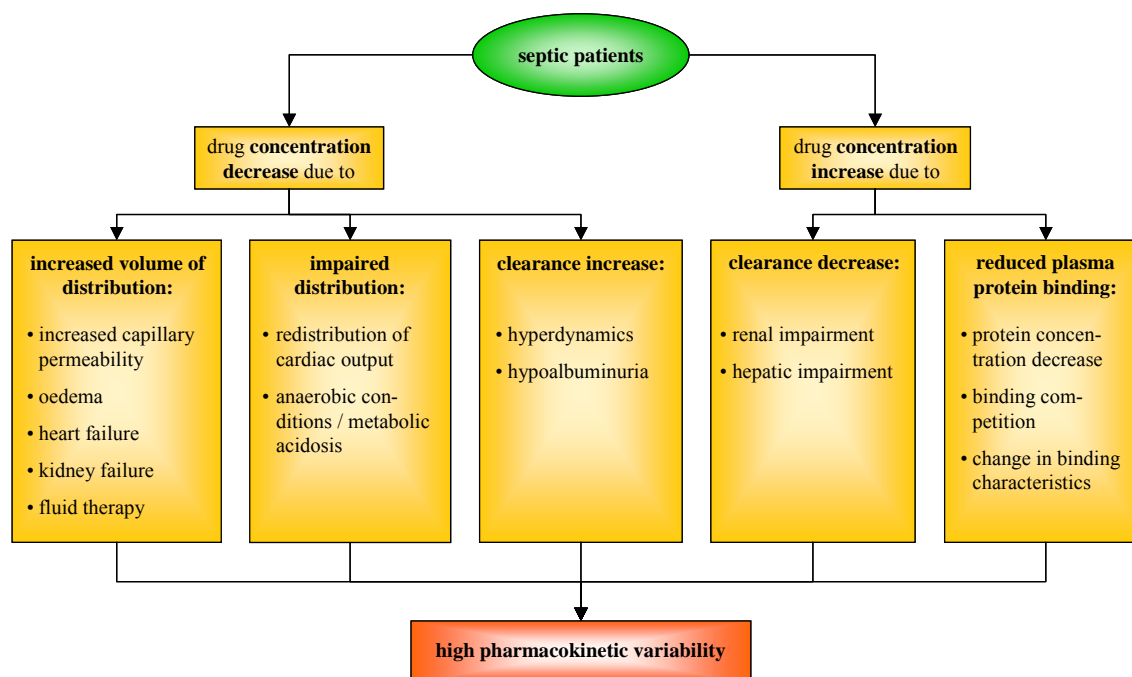
Figure 1.5: Pathophysiological conditions during sepsis

periods this difference could lead to therapeutic failure and the promotion of drug resistance. The same effect might be obtained if due to heart or kidney failure fluid is retained in the body. Moreover, the volume of distribution is increased due to extra fluid input [184]. Due to septic conditions cardiac output might be redistributed to vital organs such as the heart and the brain [187]. In consequence, the perfusion of less vital organs and tissues might be compromised. Therefore, antiinfectives might not adequately reach the microcirculation. Furthermore, reduced organ perfusion might lead to anaerobic conditions and metabolic acidosis that might alter the distribution of ionisable drugs [184].

However, a septic state can also lead to increased drug concentrations. One major reason is a compromised renal function that might result in decreased drug clearance [178]. The same effect is obtained in hepatic impairment that may result in decreased drug metabolism [188, 189]. Moreover, drug distribution is dependent on plasma protein binding. During sepsis and septic shock changes in plasma protein binding may occur due to changes in concentration of the plasma proteins as a result of reduced protein intake and increased capillary permeability [190], competition of endogenous substances or metabolites for binding sites or because of changes in the binding characteristics [183, 184, 191-195]. In consequence, a change in protein binding might lead to an increase of the free drug fraction, i.e. the pharmacologically active drug.

Considering the differences between healthy volunteers, the critically ill and septic patients in particular it becomes apparent that, pharmacokinetically, these groups are not easily comparable. This was also demonstrated in studies with critically ill patients that were able to show that antibiotic tissue concentrations in these patients differ substantially from those in healthy

volunteers [139, 144, 196-200]. Thus, higher emphasis should be placed on studying the pharmacokinetics of antimicrobial agents in this target population. In order to increase the informational value of those studies, meaningful study techniques like microdialysis should be adopted, preferably in combination with informative analysis procedures such as population pharmacokinetics.

1.5   Population pharmacokinetics

Pharmacokinetics is used to analyse and predict the concentration-time course of a drug in the body [201]. It is quite obvious that concentration-time courses of different individuals display some degree of variability. The same is true for the individual pharmacokinetic parameter estimates. A method to analyse concentration-time data of many individuals simultaneously is population pharmacokinetics. It describes the typical relations between physiology and pharmacokinetics, the interindividual variability in these relations and their residual variability [202].

The major advantage of the population pharmacokinetic approach is that it can be applied in sparse data situations as information can be 'borrowed' between individuals. Moreover, it does not require a balanced study design which permits the combination of data from different studies. Another advantage of the population approach over other pharmacokinetic analysis methods is its ability to describe the relations between covariates (i.e. individual-specific variables like creatinine clearance, weight) and model parameters (e.g. clearance, volume of distribution). This way, individual and pathophysiological factors may explain some of the variability in pharmacokinetic model parameters. As a result, patients who are at risk of receiving toxic or ineffective concentrations may be identified, a prerequisite for dose adjustment. In addition, covariate models are a valuable tool for the decision on appropriate dosage regimen [203, 204].

The population pharmacokinetic approach has been recommended by guidelines issued by the Food and Drug Administration (FDA) [205, 206] or the International Conference on Harmonisation (ICH) [207, 208] as a tool for the identification 'of the sources and correlates of variability in drug concentrations between individuals representative of those in whom a drug will be used clinically when relevant dosage regimens are administered' [209].

1.6   Objectives

In order to successfully treat bacterial infections, adequate drug concentrations have to be reached at the target site. Most bacteria reside in the extracellular space. Therefore, antibiotics have to exert their action in the interstitium. As a means to determine effective drug concentrations in this location microdialysis is the method of choice.

This thesis aims at investigating the pharmacokinetics of antiinfectives at the site of infection by means of microdialysis in order to determine if this approach might add to a more individualised antimicrobial therapy. This objective was pursued in three different projects:

I   Vancomycin and linezolid were studied in *in vitro* experiments to enable the conduction of clinical trials investigating their pharmacokinetics by using the microdialysis approach. Firstly, a fast and efficient analytical assay capable of quantifying vancomycin from small sample volumes had to be developed. Subsequently, *in vitro* microdialysis experiments had to be conducted to determine optimal conditions for vancomycin microdialysis *in vivo*. Furthermore, in order to provide for extensive pharmacokinetic analyses of linezolid a previously existing analytical assay had to be extended to the matrices urine, bone marrow, bone biopsy samples and bone microdialysate.

II   In this *in vivo* pilot study microdialysis was applied to corticancellous bone tissue of healthy sows after administration of a single intravenous linezolid infusion. It aimed at investigating the feasibility of the microdialysis technique in bone tissue to assure the validity of this approach. Furthermore, this study explored and compared the pharmacokinetics of linezolid in plasma, bone marrow, bone biopsy samples and bone microdialysate by means of a noncompartmental analysis technique.

III   The aim of this project was to design and conduct a clinical trial in order to assess the 'target site pharmacokinetics (PK) and pharmacodynamics (PD) of linezolid in healthy volunteers and septic patients after single dose administration and at steady state'. Unbound linezolid concentrations were to be determined in plasma, subcutaneous adipose tissue and skeletal muscle applying the microdialysis technique. Moreover, a population pharmacokinetic model for the simultaneous description of plasma and microdialysis tissue concentrations of unbound linezolid had to be developed and evaluated. Covariates influencing the pharmacokinetics of linezolid had to be identified. Finally, the informative sampling time points essential for the development of the pharmacokinetic model had to be determined retrospectively.

2 Materials and Methods

2.1 Chemicals, reagents and pharmaceutical products

acetonitrile HPLC gradient grade	Acros Organics, Geel, Belgium
acetylcysteine	Hexal, Holzkirchen, Germany
amitriptyline HCl	Hexal, Holzkirchen, Germany
captopril	ratiopharm, Ulm, Germany
ciprofloxacin lactate	Bayer, Leverkusen, Germany
clonidine	ratiopharm, Ulm, Germany
clopidogrel hydrogen sulfate	Sanofi Synthelabo, Paris, France
diazepam	Desitin, Hamburg, Germany
dipotassium hydrogen phosphate anhydrous	Merck, Darmstadt, Germany
disodium hydrogen phosphate	Merck, Darmstadt, Germany
enalapril maleate	Berlin-Chemie, Berlin, Germany
erythromycin	STADA, Bad Vilbel, Germany
esomeprazole	AstraZeneca, Wedel, Germany
etilefrine HCl	Boehringer Ingelheim, Ingelheim, Germany
etomidate	Braun, Melsungen, Germany
glycerol trinitrate	Pohl Boskamp, Hohenlockstedt, Germany
haloperidol	ratiopharm, Ulm, Germany
hydrochloric acid 37% (m/V)	Riedel-de Haën, Seelze, Germany
hydrocortisone	Aventis Pharma, Frankfurt, Germany
isosorbide mononitrate	Novartis Pharma, Nuremberg, Germany
linezolid (purity >99.9%)	Pharmacia, Kalamazoo, USA
metamizol sodium	Berlin-Chemie, Berlin, Germany
methanol (MeOH) HPLC gradient grade	Acros Organics, Geel, Belgium
metoclopramide	Solvay, Hannover, Germany
midazolam	Hoffmann-La Roche, Grenzach-Wyhlen, Germany
neostigmine methyl sulfate	Curasan, Kleinostheim, Germany
orthophosphoric acid	Ferak, Berlin, Germany
pantoprazole	Schwarz Pharma, Monheim, Germany
phosphate-buffered saline (PBS, 0.1 M)	80.0 g NaCL, 2.0 g KCL, 14.4 g Na_2HPO_4, 2.4 g KH_2PO_4, ad 1000 mL water, pH 7.4 with HCl
phytomenadione	Hoffmann-La Roche, Grenzach-Wyhlen, Germany
piperacillin sodium	ratiopharm, Ulm, Germany

potassium chloride	Merck, Darmstadt, Germany
potassium dihydrogen phosphate	Merck, Darmstadt, Germany
prednisolone	Jenapharm, Jena, Germany
Ringer's solution	Serumwerke Bernburg, Bernburg, Germany
sodium chloride	Merck, Darmstadt, Germany
sulbactam sodium/ampicillin sodium	Pfizer, Karlsruhe, Germany
trichloroacetic acid	Merck, Darmstadt, Germany
urapidil HCl	Byk Gulden, Konstanz, Germany
vancomycin	Lilly Reasearch Laboratories, Indianapolis, USA
water (Milli-Q)	Milli-Q^{TM} Plus water purification system, Millipore, Bedford, USA

2.2   Materials and other equipment

0.22 µm membrane filters	Sartorius, Goettingen, Germany
Centrifree$^®$ ultrafiltration devices (weight cut-off 30 kDa)	Millipore, Eschborn, Germany
microdialysis catheters (CMA60, CMA70)	CMA, Solna, Sweden
microdialysis syringes BD$^®$ 1 mL Luer Lock$^®$	Beckton Dickinson, Singapore
pipette tips	Eppendorf, Hamburg, Germany
safe lock vials (0.5-1.5 mL)	Eppendorf, Hamburg, Germany
digital analytical balance R180 D-*D1	Sartorius, Goettingen, Germany
Eppendorf centrifuge 5417 R	Eppendorf, Hamburg, Germany
Eppendorf pipettes (2-1000 µL)	Eppendorf, Hamburg, Germany
Heraeus Sepatech$^®$ Megafuge 1.0 R	Heraeus, Hanau, Germany
HPLC system	see sections 2.5.2.1 and 2.5.3.1
microdialysis precision pumps (CMA102, CMA107)	CMA, Solna, Sweden
Multipette$^®$ (5-1000 µL)	Eppendorf, Hamburg, Germany
pH meter CG 837	Schott, Mainz, Germany
Speed-Vac$^®$ Plus SC110A	Savant, Farmingdale, USA
ultrasonic bath	Bandelin electronic, Berlin, Germany
vacuum filtration device (1L)	Sartorius, Goettingen, Germany
Vibrofix$^®$ VF 1 Electronic	IKA Jahnke & Kunkel, Staufen, Germany

2.3   Descriptive statistics

Different localisation (table 2.1) and dispersion (table 2.2) parameters were employed to describe and characterise the data as well as the results obtained in this thesis. While localisation parameters describe either the location of a distribution or its central tendency dispersion parameters illustrate the variability of a distribution.

Table 2.1: Localisation parameters

arithmetic mean	$\overline{x}$	sum of all the items of the set divided by the number of items in the set
median	$\widetilde{x}$	separates the higher half of a sample, a population or a probability distribution from the lower half
5th and 95th percentile		values that cut off the lowest and highest 5% of the data

Table 2.2: Dispersion parameters

range	R	the difference between the highest and lowest value
variance	s^2	measure of statistical dispersion of a variable, indicating how far from the expected value its values typically are
standard deviation	s	measure of statistical dispersion, defined as the square root of the variance
coefficient of variation	CV%	measure of dispersion of a probability distribution, defined as the ratio of the standard deviation to the mean

2.4   Pharmacokinetic analysis

2.4.1   Non-compartmental pharmacokinetics

Non-compartmental pharmacokinetics describes the PK characteristics of a drug without assuming any kinetic compartments (see section 2.4.2). Prerequisite for universal validity of the estimated parameters is a linear PK of the investigated drug [210]. Non-compartmental pharmacokinetics does not describe the concentration-time course of a drug in different body fluids by means of different equations. Instead, it calculates PK parameters independently from those equations.

The following parameters that can be calculated by the non-compartmental approach [211] were used for evaluation purposes in this thesis:

Area under the concentration-time curve (AUC):

The AUC can be calculated by means of the linear trapezoidal rule.

$$AUC_{t_0-t_z} = \frac{1}{2} \sum_{i=1}^{z} \left[\left(C_{i-1} + C_i \right) \cdot \left(t_i - t_{i-1} \right) \right] \tag{2.1}$$

where t_{i-1} and t_i correspond to two successive measurement time points with the concentrations C_{i-1} and C_i during the time period t_0-t_z. Average concentrations can be obtained by dividing the AUC of one dosing interval by the dosing interval τ.

Clearance (CL):

$$CL = \frac{Dose_{iv}}{AUC_{0-\infty}}$$ (2.2)

where $AUC_{0-\infty}$ is obtained by addition of AUC_{0-t_z} and the AUC extrapolation till infinity.

Volume of distribution (V):

$$V = \frac{Dose_{iv}}{\lambda_z \cdot AUC_{0-\infty}}$$ (2.3)

where λ_z corresponds to the slope of the terminal elimination rate-constant.

Terminal elimination half-life ($t_{1/2}$):

$$t_{1/2} = \frac{\ln 2}{\lambda_z}$$ (2.4)

Other parameters, such as the maximum concentration (C_{max}) and time of C_{max} (t_{max}), can directly be taken from the data. All parameters were calculated using WinNonlin® (see section 2.8).

2.4.2 Compartmental pharmacokinetics

In order to describe the concentration-time course of a drug in the body it has been helpful to divide its whole distribution space into a system of pharmacokinetic compartments. Compartments can be assumed even if there is no physiological basis supporting this approach, the only aim being that the model will correctly describe the concentration-time course of the drug. If the drug transport between two compartments takes place with first-order processes and the concentration that results from the dose is proportional to that dose, the PK is linear [210].

The most simple compartmental model is shown in figure 2.1. It can be described as a one-compartment model where the drug is evenly distributed and where every part of the body to which the drug distributes is reached in a negligible period of time. Changes of drug concentration occur to the same extent per time everywhere, i.e. if the concentration in plasma is reduced by half the same is true for tissue concentrations. The simplest case for drug administration in this model is an intravenous bolus dose. In this case it is assumed that the whole drug amount is available at once in every part of the body to which the drug distributes. It is then eliminated by a first-order process.
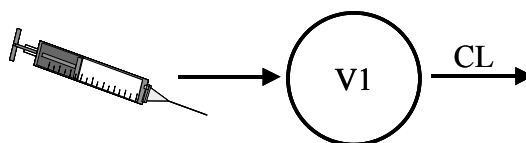
Figure 2.1: One-compartment model with intravenous bolus dosing; V1: central volume of distribution; CL: clearance

More often, however, a two-compartment model is assumed for this drug administration route (see figure 2.2). After administering the whole dose into systemic circulation at once the drug undergoes a phase of predominant distribution during which concentrations in plasma fall more rapidly than afterwards. Therefore, in a two-compartment model two different phases can be distinguished in the semi-logarithmic concentration-time plot: a rapid predominant distribution phase and a slower predominant elimination phase. In this model plasma concentrations are associated with the central compartment.
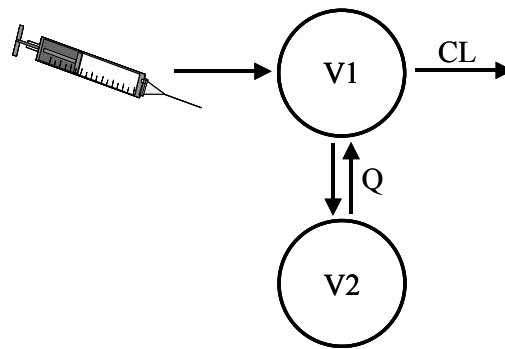
Figure 2.2: Two-compartment model with intravenous bolus dosing; V1: central volume of distribution; V2: peripheral volume of distribution; Q: intercompartmental clearance; CL: clearance

The described compartmental models can be amplified according to special needs, i.e. the number of compartments can be increased. Alternatively, other kinetic processes apart from the first-order distribution and elimination can be considered.

2.4.3   Population pharmacokinetics

There are three commonly used approaches for obtaining population PK parameters. The first is the naïve pooling procedure where all data are combined and treated as having been obtained from one individual. The method allows for the estimation of population PK parameter estimates even in sparse-data situations. However, although the deviation of the observed from the predicted values (residual variability) can be estimated, all information about the specific individual is lost in this approach [212]. Therefore, the residual variability also comprises all interindividual variability that can be described separately in the other approaches. A second method for obtaining both population and individual parameters is the standard two-stage method [213]. In this setting the data is at first analysed individually. Subsequently, a descriptive statistic is computed, thus providing typical mean parameter estimates as well as the variance and covariance of the individual parameter estimates. On the condition of a balanced study design, typical PK parameters can be estimated quite precisely. However, interindividual variability is often upwards-biased [212, 214-216]. The two-stage method is commonly used in data-rich situations, as it is dependent on availability of dense concentration-time data.

The third method available for obtaining population PK parameter estimates is the nonlinear mixed effects (NLME) modelling approach, which was first introduced by Beal and Sheiner [217]. Nonlinear mixed effects modelling also provides typical population parameters as well as variability parameters [218]. The approach can be applied to more sparse sampling schedules than the ones needed for the two-stage method, allowing a less restrictive and also unbalanced study design. Moreover, it enables study pooling and the simultaneous investigation of different drug administration routes. Therefore, it is the method of choice for analysing data obtained in routine clinical settings. The NLME modelling approach considers the population as a whole rather than the individual, but without loosing information about every individual subject. In this approach, all parameters are estimated simultaneously, and individual parameters can be determined based on the estimated variances. The term "mixed effects" is chosen because the method accounts for "fixed effects", i.e. measurable factors and population parameter estimates, and "random effects", i.e. parameter variability, in one model [219]. As NONMEM^{TM} (see section 2.8) was used for all population PK modelling in this thesis this section will focus on the NLME approach implemented in this software program.

The NLME model can be divided into three sub-models:

- the structural model
- the pharmacostatistical model
- the covariate model

Figure 2.3 illustrates the interactions between the system of sub-models. Within this system, fixed-effects parameters are estimated by the structural (section 2.4.3.1) and covariate (section 2.4.3.3) model while all random effects are provided by the pharmacostatistical model (section 2.4.3.2).
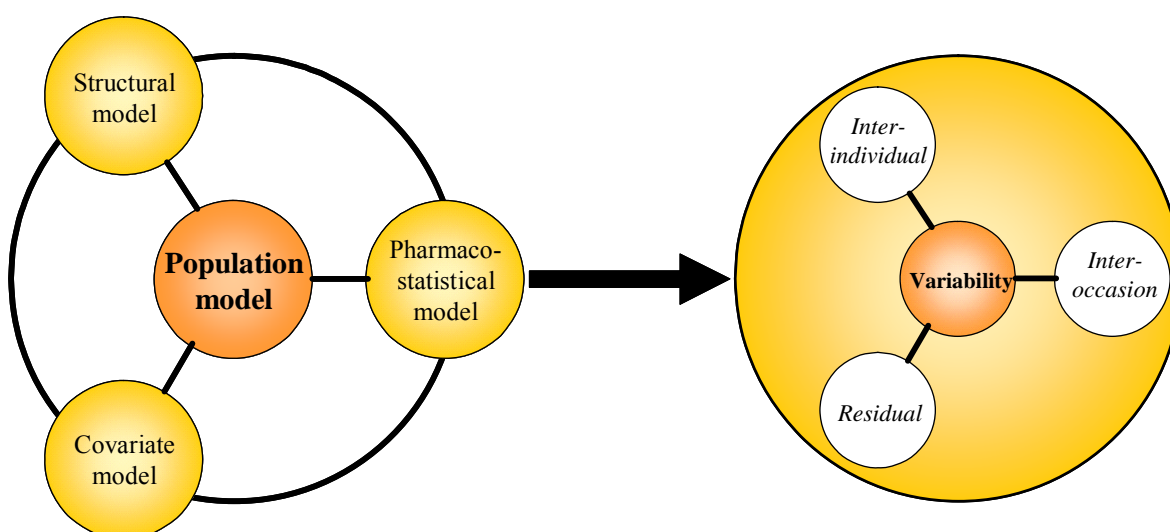
Figure 2.3: Schematic structure of the population pharmacokinetic model

2.4.3.1   Structural model

In the NLME approach the typical time profile of measured data can be described by the following function:

$$f(\phi_i, x_{ij}) \tag{2.5}$$

where the function f is the structural model relating the vector of independent variables, x_{ij} (e.g. time and dose) to the response given the *i*-th individual's vector of model parameters ϕ. Thus, the structural model describes the central tendency of the variable time course (e.g. plasma concentrations for PK) by means of certain model parameters (e.g. typical CL, typical volume of distribution) and a given dose and dosing interval.

2.4.3.2   Pharmacostatistical model

Random effects describe the variability between and within individuals as well as non-measurable and non-controllable factors, e.g. uncertainties in measurements. These random effects are accounted for by the pharmacostatistical model, which can comprise three different types of variability (see figure 2.3):

- interindividual variability (IIV)
- interoccasion variability (IOV)
- residual variability

2.4.3.2.1   Interindividual variability

Interindividual variability, also called between-subject variability, accounts for differences between individuals. It can be described with the additional parameter η_{ki} that accounts for the difference between the typical parameter θ_k and and the individual parameter θ_{ki}. In general, η_{ki}s are assumed to be symmetrically distributed with mean 0 and variance ω_k^2. The variance ω_k^2 is a diagonal element of the variance-covariance matrix Ω. In addition to the diagonal elements off-diagonal elements such as $\Omega_{k,k+1}$ (which is $\omega_{\eta_k,\eta_{k+1}}$) can be estimated as well, providing the correlation between two diagonal elements.

There are three different models widely used for the description of the individual parameter distribution that can assume normally as well as log-normally distributed parameters:

- additive error model
- proportional error model
- exponential error model

The exponential error model is the most physiological one as it assures that all individual parameters are strictly positive. Therefore, it was used in this thesis and will be discussed in more detail. The exponential error model is described by the following equation:

$$P_{ki} = \theta_k \cdot e^{\eta_{ki}} \tag{2.6}$$

where P_{ki} denotes the value of the parameter k from the individual i (= individual parameter). The model assumes that all P_{ki} values are log-normally distributed. θ_k is the typical value of the population parameter k and η_{ki} is the difference between the natural logarithm of P_{ki} and θ_k ($\eta_{ki} = \ln P_{ki} - \ln \theta_k$). After logarithmising one obtains a normal distribution, the variance ω_k^2 becomes dimensionless and, therefore, expresses approximately the coefficient of variation in the model parameters [220].

A modification of this error model that is used for confining individual parameters between 0 and 1 is provided below:

$$P_{ki} = \frac{e^{\ln(\theta_k/(1-\theta_k))+\eta_{ki}}}{1 + e^{\ln(\theta_k/(1-\theta_k))+\eta_{ki}}} \tag{2.7}$$

θ_k is the typical value of the population parameter k and $\eta_{ki} = \ln \dfrac{P_{ki}}{1 - P_{ki}} - \ln \dfrac{\theta_k}{1 - \theta_k}$.

Due to the exponential term, the numerator can only take values larger than zero. If it approximates values close to zero, P_{ki} will approach a value of 0. On the other hand, if the numerator yields values much larger than zero, P_{ki} will approach a value of 1. For small estimates of ω_k^2 the coefficient of variation can be obtained by using the following equation:

$$CV\% = \frac{\theta_k \cdot (1 - \theta_k) \cdot \omega_k \cdot 100}{\theta_k} \tag{2.8}$$

where ω_k corresponds to the standard deviation of η_k.

2.4.3.2.2 Interoccasion variability

In most cases variability within individuals is not predictable. However, this apparent random intraindividual variability can be divided into variations within one study occasion and variations between study occasions [221]. The latter is called either interoccasion variability or between-occasion variability (BOV). It arises when a parameter of the model, e.g. CL, varies within subjects between study occasions and is therefore not correctly described by IIV. For the implementation of IOV equation 2.6 is supplemented in the following way:

$$P_{kiq} = \theta_k \cdot e^{\eta_{ki} + \kappa_{kiq}} \tag{2.9}$$

where P_{kiq} denotes the individual subject's value of P_{ki} at the study occasion q. κ_{kiq} is a zero mean random variable with variance π^2, assumed to be symmetrically distributed.

An occasion can be chosen arbitrarily. However, in most cases logical time frames for an occasion, e.g. a dosing interval, are selected. In order to estimate IOV more than one observation per individual has to be available on each occasion.

2.4.3.2.3 Residual variability

A residual is the difference between an observed and a predicted measurement. The residual is an error that cannot be explained by the model. It might be due to model misspecifications, errors in the documentation of sampling time points or assay error. The most common models for the incorporation of residual variability are presented in the following. The simplest model uses an additive residual error term:

$$y_{ij} = f(\phi_i, x_{ij}) + \varepsilon_{ij} \tag{2.10}$$

where y_{ij} denotes the measured observation from the i-th individual at a certain time point j. The function $f(\phi_i, x_{ij})$ has already been introduced as the structural part of the population model, but this time it also includes IIV and IOV, thus being responsible for the individual prediction of the model. ε_{ij} denotes the random deviation between the individual prediction and the observed measurement for each individual i at a certain time point j. This model will be used if a constant variance over the whole measurement range is probable.

If the variance, however, increases with growing measurement values, a proportional residual error model will become more likely:

$$y_{ij} = f(\phi_i, x_{ij}) \cdot (1 + \varepsilon_{ij}) \tag{2.11}$$

A third commonly used model is a combination of the previous two, i.e. it uses both an additive and a proportional component:

$$y_{ij} = f(\phi_i, x_{ij}) \cdot (1 + \varepsilon_{1,ij}) + \varepsilon_{2,ij} \tag{2.12}$$

At small observation values this model acts like an additive error model while at larger observation values it will resemble a proportional error model. This type of model is very convenient because it will account for proportionally higher errors close to the lower limit of quantification (LLOQ). It is assumed that ε_{ij} is a zero mean random variable with a symmetrically distributed variance σ^2. The variance σ^2 is the diagonal element of the of the Σ matrix and is estimated as a population PK parameter.

2.4.3.3 Covariate model

One aim of a population PK analysis is the detection of factors that can explain some of the observed IIV and IOV of the model parameters. The covariate model expresses relations between covariates and model parameters by using fixed-effects parameters [222]. A covariate is any variable that is specific to an individual and may influence the PK or PD of a drug. The classification of covariates is performed by differentiating between intrinsic factors (inherited, genetically determined), such as age and height, or extrinsic factors (subject to outside environmental influences), such as dose, laboratory parameters or smoking status [223]. In general, intrinsic covariates do not change over a short period of time whereas this is not the case for extrinsic covariates. Another way for classifying covariates is their discrimination into continuous

(e.g. age), dichotomous (e.g. sex) or categorical (e.g. study centre). Continuous covariate models generally consist of one of three different functions: linear, exponential or power. As IIV, IOV and residual variability are interrelated [224] the incorporation of covariates into the population model can reduce all these types of variability. Hence, if IIV is sufficiently reduced, drug treatment can be adjusted in a more individual manner.

Before testing for covariate influences one has to identify which covariates are to be examined. For this, different screening methods are available that assess the relation between the random effects and the covariate of interest.

2.4.3.3.1 GAM analysis

GAM stands for generalised additive model. The GAM procedure was originally proposed by Mandema et al [222]. It can be used for the *a priori* identification of possibly important covariates. GAM analysis can be performed after a basic population PK model without any covariates has been developed. The estimated individual parameters P_{ki} are then treated as ordinary data and are regressed on the individual covariate X_i according to the following equation:

$$P_{ki} = \alpha_{k0} + \sum_{l=1}^{n} g_{kl}(X_{li}) \tag{2.13}$$

where α_{k0} denotes the intercept, X_{li} is the l-th covariate of the i-th individual, and the function $g_{kl}()$ represents the function describing the covariate influence on P_k. It is an arbitrary univariate function with $\sum_{i=1}^{N_i} g_{kl}(X_{li}) = 0$. In Xpose^{TM} a hierarchy of three different possible models is defined for each explanatory variable: not included, included in a linear relation, included in a nonlinear (spline) relation [225]. For each covariate, the models up and down the hierarchy are used in a stepwise addition/deletion procedure. The model discrimination is performed using the Akaike information criterion (AIC) [226]. In each step, the covariate that reduces the AIC to the largest extent is retained in the model. This procedure is repeated until no further significant decrease of the AIC is possible.

2.4.3.3.2 Graphical analysis

Another method for the selection of covariate candidates is the examination of scatter plots. In these the individual empirical Bayes estimates of the parameters of interest are plotted against a possible continuous covariate and examined for a relation between the two [223]. If the examination of the scatter plot tends to show a straight line, in general a linear model will be used. However, if the line seems to be bent then the exponential or the power model might be superior. In case of categorical covariates box whisker plots can be used for examination of covariate relations. The examination of scatter plots or box whisker plots might only be able to spot the most obvious covariate relations while covariates of only marginal significance might not be detected. Moreover,

graphical analysis may be misleading as it is based on empirical Bayes estimates obtained from a model that does not contain any covariate relations, i.e. it is based on individual values obtained from mere consideration of IIV. Hence, caution should be exercised when using this approach alone.

2.4.3.3.3 Analysis in NONMEM

The covariate analysis in NONMEM[TM] takes place in the developed base population model with respect to the significance of the covariate's influence on a PK or PD parameter. Different procedures exist for covariate model building in NONMEM[TM] [222, 227-229]. Although no consensus exists as to what the most effective procedure is, in general the covariate model building process follows the forward inclusion and backward elimination process [227]. This procedure will be described in more detail in section 2.7.6.3.

2.4.3.4   Population model

The three types of sub-models presented in sections 2.4.3.1, 2.4.3.2 and 2.4.3.3 can be merged into a single population model that is described by the following equation:

$$y_{ij} = f(g(\Theta, z_{ki}) + \eta_{ki} + \kappa_{kiq}, x_{ij}) + \varepsilon_{ij} \tag{2.14}$$

where all types of variability are exemplarily incorporated as additive components. The function f characterises the relation between all investigated data and in combination with the residual error term ε_{ij} describes every observation y of the i-th individual at the j-th time point. It comprises the measured and documented independent variables x_{ij} (e.g. dose) and z_{ki} (covariates, e.g. age or weight), the vector Θ of all fixed-effects parameters θ (which includes PK and PD as well as covariate parameters) and the vectors (or scalars, if one-dimensional) of the random-effects parameters η_{ki}, κ_{kiq} and ε_{ij}.

2.4.3.5   Population parameter estimation

Estimation of population parameters can be achieved in many different ways using different software packages [230, 231]. However, as NONMEM[TM] was used for all analyses, this section will focus on the parameter estimation methods available in NONMEM[TM].

The aim of the population analysis is to obtain parameters that result in an optimal description of the modelled data given a model function. In NONMEM[TM] this is done by minimising the extended least squares objective function (O_{ELS}):

$$O_{ELS} = \sum_{i=1}^{N} \left[\frac{(y_i - f(\theta, x_i))^2}{\upsilon(\theta, \xi, x_i)} + \ln(\upsilon(\theta, \xi, x_i)) \right] [212] \tag{2.15}$$

where $f(\theta, x_i)$ corresponds to the structural model part and a respective expected value of y_i. ξ and $\upsilon(\theta, \xi, x_i)$ correspond to any additional parameter and to the variance model, respectively. The logarithm term is included as a penalty in order to counteract the decrease in the sum of squares

term as otherwise the objective function value (OFV) would be driven to zero under any circumstances as ξ takes values that increase υ. Reasonably bounded estimates of all parameters are obtained from this approach [212]. Up to a constant, O_{ELS} is equal to minus twice the log-likelihood of the fit. Therefore, a minimum OFV reflects the maximum likelihood of parameters that maximise the probability of observing the data given a specific model.

As a closed-form solution for the minimisation of O_{ELS} is not obtainable in most PK/PD analyses, NONMEM^{TM} approximates the solution by the use of different estimation methods. The first one available in NONMEM^{TM} was the first-order (FO) method. This method produces estimates of the population parameters through a first-order Taylor series expansion of the nonlinear model around zero for the random-effects parameters. However, it does not provide any estimates of the random interindividual effects. Nonetheless, based on the first-order estimates of the population parameters these can be obtained by maximising the empirical Bayes posterior density of η_i using the 'posthoc' option available in NONMEM^{TM} [232]. The FO method performs reasonably well in sparse data situations. However, analysis of rich data situations or of models involving a larger degree of nonlinearity can lead to biased estimates. Further advancements in the estimation algorithms led to the development of the first-order conditional estimation methods (FOCE). In contrast to the FO method, the conditional estimation methods provide both estimates of the population parameters and of the random interindividual effects by using a first-order Taylor series expansion around the conditional estimates of the ηs. When this algorithm is used, estimates of the population parameters as well as the random-effects parameters are obtained during each iteration step. A conditional estimation method involves multiple minimisations within each minimisation step. Therefore, these methods are more CPU intensive and thus more time-consuming. The FOCE method is available both without (FOCE) or with (FOCE INTERACTION) interaction between η and ε. The interaction option calculates the objective function allowing for a dependence of ε on η, which is the case e.g. in a proportional residual error model. When all variances are assumed to be homoscedastic, an interaction can be excluded, otherwise one should prefer the FOCE method with interaction. All of these estimation methods have been used for model development within this thesis. However, all final results were obtained using FOCE INTERACTION. The list of mentioned estimation methods available in NONMEM^{TM} is not exhaustive, further detailed information can be found in the literature [232].

2.4.3.6   Model selection: Statistical methods

Decisions on model improvement or deterioration can be made based on the difference in the OFV of two nested models. Models can be declared as nested if the more simple model can be obtained from the more complex model by fixing one or more parameters to a certain value. The difference in OFV is approximately χ^2-distributed. Hence, a difference in OFV of 3.84 and 10.83 points

corresponds to a significance level of 0.05 and 0.001, respectively, given 1 degree of freedom (df). A p-value of 0.05 was predefined for accepting a model over a previous one for all model building procedures except the backward elimination step during covariate model building (section 2.7.6.3). In this case, a higher significance level was applied (p=0.001).

Moreover, precision of parameter estimates was attained based on their standard errors. Absolute standard errors can be obtained from the values (V_{CME}) in the covariance matrix of estimates:

$$\text{absolute standard error} = \sqrt{V_{CME}} \tag{2.16}$$

The relative standard errors (RSE) can then be calculated as follows:

$$\text{RSE,\%} = \frac{\text{absolute standard error}}{\text{parameter}} \cdot 100 \tag{2.17}$$

In general, all models were aimed at having RSE values less than 50% as otherwise the 95% confidence interval of the respective parameter would include zero.

2.4.3.7   Model selection: Graphical methods

In order to assess the goodness of fit of the models and to compare models that were not nested they were explored graphically. The graphical analysis was performed with the software Xpose [225] implemented in S-Plus® (see 2.8). Primarily, the following goodness of fit plots were investigated:

- Measured concentrations versus predicted population or individual parameter estimates
- Weighted residuals (= weighted difference between measured and predicted population or individual concentrations) versus predicted population or individual concentrations
- Weighted residuals versus independent variable (e.g. time, log time)

2.5   Project I: *In vitro* experiments

2.5.1   Objectives

This project aimed at conducting *in vitro* experiments to enable the conduction of clinical trials investigating the pharmacokinetics of vancomycin and linezolid by using the microdialysis approach. Firstly, an analytical assay for vancomycin was developed and subsequent *in vitro* microdialysis experiments were conducted. Secondly, a previously existing analytical assay for linezolid was extended to the matrices urine, bone marrow, bone biopsy samples and bone microdialysate.

2.5.2   Vancomycin: Bioanalytics and *in vitro* microdialysis

2.5.2.1   High performance liquid chromatography

Vancomycin was quantified using the high performance liquid chromatography (HPLC) method with subsequent UV detection. The separation of two sample components in chromatography is

based on their different distribution and adsorption characteristics between two non-miscible phases. The stationary phase is fixed in the system while the mobile phase is streaming through the chromatographic system.

The molecules of the analytes are distributed between the mobile and the stationary phase. Interaction with the solid phase leads to substance retention. Due to the different distribution and adsorption characteristics of the particular analytes the mean residence time in the stationary phase differs, resulting in a different net migration velocity. Analyte signals obtained from the detector can be evaluated using specific integration software [233].

All HPLC experiments were performed on a Beckman HPLC system consisting of the following components:

solvent modul 126	Beckman Coulter GmbH, Krefeld, Germany
autosampler AS 507	Beckman Coulter GmbH, Krefeld, Germany
interface AI 406	Beckman Coulter GmbH, Krefeld, Germany
UV detector LKB2151	Techlab GmbH, Erkerode, Germany

Samples were separated on a Spherimage-80 ODS2 5 µm column, 125 x 4 mm ID, with an integrated pre-column (Knauer, Berlin, Germany) as stationary phase and MeOH (reservoir A)/potassium hydrogen phosphate buffer (25 mM, pH 2.75) (reservoir B) as mobile phase at a flow rate of 1 mL/min using gradient elution. For microdialysis samples the gradient consisted of five phases:

(a) isocratic elution of 15% (A) and 85% (B) for three minutes,

(b) linear increase to 30% (A) over 0.75 min,

(c) isocratic elution of 30% (A) and 70% (B) for 2.25 minutes,

(d) linear increase to 85% (B) over 0.5 minutes,

(e) isocratic elution of 15% (A) and 85% (B) for 3.5 minutes.

For plasma samples (see section 2.5.2.2.1) an additional gradient phase was required:

(a) isocratic elution of 15% (A) and 85% (B) for three minutes,

(b) linear increase to 30% (A) over 0.75 min,

(c) isocratic elution of 30% (A) and 70% (B) for 2.25 minutes,

(d) linear increase to 80% (A) over 0.5 minutes,

(e) isocratic elution of 80% (A) and 20% (B) for 3.5 minutes,

(f) linear increase to 85% (B) over 0.75 minutes,

(g) isocratic elution of 15% (A) and 85% (B) for 5.25 minutes.

2.5.2.2   Sample preparation

Different methods for vancomycin sample preparation from biological matrices were examined. The objective of the final analytical procedure was its applicability in a routine clinical setting and a validation according to international guidelines [234].

Two stock solutions were prepared separately for the purposes of calibration and quality control (QC). For each solution, 102.5 mg vancomycin with a potency equivalent to not less than 950 µg of vancomycin per mg, calculated on the anhydrous basis [46], was dissolved in water yielding concentrations of 20.0 mg/mL each. One stock solution was diluted with water to obtain working solutions of 5.50, 13.0, 44.0, 100, 447 and 1069 µg/mL for microdialysate and plasma calibration samples. Working solutions for QC samples were prepared by diluting the second stock solution with water to yield vancomycin concentrations of 4.00, 10.0, 260 and 700 µg/mL. Aliquots of stock and working solutions were frozen at –70°C.

2.5.2.2.1 Plasma

Plasma calibration samples were prepared prior to each analytical run by mixing 10 µL of aqueous working solution with analyte-free human plasma to yield vancomycin concentrations of 0.400, 1.00, 3.30, 7.40, 33.0 and 80.0 µg/mL. In addition, QC samples were prepared from aqueous working solutions by dilution with plasma. They contained 0.400, 1.00, 26.0 and 70.0 µg/mL vancomycin. QC samples at the LLOQ were used for pre-study validation only. Aliquots of QC samples for pre- and in-study validation were stored at –25°C until analysis.

Plasma samples were prepared by mixing a 100 µL aliquot with 100 µL MeOH and 100 µL trichloroacetic acid (5%). The mixtures were allowed to rest at ambient temperature for 10 min and centrifuged at 10,000 g for 5 min. 230 µL of the supernatant were evaporated to dryness by a Speed-Vac® and redissolved in 75 µL water. A volume of 20 µL was injected into the HPLC system.

2.5.2.2.2 Microdialysate

In analogy to the procedure for plasma calibration sample preparation, microdialysate calibration samples were prepared prior to each analytical run by mixing 4 µL of aqueous working solution with analyte-free Ringer's solution to yield vancomycin concentrations of 0.400, 1.00, 3.30, 7.50, 33.0 and 80.0 µg/mL. QC samples for microdialysate were obtained in the same way as plasma samples, diluting with Ringer's solution instead of plasma.

For microdialysate, a simple one-step dilution preparation procedure was developed due to the lack of proteins. After the described dilution process for obtaining the calibration solutions, 40 µL of every microdialysate sample were mixed with 20 µL of water. Following dilution, a volume of 20 µL was injected into the HPLC system.

2.5.2.3   Method validation

Validation was carried out according to FDA guidelines [234]. In the context of pre-study validation the analytical method was examined in terms of analyte stability and recovery as well as method specificity, accuracy, precision and linearity. If applicable, results will be presented as mean (coefficient of variation).

2.5.2.3.1 Specificity

In order to evaluate the specificity of the analytical method vancomycin-free artificial microdialysate, i.e. Ringer's solution, and plasma from six different healthy human sources were investigated for compounds influencing vancomycin during analysis. In addition, to investigate interference of drugs commonly used in patients, a broad variety of drugs that could possibly be co-administered with vancomycin were assayed (see section 2.1). For this purpose, solutions of the drugs were diluted to yield final concentrations that were at least within clinically relevant ranges. Samples were prepared and assayed as described above.

2.5.2.3.2 Stability

Vancomycin stability was assessed in microdialysate and plasma, reflecting situations likely to be encountered during actual sample collection, storage, preparation and analysis. Low and high QC concentrations were investigated in triplicate under three different conditions for both matrices. Three sets of QC samples were assayed after one, two or three freeze-thaw cycles (-25°C versus room temperature) and were compared to freshly prepared QC samples. Equation 2.18 was used to determine the freeze-thaw stability of vancomycin in microdialysate and plasma, respectively.

$$\text{stability, \%} = 100 \cdot \frac{\text{result}_{\text{stored sample}}}{\text{result}_{\text{freshly prepared sample}}} \tag{2.18}$$

To evaluate stability at room temperature, QC samples were thawed at ambient temperature and kept under these conditions for 4 h or 24 h. The data were compared to results from freshly thawed QC samples as described above.

To determine the stability of the drug in prepared samples, two sets of QC samples were prepared as described above. One set was stored in the sample tray of the autosampler at room temperature for 24 h or 27 h, depending on the matrix studied. The other set was frozen at −25°C after preparation for at least 24 hours. These results were compared with those of new QC samples measured immediately after preparation using equation 2.18. A student's t-test was applied to test for statistically significant differences.

2.5.2.3.3 Accuracy and precision

Accuracy, or more precisely inaccuracy, was assessed by calculating the mean percentage deviation (relative error, RE) of measured concentrations of QC samples from their nominal concentration.

For pre-study validation, 5 QC samples per concentration and matrix were analysed on three different days. Precision, or more precisely imprecision, was evaluated using the coefficient of variation (CV) of multiple determinations. For both parameters, the within-day and between-day results were determined. In each instance, four concentrations covering the whole concentration range were investigated.

2.5.2.3.4 Linearity and determination of lower limit of quantification

Linearity was evaluated using freshly prepared, spiked matrix samples in a concentration range from 0.400-80.0 μg/mL for microdialysate and plasma samples (n = 5). Each calibration function consisted of 6 calibrator concentrations.

LLOQ was assessed by comparing the chromatograms of analyte-free matrix with those obtained from 5 spiked matrix samples at each concentration. Vancomycin working solution was added to Ringer's solution and analyte-free plasma yielding concentrations from 0.200 to 0.800 μg/mL. The LLOQ for each matrix was defined as the lowest concentration within acceptable ranges of accuracy and precision that could be analysed [234].

2.5.2.3.5 Recovery of the analyte

Peak area data of 5 spiked matrix samples at 3 QC concentrations were compared to the results of 3 diluted aqueous solutions. The aqueous solutions had the the same nominal concentration as the spiked matrix samples. The recovery was calculated in analogy to equation 2.18.

2.5.2.4 *In vitro* microdialysis

As obligatory experiments prior to the planned use of the drug in pre-clinical and human microdialysis investigations, the characteristics of vancomycin in the microdialysis probes were evaluated *in vitro*.

2.5.2.4.1 Probes

For microdialysis investigations *in vitro*, commercially available microdialysis probes with a molecular weight cut-off of 20 kDa, an outer diameter of 0.6 mm and a membrane length of 30 mm were used. Probes were perfused with Ringer's solution at different flow rates (see below) and with potassium hydrogen phosphate buffer (50 mM, pH 7.4) at a constant flow rate by using a precision pump.

2.5.2.4.2 Recovery experiments

A microdialysis probe was placed in a vial containing Ringer's solution. The perfusion medium consisted of vancomycin in Ringer's solution at a concentration of 80 μg/mL. In order to determine an optimal flow rate for subsequent *in vitro* and *in vivo* experiments recovery was assessed at flow rates of 1, 2, 3 and 4 μL/min, performing the retrodialysis method [164]. Samples (n = 3) were collected at intervals of 10 min for a flow rate of 4 μL/min, 14 min for 3 μL/min, 20 min for

2 µL/min and every 40 min for a flow rate of 1 µL/min. RR was calculated according to equation 1.1.

To investigate the effects of concentration on RR, a probe was perfused with either Ringer's solution or 50 mM potassium phosphate buffer (pH 7.4), both containing vancomycin concentrations of 1.00, 10.0, 40.0 or 80.0 µg/mL, at a flow rate of 4 µL/min. The experiment was performed in two different settings for two possible directions of diffusion: (1) as delivery (retrodialysis) and (2) as recovery experiment (diffusion of drug from the surrounding medium into the probe). Samples (n = 3) were taken every 10 min.

2.5.3   Linezolid: Bioanalytics

2.5.3.1   High performance liquid chromatography

Linezolid was quantified by means of an HPLC system with UV detection. It consisted of the following components:

solvent modul 422 and 420	Kontron, Neufahrn, Germany
autosampler SA 360	Kontron, Neufahrn, Germany
UV detector 430	Kontron, Neufahrn, Germany
multiport	Kontron, Neufahrn, Germany
HPLC column Spherimage-80 ODS2 5 µm, 125 x 4 mm ID with integrated pre-column	Knauer, Berlin, Germany

2.5.3.2   Sample preparation

2.5.3.2.1   Plasma, ultrafiltrate and microdialysate

The preparation procedure for plasma, ultrafiltrate and microdialysis samples had been developed at the Department prior to all investigations [159]. It was employed unchanged and provided the basis for the sample preparation procedures of other matrices (sections 2.5.3.2.2, 2.5.3.2.3, 2.5.3.2.4).

2.5.3.2.2   Bone marrow

As bone marrow exhibits similar characteristics as blood it was hypothesised that bone marrow samples could be measured using plasma calibration samples. In order to confirm this, empty bone marrow was obtained from healthy piglets and centrifuged. The supernatant was spiked with linezolid working solutions to obtain the concentrations 0.2, 0.5, 1, 5, 10 and 20 µg/mL. It was prepared and assayed like plasma samples using plasma working solutions for calibration. 50 µL of bone marrow sample were mixed with 200 µL acetonitrile. The mixtures were allowed to rest at ambient temperature for 10 min and centrifuged at 10,000 g for 5 min. Subsequently, 200 µL of the supernatant were removed and evaporated to dryness. The residue was redissolved in 50 µL 80/20 H_2O/ACN (v/v). A volume of 20 µL was injected into the HPLC system [159].

2.5.3.2.3 Bone

For the sample preparation of bone the assay was modified according to the preparation procedure described by Lovering et al. [94]. Bone samples (m = 113.9-114.5 mg) were crushed after adding liquid nitrogen. Afterwards, a volume of 0.1 M PBS equal to twice the weight of bone was added (where 1 mL = 1 g). Linezolid was extracted from the bone/PBS mixture at 8°C for 5 h. During this period the samples were vortexed every 30 min. After extraction the samples were centrifuged at 10,000 g and an aliquot of the aqueous layer was treated with an equal volume of acetonitrile. The supernatant was diluted to achieve a minimal volume of 40 µL. A volume of 20 µL was injected into the HPLC system. In order to corroborate the hypothesis that bone concentrations can be determined using plasma working solutions for calibration [159], crushed bone samples from healthy piglets were lyophilised. Subsequently, they were spiked with a volume of linezolid working solution that exactly replaced the water loss from the lyophilisation process. This way three samples were obtained containing 0.395 µg/mL, 1.02 µg/mL and 2.05 µg/mL linezolid. The samples were treated as described above and measured against plasma calibration samples.

2.5.3.2.4 Urine

Urine samples from healthy pigs do not contain any proteins. Therefore, sample preparation included a simple one-step dilution preparation procedure only. In analogy to the preparation of microdialysate samples [159] 10 µL of urine were mixed with 30 µL of water. Following dilution, a volume of 20 µL was injected into the HPLC system using microdialysate working solutions for calibration.

2.6   Project II: Linezolid pharmacokinetics in bone tissue

2.6.1   Objectives

The project was carried out in cooperation with Dr. L. Stolle (Clinical Institute & Department of Clinical Microbiology, Aarhus University Hospital, Denmark). The aim of this study was to apply the microdialysis technique to corticocancellous bone ISF of 10 sows in order to investigate the feasibility of the technique. Moreover, it was evaluated if linezolid sufficiently penetrated into bone tissue to successfully treat gram-positive bone infections. In addition to microdialysate concentrations, the concentrations in other investigated matrices were measured using the described analytical procedures (section 2.5.3). Subsequently, the pharmacokinetics of linezolid was explored in a non-compartmental approach (see section 2.3) and the values obtained in plasma, bone marrow and finally bone concentrations obtained from bone biopsy and bone microdialysis samples were compared intraindividually.

2.6.2   Study design, treatment and sample collection

Ten sows were included into the study. In order to implant microdialysis probes animals underwent surgery in general anaesthesia [235]. In an angle of 90° to the bone surface two holes with a diameter of 1.1 mm and depth of 15 mm were drilled into the corticocancellous bone of the right tibia and the microdialysis catheters were inserted into the channels. In order to let the tissue recover from insertion trauma a period of 1 h was allowed before the start of the experiment. The positions of the catheters were controlled by autopsy. All animals received 600 mg linezolid (Zyvoxid® 2 mg/ml, 300 ml, Pfizer) as a 30 min intravenous infusion. Microdialysis was carried out with a flow rate of 1 µL/min using Ringer's solution as perfusate. Beginning with linezolid administration (T_0) dialysates were collected every 30 min over a period of 6 hours. The concentration in bone ISF ($C_{bone,ISF}$) was defined as:

$$C_{bone,ISF} = 100 \cdot \frac{C_{dialysate}}{RR} \tag{2.19}$$

Bone biopsy samples were obtained from the proximal part of the left tibia. Starting with T_0, they were harvested by a Coombs bone drill at intervals of 1 hour. The number of bone specimens was limited as further biopsies would have damaged the bone structure to a large extent. From all samples, periosteum and cortical bone was removed.

Blood was collected from a sheath placed in the external jugular vein. The samples were collected every 15 min from T_0 until 6 h. After centrifugation for 10 minutes all samples were immediately frozen to -80°C. Bone marrow was obtained with a cannula inserted into the bone marrow of the left tibia and collected at 30 min intervals until 6 h after the start of linezolid administration. The sampling schedule for the different matrices is illustrated in table 7.1. All surgical procedures were performed under the approval and guidelines of the Danish Ministry of Justice, Animal Experimentation Inspectorate.

2.6.3   Calibration of microdialysis catheters

In vivo RR of linezolid was determined by use of the retrodialysis method [164]. Two different perfusates containing different concentrations of linezolid (25 and 75 µg/mL) were used applying a flow rate of 1 µL/min. The *in vivo* RR was calculated according to equation 1.1.

2.6.4   Building the dataset and missing values

For each subject a single dataset was created. It included information about the individual subject, sampling time points and measured concentrations in the different matrices studied. Final unbound matrix concentrations were calculated, taking into account ultrafiltration and recovery results for plasma and microdialysates, respectively. All datasets were merged into one single analysis dataset that in the end contained data from 10 subjects and all studied matrices. Missing data items were not included in the data analysis. Values below the LLOQ were excluded from data analysis.

However, if the value below the LLOQ was obtained before the first quantifiable value after drug administration, the concentration was set to zero.

2.6.5 Pharmacokinetic analysis

The pharmacokinetics of linezolid in plasma, bone marrow, bone biopsy and bone microdialysate was determined using a non-compartmental approach (see section 2.3) implemented in the software WinNonlin® (see section 2.8). For each matrix, the parameters t_{max}, C_{max}, AUC_{0-6h}, volume of distribution, CL and $t_{1/2}$ were estimated. In addition, tissue penetration factors (PF) were calculated according to the following equation:

$$PF = \frac{AUC_{tissue}}{AUC_{plasma}} \qquad\qquad (2.20)$$

where AUC_{tissue} and AUC_{plasma} correspond to the area under the concentration-time curve for unbound tissue and plasma concentration data from 0-6 h, respectively. Apart from t_{max} and $t_{1/2}$, which will be given as median, parameters will be presented as geometric mean values.

2.7 Project III: Target site pharmacokinetics of linezolid during sepsis

2.7.1 Objectives

In cooperation with Dr. C. Joukhadar (Department of Clinical Pharmacology, Medical University Vienna, Austria) and Dr. S. Ključar (Central Department of Anaesthesiology and Intensive Care, DRK-Kliniken Berlin, Germany) a clinical study for the 'Assessment of target site pharmacokinetics and pharmacodynamics of linezolid in healthy volunteers and septic patients after single dose administration and at steady state' was carried out. It was a multi-centre, open-labelled, prospective comparative study approved by the local ethics committees in Vienna and Berlin. In total, 10 healthy volunteers and 12 patients with either sepsis or septic shock were included in the study in Vienna. At the Berlin study site 12 patients were enrolled in the trial.

The aim of the study was to investigate unbound linezolid plasma concentrations as well as its distribution characteristics into subcutaneous adipose (s.c.) ISF and skeletal muscular (i.m.) ISF after single (study visit 1) and multiple (study visit 2) dosing by means of the microdialysis technique (see section 1.3). This technique measures unbound drug concentrations. Therefore, only the active fraction of linezolid was determined. The samples from the described matrices were measured as described in section 2.5.3. The obtained data was then used to describe the PK of linezolid. Moreover, the PK of healthy volunteers and critically ill patients was compared. The model was developed and evaluated in order to enable predictions for an improved, more individualised antimicrobial therapy.

2.7.2   Study design, treatment and sample collection

2.7.2.1   Healthy volunteers

Inclusion and exclusion criteria for healthy volunteers are summarised in table 7.2. Volunteers enrolled in the study were provided with a perivenous inlet for the administration of linezolid and the withdrawal of blood samples. Two microdialysis catheters were placed into either s.c. or i.m. ISF of the lower extremities and perfused with Ringer's solution at a flow rate of 1.5 µL/min. A baseline microdialysate sample was collected before calibrating the probe (see section 2.7.3) according to the retrodialysis method (see section 1.3.2). Following calibration, a 30 min washout period with Ringer's solution was allowed. Afterwards, 600 mg linezolid were administered as a short-term infusion over 30 min. Samples were taken as described in table 7.3.

After the 8 h sampling period microdialysis catheters were removed. Subsequent doses of 600 mg linezolid tablets were taken in intervals of 12 h. The responsibility for the administration of the tablets was taken by the subjects themselves. Volunteers documented the actual time of linezolid intake in a diary. This visit was carried out after multiple dosing. The sampling schedule as well as the procedure of the visit were the same as described above and as in table 7.3. However, calibration was performed after the 8 h sampling period.

2.7.2.2   Patients

Inclusion and exclusion criteria for patients are summarised in table 7.4. The study procedure for septic patients and patients with septic shock was mainly the same as that described for healthy volunteers (section 2.7.2.1). However, patients received all linezolid doses as a short-term infusion over 30 min. The dosing intervals as well as the sampling schedule remained unchanged.

For patients recruited in Berlin a deviating schedule was necessary for the subsequent analytical measurements in order to obtain study approval by the local ethics committee. Microdialysis samples had to be measured within the next 24 h after study visit 2. If deemed necessary, the dosing regimen of linezolid could then be adjusted on the day following study visit 2. The decision was based on clinical evaluation and individual ISF concentrations with respect to the MIC_{90} of the respective pathogen. If a dose increase was considered to be beneficial for the patient, the dosing regimen of linezolid would be adjusted from 600 mg every 12 hours (twice daily) to 600 mg every 8 hours (3 times a day), i.e. the daily dose would be increased from 1200 mg to 1800 mg.

2.7.3   Calibration of microdialysis catheters

The calibration procedure was the same for both healthy volunteers and patients. Catheters were calibrated according to the retrodialysis method (see section 1.3.2). On study visit 1 the calibration was performed using a perfusate containing 10 µg/mL linezolid and a flow rate of 1.5 µL/min. Two dialysate fractions were collected in intervals of 15 min. On study visit 2 the perfusate

concentration was changed to 150 µg/mL in order to allow for calibration after multiple dosing. Concentrations in the dialysate and perfusate were determined and the recovery of the catheter calculated according to equation 1.1. Retrospectively, it was investigated if the used perfusate concentration on study visit 2 was sufficient for *in vivo* experiments, i.e. if it exceeded ISF concentrations by more than the tenfold.

2.7.4 Building the NONMEM dataset

In general, a dataset readable by the NONMEM^{TM} software (see section 2.8) has to be structured in a special way [232]. It commonly consists of dependent variables (DV), e.g. measured concentrations, and independent variables such as dosing information records and covariates (e.g. demographic, disease and other individual factors which might influence drug PK). The dataset created for the population PK analysis contained the items listed in table 7.5.

Creatinine clearance (CLCR) was calculated by the Cockcroft-Gault equation [236] based on serum creatinine concentrations. Age was given in years, weight in kg and serum creatinine concentrations in mg/dL. The calculations were performed in Excel (see section 2.8).

$$\text{CLCR (mL/min)} = \frac{(140 - \text{age}) \cdot \text{weight}}{72 \cdot \text{creatinine concentration}} \left(\cdot \, 0.85 \text{ for females} \right) \tag{2.21}$$

Missing DV data items were not included in the data analysis. Values below the LLOQ were excluded from data analysis unless they were obtained before the first quantifiable value after drug administration. In this case, the DV data item was set to zero. Covariates missing within a subject were replaced by the measured value closest to that certain time point. In patients, completely missing continuous values were replaced by the median of the patient population. If a continuous covariate was missing in all healthy volunteers simultaneously, it was replaced by the arithmetic mean reference values for healthy people. This procedure was adhered to as the obtained median values of the patient population were not expected to reflect the missing data of healthy volunteers. Completely missing categorical covariate values were planned to be replaced by the mode of the study population. The dataset was created manually and was subject to an intensive data checkout procedure (see section 2.7.5).

2.7.5 Data checkout

Before analyses, datasets were checked in terms of completeness, accuracy and plausibility. In a first exploration the dataset was subjected to a column check in Excel (see section 2.8). Single columns were examined for their minimum and maximum values. These were compared to reference values and checked for their plausibility. In addition, the dataset was subject to a cross-column check, identifying combinations that necessarily belonged together. The plausibility check was assisted by the creation of "index plots". In these plots every item in the dataset was plotted

against the individual subject records (ID). The appendix contains an example of such an index plot (figure 7.1).

2.7.6   Strategies for population pharmacokinetic model development

The whole model building procedure was performed according to the following concept:

- Development of the structural model
- Implementation of IIV, IOV and residual variability, hence obtaining the 'base model'
- Identification of covariates (covariate analysis), hence obtaining the 'final covariate model'

It was planned to perform the population PK modelling in a sequential manner. Data was available from three different matrices: ultrafiltrate (unbound plasma concentrations), subcutaneous ISF and muscular ISF (see section 2.7.1). The first modelling approach aimed at developing a model for the description of unbound plasma concentrations. Afterwards, the joint model combining microdialysis ISF as well as ultrafiltrate data was developed based on the final covariate model for unbound plasma concentrations (see section 2.7.6.3).

2.7.6.1   Structural model

The structural model describes the typical time profile of the measured concentration as a function of model parameters, the dosing schedule and the administered dose. For nested models discrimination between rival structural models was performed based on the difference in OFV. Otherwise, graphical analysis using goodness of fit graphics was employed. Furthermore, parameter estimates were checked for plausibility. Parameter precision was evaluated by examining the size of the RSEs.

2.7.6.1.1   Model for unbound linezolid plasma concentrations

Before the start of the analysis, several structural models for the description of linezolid PK in plasma had been published. The concentration-time profiles had either been described by a two-compartment model with linear elimination kinetics [97] or a two-compartment model with parallel linear as well as Michaelis Menten elimination [100]. As a consequence, the first strategy was aimed at examining whether one of these models was suitable for the adequate description of unbound linezolid plasma concentrations. Furthermore, different simple structural base models (one-, two- and three-compartment) were explored. In addition, more complex models were developed in order to assess whether the observed nonlinearity in linezolid PK could be described more precisely. This approach was based on the results obtained from the analysis using the two-compartment model with linear elimination kinetics as well as the two-compartment model with parallel linear and Michaelis Menten elimination.

All models for the description of unbound linezolid plasma concentrations were parameterised in terms of distribution and elimination clearances, volumes of distribution and absorption rate-constants.

2.7.6.1.2 Joint model for unbound linezolid ISF and plasma concentrations

The final covariate model for unbound plasma concentrations (see 2.7.6.3) was used for the development of the joint model. Two additional compartments were added for the inclusion of ISF concentration data. Manifold connections between these two compartments and the plasma model were explored, using distribution and elimination rate-constants, apparent volumes of distribution or coding as in an effect compartmental approach [237], including partition coefficients [238].

Two basic approaches for the inclusion of microdialysis ISF concentration data were conceivable. In the first approach, all parameters of the joint model would be estimated simultaneously. This approach would correctly account for the uncertainties in the data and would also allow ISF concentration data to influence PK parameters for unbound plasma concentrations. However, in this approach fitting any single model to all the data might be computationally burdensome. A second approach would be to estimate the parameters for plasma and ISF concentrations sequentially, thus disconnecting their estimation. As a result, the parameters estimated for the description of unbound ISF concentrations would be conditioned on the previously obtained parameters based on unbound plasma concentrations. In general, the model development aimed at estimating all parameters simultaneously. However, if it became obvious that a simultaneous approach was not feasible due to long model run times, a sequential approach would be taken.

2.7.6.2 Pharmacostatistical model

In general, the strategies for model building in NONMEM^{TM} are twofold: either a bottom up to or a top down approach is chosen. The bottom up approach starts out with the most simple model, including variability on only one fixed-effects parameter. From this, the model is expanded to more complexity until further additions fail to improve the model fit. In the top down approach IIV is included into the model for every fixed-effects parameter, meaning that the most complex model is chosen. In subsequent steps, every random-effects parameter is individually removed from the model. If the removal does not lead to a significant worsening of the model (see 2.4.3.6), the random-effects parameter is excluded. This procedure is repeated until no further elimination of random-effects parameters can be performed without impairing the model fit. The top down approach has the advantage of including every possible parameter, meaning that it may be closer to the true model. However, this modelling approach is very time-consuming and in addition, inclusion of variability on every parameter leads to numerical model instabilities. In most cases, it is advisable to employ the bottom up approach as run times are significantly reduced and in most cases the data situation does not allow using the most complex model [232]. Therefore, it was applied in this thesis.

In most cases, IIV and IOV was modelled using an exponential random-effects model, and residual variability was modelled using a combined (additive/proportional) error model (see section

2.4.3.2). If individual parameter estimates had to be restricted to values between 0 and 1, the error model described in equation 2.7 was used.

2.7.6.3 Covariate model

Covariate analysis was separately carried out with the model for unbound linezolid plasma concentrations and the joint model for unbound linezolid ISF and plasma concentrations, respectively. The proceedings are illustrated in the flowchart in figure 2.4.

2.7.6.3.1 Covariate screening and univariate covariate implementation

In a first step, a GAM analysis (as described in section 2.4.3.3) was performed and possible covariates were pre-selected. In addition, further covariates were selected if either a relation to the individual empirical Bayesian parameter estimates seemed conceivable from the examination of the scatter plots (see section 2.4.3.3) or if it seemed physiologically plausible (e.g. CLCR was selected for covariate analysis as a possible influence on the CL of linezolid independent of the results obtained in the GAM analysis).

These pre-selected covariates were then individually added to the base model. Continuous covariates (Cov) were implemented into the model using a linear relation:

$$\theta_{P_{Cov}} = \theta_P \cdot \left(1 + \theta_{Cov} \cdot \left(Cov - Cov_{median}\right)\right) \tag{2.22}$$

where $\theta_{P_{Cov}}$ depicts the typical parameter value of an individual with a certain covariate value. θ_P is the typical parameter value of an individual possessing the median covariate value. θ_{Cov} describes the influence of the covariate as a proportionate change from θ_P per change of one covariate unit from the median covariate value Cov_{median}.

In some cases, however, the data may not have been satisfactorily described by the linear model presented above. If the covariate values were spread over a wide range, the hockey-stick or two-spline model could be used:

$$\theta_{P_{Cov}} = \begin{cases} \theta_P \cdot \left(1 + \theta_{Cov} \cdot \left(Cov - Cov_{median}\right)\right) & \text{if covariate} < \text{node point of spline function} \\ \theta_P & \text{if covariate} \geq \text{node point of spline function} \end{cases} \tag{2.23}$$

Depending on whether an individual covariate value was higher or lower than the chosen node point of the spline function, different relations were assumed. In the equation described above a linear relation was used until the node point was reached, afterwards $\theta_{P_{Cov}}$ took the value of θ_P.

In all cases, the linear relation was implemented into the model. If indicated by the results of the GAM analysis or after visual inspection of the scatter plots, the hockey-stick function would be examined in addition. The function that resulted in the lower OFV was selected for further model development.
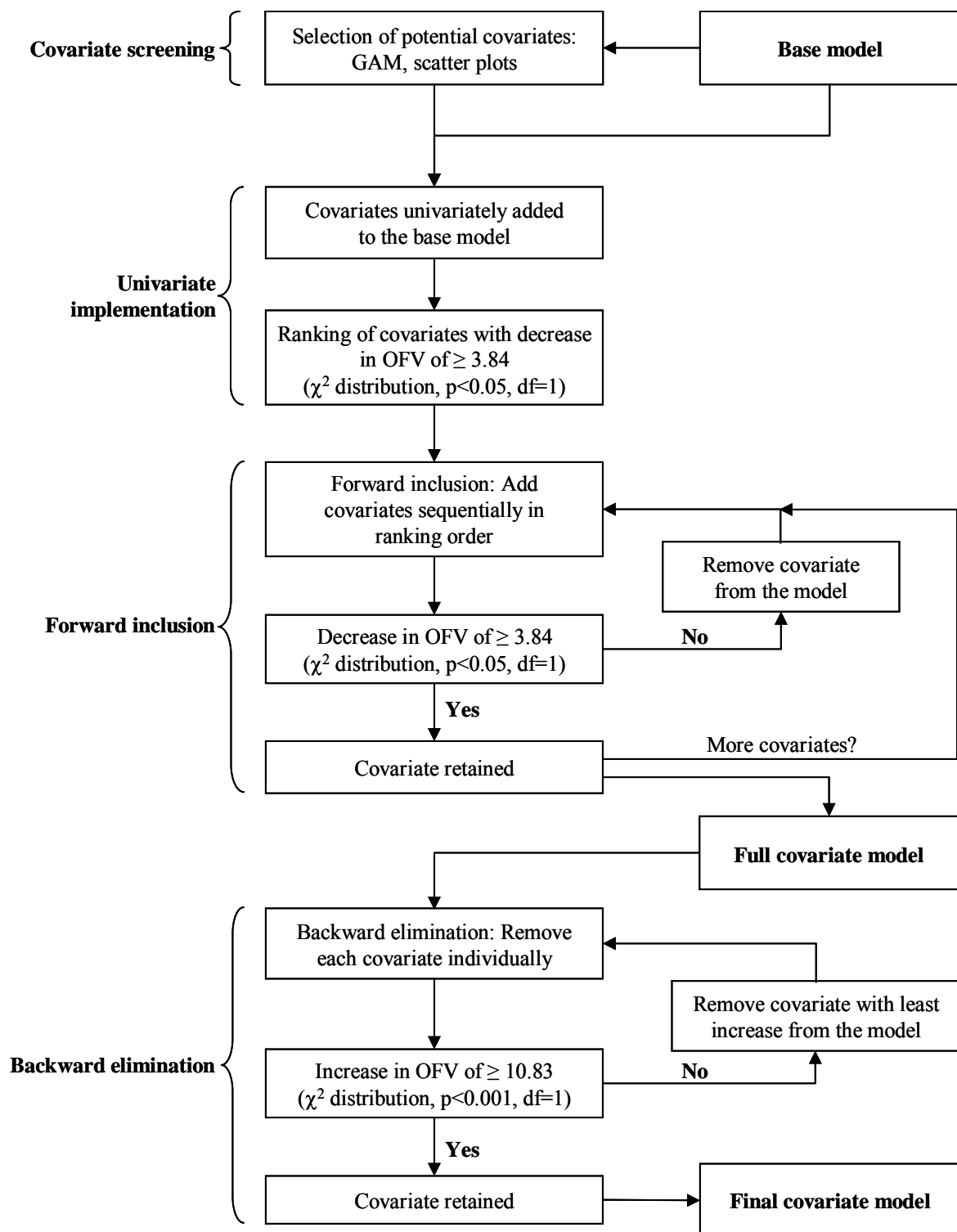
Figure 2.4: Flowchart of the covariate model development process

Categorical covariates were incorporated using a fractional change model. The covariate sex is used as an example in the following function:

$$\theta_{P_{Cov}} = \begin{cases} \theta_{P,male} \\ \theta_{P,male} \cdot \theta_{fraction,female} \end{cases} \qquad (2.24)$$

In this function, a typical parameter is estimated for a male individual ($\theta_{P,male}$). The typical parameter value of a female individual is the fraction $\theta_{fraction,female}$ of the typical male parameter estimate.

If inclusion of the respective covariate did not lead to a drop in OFV of at least 3.84 points, it was dismissed from further analysis. All other covariates were put in a ranking order and carried forward to the next level, the forward inclusion process.

2.7.6.3.2 Forward inclusion

In the forward inclusion step the covariates were sequentially added to the model containing the covariate with the strongest influence. Inclusion was performed according to the ranking order of the significance level obtained from the univariate implementation step. All covariates that led to a decrease in OFV of at least 3.84 were retained in the model. All others were excluded from further analysis. The forward inclusion process was repeated until no further covariates assessed as statistically significant during the univariate testing remained. After finishing the forward inclusion process the 'Full Covariate Model' was obtained.

2.7.6.3.3 Backward elimination

In the backward elimination process each covariate contained in the full covariate model was individually removed. For the decision on whether or not to keep the covariate in the model a stricter significance level ($p<0.001$) was applied. If omitting one or more covariates led to an increase in OFV of less than 10.83, the covariate with the least OFV increase would be eliminated from the model and the procedure repeated. It would be carried on until the removal of any covariate resulted in a significant worsening of the model. A model thus obtained was called the 'Final Covariate Model'.

2.7.7   Model evaluation

2.7.7.1   Log-likelihood profiling

For all parameters estimated with a RSE larger than 50% a log-likelihood profiling was carried out to assess the 'true' confidence interval of the respective parameter. Standard errors reported by NONMEM^{TM} are estimates based on assuming symmetrical confidence intervals. In contrast, log-likelihood profiling does not assume symmetry around the respective estimate [239, 240]. In this approach, the parameter of interest was fixed to several values close to the final estimate. A log-likelihood profile was generated by refitting the other parameters of these nested models. The

resulting changes in the OFV were plotted as a function of the fixed parameter value. The fixed parameter values yielding an increase in OFV equal to 3.84 corresponded to the upper and lower limits of the 95% confidence interval. Log-likelihood profiling was performed for both final covariate models (i.e. model for unbound plasma concentrations and joint model for unbound plasma and ISF concentrations, respectively).

2.7.7.2 Bootstrap

The bootstrap is a technique that can be used to determine the bias and precision of a population PK model. It can be performed as either a parametric or nonparametric bootstrap. In the parametric approach, parameters are fixed to the final model estimates. Afterwards, a series of datasets of a size equal to the original dataset is simulated. In a subsequent step, the final model is fit to each of the simulated datasets. The most common approach, however, is the nonparametric bootstrap in which a series of datasets of equal size to the original dataset is generated by repeatedly sampling individuals from the original dataset. The generated datasets thus contain 'real' data. However, not every individual might be represented in these datasets whereas some might be represented more than once. A sampling procedure like this is called 'sampling with replacement' [241]. The final model was fit to each of the generated datasets. In the following the obtained PK parameters were examined for bias and precision. Bias and variance were calculated according to the following equations:

$$\text{Bias} = \theta_k - \frac{\sum_{i=1}^{B} \theta_{k_B}}{B} \tag{2.25}$$

$$\text{Variance} = \frac{\sum_{i=1}^{B} \left[\theta_{k_B} - \frac{\sum_{i=1}^{B} \theta_{k_B}}{B} \right]^2}{B-1} \tag{2.26}$$

where θ_k is the population parameter estimate of parameter k obtained from the estimation based on the original dataset, B is the number of bootstrap repetitions and θ_{k_B} is the population parameter estimate of parameter k and bootstrap run B. The square root of the variance yielded the estimate of the standard error of the respective parameter.

There is no general rule defining the size of B in order to obtain valid results. It is recommended to perform 50-100 bootstrap runs for the estimation of bias and at least 100 for the estimation of variance [223].

Bootstrap analysis was performed for both final covariate models (i.e. model for unbound plasma concentrations and joint model for unbound plasma and ISF concentrations, respectively). However, as run times were expected to be high and a hundredfold repetition therefore not feasible,

only 20 bootstrap runs were performed with either of the final covariate models. In consequence, only parameter bias was calculated as the number of bootstrap runs was not sufficient to calculate a valid variance.

2.7.7.3   Case deletion diagnostics

The robustness of the model was evaluated by case deletion procedures. Case deletion diagnostics were performed for either of the final covariate models (i.e. model for unbound plasma concentrations and joint model for unbound plasma and ISF concentrations, respectively). All 34 subjects were randomly allocated into 11 groups, each consisting of roughly 10% of the total number of subjects. By subsequently excluding subjects from 1 of 11 groups from the full dataset (i.e. each time 3-4 individuals) 11 new datasets were created. After fitting the final covariate model to each of the resulting datasets, the model parameters were compared with the estimates and the confidence intervals of the full dataset. In addition, each subject was individually removed from the full dataset, resulting in 34 more datasets. After fitting the final covariate model to each of these, the obtained model parameters were compared with the estimates and the confidence intervals of the full dataset. This analysis technique was used to evaluate whether selected subjects exerted a strong influence on the model. Hereby, it is accepted that exclusion of a small fraction of subjects at a time should not significantly influence the parameter estimates. Similarity of the parameter estimates obtained from the full data set to that obtained from each of the reduced analysis data subsets ensures that none of the subjects exhibit an immoderately strong influence on the population model [242].

2.7.7.4   Predictive check

One goal of a PK model is its predictive performance, especially if clinical decision-making will be based upon the model. Therefore, in an internal evaluation procedure 1000 new individual concentration-time profiles were simulated based on the parameter estimates from the final base model. The simulation was performed for intravenous dosing only. From all simulated concentrations the median and the 5% and 95% quantile were calculated for each time point. Based on these calculations the 90% prediction interval and the median concentration-time course separated by study visit were presented graphically. All measured unbound linezolid concentrations were then compared to the corresponding 90% prediction interval. The predictive check was performed for both the model describing unbound plasma concentrations as well as the joint model for unbound plasma and ISF concentrations. Moreover, the same procedure was performed for those models that had previously been reported in the literature (section 2.7.6.1). Their predictive performance was compared to the developed base model by visual inspection of the corresponding 90% prediction intervals.

2.7.7.5 Evaluation of tissue penetration

In order to determine if the same results for tissue penetration would be obtained based on a linear two-compartment model, tissue penetration parameters were estimated based on a two-compartment model with linear elimination in addition to the base model for the simultaneous description of unbound linezolid tissue and plasma concentrations. For this purpose, all parameters except those describing the distribution into ISF were fixed to values previously estimated by the linear model. The individual parameter estimates of both models describing the extent of ISF distribution were then compared.

2.7.8 Evaluation of covariate relations

In order to assess the influence of the covariates retained in the final covariate model after the backward elimination procedure on the unbound linezolid concentration-time profiles a simulation was performed using the parameter estimates of the final covariate model. For each covariate the 5th and 95th percentile values of the study population were used while all other covariates were assumed to take the median values. Subsequently, their influence on the concentration-time profiles was assessed. If a two-spline function was used and the node lay between the 5th and 95th percentile of the covariate range, this covariate value was used instead of one of the percentile values. In order to assess which patients would potentially be at risk of subinhibitory or toxic concentrations two 'worst-case scenarios' were simulated using the 5th and 95th percentile covariate values that in combination would yield the lowest and highest possible concentrations, respectively. Moreover, concentration-time profiles of all subjects studied in this clinical trial were simulated using the actual observed covariate value combinations.

2.7.9 Development of an optimised sampling strategy

As can be seen in section 2.7.2 the clinical study was performed using an intensive sampling schedule. However, in order to reduce the burden on the patient it would have been desirable to reduce the number of sampling points to the minimum needed for the estimation of population PK parameters. The accuracy of parameter estimates in mixed-effect models is highly dependent on the design of the experiment [243]. A poor experimental design can lead to unreliable or inaccurate estimates of model parameters [244]. Therefore, the software POPT® written in MATLAB® was used to retrospectively design an optimised sampling schedule for the developed population PK model (see section 2.8). POPT® calculates a D-optimal design based on the Fisher information matrix. The D-optimal design criterion aims at maximising the determinant of the Fisher information matrix. Because the inverse of the information matrix is the lower bound of the estimation variance matrix this approach is equivalent to minimising the determinant of the variance matrix [245]. In more general terms: the Fisher information 'measures' how much information is available about a parameter θ.

In the simplest case of a population design where all individuals receive an identical design and dosing regimen the minimum number of samples has to be at least equal to the number of fixed-effects parameters since in this case information cannot be borrowed between individuals [246]. If the design differs between individuals, less samples per individual are possible.

Thirty individuals, i.e. a group of similar size compared to the one studied in this thesis, with intravenous multiple linezolid administration were included for retrospective evaluation. A sequential approach was taken for optimisation. At first, optimised sampling was obtained for the model describing unbound linezolid plasma concentrations. In a second step, the joint model decribing microdialysis ISF and unbound plasma concentrations was implemented. The sampling times previously obtained for plasma concentrations were fixed. Moreover, POPT® only allows for the simultaneous optimisation of sampling time points from two different matrices. In consequence, the two investigated tissue matrices (subcutaneous and muscular ISF) were implemented separately, assuming that the residual error previously estimated for all three matrices would also be true for a combination of plasma and each single tissue matrix. The obtained optimised design was evaluated by simulating data from 30 individuals and re-estimating the PK parameters using NONMEM™. The obtained RSEs were used to assess whether all population PK parameters could be precisely estimated with the reduced design. For the joint model decribing microdialysis ISF and unbound plasma concentrations two residual errors and respective standard errors were obtained after simulation and re-estimation due to the separate optimisation processes. Therefore, the results section will report both values obtained for the two matrices.

2.8   Software

Non-compartmental pharmacokinetics was calculated using the software WinNonlin® Professional (Pharsight Corporation, Version 4.0, 2002). All population models presented in this thesis were obtained using the software NONMEM™ (Globomax, Version V, Level 1.1, 1998). Graphical analysis was carried out with WinNonlin® Professional or S-Plus® (Insightful Corporation, Version 6.0 Professional Release 2, 2001) in co-action with Xpose (Niclas Jonsson and Mats Karlsson, Version 3.104). All simulations were performed using NONMEM™, Berkeley Madonna™ (Robert I. Macey & George F. Oster, Version 8.0.1, 2000) and S-Plus®. Optimised design was obtained using MATLAB® (The MathWorks, Inc., Version 7.2.0.232) and POPT® (Stephen Duffull, Version 3.0).

Datasets including derived covariates for the NONMEM™ dataset were created by Microsoft® Excel (Microsoft Corporation, Version 9.0.6926 SP-3, 2000). Statistics were calculated using Microsoft® Excel, WinNonlin®, S-Plus® or SPSS® (SPSS Inc., Version 7.5.1, 1996).

3   Results

3.1   Project I: *In vitro* experiments

3.1.1   Vancomycin: Bioanalytics and *in vitro* microdialysis

3.1.1.1   High performance liquid chromatography

The bioanalytical method developed for the quantification of vancomycin consisted of a high performance liquid chromatography system with UV detection at 240 nm. Vancomycin was eluted with a retention time (t_R) of approximately 6.5 min.

3.1.1.2   Method validation

3.1.1.2.1 Specificity

In all vancomycin-free microdialysate and plasma samples measured, an interference with the signal of the analyte could not be observed (see figures 3.1 and 3.2). Furthermore, no interactions with vancomycin and matrix components were detected. Urapidil HCl ($t_R = 8.1$ min), diazepam ($t_R = 7.0$ min), etilefrine HCl ($t_R = 10.9$ min), isosorbide mononitrate ($t_R = 3.4$ min), pantoprazole ($t_R = 9.6$ min), clopidogrel hydrogen sulfate ($t_R = 11.8$ min), esomeprazole ($t_R = 9.8$ min), piperacillin sodium ($t_R = 9.2$ min), ciprofloxacin lactate ($t_R = 9.0$ min) and sulbactam sodium/ampicillin sodium ($t_R = 8.0$ min) were eluted without interfering with the signal of vancomycin. All other substances tested were not detectable due to e.g. the sample preparation procedure, low recovery or the particular wavelength required for vancomycin. In conclusion, none of the possibly co-administered drugs investigated showed any interference with the signal of vancomycin.
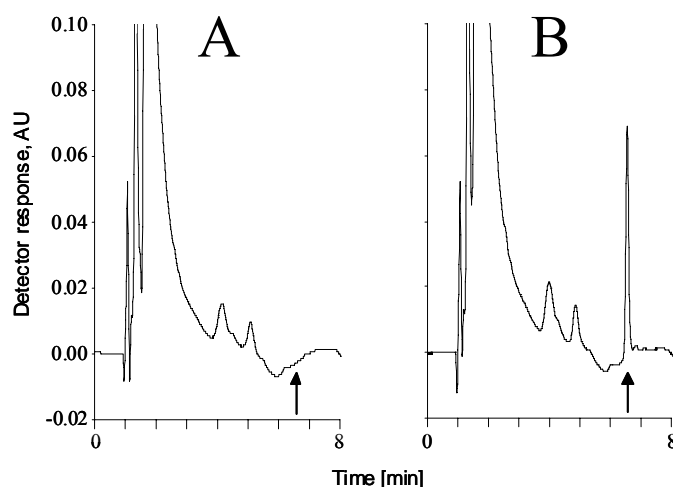

Figure 3.1: HPLC chromatograms of vancomycin in plasma. (A) Analyte-free plasma; (B) Plasma calibrator (33 µg/mL). Arrows indicate the signal of vancomycin (6.5 min).
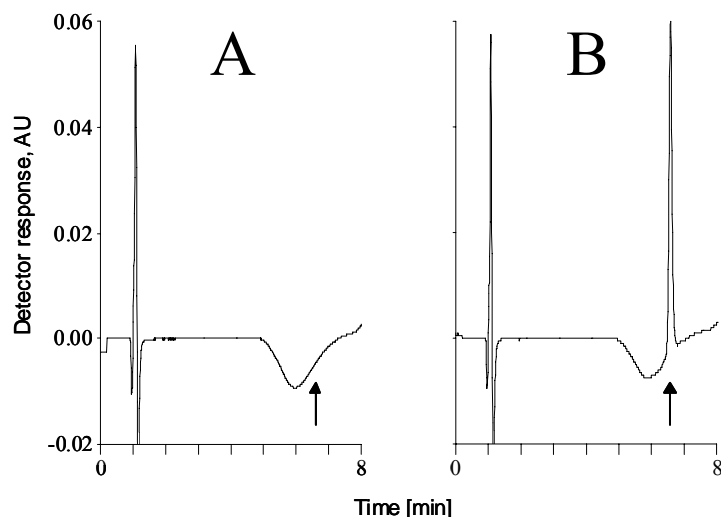
Figure 3.2: HPLC chromatograms of vancomycin in microdialysate. (A) Analyte-free microdialysate; (B) Microdialysate calibrator (33 µg/mL). Arrows indicate the signal of vancomycin (6.5 min).

3.1.1.2.2 Stability

The results of the microdialysate stability investigation of vancomycin are summarised in table 7.6. Plasma stability is displayed in table 7.7. Exposure of vancomycin in microdialysate to one to three freeze-thaw cycles revealed a drug recovery of 100.5% (1.7%) to 102.4% (1.4%) on average compared to stored and freshly prepared QC samples.

Vancomycin microdialysate samples were stable at room temperature for 4 h or 24 h. Mean vancomycin concentrations ranged from 98.7% (4.6%) to 106.1% (1.1%). In addition, an evaluation of vancomycin stability after sample preparation where one set of QC samples was frozen after preparation for at least 24 h and another set was stored in the sample tray of the autosampler for 24 h revealed no drug degradation. Average concentrations varied from 100.8% (3.6%) to 104.8% (0.7%). No tendency towards degradation or enrichment related to the various storage conditions could be detected. In addition, with the exception of the sample frozen after preparation (p=0.027) the statistical evaluation showed no statistically significant differences (p≥0.113) between the examined and freshly prepared samples. This one exception yielded a mean recovery of 104.1% (1.9%).

The storage of vancomycin in plasma under freeze-thaw conditions yielded mean recoveries between 81.6% (20.7%) and 108.1% (12.4%). One sample investigated after three freeze-thaw cycles yielded a recovery of only 69%. However, as all other recoveries were higher it was considered to be an outlier. Plasma samples left at room temperature for 4 h or 24 h contained average concentrations between 87.9% (9.0%) and 99.6% (8.8%). Post-preparative QC samples analysed after storage at ambient temperature for 27 h or in a freezer after processing showed mean results between 91.3% (5.9%) and 120.6% (3.2%). None of the observed differences were statistically significant (p≥0.148).

3.1.1.2.3 Accuracy and precision

The results for within- and between-day accuracy and precision are listed in tables 7.8 and 7.9. Overall, CV remained below 10.9% and RE data ranged between -9.1% and +5.6% for microdialysate samples. Plasma samples displayed a CV below 9.4% while RE ranged between -6.7% and +11.5% under all circumstances investigated. Thus, the investigation of accuracy and precision met the acceptance criteria for pre-study validation specified in the FDA guideline [234].

3.1.1.2.4 Linearity and determination of lower limit of quantification

The analytical assay was validated for concentrations of 0.400-80.0 µg/mL for both plasma and microdialysate. This range comprised almost all concentrations likely to be encountered during clinical treatment. A linear regression analysis was performed (peak area versus nominal vancomycin concentrations) to describe the relation between detector response and concentration using the reciprocals of squared concentrations as weighting factor [247]. Vancomycin displayed linearity in the attempted concentration ranges with correlation coefficients of 0.999 (CV≤0.036%, n=3) in both matrices investigated. A representative calibration function is shown in figure 7.2. The mean regression parameters of three calibration functions for each matrix are given in table 7.10.

The LLOQ was determined to be 0.400 µg/mL for both microdialysate and plasma. Concentrations of 5 back-calculated samples in this range resulted in a CV of 10.9% (RE -9.1%) and 6.7% (RE +11.5%) for microdialysate and plasma samples, respectively (see tables 7.8 and 7.9). In summary, the same LLOQ was achieved in microdialysate even though microdialysis samples contained very small sample volumes, i.e. 40 µL.

3.1.1.2.5 Recovery of the analyte

The recovery of spiked microdialysate samples was 98.3% (CV 15.4%, n=15) on average. The comparison between peak area data obtained from spiked plasma and aqueous solution produced a mean recovery of 86.7% (CV 8.1%, n=15).

3.1.1.3 *In vitro* microdialysis

3.1.1.3.1 Flow rate dependence

Figure 7.3 depicts the relation between the RR of vancomycin and the flow rate. In the delivery experiments, a flow rate reduction from 4.0 µL/min to 3.0 µL/min resulted in an increase in RR from 25.4% (CV 2.8%) to 37.2% (CV 3.7%); a further reduction to a flow rate of 2.0 µL/min increased the RR to 50.3% (CV 3.0%). A decrease in the flow rate to 1.0 µL/min yielded a RR of 73.3% (CV 1.2%). The relation between the flow rate and the RR can be described by the following equation:

$$RR = 1 - e^{-1.336/F} \tag{3.1}$$

with F = flow rate. However, lower flow rates require a longer sampling interval for sufficient sample volume (40 min vs. 10 min for 1 µL/min and 4 µL/min, respectively). Thus, in order to comprehensively characterise the PK profile while retaining adequate recovery, a flow rate of 4.0 µL/min was chosen for all following *in vitro* recovery experiments.

3.1.1.3.2 Concentration dependence

A concentration change of the medium perfusing the probe affected the RR. In delivery experiments the RR changed from 25.8% (CV 12.1%) for a vancomycin solution of 1 µg/mL in Ringer's solution to 35.9% (CV 5.7%) for a concentration of 80 µg/mL (figure 7.4). Statistical evaluation between the RR and the concentration of the surrounding or perfusing medium yielded a regression line with a slope of 0.11%·mL/µg (standard error [SE] 0.025%·mL/µg) and an intercept of 27.8% (SE 1.136%). As the 95% confidence interval of the slope did not include zero the line did not run parallel to the x-axis. In order to assess if this concentration dependence could be observed at lower flow rates the same experimental setup as in a study conducted by Luer et al. [248] was used under *in vitro* conditions using a flow rate of 1.7 µL/min and Ringer's solution as perfusate. In this setting a perfusate concentration change from 1.00 µg/mL to 80.0 µg/mL led to RR changes of more than 30% (figure 7.5).

Based on these findings all recovery experiments were repeated under the same experimental conditions. However, as it was observed that a concentration change resulted in a change of pH value and that this pH value might be responsible for changes in RR (figure 7.6), physiological conditions were simulated. The pH value was kept at a constant value of 7.4 by means of using 50 mM potassium phosphate buffer instead of Ringer's solution. This resulted in a constant RR value of 27.8% (CV 11.1%) for retrodialysis experiments. Results of the recovery experiments were comparable with a mean RR of 33.2% (CV 8.3%) (figure 7.7). Linear regression between the RR, achieved in the delivery and recovery experiments, and the concentration of the surrounding or perfusing medium yielded a regression line with a slope of 0.023%·mL/µg (SE 0.020%·mL/µg) and an intercept of 28.6% (SE 0.914%). The line was assumed to run parallel to the x-axis because the 95% confidence interval of the slope included zero.

3.1.2   Linezolid: Bioanalytics

3.1.2.1   Bone marrow sample preparation

The results of the recovery experiments of linezolid in bone marrow are displayed in table 7.11. Mean RR of all concentrations was 112%. The exclusion of the lowest concentration of 0.200 µg/mL reduced this RR value to 107%. A linear regression of nominal bone marrow concentrations vs. peak area leaving out the concentration 0.200 µg/mL resulted in a correlation coefficient of 0.999 and acceptable relative errors as specified in the FDA guideline [234]. It was

concluded that plasma calibration samples could be used for the measurement of linezolid bone marrow concentrations but that the concentration range would be reduced to 0.500 – 20.0 µg/mL.

3.1.2.2   Bone sample preparation

The bone biopsy recovery experiments investigated a linezolid concentration range of 0.395-2.05 µg/mL. The results of the recovery experiments are displayed in table 7.11. Mean RR was 105.5% and a linear regression of the bone sample concentrations vs. peak area yielded a correlation coefficient of 0.991 and relative errors in accordance with the FDA guideline [234]. Bone biopsy concentrations could therefore be correctly determined using plasma calibration samples.

3.2   Project II: Linezolid pharmacokinetics in bone tissue

3.2.1   Dataset

The PK evaluation was based on a dataset containing linezolid concentration data from 10 sows (Danish Landrace Breed, weight range 38-43 kg). The dataset contained 605 linezolid concentrations. Of these concentrations 164 (27.1%) were obtained from plasma and 124 (20.5%) from bone marrow measurements. Moreover, 128 (21.2%) and 129 (21.3%) concentrations were available from the medial and lateral microdialysis catheter, respectively. The dataset contained 60 (9.92%) concentrations from bone biopsy samples.

3.2.2   Concentration-time profiles of linezolid

The data included in the dataset was collected over a time period of 6 h after intravenous linezolid infusion. Figure 7.8 shows all measured concentrations against time as well as the median concentration-time profiles grouped by matrix. A linezolid dose of 600 mg given over 30 min resulted in observed individual plasma and bone marrow concentrations of up to 39.2 µg/mL in both matrices. Overall, the median profiles in these two specimens closely resembled each other. Only C_{max} values in bone marrow significantly differed (paired t-test, p=0.024) to those in plasma. Median concentrations and variability in bone measured by microdialysis were very similar when comparing the data from the lateral and medial catheter. In contrast, the bone concentration-time course obtained from bone biopsies differed from those in microdialysate by showing a shallower slope in the terminal phase. Variability in bone biopsy as well as in microdialysis concentrations was higher when compared to concentration values in plasma and bone marrow.

3.2.3   Pharmacokinetic analysis

The geometric mean parameters and their coefficients of variation obtained in the non-compartmental analysis are summarised in table 7.12.

3.2.3.1   Plasma

In plasma, linezolid reached a geometric mean C_{max} of 26.1 µg/mL. T_{max} was directly extracted from the concentration-time profiles and was 0.5 h (R: 0.5-0.75). Six hours after infusion the geometric mean concentration (C_{6h}) had declined to 9.7 µg/mL. CL was calculated to be 2.9 L/h and V was estimated to be 37.9 L, corresponding to a $t_{1/2}$ of 9.2 h. The AUC_{0-6h} was 75.7 µg·h/mL. T_{max} obtained in this analysis was in close agreement with the literature while $t_{1/2}$ was slightly longer [79].

3.2.3.2   Bone marrow

C_{max} of linezolid in bone marrow was 21.9 µg/mL. It was reached at 0.5 h, i.e. at the end of the linezolid infusion. After 6 h the linezolid concentration in bone marrow decreased to 9.4 µg/mL. CL was calculated to be 3.1 L/h and V was estimated to be 38.1 L, corresponding to a $t_{1/2}$ of 8.3 h. The AUC_{0-6h} was calculated to be 72.8 µg·h/mL, resulting in a PF of 0.96 (R: 0.91-1.13).

In an analysis of variance (ANOVA) the PK parameters were compared to those obtained from plasma data. The investigated parameters did not show any statistically significant difference (p≥0.9995). In total, the penetration into bone marrow could be regarded as virtually complete. Moreover, it occurred as fast as in plasma, i.e. both matrices displayed similar kinetics.

3.2.3.3   Bone biopsy

On average, in bone biopsy samples t_{max} was reached 0.5-1 h later than in plasma with a C_{max} of 12.5 µg/g. Six hours later the linezolid concentration in bone had decreased to 8.8 µg/g. CL was calculated to be 3.5 L/h and V was estimated to be 48.1 L, corresponding to a $t_{1/2}$ similar to plasma and bone marrow (8.8 h). The calculated AUC_{0-6h} amounted to 53.1 µg·h/g.

In order to enable a comparison of bone biopsy results to other matrices the bone density was determined by means of water displacement where 1 gram of cancellous bone tissue corresponded to 0.57 mL. Taking the density into account, the geometric means of C_{max}, C_{6h} and AUC_{0-6h} were 21.9 µg/mL, 15.4 µg/mL and 92.9 µg·h/mL, respectively. In an ANOVA the PK parameters were compared to those obtained from plasma and bone marrow data. The investigated parameters did not show any statistically significant differences (0.147≤p≥0.9995). However, these results should be regarded with caution because of the large variability in concentrations among the animals which can also be seen in the concentration-time profiles in figure 7.8. The geometric mean PF that was calculated to be 1.23 (R: 0.79-2.53) supported the hypothesis that in general PK in bone differed from that in plasma.

3.2.3.4   Bone microdialysate

Bone microdialysate was obtained from two locations, the lateral catheter (lc) and the medial catheter (mc). The median *in vivo* RR of mc and lc for all animals was 34.1% (R: 22.3-97.4%,

n=10) and 37.8% (R: 14.4-90.2%, n=10), respectively. The large inter-probe variability supports the procedure of calibrating each microdialysate probe separately. At both locations the maximum concentration was reached after a time period of 1.0 h with values of 11.8 µg/mL and 13.2 µg/mL for the lateral and medial catheter, respectively. After six hours the concentrations had decreased to 6.1 µg/mL (lc) and 6.6 µg/mL (mc) with a calculated CL of 5.5 L/h and 4.8 L/h for the lateral and medial catheter, respectively. The two sampling sites showed a V of 61.0 L (lc) and 57.1 L (mc). Compared to plasma, bone marrow and bone biopsy samples these parameters resulted in slightly shorter half-lives of 7.9 h (lc) and 7.1 h (mc). The AUC_{0-6h} was calculated to be 42.5 µg·h/mL and 45.8 µg·h/mL. An ANOVA comparison between the two sampling sites did not show any statistically significant differences in any PK parameter ($p \geq 0.515$). However, a high interindividual variability was observed within one location.

When comparing the AUC from the lateral catheter to that obtained in plasma, a statistically significant difference was identified ($p=0.048$). A statistical comparison between the medial catheter and plasma yielded a p-value of 0.123. Thus, a statistically significant difference could not be ascertained. In addition, C_{max} values between bone microdialysates and plasma displayed a statistically significant difference ($p=0.003$, lc and $p=0.008$, mc). This difference was expected as the equilibration process between plasma and bone ISF may have taken some time. Thus, similar concentrations could only be assumed after the initial distribution phase.

Most other PK parameters did not show any statistically significant difference ($p \geq 0.101$) when compared to the corresponding parameters from other matrices. One exception was the comparison of AUC values from bone microdialysate to that of bone biopsy samples ($p<0.0005$, lc and $p=0.001$, mc).

The geometric mean PF was calculated to be 0.56 (R: 0.23-1.51) and 0.61 (R: 0.34-1.95) for lc and mc, respectively. Thus, when examining unbound concentrations in bone ISF by applying the microdialysis technique one could observe that on average ISF penetration was not complete. Applying a paired t-test no statistically significant difference between the two tissue penetration factors could be identified ($p=0.690$).

3.3 Project III: Target site pharmacokinetics of linezolid during sepsis

3.3.1 Data observations

The population PK analysis was based on data from 10 healthy volunteers and 24 patients. Three datasets were generated for the model development process. The first one only included unbound plasma concentrations from healthy volunteers after single intravenous dosing (preliminary dataset). The second one contained unbound concentration data from plasma measurements of all investigated subjects (dataset A), while the last one consisted of unbound concentrations from both plasma and microdialysate of all individuals (dataset B). As the concentration profiles of one

healthy volunteer which had been obtained after oral multiple dosing differed completely from all other profiles and the primary objective of the analysis was not to describe differing absorption profiles after oral dosing, the corresponding 20 plasma as well as 40 microdialysis observations were excluded from the analysis. In addition, 8 observation records were not incorporated into the datasets (6 plasma and 2 microdialysis observation records) as for those the exact sampling time point was not documented. Thus, 1176 and 3501 observation records were included into dataset A and B, respectively. The distribution of observations for healthy volunteers and patients for the different matrices and administration routes is summarised in table 7.13. The number of samples was equally distributed over all investigated matrices. Overall, only a small amount of samples was obtained after oral dosing. Therefore, parameters that describe absorption processes from the gastrointestinal tract were not expected to be easily and precisely assessable and were thus not primarily focused on.

All 34 individuals were studied after single dosing. Multiple dose data could be investigated in 9 healthy volunteers (90%), 7 septic patients (88%) and 12 patients with septic shock (75%), adding up to a total of 82%.

3.3.2   Population characteristics

The demographics of the studied population are summarised in table 7.14. The population had a median age of 62 years. Healthy volunteers were younger than the patients. All groups had a similar median height of 170 cm. Median body weight (WT) of the total population was 67 kg. The WT of healthy volunteers and septic patients was comparable while the WT of patients with septic shock substantially exceeded that of the other groups.

Covariate histograms including reference ranges are shown in figure 7.9. Most of the covariates were not normally distributed. Laboratory parameters were anticipated to differ between healthy volunteers and patients, thus influencing the shape of the distribution. In addition, in a patient collective of septic patients outliers are likely to be encountered in extreme pathological conditions. The median thrombocyte (THRO) value of the population was 201 nL^{-1}. THRO values of healthy volunteers and septic patients were comparable whereas those of patients with septic shock were significantly reduced. 11 patients had initial THRO values below the reference range. CLCR varied noticeably with values ranging from 16.5 – 200 mL/min. The high value of 200 mL/min is a result of one patient having a combination of high body weight and height and a low serum creatinine value. The majority of 24 subjects (70%) suffered from no or only mild renal impairment, while 10 subjects (30%) were moderately or severely impaired in their renal function (table 7.15).

Missing values were imputed as described in section 2.6.4. However, after the PK analysis the covariate relations that remained in the model were not based on any individual value imputations but instead for these individual information was not missing. As the imputations were therefore not of any relevance to the final model they will not be commented on any further.

3.3.3   Calibration of microdialysis catheters after multiple dosing

Geometric mean s.c. ISF concentrations 8 hours after linezolid administration on study visit 2 were 6.33 µg/mL and 4.54 µg/mL for healthy volunteers and patients, respectively. The corresponding i.m. ISF concentrations were 6.90 µg/mL and 4.42 µg/mL. In consequence, perfusate concentrations used for multiple dose calibration exceeded ISF concentrations by more than tenfold. In one patient, ISF concentrations after 8 hours were determined to be 30 µg/mL. Thus, in this patient the perfusate concentration was only the fivefold of the ISF concentration, which might have led to a slight overestimation of ISF concentrations. However, it can be concluded that perfusate concentrations were generally sufficient for calibration procedures on study visit 2.

3.3.4   Concentration-time profiles of linezolid

The semilogarithmic concentration-time scatterplots of healthy volunteers and patients after single and multiple dosing separated by administration route and matrix are presented in figures 7.10 and 7.11. Moreover, geometric mean ultrafiltrate concentration-time profiles of healthy volunteers and patients after intravenous single and multiple dosing are shown in figure 7.12 and 7.13. After intravenous dosing, two disposition phases, i.e. two slopes could be observed that presumably belonged to a predominant early distribution and a later predominant elimination phase. In contrast, after oral dosing the early distribution phase did not become apparent (figure 7.10). Furthermore, figure 7.12 and 7.13 revealed a change in the disposition of linezolid, i.e. the slope of the elimination phase became more shallow over time, indicating nonlinearity in the PK of linezolid. The same phenomenon, although not as explicit, was also met in the other matrices studied.

The concentration range in patients was much wider than that observed in healthy volunteers, also indicating a wider range in distribution and/or elimination PK parameters.

3.3.5   Population pharmacokinetic model for unbound linezolid in plasma

The development process of the population PK model for linezolid was performed in a sequential approach. At first, a model for unbound plasma concentrations was developed.

3.3.5.1   Structural and pharmacostatistical model

3.3.5.1.1 Model development

By analysing the preliminary dataset (i.e. concentration data from healthy volunteers obtained after single dosing) it could be confirmed that a two-compartment model should be the basis for all further model building activities. This preliminary structural model consisted of a linear CL, a central (V2) and peripheral (V3) volume of distribution and an intercompartmental clearance (Q). CL was estimated to be 7.7 L/h, and V was 49.4 L in total. IIV was implemented on CL (ωCL) and both volumes of distributions (ωV2, ωV3). The parameters showed a moderate IIV with values ranging between 31 and 36% CV. The additive error, which was used to describe the residual error,

was estimated to be 0.432 mg/L. Overall, parameters were estimated precisely with only $\omega V3$ having a standard error larger than 50%.

After finishing the preliminary analyses a two-compartment model with first-order absorption and linear elimination was fitted to dataset A (model DSA1). IIV was included for V2 and V3, CL and the absorption rate-constant (ωKA). Residual variability was described by a combined random-effects model. The model consisted of a linear CL estimated to be 6.85 L/h and V was 67.7 L. KA was estimated to have a value of 1.93 h^{-1}. In addition, a lag-time was incorporated into the model. However, as oral data was only available from 9 healthy volunteers it was not possible to estimate the lag-time for all individuals simultaneously. Therefore, three individuals were selected after visual inspection of concentration-time data. Only for these individuals a lag-time was estimated, yielding a value of 1.55 h. Initial bioavailability estimation yielded a value of 100% which is in close agreement with literature values [81]. Therefore, it was fixed to 100% in all further analyses.

IIV was moderate to high with values of 54% CV (ωCL), 26% CV ($\omega V2$), 108% CV ($\omega V3$) and 62% CV (ωKA). The proportional residual error had a moderate value of 17% while the additive error component was negligible and fixed to 0.01 µg/mL for reasons of model stability.

Goodness of fit plots for model DSA1 are shown in figure 7.14. Inspection of the plot showing population predictions against observed concentrations revealed some degree of model misspecification. Some of the observed low values were overestimated by the model. This became even more apparent in the plot of logarithm of time against weighted residuals which showed an explicit trend in the early time phase. Values of the elimination phase after single dosing were overestimated, which further supported the assumption that nonlinearity in linezolid PK was involved, changing its disposition in the course of therapy. As nonlinearity in CL had already been reported in the literature [100] and the authors suggested the use of a model with parallel linear and Michaelis Menten elimination this approach was implemented during the next step (model DSA2). The parameters to be estimated were the same as in the linear model. In addition, a maximum elimination rate V_{max} and the Michaelis Menten constant K_m were estimated. IIV was included for V2 and V3, CL, V_{max} (ωV_{max}), Q (ωQ) and KA. Residual variability was described by a combined additive and proportional random-effects model. Model DSA2 consisted of a linear CL estimated with a value of 2.72 L/h and a total V of 67.0 L. KA was estimated with a value of 1.90 h^{-1} and the lag-time, which was only included for three individuals, had a value of 1.26 h. V_{max} and K_m were estimated to be 26.6 mg/h and 0.10 mg/L, respectively.

IIV was moderate to high with values of 98% CV (ωCL), 74% CV (ωQ), 41% CV (ωV_{max}), 32% CV ($\omega V2$), 63% CV ($\omega V3$) and 87% CV (ωKA). The proportional residual error was low with a value of 10%. The additive error component was estimated to be 0.33 µg/mL, which corresponded to approximately twice the lower limit of quantification.

Goodness of fit plots for model DSA2 are shown in figure 7.15. The trend that was visible in the model with linear elimination was less pronounced, however it was still distinguishable. Although the model had a good individual fit, low concentrations at the start of linezolid treatment were overerstimated. This observation led to the conclusion that the change in CL was not only an effect of concentration differences but only took place after a certain time of linezolid treatment. This conclusion was also supported by individual concentration-time data. In 26.5% of all subjects a similar C_{max} could be observed after single and multiple dosing despite the change in CL. One concentration-time profile of such an individual is shown in figure 7.16. This observation invalidated the Michaelis Menten model theory which solely depends on concentration differences.

In a subsequent approach the nonlinearity was implemented into the model as a function of time (model DSA3). This model contained two linear elimination pathways. One of these was allowed to be inhibited depending on the concentration in an imaginary additional compartment. In this model the additional compartment was coded in the same way as an effect compartment. In consequence, while concentrations in the central compartment instantly rose as soon as a dose was given, the effect compartment only approached concentrations similar to those in the central compartment over time. The nonlinear effect was therefore delayed. Application of this modelling approach resulted in better fit as can be seen in figure 7.17. The noninhibitable and inhibitable CL values were estimated to be 6.11 L/h and 2.07 L/h, respectively. The rate-constant into the effect compartment (KIC) and the concentration in the effect compartment yielding 50% of CL inhibition (IC50) were estimated to be 0.0038 h^{-1} and 0.139 µg/mL. This resulted in a reduction of the inhibitable CL fraction to values of 1 L/h, 0.75 L/h, 0.5 L/h and 0.25 L/h after 4.7 h, 11.5 h, 18.0 h and 43.0 h, respectively. Examining the logarithm of time vs weighted residuals plot the trend of overestimation, which could be observed in the linear and Michaelis Menten model, was eliminated. Model misspecifications were therefore reduced. However, the plot showing population predictions against observed concentrations revealed that in general model DSA3 overestimated the observed concentrations as the predictions were not uniformly spread around the line of unity. A second disadvantage of this model was its instability, which presumably resulted from the two implemented CL pathways (one linear and one nonlinear).

Therefore, in the next step only one CL was estimated by applying the following code:

$$INH = VAR + (1 - VAR) \times e^{-KINH \times T} \tag{3.2}$$

where T was the time elapsed since the first dose and VAR was the part of the CL that could not be inhibited (model DSA4). KINH corresponded to the inhibition rate-constant that expressed the rate of change in CL. The term INH was then multiplied with the elimination rate-constant, which resulted in decreasing clearance values over time. VAR was restricted in a way so that for each individual it could only take values between 0 and 1 (see equation 2.7, section 2.4.3.2.1).

The implementation of model DSA4 led to an estimated CL of 10.2 L/h, which represented the maximum possible population value. This value represented the clearance which was only applicable for the first dose of linezolid when inhibition was negligible. Furthermore, estimation led to a V2 and V3 of 20.6 L and 29.3 L, respectively, and a Q of 73.3 L/h. KA was estimated with a value of 1.79 h^{-1} while the lag-time for three selected individuals was fixed to a value of 1.23 h. The estimate for VAR was 0.873. Thus, 87.3% of CL could not be inhibited while 12.7% were inhibitable. KINH was estimated to have a value of 0.055 h^{-1}.

In general, IIV was moderate to high with values of 44% CV (ωCL), 38% CV (ωV2), 34% CV (ωV3) and 75% CV (ωKA). The IIV on VAR (ωVAR) calculated according to equation 2.8 was 38% CV. The proportional residual error was low with a value of 9%. The additive error component was estimated to be 0.29 µg/mL, which was slightly above the lower limit of quantification of the analytical assay.

Examining the logarithm of time vs weighted residuals plot of model DSA4 (figure 7.18) the trend of overestimation, which could be observed in the linear and Michaelis Menten model, was again not observable. Furthermore, in the plot showing population predictions against observed concentrations all concentrations were uniformly spread around the line of unity, indicating that the data was well described by the model.

In a final step, a more mechanistic approach was taken. In the term INH the time dependence was replaced by implementation of a dependence on the concentration in an inhibition compartment (model DSA5), this way re-introducing a term similar to the one used in the Michaelis Menten model. The full code is provided in the appendix (NONMEM code 7.1). The goodness of fit for model DSA5 (see figure 3.3) was essentially the same as in the time-dependent model. As the model was more mechanistic and closer to physiology, it was chosen as the base model and will be described in section 3.3.5.1.2.

3.3.5.1.2 Base model

The unbound linezolid plasma concentrations were best described by a two-compartment model with first-order absorption. An additional inhibition compartment was implemented. Depending on the concentration in this empirical compartment CL was inhibited and was in course of time allowed to take values between 0 and 100% of the original value estimated for the time of the first linezolid administration. A schematic illustration of model DSA5 is presented in figure 3.4 while the simulated concentration-time course in the inhibition compartment is presented in figure 7.19.

The following fixed-effects parameters were included into the model: CL, V2, Q, V3, KA, VAR (fraction of CL which cannot be inhibited), KIC and IC50. ALAG1 (absorption lag-time after oral dosing) was included for three selected individuals.

IIV was incorporated for CL, V2 and V3, KA and VAR. In addition, the correlation between CL
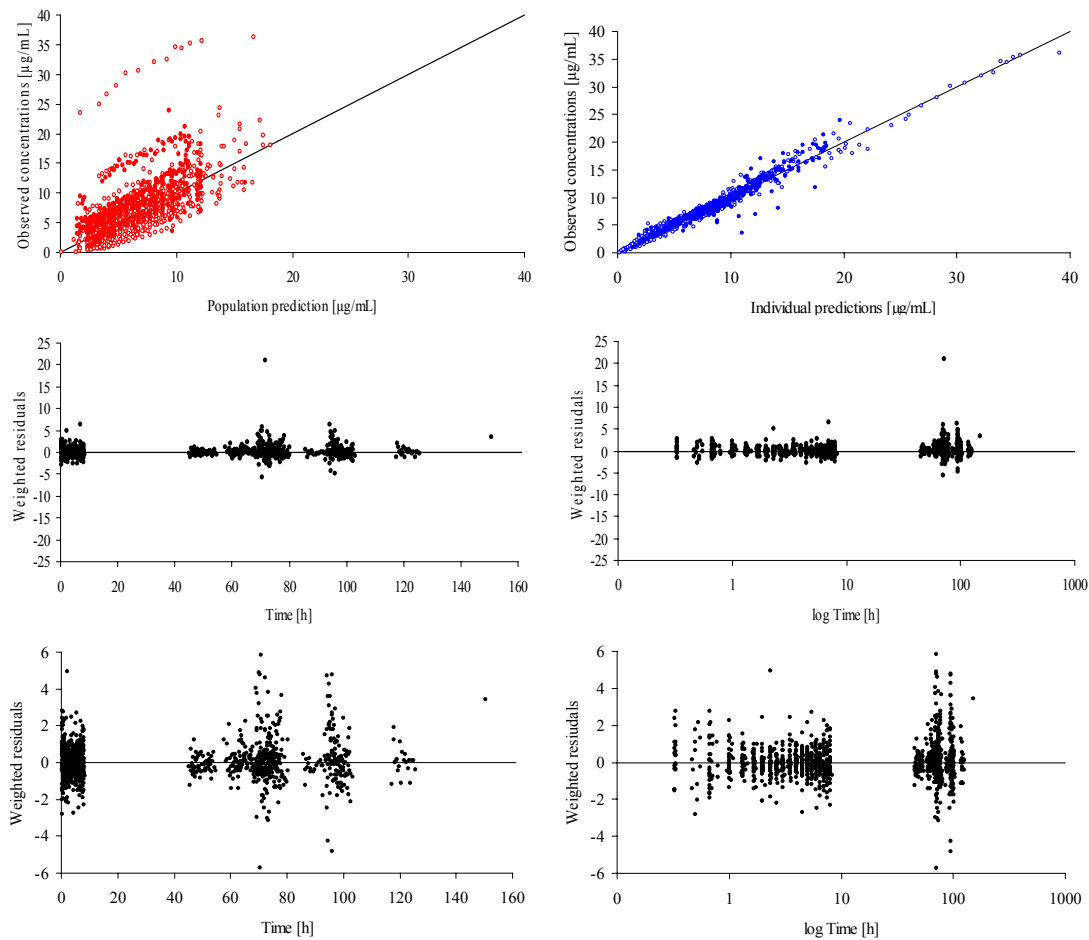
Figure 3.3: Goodness of fit plots for unbound plasma data; clearance was inhibited based on the concentration in an inhibition compartment; upper panel: filled circles: healthy volunteers, empty circles: patients. The lower panel represents an enlarged section of weighted residuals against time or logarithm of time.

and V3 (Corr_CL/V3) as well as V2 and VAR (Corr_V2/VAR) was estimated. Residual variability was described by a combined additive and proportional random-effects model.

In general, IIV was moderate to high with values of 42% CV (ωCL), 40% CV (ωV2), 35% CV (ωV3) and 72% CV (ωKA). ωVAR calculated according to equation 2.8 was 81% CV. This corresponded to a 95% confidence interval of 0.00374-0.99963. The proportional residual error was low with a value of 9%. The additive error component was estimated to be 0.29 µg/mL, which
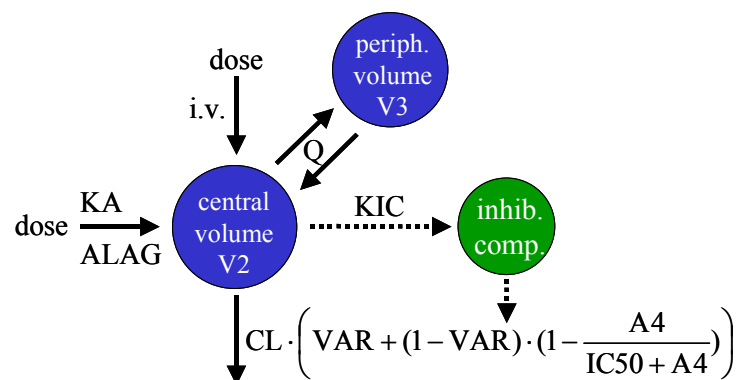

Figure 3.4: Final structure of the population pharmacokinetic model for unbound plasma concentrations. A4 corresponds to the concentration in the inhibition compartment.

Table 3.1: Parameter estimates of the base and final model for unbound plasma concentrations.

Model parameter		Base model		Final model	
		Estimate	RSE[#] %	Estimate	RSE[#] %
CL	[L/h]	11.1	7.84	11.5	8.78
V2	[L]	20.0	8.15	19.8	8.38
Q	[L/h]	75.0	8.55	76.8	8.16
V3	[L]	28.9	7.99	27.0	6.26
KA	[1/h]	1.81	25.9	1.85	27.9
ALAG	[h]	1.27 FIX	-	1.27 FIX	-
VAR		0.764	14.3	0.567	19.9
KIC	[1/h]	0.0019	5.19	0.0027	12.6
IC50	[mg/L]	0.1 FIX	-	0.1 FIX	-
Covariate influence, %					
θ_{CLCR_CL}[§]		n.a.	-	0.911	12.0
θ_{WT_CL}[§]		n.a.	-	1.13	62.7
θ_{THRO_CL}[§]		n.a.	-	0.229	47.0
θ_{WT_V3}		n.a.	-	1.52	16.6
Interindividual variability					
ωCL	[CV%]	41.7	22.2[*]	49.8	40.7[*]
ωV2	[CV%]	40.1	22.3[*]	37.1	25.1[*]
ωV3	[CV%]	34.8	31.0[*]	20.5	46.2[*]
ωKA	[CV%]	72.4	57.1[*]	78.9	59.0[*]
ω^2VAR		11.8	52.5	6.36	43.7
Corr_CL/V3		0.383	49.5[$]	n.a.	-
Corr_V2/VAR		0.384	62.2[$]	0.573	38.7[$]
Residual Variability					
σ proportional	[CV%]	8.96	9.50	9.59	7.60
σ additive	[mg/L]	0.292	31.8	0.042	74.3

[#] = relative standard error, [§] = percent change with regard to the population parameter estimate, [*] = Standard error given on the variance scale; [$] = Standard error of the covariance estimate; n.a. = not applicable;

was slightly above the lower limit of quantification.

Parameter estimates of the final base model are presented on the left of table 3.1. All fixed-effects parameters as well as residual variability were estimated with good precision (RSE <32%). Precision for IIV was lower. ωKA, ωVAR and Corr_V2/VAR were estimated with RSE values higher than 50%. The goodness of fit plots are shown in figure 3.3. All concentrations were spread uniformly around the line of unity, indicating that the data was well described by the model.

3.3.5.2   Covariate model

3.3.5.2.1 Model development

The covariate analysis was performed according to the procedure described within section 2.7.6.3. The covariates that were selected by the GAM analysis and all other covariates that were tested for

reasons of plausibility after inspection of the scatterplots are listed in table 7.16. After inspection of the scatterplots it was realised that no covariate seemed plausible for ωVAR. However, as VAR was directly related to the parameter CL, it was expected that a covariate affecting ωCL might possibly influence ωVAR as well. ωKA was not considered in the covariate analysis as no covariate-parameter relation seemed reasonable after graphical inspection. This might be due to the limited number of individuals who contributed data after oral dosing (9 out of 34).

During the forward inclusion process the correlation between CL and V3, which had been included in the base model, was found to be unnecessary as its inclusion only led to an OFV drop of 1. Therefore, it was deleted from the model. The full code for the covariate model is provided in the appendix (NONMEM code 7.2).

3.3.5.2.2 Final covariate model

After performing the forward inclusion and the backward elimination procedure the number of covariates having a significant effect on the OFV was noticeably reduced. Covariate analysis identified a significant influence of CLCR, WT and THRO on CL using the following expression:

$$CL = \theta_{CL} \cdot \begin{pmatrix} 1 + \theta_{CLCR\_CL} \cdot (CLCR - 65) + \theta_{WT\_CL} \cdot (WT - 67) \\ + \theta_{THRO\_CL} \cdot (THRO - 220) \end{pmatrix} \cdot e^{\eta_{CL}} \qquad (3.3)$$

According to this relation and using the 5th and 95th CLCR percentiles of the study population while using the median of all the other relations, CL values changed from 6.6 to 15.1 L/h as CLCR increased from 18.4 to 99.0 mL/min. Moreover, compared to individuals with median CLCR values, CL was reduced by 31.9% in individuals with severe renal impairment (CLCR = 30 mL/min). For WT, the typical CL increased from 8.7 to 17.8 L/h as WT increased from 45.1 to 115.3 kg, corresponding to a change of -24.3 and 54.8% compared to the population parameter estimate. Thrombocyte changes from 81.2 to 439.5 nL^{-1} caused a change in typical CL from 7.8 to 17.3 L/h, a change of -32.2 and 50.4% compared to the population parameter estimate.

A significant influence on V3 could be identified for WT. The mathematical expression for this relation was as follows:

$$V3 = \theta_{V3} \cdot \left(1 + \theta_{WT\_V3} \cdot (WT - 67)\right) \cdot e^{\eta_{V3}} \qquad (3.4)$$

According to this relation and using the 5th and 95th WT percentiles of the study population V3 changed from 18.0 to 46.8 L as WT increased from 45.1 to 115.3 kg, a change of -33.3 and 73.3% compared to the population parameter estimate, respectively.

The final parameter estimates including the covariates are summarised on the right in table 3.1. Overall, estimated fixed-effects parameters did not change much. The only obvious change took place in the value for VAR, which changed from 0.764 to 0.567, meaning that for a typical individual the CL could now be inhibited to 56.7% of the original value instead of 76.4%. Moreover, the rate into the inhibition compartment (KIC) changed noticeably to a value of

0.0027 h^{-1}. Therefore, the typical change of CL occured faster compared to the base model. This result might be due to the close relation of KIC to the parameter CL. Some of the changes in CL would already have been accounted for by the found covariate relations, as these changed over time, which in turn led to an altered KIC estimate in the final covariate model.

IIV was moderate to high with values of 50% CV (ωCL), 37% CV (ωV2), 20% CV (ωV3), 109% CV (ωVAR) and 79% CV (ωKA). Compared to the base model ωCL increased slightly by 19.4% (i.e. 8.1 percent points). The variability was reduced by 7.5% (i.e. −3.0 percent points) for ωV2 and 41.1% (i.e. -14.3 percent points) for ωV3. ωKA slightly increased by 9.0% (i.e. 6.5 percent points). Moreover, ωVAR seemed to have increased by 34.8% (i.e. 28.0 percent points). However, it has to be kept in mind that VAR, due to the restricting code, is not normally distributed but takes a U-shape (figure 7.20). When variability is high one should therefore not evaluate it in terms of coefficients of variation but rather by the corresponding 95% confidence intervals. This included values between 0.00955 and 0.99466. Thus, ωVAR was reduced by inclusion of the covariate influences. The proportional residual error was low with a value of 10%.

The additive error component was estimated to be 0.04 μg/mL, which was below the lower limit of quantification and therefore negligible. Most parameters were estimated with good precision (RSE between 6.3 and 47%). Merely θ_{WT_CL} and ωKA were estimated less precisely with standard errors of 62.7 and 59.0%, respectively. The goodness of fit plots for the final covariate model are presented in figure 3.5. All concentrations were uniformly spread around and, compared to the base model, closer to the line of unity. Especially the concentrations of one individual that had concentrations higher than 25 μg/mL were much better described by the final covariate model. This indicated a good model choice.
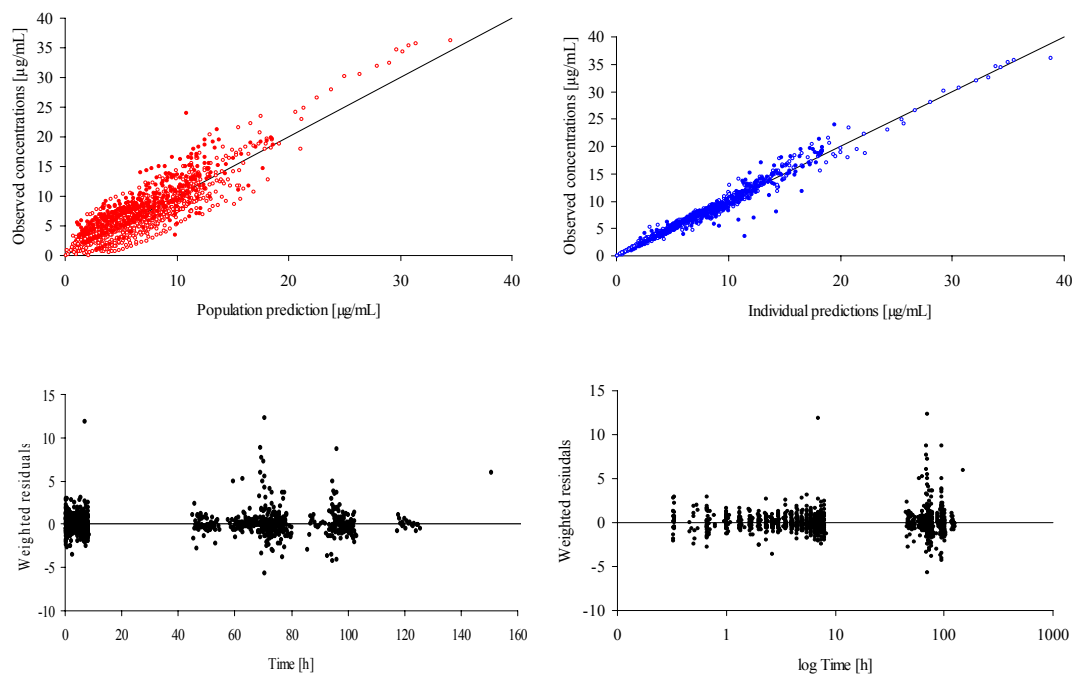

Figure 3.5: Goodness of fit plots of the final plasma covariate model; upper panel: filled circles: healthy volunteers, empty circles: patients.

3.3.5.3 Model evaluation

3.3.5.3.1 Log-likelihood profiling

Two parameters, namely ωKA and θ_{WT_CL}, were estimated with a RSE larger than 50%. For these parameters a log-likelihood profiling was performed. ωKA was coded as a fixed-effects parameter, i.e. as a θ instead of ω, as otherwise a difference in OFV of 3.84 points might not correspond to a significance level of 0.05. The results of the procedure are presented in figure 7.21 and the upper part of table 7.17. For both parameters the 95% confidence interval determined by log-likelihood profiling did not include zero. Compared to the 95% confidence interval estimated by the covariate model (see table 7.17) it was noticeably reduced for θ_{WT_CL} whereas interval width increased for ωKA. This was mainly due to the shape of the obtained profile, which decidedly differed from the expected symmetrical profile. The result of the log-likelihood profiling for ωKA supports the results from bootstrap analysis (see section 3.3.5.3.2), indicating that the estimated parameter might be biased and imprecise. The expected symmetrical profile was, however, obtained for θ_{WT_CL}. Thus, it can be concluded that θ_{WT_CL} was estimated with higher precision than originally predicted by the final model and should therefore remain part of the model.

3.3.5.3.2 Bootstrap

The results of the bootstrap analysis are presented in table 7.18. Most fixed-effects parameters describing the structural model were estimated with low bias. The relative bias for these parameters ranged between -11.6 and 23.7%. A higher bias could be observed for KA (50.5%). Moreover, a slightly higher bias could be identified for IIV as well as for residual variability and all covariate relations apart from θ_{WT_V3} (-2.07%). Relative bias ranged between -21.8 and 40.6%. The largest bias was observed in ωKA with a relative value of -389%. This can be explained by the poor data situation after oral dosing. In conclusion, the results indicate that, apart from the absorption process after oral dosing, the used data was sufficient to accurately estimate structural model parameters and IIV.

3.3.5.3.3 Case deletion diagnostics

During the case deletion procedure 11 new datasets were created by randomly deleting 10% of the individuals of the original dataset. Moreover, 34 new datasets were created in which only one individual was removed. In both approaches each individual was only deleted once. The results of the case deletion procedure are displayed in figures 7.22 and 7.23. All structural parameter estimates from the subject subsets except KIC, all estimates for IIV as well as θ_{THRO_CL} and θ_{WT_V3} obtained from the case deletion procedure lay within the respective 95% confidence intervals. To investigate if the deviation of the parameter KIC had any relevance for the model, concentration-time profiles were simulated using the minimum and maximum values of KIC obtained during case deletion procedures while setting all other parameter values to the final model estimates (see figure

7.24). In the following, the simulated concentration-time profiles were analysed by noncompartmental analysis. The area under the curve during one dosing interval after multiple dosing ($AUC_{ss,\tau}$) as well as C_{max} were calculated. A reduction of KIC from 0.0029 to 0.0006 h^{-1} resulted in a reduction of $AUC_{ss,\tau}$ by 5.12%. C_{max} was only reduced by 1.97%. As these small deviations originated from extreme KIC values it was concluded that the influence of KIC on the overall concentration-time profiles could be regarded as rather small. Thus, although some individuals might largely influence the value of KIC this would not have any influence on the overall structural model. A strong individual influence, however, could be ascertained for θ_{CLCR_CL} and θ_{WT_CL}. Both were influenced by a single individual with extremely low body weight (39.5 kg) and changes in CLCR from single to multiple dosing (63.3 mL/min versus 106 mL/min, respectively). In consequence, it can be concluded that these covariate relations should be reinvestigated with more individuals. However, the relations seem reasonable as they have been reported in the literature before [100].

3.3.5.3.4 Predictive check

The results of the predictive check after intravenous single as well as multiple dosing are presented in figures 7.25 and 7.26, respectively. Red lines represent the simulated median concentration-time profile whereas blue lines represent the 5% and 95% quantile and enclose the 90% prediction interval. The black symbols correspond to the measured concentrations either after single or multiple dosing. After single dosing, all models captured the median concentration-time course well. Although C_{max} values were best predicted by the competing models the best overall prediction of single dose data was obtained when the parameters of the final model were used for simulation and ωVAR was set to zero (figure 7.25 B).

The differences in the models were more pronounced after multiple dosing. The inhibition compartment model (figure 7.26 A) resulted in a wide 90% prediction interval, which did not adequately predict the observed concentrations. This was due to the special individual parameter distribution of VAR, which was not normally distributed but instead took a U-shape (see figure 7.20). In consequence, many small values were simulated for VAR, which widened the 90% prediction interval. The prediction interval was narrowed by the model with parallel linear and Michaelis Menten elimination (figure 7.26 C) and was even smaller in the model using a linear elimination pathway only (figure 7.26 D). However, in all these models the predicted concentration range as well as the predicted median concentration-time course exceeded the observed one. The best predictions were obtained by using the inhibition compartment model. However, ωVAR had to be set to zero (figure 7.26 B). This way it could be prevented that individual VAR values took a U-shape in simulation. Using this approach the simulated median concentration-time profile as well as the 90% prediction interval closely reflected the observed concentrations. It can therefore be concluded that the developed inhibition compartment model can be used to adequately predict

unbound concentration-time profiles of linezolid in plasma on the condition that ωVAR is set to zero.

3.3.5.4 Evaluation of covariate relations

A simulation was performed to assess the influence of the covariates on the unbound linezolid plasma concentration-time profiles using the parameter estimates of the final covariate model.

3.3.5.4.1 Influence of creatinine clearance

In order to assess the influence of CLCR on the concentration-time profiles of unbound linezolid the 5th and 95th percentile values of the study population were used. The profiles of the central and the inhibition compartment are presented in figure 7.27. The central compartment represented unbound plasma concentrations while steady state concentrations in the inhibition compartment can be used to visualise the calculated average steady state concentrations for the central compartment. The concentrations obtained from the different CLCR values differed remarkably. An individual with CLCR values in the reference range eliminated most of the drug before the administration of the next dose, resulting in low plasma concentrations, while individuals with low CLCR values reached distinctly higher concentration levels. Average concentrations of individuals with low CLCR values (18.4 mL/min) were increased by 129% compared to a CLCR value of 99 mL/min.

3.3.5.4.2 Influence of weight

The influence of WT on the concentration-time profiles was studied using the 5th and 95th percentile values of the study population. In the first case the covariate was only considered in the mathematical expression for the relation to CL. The results were very similar to the ones obtained for CLCR. Average concentrations increased by 108% when WT changed from 45.1 to 115.3 kg. The second case examined the effect of WT on V3. This relation did not have any effect on average concentrations. However, for heavy individuals C_{max} values were lower and tended to decrease more rapidly in the early distribution phase. However, the slope of the predominant elimination phase was more shallow, which resulted in higher minimum concentrations. When combining those two influences of WT the results were similar to those obtained when investigating the influence of WT on CL alone: as seen previously the average concentrations of lightweight individuals (45.1 kg) were 107% higher than those of heavy ones (115.3 kg). This went along with a change in terminal elimination half-life from 4.0 h to 3.4 h for lightweight and heavy individuals, respectively. The concentration-time profiles of the central and the inhibition compartment, considering both influences, are presented in figure 7.28.

3.3.5.4.3 Influence of thrombocytes

The influence of THRO on the concentration-time profiles was simulated using the 5th and 95th percentile values of the study population. The profiles of the central and the inhibition

compartment are presented in figure 7.29. An individual with high thrombocyte values showed low plasma concentrations, while individuals with low thrombocyte values reached distinctly higher concentration levels. Compared to the 95th percentile values, average concentrations of individuals with low thrombocyte values (81.2 nl[-1]) were increased by 123%.

3.3.5.4.4 Worst-case scenario

A combination series of 5th and 95th percentile covariate values was investigated in order to determine which combination would yield the lowest possible concentrations. Lightweight patients with high CLCR and thrombocyte values would potentially show the highest risk of having subinhibitory linezolid concentrations over a long time period. Assuming a MIC_{90} of 2 µg/mL and a dosing interval of 12 h these patients would have subinhibitory concentrations over a time period of 37.5% of the dosing interval at steady state. If the MIC_{90} was assumed to be 4 µg/mL this interval would even increase to a value of 58.3%. In contrast, individuals with median covariate values would have sufficient linezolid concentrations over the complete dosing interval. The results are displayed graphically in figure 3.6 showing concentration-time profiles over a period of 240 h as well as one dosing interval after multiple dosing.
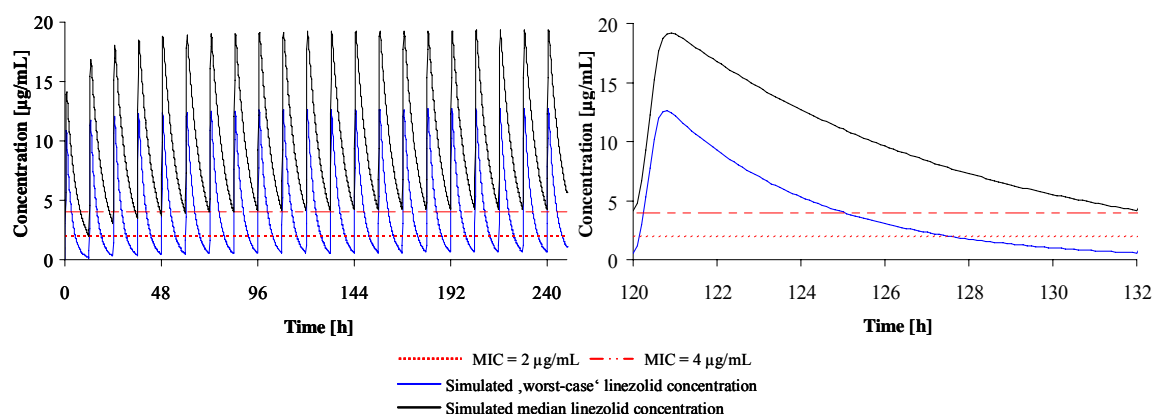

Figure 3.6: Simulated 'worst-case scenario' using a combination of 5th and 95th percentile covariate values yielding the lowest possible concentrations, compared to simulated median concentration-time profile. Left: Concentration-time profile over a period of 240 h; right: one dosing interval after multiple dosing

Moreover, it was investigated which covariate combination would yield the highest possible concentrations. The highest concentrations would be reached in patients having the opposite covariate values to those presented above, i.e. heavy patients with low CLCR and thrombocyte values. In consequence, these patients would be at higher risk of suffering from linezolid toxicity.

3.3.5.4.5 Simulation using actual subject's covariate values

In this simulation, all observed combinations of covariate values were simulated to obtain a concentration range that would probably be observed in further studies using similar subjects. The results are presented in figure 7.30. After multiple dosing, predicted C_{max} values ranged between 15 and 35 µg/mL and C_{min} values between 1 and 20 µg/mL. Overall, subjects reached adequate

linezolid concentrations on the condition that MIC_{90} took a value of 2 µg/mL. However, the simulation showed that if MIC_{90} were 4 µg/mL some individuals might potentially be underdosed. The identified covariate influences might therefore help to guide dose selection.

3.3.5.5   Development of an optimised sampling strategy

The number of samples needed for the determination of PK parameters describing the concentration-time profiles of unbound linezolid in plasma was reduced to 6 per studied individual. The 30 individuals included in the study were divided into three groups of equal size. The best performance was obtained when sampling times were equal for all individuals, but the dose after which the samples were taken was allowed to differ between groups. By using this approach especially parameters describing the change in PK over time (e.g. KIC) could be estimated with higher precision. The optimised sampling time points are presented in table 7.19.

After the optimisation process the design was evaluated by simulating data from 30 individuals and re-estimating the PK parameters. The resulting parameters are presented in table 7.20. They were in good agreement with those obtained from the intensive sampling design. Moreover, overall precision was not impaired. RSE values all ranged between 4.82-41.6%.

3.3.6   Joint model for unbound linezolid in plasma and ISF

3.3.6.1   Structural and pharmacostatistical model

In order to simultaneously describe unbound linezolid plasma as well as subcutaneous and muscular ISF concentrations within one population PK model a joint analysis was performed using dataset B.

3.3.6.1.1 Model development

As the parameter estimation in a nonlinear model was expected to be very time-consuming, the modelling process was started using a model with linear elimination from the central compartment. After gaining knowledge about the general ISF distribution of linezolid a model analogue to the plasma base model was applied, which was extended to account for the additional ISF data.

The model development process was started using a four-compartment model with an additional absorption compartment and first-order absorption and elimination. Unbound plasma concentrations were assigned to compartment 2, subcutaneous ISF concentrations to compartment 3 and muscular ISF concentrations to compartment 4. The different investigated model structures are presented in figure 7.31. Model A was varied with respect to its number and location of intercompartmental and elimination clearances. In order to run model A the volumes of distribution for the ISF compartments 3 and 4 had to be fixed to avoid identifiability problems. However, the model was still overparameterised, leading to numerical model instability. Furthermore, a major concern of model A was the difficulty of interpreting the obtained parameters. These disadvantages

were resolved by introducing model B. In this approach only two volumes of distribution were estimated, whereas no volume was assigned to the ISF compartments. Instead, the subcutaneous and muscle compartments were coded as effect compartments in which the rate into the compartment was equated with the output rate. The extent of ISF distribution was accounted for by introducing tissue partition coefficients (PC), which could easily be interpreted. The number of estimated fixed-effects parameters was reduced from 14 to 10. This way, stability problems were overcome.

3.3.6.1.2 Base model

The structure of the base model is shown in figure 3.7. It merged the plasma base model (see section 3.3.5.1.2) and model B (section 3.3.6.1.1) into one structure. Thus, it was a four-compartment model with an additional absorption compartment and first-order absorption. Unbound plasma concentrations were assigned to compartment 2, subcutaneous ISF concentrations to compartment 3 and muscular ISF the concentrations to compartment 4. The model incorporated a linear elimination process from compartment 2 that could be inhibited depending on the concentration in an inhibition compartment (same as in section 3.3.5.1.2). The model structure for ISF compartments was the same as described for model B in section 3.3.6.1.1. Thus, the following fixed-effects parameters were included into the model: CL, V2, Q, KA, ALAG1, VAR, KIC and IC50, which had the same meaning as in the plasma base model described in section 3.3.5.1.2, V5 (peripheral volume of distribution), PC23 (partition coefficient between plasma and subcutaneous ISF), PC24 (partition coefficient between plasma and muscle ISF), K30 (monodirectional rate-constant into and from compartment 3) and K40 (monodirectional rate-constant into and from compartment 4).

In order to estimate ISF parameters in acceptable run times all parameters that had previously been estimated for unbound plasma data had to be fixed to values obtained in the final plasma covariate
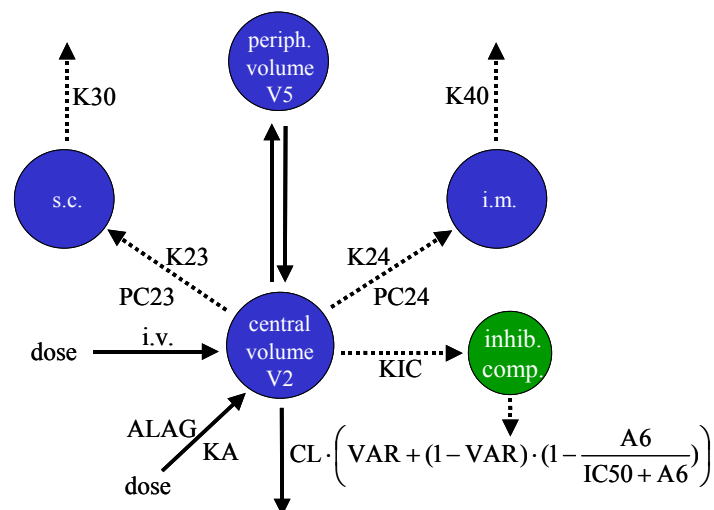

Figure 3.7: Final structure of the joint base model simultaneously describing unbound linezolid plasma and ISF concentrations. A6 corresponds to the concentration in the inhibition compartment.

model. It was not possible to selectively estimate some of these parameters. In addition, the model already contained the covariate relations described in section 3.3.5.2.2. A coding example is given in the appendix (NONMEM code 7.3).

Estimation of K30 resulted in extremely high values $(1360\,h^{-1})$ and was accompanied by unsuccessful run terminations. Sensitivity analysis using Berkeley Madonna showed that it was possible to reduce the value of K30 to $100\,h^{-1}$ without any changes in the concentration-time profiles in compartment 3. Therefore, K30 was fixed to a value of $100\,h^{-1}$.

IIV was incorporated for K40 (ωK40) and was estimated with a high value of 77% CV. IIV on PC24 (ωPC24) took a moderate value of 30% CV. Variability for PC23 was modelled using IOV (πPC23). It was estimated to be 43% CV, which was slightly higher than ωPC24. Residual variability was described by a combined additive and proportional random-effects model. A moderate proportional residual error was estimated (20%) whereas the additive error term was only included for reasons of model stability and was fixed to a value of 0.01 µg/mL.

Parameter estimates of the final base model are presented on the left in table 3.2. All fixed-effects parameters as well as IIV and residual variability were estimated with good precision (RSE ≤41%). Only πPC23 was estimated with lower precision (RSE 68%). The goodness of fit plots separated by matrix are shown in figure 7.32. In all plots showing population predictions against observed concentrations, the concentrations were spread uniformly around the line of unity, indicating that the data was well described by the model. However, when examining the plots showing individual predictions against observed concentrations it became obvious that unbound plasma concentrations were better described than data obtained from microdialysis measurements as concentrations were closer to the line of unity. A comparison of the individual fit for all matrices revealed that the best fit was obtained for unbound plasma concentrations, followed by muscle and then subcutaneous concentrations. A slight worsening of model fit could be observed for unbound plasma concentrations when comparing the joint model to the model obtained for unbound plasma concentrations only (see section 3.3.5.1.2).

3.3.6.2 Covariate model

3.3.6.2.1 Model development

In general, covariate analysis was performed according to the procedure described within section 2.7.6.3. However, the covariate model building process was started with a model that already contained the fixed covariate relations obtained in the covariate analysis for unbound plasma concentrations. Based on this model a GAM procedure was performed. The covariates that were selected by the GAM analysis and all other covariates that were investigated for reasons of plausibility after inspection of the scatterplots are listed in table 7.16.

Table 3.2: Parameter estimates of the joint base and final model for plasma and ISF concentrations.

Model parameter		Base model		Final model	
		Estimate	RSE[#] %	Estimate	RSE[#] %
CL	[L/h]	11.5 FIX	-	11.5 FIX	-
V2	[L]	19.8 FIX	-	19.8 FIX	-
Q	[L/h]	76.8 FIX	-	76.8 FIX	-
V3	[L]	27.0 FIX	-	27.0 FIX	-
KA	[1/h]	1.85 FIX	-	1.85 FIX	-
ALAG	[h]	1.27 FIX	-	1.27 FIX	-
VAR		0.567 FIX	-	0.567 FIX	-
KIC	[1/h]	0.0027 FIX	-	0.0027 FIX	-
IC50	[mg/L]	0.1 FIX	-	0.1 FIX	-
PC23		1.05	6.40	1.05	6.39
PC24		1.03	5.38	1.07	5.87
K30	[1/h]	100 FIX	-	100 FIX	-
K40	[1/h]	12.3	17.1	13.0	14.5
Covariate influence, %					
θ_{CLCR_CL}[§]		0.91 FIX	-	0.91 FIX	-
θ_{WT_CL}[§]		1.13 FIX	-	1.13 FIX	-
θ_{THRO_CL}[§]		0.23 FIX	-	0.23 FIX	-
θ_{WT_V3}		1.52 FIX	-	1.52 FIX	-
θ_{THRO_K40}		n.a.	-	0.211	1.96
θ_{CLCR_PC24}		n.a.	-	0.382	75.4
Interindividual and interoccasion variability					
ωCL	[CV%]	49.8 FIX	-	49.8 FIX	-
ωV2	[CV%]	37.1 FIX	-	37.1 FIX	-
ωV3	[CV%]	20.5 FIX	-	20.5 FIX	-
ωKA	[CV%]	78.9 FIX	-	78.9 FIX	-
ω^2VAR		6.36 FIX	-	6.36 FIX	-
πPC23	[CV%]	43.5	41.0*	43.6	41.0*
ωPC24	[CV%]	30.1	68.1*	28.0	71.9*
ωK40	[CV%]	77.4	24.7*	63.6	36.4*
Corr_V2/VAR		0.573 FIX	-	0.573 FIX	-
Residual Variability					
σ proportional	[CV%]	20.3	4.30	20.2	4.18
σ additive	[mg/L]	0.01 FIX	-	0.01 FIX	-

[#] = relative standard error, [§] = percent change with regard to the population parameter estimate, * = Standard error given on the variance scale; n.a. = not applicable; [#] = relative standard error

3.3.6.2.2 Final covariate model

The covariate model code is presented in the appendix (NONMEM code 7.4). Covariate analysis identified a significant influence of CLCR on PC24 using the following two-spline function:

$$PC24 = e^{\eta_{PC24}} \begin{cases} \theta_{PC24} \cdot \left(1 + \theta_{CLCR\_PC24} \cdot (CLCR - 65)\right) & \text{if } CLCR < 80 \\ \theta_{PC24} & \text{if } CLCR \geq 80 \end{cases} \qquad (3.5)$$

A value of 80 mL/min was chosen as node point as this is an acknowledged cut-off value for renal impairment [249]. The value of 65 mL/min was chosen because it represents the median of the study population. According to this relation and using the 5th and 95th CLCR percentiles of the study population while using the median of all the other relations, PC24 values changed from 0.880 to 1.13 as CLCR increased from 18.4 to 80.0 mL/min, a change of -17.8 and 5.61% compared to the population parameter estimate.

A significant influence of THRO on K40 could be identified. The mathematical expression for this relation was as follows:

$$K40 = \theta_{K40} \cdot \left(1 + \theta_{THRO\_K40} \cdot (220 - THRO)\right) \cdot e^{\eta_{K40}} \qquad (3.6)$$

According to this relation and using the 5th and 95th THRO percentiles of the study population K40 decreased from 16.8 to 6.98 h^{-1} as THRO increased from 81.2 to 439.5 nL^{-1}, corresponding to a change of -29.3 and 46.3% compared to the population parameter estimate. The final parameter estimates including the covariates are summarised on the right in table 3.2. Overall, estimated fixed-effects parameters did not change much. A slight increase in typical population parameter estimates could be observed for PC24 and K40. IIV was moderate to high with values of 28% CV (ωPC24) and 64% CV (ωK40). πPC23 was estimated to be 44% CV. Compared to the base model ωPC24 slightly decreased by 7.0% (i.e. –2.1 percent points). The variability was reduced by 17.8% (i.e. –13.8 percent points) for ωK40 whereas it slightly increased by 0.2% (i.e. 0.1 percent points) for πPC23. The proportional residual error had a moderate value of 20%. The additive error component was fixed to 0.01 µg/mL for reasons of model stability. Most parameters were estimated with good precision (standard errors ranging from 2 to 41%). Merely the covariate influence θ_{CLCR_PC24} and ωPC24 were estimated less precisely with standard errors of 75.4% and 71.9%, respectively. However, the resulting 95% confidence intervals were scrutinised and corrected by log-likelihood profiling (see section 3.3.6.3.1). The goodness of fit plots for the final covariate model are presented in figure 3.8. As most concentrations were uniformly spread around the line of unity the model can be regarded as well suited for describing unbound linezolid plasma and ISF concentrations.

3.3.6.3   Model evaluation

3.3.6.3.1 Log-likelihood profiling

Two parameters, namely ωPC24 and the covariate influence θ_{CLCR_PC24}, were estimated with a RSE larger than 50%. For these parameters a log-likelihood profiling was performed. The results of the procedure are presented in figure 7.33 and the lower part of table 7.17. For both parameters the
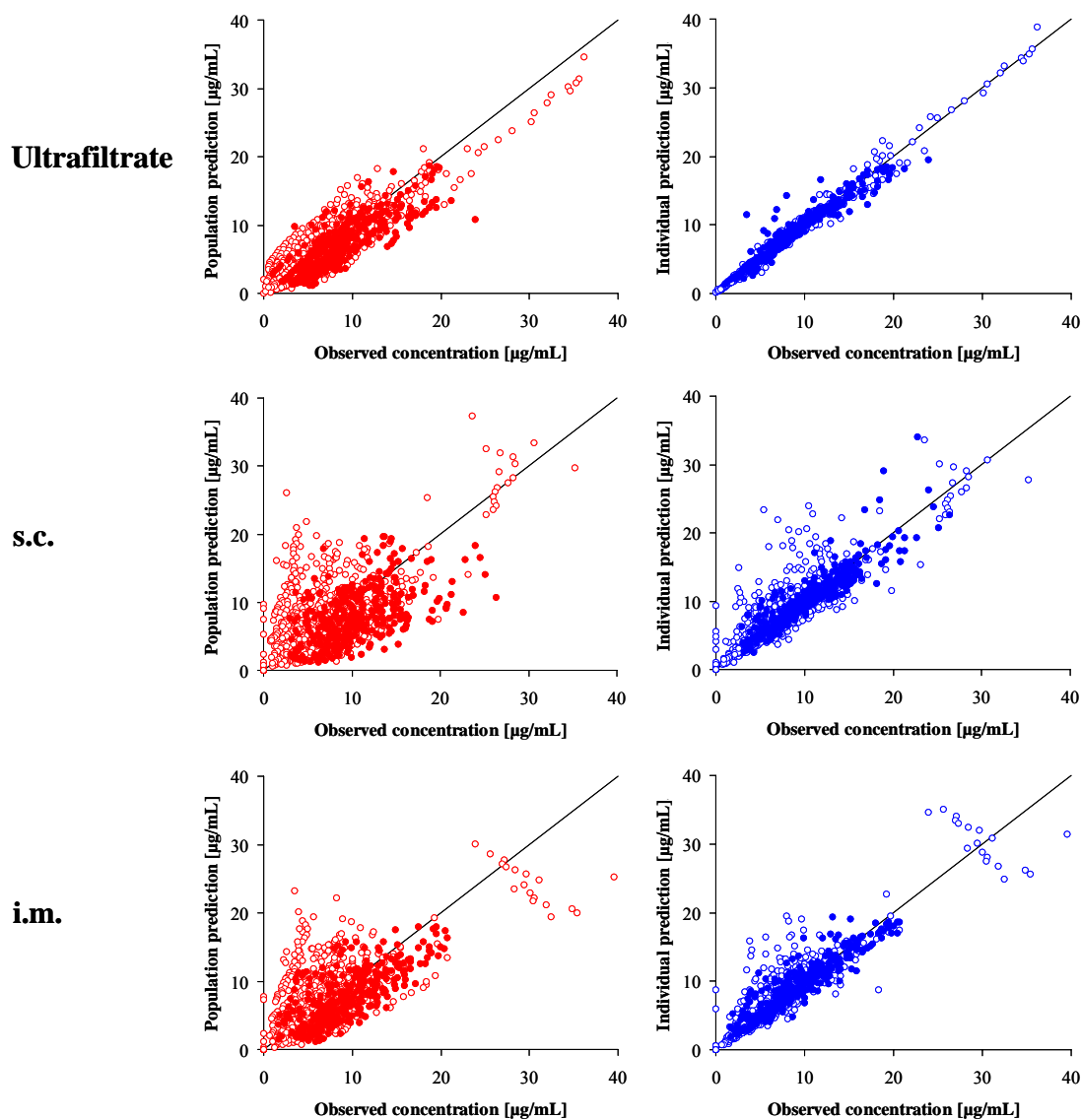
Figure 3.8: Goodness of fit plots of the final covariate model describing ultrafiltrate, s.c. and i.m. concentrations; filled circles: healthy volunteers; empty circles: patients.

95% confidence interval determined by log-likelihood profiling was noticeably reduced compared to the 95% confidence interval estimated by the covariate model (see table 7.17) and did not include zero. Thus, it can be concluded that both $\omega PC24$ and θ_{CLCR_PC24} were estimated with higher precision than originally predicted by the final model and should therefore remain part of the model.

3.3.6.3.2 Bootstrap

The results of the bootstrap analysis are presented in table 7.21. All parameters describing the structural and pharmacostatistical model were estimated with very low bias and with relative values ranging between –8.90 and 3.07%. Slightly higher values were observed for covariate influences with relative values between 13.0 and 28.4%. It can be concluded that all parameters describing linezolid distribution into muscle and subcutaneous ISF were accurately estimated using the available data.

3.3.6.3.3 Case deletion diagnostics

By randomly deleting 10% of the individuals of the original dataset 11 new datasets were created. Moreover, 34 new datasets were created in which only one individual was removed. In both approaches each individual was only deleted once. The results of the case deletion procedure are displayed in figures 7.22 and 7.23. All parameter estimates from the subject subsets except ωPC24 and the covariate influence θ_{THRO_K40} obtained from the case deletion procedure lay within the respective 95% confidence intervals. ωPC24 was influenced by a single patient who had significantly lower ISF than plasma concentrations. In this context this patient decidedly differed from all other studied subjects. It was therefore not surprising that this patient should influence ωPC24. However, the patient did not influence the mean population parameter estimate or any covariate influence on PC24. Therefore, the observed difference can be regarded as negligible. To investigate if the deviation of the parameter θ_{THRO_K40} had any relevance for the concentration-time profiles, simulations were performed using the minimum and maximum values of θ_{THRO_K40} obtained during case deletion procedures as well as the 5th and 95th percentile thrombocyte values of the study population, while setting all other parameter values to the final model estimates. The concentration-time profiles obtained with different values of θ_{THRO_K40} barely differed from each other (see figure 7.34). In the following, the simulated concentration-time profiles were analysed by noncompartmental analysis and the $AUC_{ss,\tau}$ as well as C_{max} were calculated. Using a thrombocyte value of $81.2\ nL^{-1}$ a reduction of θ_{THRO_K40} from 0.0021 to 0.0017 resulted in a reduction of C_{max} by 0.381%. $AUC_{ss,\tau}$ was only reduced by 0.003%. At thrombocyte values of $439.5\ nL^{-1}$ a reduction of θ_{THRO_K40} from 0.0021 to 0.0017 resulted in an increase in C_{max} by 1.97%. $AUC_{ss,\tau}$ was increased by 0.023%. As these influences can be regarded as negligible it can be concluded that, although the parameter value θ_{THRO_K40} was significantly influenced by a single individual, this did not have any relevance on the prediction of concentration-time profiles.

3.3.6.3.4 Predictive check

The results of the predictive check for subcutaneous and muscle ISF after intravenous single as well as multiple dosing are presented in figures 7.35 and 7.36, respectively. Red lines represent the simulated median concentration-time profile whereas blue lines represent the 5% and 95% quantile and enclose the 90% prediction interval. The black symbols correspond to the measured concentrations after single or multiple dosing. After single dosing, the 90% prediction interval in subcutaneous ISF was well captured. However, median concentration-time profiles were slightly underpredicted. In muscular ISF the median was predicted well while the upper limit of the 90% prediction interval was higher than observed values. This tendency could be observed using the final model as well as when using the inhibition compartment model, with setting ωVAR to zero. Moreover, as a result of the coding for ISF concentrations, which was a function of concentrations

in the central compartment, C_{max} values were lower than predicted and could be observed later than anticipated.

As previously observed in section 3.3.5.3.4 the 90% prediction interval was also wide for subcutaneous and muscle concentrations after multiple dosing. This fact can be explained as in the used model ISF concentrations were a function of unbound plasma concentrations. Thus, if unbound plasma concentrations were not well predicted the same would apply for ISF data. In consequence, ωVAR was set to zero. This resulted in a much narrower prediction interval. However, although median concentration-time profiles apart from C_{max} were well predicted for both matrices the upper boundary of the 90% prediction interval was still a bit too high for subcutaneous ISF.

It can be concluded that ωVAR should be set to zero in order to predict concentrations in subcutaneous and muscular ISF. This way, median concentration-time profiles will be adequately predicted. A slight overprediction of the upper limit of the 90% prediction interval might result.

3.3.6.3.5 Evaluation of tissue penetration

Tissue partition coefficients estimated by the model with linear elimination closely resembled those estimated by the inhibition compartment model (see table 7.22). While median PC23 increased by 2.96%, median PC24 decreased by 0.04%. However, some individual partition coefficients for subcutaneous ISF significantly differed from those obtained using the inhibition compartment model. These derived exclusively from individuals whose concentration-time profiles after multiple dosing contained strong fluctuations and whose partition coefficient could thus be regarded as not well assessable. In consequence, it can be concluded that partition coefficients of both models were similar. If the aim of a study was to estimate ISF penetration one could therefore use a model with linear elimination. This would save calculation time.

3.3.6.4   Evaluation of covariate relations

A simulation was performed to assess the influence of the covariates on the unbound linezolid muscle concentration-time profiles using the parameter estimates of the final covariate model.

3.3.6.4.1 Influence of creatinine clearance

In order to assess the influence of CLCR on the concentration-time profiles of linezolid in skeletal muscle the 5th percentile value of the study population and the node of the hockey-stick function were used. Two different scenarios were simulated. The first one incorporated only the influence of CLCR on PC24 whereas the second scenario also took the influence of CLCR on CL into account. The respective profiles of the muscle compartment in scenarios one and two are presented in figure 7.37. An increase in CLCR values was accompanied by an increase in skeletal muscle concentrations due to higher PC24 values. When CLCR influence on CL was taken into account C_{max} values remained higher if CL values increased. However, the additional influence on CL also

resulted in lower minimum concentrations. Average concentrations in skeletal muscle decreased by 20% as CLCR values increased from 18.4 to 80.0 mL/min. This result might be clinically relevant as concentrations at the 95th percentile resulted to be below 4 µg/mL for 25% of the dosing interval.

3.3.6.4.2 Influence of thrombocytes

The influence of THRO on the concentration-time profiles was studied using the 5th and 95th percentile values of the study population. The resulting profiles are presented in figure 7.38. In the first scenario the covariate was only considered to have an influence on K40. Concentration-time profiles in skeletal muscle closely resembled each other. The only observable change was a decrease in multiple dose C_{max} values from 19.16 to 17.84 µg/mL, i.e. by 6.9%, as thrombocyte values increased from 81.2 to 439.5 nL^{-1}. In the second approach THRO were considered to have an effect on K40 as well as on CL. This resulted in an average concentration decrease of 52% as thrombocyte values changed from 81.2 to 439.5 nL^{-1}. This result might be clinically relevant as concentrations at the 95th percentile resulted to be below 4 µg/mL for 37.5% of the dosing interval. Moreover, both C_{max} and C_{min} values were distinctly lower at the 95th percentile value.

3.3.6.5   Development of an optimised sampling strategy

In order to determine optimised sampling times for parameters describing ISF distribution the design developed for the plasma model was retained and corresponding sampling time points were fixed. In consequence, this optimisation yielded the additional microdialysis sampling time points. In principle, using 2 samples for each matrix yielded similar precision as with 4 samples. However, in order to enable the estimation of IOV in further studies it was decided that 4 samples (2x2 at different occasions) should be taken in every ISF matrix. For reasons of practicability these samples were assigned to be taken after doses where plasma sampling took place as well. The resulting sampling schedule for subcutaneous and muscular ISF is presented in table 7.23. After the optimisation process the design was evaluated by simulating data from 30 individuals and re-estimating the PK parameters. The resulting parameters are presented in table 7.24 and were in good agreement with those obtained from the intensive sampling design. Moreover, overall precision was not impaired. However, ωPC24 was estimated with higher precision than before whereas ωK40 was estimated less precisely. Precision could not be improved by adding additional sampling time points. RSE values ranged between 4.93-89.6%.

4   Discussion

4.1   Project I: *In vitro* experiments

4.1.1   Vancomycin: Bioanalytics and *in vitro* microdialysis

A new analytical method for the quantification of vancomycin had to be developed in order to be able to quantify vancomycin from small sample volumes like those obtained during microdialysis experiments. This aim was accomplished by the development of an HPLC method with UV detection that was able to quantify vancomycin from sample volumes of 100 µL and 40 µL for plasma and microdialysate, respectively. Moreover, as the assay had to meet international criteria it was validated according to guidelines issued by the FDA [234]. In addition, *in vitro* microdialysis experiments were performed with vancomycin to determine if it was possible to investigate the *in vivo* PK of the drug with the application of this technique.

This chapter will discuss the investigations performed with vancomycin and the results obtained. The following items will be addressed:

- vancomycin quantification
- *in vitro* microdialysis experiments

4.1.1.1   Vancomycin quantification

Before the method development process was initiated several methods for the quantification of vancomycin from plasma had been published. In these publications vancomycin was either quantified by the use of a fluorescence polarisation immunoassay (FPIA) [250], which is often employed for routine clinical drug quantification, or by HPLC, using different detection methods such as UV [251-259] and electrochemical detection [260] or tandem mass spectrometry [261, 262]. A thorough search of the literature revealed that FPIA might result in an overestimation of vancomycin concentrations [255, 263-268]. This result was attributed to the fact that a vancomycin crystalline degradation product (CDP-1) has a similar chemical structure to that of vancomycin and was therefore falsely recognised by the immunoassay [269]. CDP-1 is formed at temperatures of 37°C [269] and thus may be present in patients treated with vancomycin. An accumulation can occur predominantly in patients with decreased renal function [270]. However, as CDP-1 does not show any antimicrobial activity its false recognition would result in apparent elevated concentrations of vancomycin. All methods that resulted in an overestimation were performed using a sheep-derived polyclonal antibody for the FPIA. Therefore, a modified assay was developed using murine-derived monoclonal antibodies in an attempt to make it more specific for vancomycin [271]. Evidently, previous problems were resolved as the new assay did not cross-

react with CDP-1 [269-272]. Nevertheless, it was decided to develop a vancomycin quantification method based on HPLC.

The most sensitive HPLC methods used electrochemical or mass tandem spectrometry detection and had a lower limit of quantification of 0.001-0.500 µg/mL [260, 261]. However, the aim of the method development was the use of common HPLC equipment in order to make the method applicable for any laboratory performing biomedical analyses. Hence, UV detection was chosen for further experiments.

Authors of articles published prior to the method development process had mostly used a mixture of acetonitrile and buffer as mobile phase. Lukša and Marušič used an isocratic elution procedure on an RP-18 column. Their mobile phase was prepared by mixing 0.005 M KH_2PO_4 (pH 2.8) and acetonitrile in a 90:10 (v/v) ratio, using a flow rate of 1 mL/min [257]. Other publications recommended the use of buffer in higher concentrations. Favetta et al. used a 0.025 M sodium phosphate buffer [260] while Hu et al. even used a concentration of 0.050 M [255]. Therefore, method development was started by using an RP-18 column and a mixture of 0.025 M KH_2PO_4 (pH 2.75) and acetonitrile in a 90:10 (v/v) ratio, applying a flow rate of 1 mL/min and isocratic elution. This approach resulted in retention times of approximately 5 minutes, which was in good accordance with the literature [257]. The use of buffer during HPLC experiments may result in damage of the HPLC pump over time as buffer might crystallise and cause friction. Therefore, the subsequent experiments aimed at replacing buffer by water. However, this approach was not successful as vancomycin could not be detected by the HPLC system. This observation can be explained by the chemical structure of vancomycin. The molecule is a compound with 6 pk_a values covering a range from 2.18 to 12.0 [273]. Two of those pk_a values belong to basic structural compounds whereas the other four are acidic groups. This complexity results in the molecule almost always having some net charge, except at its isoelectric point (pH 7.2 [274]). The net charge changes with only minor variations in the pH value and with vancomycin concentration. Thus, the interaction of vancomycin with the HPLC column will vary if water is used as mobile phase as this allows pH to change. The use of water would therefore result in unpredictable shifts of retention times. Consequently, buffer remained part of the mobile phase. In a next step it was investigated if acetonitrile could be replaced by less toxic agents such as MeOH. As reasonable retention times with similar peaks could be obtained by this mobile phase composition, acetonitrile was replaced by MeOH in all subsequent experiments.

Although previously published methods used isocratic elution this resulted in vancomycin peak widths of 1.5 min. Introduction of gradient elution and variation of the pH of the mobile phase resulted in a decrease of this interval to 0.3 min; a prerequisite for the quantification of even low amounts of vancomycin.

The aim of the method development process was to establish an analytical assay capable of quantifying vancomycin from plasma and even from small volumes such as microdialysate.

Moreover, it needed to cover a concentration range expected in humans *in vivo*, and this with low expenditure of time. Therefore, the development process aimed at using time saving sample preparation procedures. In consequence, solid phase extraction, as used by Greene et al. [254], was replaced by a protein precipitation method for plasma samples. Even more time could be saved when preparing microdialysis samples. As these only contain an aqueous solution it was possible to directly inject the diluted samples into the HPLC system.

After introducing a gradient elution procedure the lower limit of quantification was reduced to a value of 0.400 μg/mL. This value conformed to other LLOQs reported for vancomycin in bioanalytical assays using HPLC with UV detection [252, 256]. In some cases it was even lower [251, 253-255, 257, 259]. It allowed for the measurement of antibiotic concentrations in small sample volumes (e.g. 40 μL microdialysate) in plasma and ISF down to the MIC_{90} values reported for most relevant gram-positive pathogens, including MRSA [275]. Accuracy and precision of the method were in accordance with other methods [256, 257]. All validation parameters met the criteria set in the international guideline for bioanalytical methods [234]. Moreover, the aim of reducing the sampling volume and thus reducing the burden for eventual study subjects was achieved. Plasma sampling volume could be reduced from 1000 μL [257] to 100 μL; a *sine qua non* when applying the method during a pharmacokinetic clinical trial depending on multiple plasma samples per subject. In conclusion, a rapid and reliable HPLC assay validated for the determination of vancomycin concentrations in microdialysate and plasma was developed that is suitable for application in (pre-)clinical trials.

4.1.1.2   *In vitro* microdialysis experiments

The analytical assay for vancomycin was developed in order to measure its concentrations in microdialysis samples in further clinical studies. After assay development had been completed, further experiments therefore aimed at investigating the feasibility of the microdialysis method with respect to vancomycin. The drug has a molecular weight of 1486 Da. For eventual clinical trials it was planned to use microdialysis probes with a molecular weight cut-off of 20000 Da. From a theoretical point of view it was expected that vancomycin would pass the microdialysis membrane in quantifiable amounts as acceptable RR will be attained with substances having a molar mass lower than approximately one-fourth of the membrane cut-off [158]. In *in vitro* experiments it was investigated whether vancomycin was able to pass the probe membrane and if this process was dependent on the flow rate. Recovery was observed to be relatively low compared to other drugs such as linezolid [159]. This observation can be explained by the fact that linezolid has a much lower molecular weight than vancomycin. It was expected that the RR would be dependent on the flow rate. The observed flow rate dependence was in accordance with other inverstigations [159, 276]. *In vitro* microdialysis experiments revealed that vancomycin concentrations achieved in the dialysate would be sufficient for *in vivo* investigations.

A prerequisite for conducting microdialysis experiments is a concentration independence of RR. Experiments were started using Ringer's solution as perfusate as *in vivo* this is the standard perfusion medium reported for many drugs [277-280] and as it has also been used for vancomycin [248]. However, when applying this experimental setting, the essential requirement of concentration independence was not met. Vancomycin recovery increased with increased drug concentrations. This effect can be explained by the changing pH value obtained from vancomycin solutions of different concentrations. This might have been the cause for the change in its diffusion characteristics. This assumption could be confirmed in further experiments where the perfusate composition was changed from Ringer's solution to phosphate buffer. This resulted in constant relative recoveries over the whole investigated concentration range. Coefficients of variation were below 11.1% which corresponded to values observed for intraday variability of the analytical assay. However, mean RR varied with values of 27.8% (CV 11.1%, n=3) and 33.2% (CV 8.3%, n=6) for retrodialysis and recovery experiments, respectively. The difference was statistically significant (student's t-test: $p < 0.0005$), indicating that the extent of membrane passage was not equal in both directions. However, in general variations in RR of 20% are accepted under *in vivo* conditions [281]. In consequence, these could be regarded as not being of relevance to the practical implementation of microdialysis. In addition, the results from the performed linear regression confirmed that RR was not influenced by vancomycin concentrations and that by keeping the pH value constant the diffusion process through the semipermeable membrane was quantitatively equal in both directions. It can be derived from the *in vitro* results that microdialysis experiments cannot be carried out using Ringer's solution as a perfusate. It is therefore recommended to replace Ringer's solution by phosphate buffer in all subsequent experiments. Thus, by taking into consideration the special phenomenon observed during *in vitro* experiments optimal conditions for the *in vivo* microdialysis procedure were determined. It can be concluded that vancomycin is suitable for *in vitro* and *in vivo* microdialysis experiments.

4.1.2   Linezolid: Bioanalytics

Prior to all investigations the analytical assay for linezolid in plasma, ultrafiltrate and microdialysate had been developed in the department [159]. The aim of further investigations was to transfer the developed method to other matrices which might possibly be investigated in (pre-)clinical studies. In consequence, the assay and/or preparation procedure were modified to quantify linezolid in bone marrow, bone biopsy samples and urine. Provided that the studied subject does not suffer from any renal illness urine can be characterised as an aqueous medium that does not contain any proteins. Therefore, it was assumed that this matrix could be assayed like microdialysis samples and no further method development or validation was performed. However, if linezolid was studied in urine of patients, it would have to be tested for proteins. If proteins were present it would not possible to use the simple one-step dilution procedure as proteins might

denature and precipitate as soon as the mobile phase used in HPLC would be added. In consequence, a method similar to plasma preparation would become necessary, which would require further method validation.

Bone marrow fills the cavities of bones and produces the cellular components of blood. It contains progenitor and mature blood cells, including leukocytes, erythrocytes and platelets as well as proteins. It therefore has a similar complex composition as blood. Consequently, it was hypothesised that bone marrow samples could be measured using plasma calibration samples. The results showed that acceptable accuracy could be obtained for a concentration range from 0.500-20.0 µg/mL whereas the relative error of the nominal concentration of 0.200 µg/mL exceeded the value demanded by the FDA guideline [234].

The bone marrow used for the experiments was obtained from healthy piglets. Due to the limited number of piglets available only a small amount of bone marrow was available for experiments. In consequence, the experiments could not be repeated indefinitely. The results of the recovery experiments emanated from a single experiment whereas repeated measurements would have been desirable. It could therefore not be determined if the large relative error of the lowest concentration was an artefact of sample preparation errors. Investigations performed with bone marrow that had been centrifuged after it had been deep-frozen indicated that in principle it might be possible to obtain accurate results using plasma calibration samples even when including the concentration of 0.200 µg/mL, as these investigations resulted in a relative error of only 1.3%.

Bone marrow contains more connected protein fibres which when pipetted could have caused errors in sample volumes. Moreover, it was not investigated if the concentration of linezolid differed in those protein fibres. If linezolid accumulated in protein fibres and if proteins were accidently carried over into the assayed samples it would result in higher total concentrations than originally anticipated. In conclusion, it might be possible that the observed high relative error at the original lower limit of quantification might be the result of errors in sample preparation procedures. However, as a concentration of 0.500 µg/mL was still well below the threshold of 2-4 µg/mL, which is defined as the MIC_{90} for many relevant pathogens [282], it was decided that for further studies in bone marrow this concentration would be sufficient as a lower limit of quantification.

Due to the small number of bone biopsy samples available for method development it was not possible to fully validate the sample preparation procedure with repeated measurements. The proceedings were therefore very similar to those performed with bone marrow. Three different linezolid concentrations were assayed and the results indicated that it was possible to measure bone biopsy concentrations using plasma calibration samples. One drawback might be that the three concentrations only covered the small concentration range of 0.400-2.00 µg/mL, thus the validity of this approach was not demonstrated for higher concentrations. However, the same procedure was applied by Rana et al. [93] and Lovering et al. [94] who determined a recovery of linezolid from bone of 95-110% that exactly corresponds to the results described in this thesis. They used an

analytical assay that was validated for a range of 0.1-30 μg/mL. It can therefore be assumed that the investigated bone concentrations covered this range as well. As it would not be feasible to prepare calibration samples from bone biopsies in a routine clinical setting and, in addition, such an approach would not be justifiable from an ethical point of view, the measurement against plasma calibration samples was chosen as the best method available to determine linezolid concentrations from bone biopsy samples.

4.2   Project II: Linezolid pharmacokinetics in bone tissue

The aim of the experimental study was to apply microdialysis to cancellous bone ISF of healthy pigs in order to investigate the feasibility of the technique. Furthermore, it was aimed to examine the PK of linezolid at a possible site of infection. So far, linezolid PK had mostly been studied with techniques such as biopsy sampling, a method that only yields information about total concentrations in tissue homogenate. The PK parameters obtained from bone ISF were compared to those obtained from plasma, bone marrow and bone biopsy samples.

This chapter will address the following items:

- feasibility of microdialysis in bone ISF compared to bone biopsy sampling
- pharmacokinetics of linezolid in plasma, bone marrow, bone ISF and bone biopsy

4.2.1   Feasibility of microdialysis in bone ISF

Prior to this study, microdialysis experiments in bone had been scarce and had never been performed with linezolid. Gentamicin pharmacokinetics was studied in pigs over a period of 6 h after single drug administration [235, 283]. The studies concluded that microdialysis was a suitable, relatively non-invasive and reproducible technique for dynamic and quantitative measurement of gentamicin concentrations in bone ISF. The only application of bone microdialysis in humans – although not after any drug administration – was performed by Thorsen et al. in order to study the release of prostaglandin E2 in the proximal tibia metaphysis in six healthy females after mechanical loading [284]. Three additional healthy females served as control group. In this group, major prostaglandin E2 alterations were not observed whereas a statistically significant increase was observed in the verum group. The authors therefore concluded that microdialysis was a useful tool to study prostaglandin E2 production in human bone.

The study presented in this thesis applied the microdialysis technique by drilling a channel of 1.1 mm in diameter and 15 mm of depth. A concern was that this mechanical procedure would have caused tissue trauma which could have influenced the distribution characteristics of the drug. In general, an inflammatory response can be observed in all tissues. Yet, previous studies showed that trauma developed mostly after longer microdialysis application over many days [285, 286]. However, directly after probe implantation an immediate evidence of edema or tissue disruption

was not observable [287]. Although some of these studies were performed in tissue more easily accessible, i.e. skin, Thorsen et al. also presented direct evidence for the feasibility of the technique in bone by comparing measured values to a control group [284]. With a diameter of 2 mm and depth of 50 mm the drill channel in Thorsen's study was larger than the one used in this experiment. If tissue trauma had influenced prostaglandin E2 release one would have expected a change in release over the measurement period as tissue was recovering. However, in the control group prostaglandin E2 concentration changes were not observed. It can therefore be concluded that the drilling procedure will not have largely influenced linezolid concentrations.

In general, the variability in microdialysate concentrations was higher than in plasma or bone marrow measurements. This variability also became apparent in the calculated tissue penetration factors. One explanation might be that the characteristics of blood differ less between individuals. In order to become available in bone, however, the drug has to penetrate through various tissues. The diffusion ability is influenced by the tortuosity of the tissue, i.e. the increase in diffusion length caused by the hindrance that is imposed by the cellular structures as well as the connectivity of the spaces [288, 289]. Mathematically, the diffusion into tissues can be described by transfer time functions where transfer times are exponentially distributed due to the included variance term [290]. In consequence, if a drug has to diffuse through various tissues, the increasing number of subsequent transit functions results in increased variability. Moreover, ISF penetration might differ due to the presence of diffusion barriers. In consequence, the ability of a drug to reach the bone tissue might differ according to the differences in the tissue structure. Nevertheless, the increased variability might also have been due to the probe calibration procedure. The determination of precise ISF values of unbound linezolid from microdialysates demands calibration of the probes. Two standard solutions of linezolid were used for the determination of RR of the microdialysis catheter. In some cases a recovery value could only be obtained for the calibration solution with the higher linezolid concentration. Thus, the concentration calculation was based on only one recovery measurement although repeated measurements would be more favourable to minimise imprecision. This could have led to a larger range of ISF concentrations. However, it should not have influenced geometric mean concentrations as variations in recovery can be expected to occur randomly. In addition, when inspecting the concentration-time plots of a single pig, smooth individual profiles with almost no outliers were observed (see figure 7.39), substantiating the reliability of the microdialysis measurements within one individual. However, for future studies it would be desirable to calibrate the probe with only one high concentration while repeating the calibration process at least once to obtain more information about RR precision.

4.2.2   Pharmacokinetics of linezolid in plasma and bone

Comparing the PK of linezolid in bone marrow and plasma the penetration into bone marrow was as fast as in plasma and virtually complete. This result was not surprising and cofirmed previous

expectations. Bone marrow has proven to be in constant exchange with blood. Hence, it consistently gains in importance as a route of drug administration. The intraosseous route provides a valuable alternative to the intravenous administration [291-293] as it has been demonstrated that the central circulation is quickly reached from multiple intraosseous sites [294]. In conclusion, it can be stated that further studies investigating linezolid PK in bone marrow are not required as they can easily be derived from plasma PK.

Before a comparison between the PK of linezolid in bone, which was determined by biopsy sampling, and other matrices could be undertaken, measured concentrations had to be transformed. Due to the experimental design, sample preparation and analysis concentration values obtained from bone biopsy samples carried the unit µg/g and thus, a statistical comparison to other matrices, e.g. plasma, became difficult. An obvious approach would be to convert values of other matrices from µg/mL to µg/g. However, for the effect of an antibiotic the volume in which it is distributed is far more meaningful than its mass. Therefore, concentration values should preferably be presented in the unit µg/mL. In order to perform comparisons and statistical analyses and to enable PK parameter estimation on a volume basis a bone density of approximately 1.75 g/mL was determined by means of water displacement. By using these volume terms a high tissue penetration was observed. It can be explained by the anatomy of the cancellous bone in young pigs that is characterised by a high content of blood, bone marrow and connected tissues. However, another explanation might be that bone concentrations were overestimated due to an overestimation of bone density as this would increase the PK values when transforming them from µg/g to µg/mL. Water displacement might not be a very accurate method for determining bone density as bone tissue is not one solid mass. It contains spaces which might be filled with air. This might have led to modified results. Moreover, for a precise density determination replicate experiments should be performed. However, this was not possible due to the limited number of samples available. This shows the difficulties involved with homogenated bone samples. While concentrations in µg/g could not be directly compared to other matrices, their recalculation to values in µg/mL was associated with a high error risk. In addition, the intraindividual variability in bone biopsy concentrations was very high. It indicated that the extraction of linezolid from bone homogenates was difficult and in some cases might not have been complete. Another limitation of bone biopsy sampling occurs from the fact that it represents tissue homogenate. Thus, it represents a mixture of intra- and extracellular compounds. Moreover, it does not allow for discrimination between bound and unbound drug. Therefore, the value of results obtained from bone biopsy sampling remains questionable. In conclusion, PK estimations performed on homogenated tissue samples could be misleading and might even result in an overestimation of the efficacy of the antimicrobial agent.

PK parameters obtained from bone microdialysis measurements differed substantially from those in plasma and were also well distinguishable from those obtained after bone biopsy sampling. In general, the results indicated that linezolid did not penetrate into bone ISF as well as it might have

been expected from bone biopsy results. Both AUC and C_{max} values of bone ISF were considerably below those of all other matrices. These results were also reflected in the low PF values, indicating that on average penetration into bone tissue was not complete.

Clearance values and volumes of distribution of bone ISF were higher than those in plasma and bone biopsy samples. Furthermore, $t_{1/2}$ was slightly shorter. The most reasonable explanation might be that those were parameters that were obtained by an extrapolation until infinity [211]. However, not more than 20% of the total AUC should be based on extrapolation [295] in order to be able to obtain reliable parameter estimates. However, in the present study sampling was only performed over a period of 6 h. Surgical procedures, tissue recovery, recovery measurements and the 6 h of sampling added to a total of 12 h of anaesthesia which presented a very long time for a pig. The study could, therefore, not be extended beyond 6 h. Due to the lack of other alternatives PK parameter calculation was based on this data. Thus, those parameters should be regarded with care and small differences between matrices should not be overinterpreted.

In plasma, linezolid reached geometric mean maximum concentrations of 26.1 µg/mL after single linezolid administration. This value exceeded the one observed for humans by a factor of ~2 [79, 85]. However, compared to humans the pigs used in this study had a significantly lower WT. Taking this difference into consideration, pigs received a dose of 15 mg/kg whereas humans with a WT of 70 kg would receive only 8.5 mg/kg with the same absolute dose. Thus, pigs received approximately the 1.75-fold dose of humans. Although at first sight the approach of higher doses might not seem reasonable it assured that analytical problems could be precluded. Taking the higher dose into account, the observed C_{max} values were very similar to those reported for humans. Moreover, time of C_{max} in this analysis was in close agreement to values reported for humans in the literature while $t_{1/2}$ was slightly higher [79]. Concentrations in bone microdialysate exceeded the MIC_{90} of important pathogens (MIC_{90}>2-4 mg/L) [282] during all experiments performed. However, as the dose administered to the animals exceeded the human dose by a factor of 1.75 the results indicate that unbound tissue concentrations reached in human bone might in some cases not be sufficient given the standard dosing regimen of 600 mg linezolid bid. Moreover, AUC_{0-24h}/MIC_{90} is a primary predictor for linezolid therapy outcome and should take values larger than 100 in order to successfully eradicate relevant bacteria [296, 297]. In this study, only AUC_{0-6h} values could be calculated. Although it would be desirable to calculate AUC_{0-24h}, an extrapolation of the obtained value over a period of 24 h is not recommended [295]. However, when relating the obtained AUC to pharmacodynamics by using the AUC_{0-6h}/MIC_{90} ratio, values of 21.3 and 22.9 were obtained for the lateral and medial catheter, respectively, given a MIC_{90} of 2 µg/mL. Even when quadruplicating these values, which would definitely present an overestimation of AUC_{0-24h}, the limit of 100 would not be reached. This result indicates that the given dose might not be sufficient for the treatment of bone infections in both animals and humans.

Prior to this study, linezolid bone penetration had only been investigated using tissue homogenates. The conclusions drawn suggested that the concentrations in bone tissue were sufficient for the treatment of bone infections [94]. Others reasoned, though, that linezolid did not penetrate well into bone tissue [82, 298]. From the results presented here it can be concluded that investigating tissue PK by *in situ* microdialysis was superior to investigating homogenated tissue samples. Analysis of tissue homogenates yielded less reliable results than microdialysis and could from a theoretical point of view have overestimated pharmacokinetic values which in turn might have led to insufficient concentrations in a patient and caused subsequent clinical failure. Results from microdialysis measurements indicated that the chosen dose of linezolid might not have been sufficient for the treatment of bone infections. This issue needs further investigation, especially for septic patients with a locally infected area where the concentrations at the target site are the most relevant and should therefore be determined with the highest accuracy possible.

4.3   Project III: Target site pharmacokinetics of linezolid during sepsis

Based on data obtained from 34 subjects a population PK model for the simultaneous description of unbound linezolid concentrations in plasma and ISF of healthy volunteers and septic patients was developed. The studied individuals were examined after single and multiple linezolid administration, applying an intensive sampling schedule for both blood and ISF. In parallel, different intrinsic and extrinsic covariates were collected in order to investigate their influence on PK parameters. The developed model was evaluated in terms of accuracy, robustness and its ability to predict concentration-time profiles of unbound linezolid. Furthermore, the aim was to retrospectively identify the informative sampling time points that would have been needed for the development of the PK model and for further studies.

This chapter will discuss the developed model based on the following items:

- modelling approach
- model structure
- covariate influence
- model evaluation
- optimised sampling design
- practical model implementation

4.3.1   Modelling approach

Parameters for unbound plasma and ISF concentrations were estimated sequentially. As a result, the parameters estimated for the description of unbound ISF concentrations were conditioned on the previously obtained parameters based on unbound plasma concentrations. In principle, this approach may lead to biased parameter estimates, and conditioning on some of the data or on prior

fits to them may yield inaccurate standard errors [299]. Nevertheless, this approach has the advantage of obtaining parameter estimates in a reasonable period of time. As during model development it became obvious that a simultaneous estimation of all parameters would not be feasible due to long model run times, the sequential approach was chosen.

4.3.2   Model structure

The PK of unbound linezolid was best described by a two-compartment model with linear elimination. However, this linear CL could be inhibited dependent on the concentration in an empirical inhibition compartment, resulting in an overall nonlinearity in CL. This model structure was superior to all other investigated alternatives with respect to goodness of fit and model stability. The population PK of linezolid had been described in the literature prior to this investigation. Whitehouse et al. investigated linezolid PK by means of a linear one- and two-compartment model [97]. The one-compartment model underestimated all concentrations, most pronounced for C_{max} values. The authors therefore concluded that this misspecification would be removed by using a two-compartment model. This was implemented using the FO algorithm with the POSTHOC option available in NONMEM^{TM}. However, although the individual goodness of fit was shown for one subject an overall goodness of fit plot showing observed versus predicted values was not presented. The obtained PK parameters were not in accordance with any other investigations, e.g. the volume of distribution was estimated to be 284 L for an individual weighing 70 kg whereas other authors reported a volume of distribution of 40-50 L [84]. Own estimations using a linear two-compartment model (model DSA1, section 3.3.5.1.1) resulted in a volume of distribution of 68.2 L and – although being slightly higher – confirmed the usually reported values. Moreover, the authors stated that for multiple dose data the FOCE algorithm in NONMEM^{TM} failed to converge. Standard errors for the central volume of distribution and all variability parameters exceeded 50%. This leads to the conclusion that both a linear one- and two-compartment model are not sufficient to describe linezolid PK, although stated otherwise by the authors. This conclusion was confirmed by own investigations. Examination of the individual concentration-time profiles as well as the measures of central tendency clarified that, firstly, two disposition phases could be identified, indicating the use of a two-compartment model. Secondly, a change in the disposition of linezolid was visible when comparing concentration-time profiles obtained after single dosing to those obtained after multiple dosing, suggesting PK nonlinearity which might presumably be attributed to CL. Fitting a two-compartment model with linear elimination to the data resulted in an overall good fit although small individual concentrations tended to be overestimated. The model misspecification became apparent when plotting weighted residuals against the logarithm of time (figure 7.14), thus making early time points after single dosing visible more clearly. As a result of the underlying assumption of a constant CL for single and multiple dose data concentrations were

underestimated right after giving a dose while they were distinctly overestimated in the drug elimination phase of the first dose.

Models accounting for nonlinearity in CL have been described in the literature as well. The first of these has been presented by Antal et al. [99]. It was a one-compartment model with parallel linear and Michaelis Menten elimination developed based on data from Phase I (number of individuals and data points not mentioned), II (number of individuals: 655, data points: 3238) and III (number of individuals: 232, data points: 729) studies. With a value of 48.0 L for a 50-year old male subject with a WT of 70 kg the volume of distribution was comparable to other values published [84]. Clearance estimation resulted in values of 10.99, 6.96, and 4.51 L/h for concentrations of 1.02, 5.86 and 13.94 µg/mL, respectively. Meagher et al. developed a two-compartment model with parallel linear and Michaelis Menten elimination using an iterative two-stage analysis [100]. They estimated a total V of 65.8 L/65 kg which was slightly higher than in most reports [84]. A combination of the linear and nonlinear elimination resulted in a total average CL of 6.85 L/h/65 kg calculated over the first 7 days of treatment. A model using only a Michaelis Menten process for the description of linezolid CL was presented by Beringer et al. [98] for the description of single dose data obtained after either intravenous or oral administration. Its performance was compared to that of a linear model. They estimated a total V of 55.0 L/70 kg and 42.7 L/70 kg for the saturable and linear elimination model, respectively, which is in accordance with values mentioned in the literature [84]. The maximum elimination rate V_{max} and the Michaelis Menten constant K_m were in the same range as those estimated before [100], resulting in a nonlinear clearance between 4.5-22.1 L/h for concentrations between 0-14 µg/mL. Due to the fact that the study was limited to administering the same dose in every subject and to the fact that data was only available after single dosing, K_m had to be fixed as an estimation of both parameters was not possible. In the linear model CL was estimated to be 11.2 L/h for a subject with a WT of 70 kg.

Although the presented studies all claimed to have successfully described the PK of linezolid some major concerns became apparent: if a model with Michaelis Menten elimination was used, one would expect a decrease in CL with increasing doses as concentration would be a function of dose. However, in the study performed by Antal et al. [99] a plot showing weight-normalised CL against weight-normalised dose reveals that CL varied randomly with differing doses and no clear pattern towards lower CL with higher doses could be observed. Although the model was successfully fit to the data this might be an indication that the Michaelis Menten model theory does not sufficiently explain the PK of linezolid. Meagher et al. [100] reported that CL seemed to change with an increasing number of doses. Unfortunately, the authors did not report if the change in clearance was only observed when plasma concentrations increased or if this change also became apparent in subjects who had similar maximum concentrations after single and multiple dosing. However, they described an apparent change in V_{max} and K_m with increasing doses when applying a model with sole Michaelis Menten elimination. This, however, might also indicate that this type of model still

contained some misspecifications. Finally, the model presented by Beringer et al. [98] was based on single dose data and every subject was given the same dose. The authors concluded that the model with linear elimination and the one with Michaelis Menten elimination performed equally well. However, this is not surprising due to the chosen study design. Since it was not possible to precisely estimate the Michaelis Menten parameters, one of these parameters was fixed. The reliability of the obtained results thus remains questionable. If the authors had investigated multiple doses using different drug amounts, the performance of the two competing models might not have been equal. The last indication that Michaelis Menten elimination was not suitable for the description of linezolid PK was obtained from own investigations. Firstly, examination of the individual concentration-time profiles of some individuals after single and multiple dosing revealed that linezolid disposition changed over time although C_{max} values were almost equal. Even when using a Michaelis Menten model this change in CL would not have been adequately described as the model would only have predicted a difference in CL if C_{max} values had been different. Thus, by mere visual inspection of individual concentration-time profiles the Michaelis Menten model could be excluded from further considerations. Nevertheless, a model with parallel linear and Michaelis Menten elimination was fitted to the available data (model DSA2, section 3.3.5.1.1). When plotting observed concentrations against population predictions, the observed values were not all uniformly spread around the line of unity (figure 7.15). However, as in the studies presented above, the model seemed to describe the concentrations reasonably well although again, small individual concentrations were overestimated. The model misspecification became apparent when plotting weighted residuals against the logarithm of time (figure 7.15). Although the trend was reduced in comparison to the model with linear elimination, concentrations were still overestimated in the drug elimination phase of the first dose as a result of the misspecifications in the description of the drug elimination process. After all these considerations it can be concluded that:

- nonlinearity is involved in the elimination of linezolid and
- the nonlinearity cannot be adequately explained by saturable elimination pathways.

Consequently, other approaches had to be investigated. As direct concentration-dependence could be excluded from further consideration another possible explanation was an auto-inhibition of CL over time. Auto-inhibition of CL has been described in the literature for many different drugs including moclobemide [300], mibefradil [301], propranolol [302], letrozole [303] or ketoconazole [304] and it is usually explained by a reduction of metabolic CL due to e.g. enzymatic down-regulation. However, so far it has not been described for linezolid.

Modelling linezolid CL as a function of time (model DSA4, section 3.3.5.1.1) resulted in an improved model fit. The trend previously observed when plotting weighted residuals against the logarithm of time was eliminated. The data was adequately described by the model. This approach, however, gave no indication as to the reasons for the inhibition. This limitation was overcome by the subsequent more mechanistic approach (model DSA5, sections 3.3.5.1.1 and 3.3.5.1.2). It was

hypothesised that linezolid exerted an inhibitory action – presumably on enzymes responsible for its metabolism – with a changing degree of inhibition over time. To account for this, an additional empirical inhibition compartment was introduced. Consequently, based on the concentrations in this compartment CL was inhibited. This modelling approach was successful as well. The observed concentrations were adequately described by the model.

Most of the estimated parameters corresponded to those presented in the literature before. The total volume of distribution with a value of 46.8 L corresponded to the amount of total body water which indicates a drug distribution into intra- and extracellular fluid compartments. However, the estimate for CL (11.5 L/h) exceeded that of other investigations. Stalker et al. observed a CL of 7.38 L/h after multiple administration of 625 mg of linezolid [79]. Meagher et al. estimated a total average CL of 6.85 L/h/65 kg calculated over the first 7 days of treatment [100]. Another study yielded an even lower value of 4.85 L/h [305]. However, this value was calculated for an individual with a body surface area of 1.73 m^2. In order to correctly interpret the observed higher CL value one has to consider that the CL estimated by the model presented in this thesis was the maximum possible value. This value decreased over time. In consequence, it would only have been applicable for the first dose of linezolid when inhibition is negligible. Considering this, the estimated value of 11.5 L/h well corresponded to e.g. the value of 11.2 L/h estimated by a linear model for a subject with a WT of 70 kg after single dose administration [98]. The decrease in CL was triggered by the parameters VAR and KIC. KIC described the rate of CL inhibition. The estimate of 0.0027 h^{-1} denoted that maximum inhibition was reached after approximately 54 days. The estimate of VAR revealed that CL could be inhibited to 56.7% of its original value. Consequently, CL changed to 6.52 L/h over time, which was in accordance with CL values mentioned above. In conclusion, the different CL estimates at different time points well agreed with other values reported.

In order to explain the CL inhibition the following has to be noted: firstly, one of the major metabolites of linezolid is the hydroxyethyl glycine metabolite (1.1.2.2). It is produced via formation of its precursor hydroxylinezolid [306]. The production of hydroxylinezolid was demonstrated to be dependent on NADPH *in vitro* [77]. Secondly, it was hypothesised that linezolid inhibited mitochondrial activity [307], and only recent investigations provided direct evidence that linezolid induces a dose- and time-dependent decrease of mitochondrial respiratory chain enzyme activity at therapeutic concentrations [308].

These results can be regarded as being closely connected. NADPH is formed in the pentose phosphate pathway. Two molecules of NADP are reduced to NADPH, utilising the energy from the conversion of glucose-6-phosphate into ribulose-5-phosphate. Glucose-6-phosphate originates from the first step of glycolysis. In this process, one phosphate moiety is transferred to glucose under adenosine triphosphate (ATP) consumption. The ATP used for this reaction is produced by complex V of the mitochondrial respiratory chain. It is a product of the citric acid cycle and oxidative phosphorylation which account for 95% of all energy used by aerobic human cells [309].
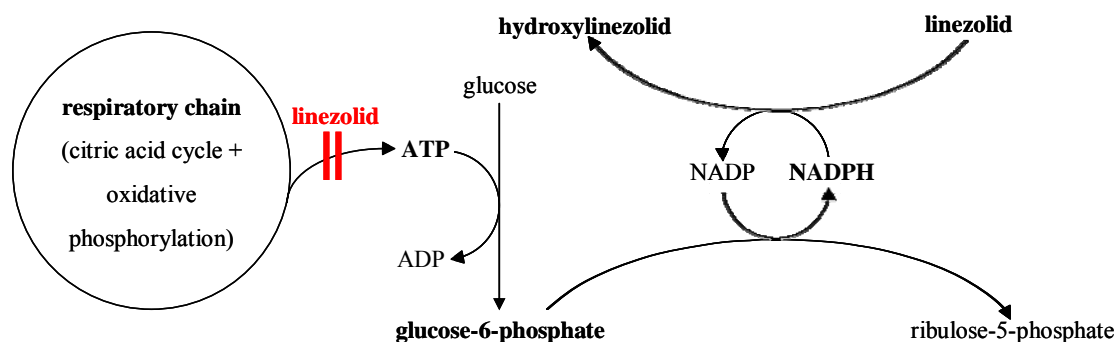
Figure 4.1: Proposed mechanism of linezolid clearance inhibition. Linezolid inhibits its own metabolism via inhibition of the mitochondrial respiratory chain enzyme activity.

In consequence, as NADPH is only produced when glucose-6-phosphate is present and this depends on the presence of ATP obtained from the respiratory chain, the formation of NADPH and consequently the metabolism of linezolid is dependent on the respiratory chain enzyme activity as well. Thus, the hypothesis can be generated that linezolid inhibits its own metabolism via inhibition of the mitochondrial respiratory chain enzyme activity (figure 4.1). It is highly probable that the observed PK nonlinearity is a result of the CL inhibition which is due to the inhibition of the formation of the major linezolid metabolite.

Theoretically, an inhibition of one metabolic pathway may be compensated for an increased second metabolic pathway. However, the given explanation is supported by previous publications. It has been reported that 40% of the administered linezolid dose are eliminated as the hydroxyethyl glycine metabolite via the formation of hydroxylinezolid [74]. The final covariate model estimated an inhibitable clearance fraction of 43.3%. If one assumed that this metabolic pathway was completely inhibited in the course of linezolid treatment the final model estimate supported the proposed mechanism for linezolid clearance inhibition. Moreover, the explanation was in accordance with adverse events observed after longer linezolid treatment. Over time, linezolid might cause myelosuppression (e.g. anaemia, leukopenia and thrombocytopenia) [74]. The formation of blood cells is dependent on the supply of energy in the form of ATP. If linezolid inhibited this essential formation pathway the myelosuppresion might be caused by the same mechanism which was presumably responsible for the nonlinearity in linezolid PK.

So far, this mechanism has not been fully implemented in the population pharmacokinetic model as, until now, CL inhibition has been described as being dependent on linezolid concentrations in an inhibition compartment. In following analyses it might therefore be investigated if the nonlinearity might also be described by using an indirect response model [310]. These models are based on drug effects that either stimulate or inhibit the production or loss of a response variable. The proposed model structures are presented in figure 4.2. The hypothesised model A incorporates the formation of e.g. ATP as a respective variable which could then be inhibited based on linezolid concentrations in the central compartment. The changing amount of intracellular ATP would in turn be responsible for the change in metabolic linezolid CL. For model refinement transit
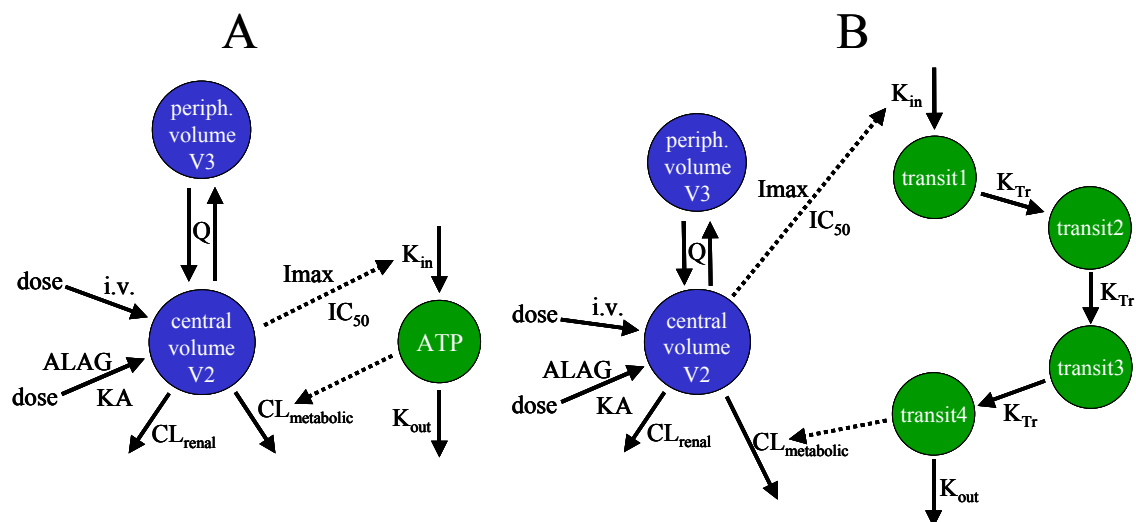
Figure 4.2: Proposed model structures including a mechanistic approach for clearance inhibition. Both models include two CL pathways. The noninhibitable CL corresponds to renal elimination, the inhibitable CL to all metabolic pathways. Thus, inhibition of the metabolic CL would not be expected to be complete as only the formation of metabolite B would be inhibited. Hypothesised model A: The response variable (e.g. ATP) is formed with the rate K_{in} which can be inhibited dependent on linezolid concentrations in the central compartment using a saturable process coded by the parameters Imax and IC_{50}. Loss of the response variable is coded by K_{out}. Hypothesised model B: Model includes transit compartments and an additional rate-constant K_{Tr} which account for time delay between inhibition of ATP formation and inhibition of clearance. The number of transit compartments might reflect the stages of inhibition: mitochondrial inhibiton → ATP → glucose-6-phosphate → NADPH.

compartments might be included (hypothesised model alternative B) to account for the time delay between intracellular ATP formation and decrease of intracellular NADPH concentration. If further studies were conducted one should aim at measuring NADPH blood concentrations in addition to linezolid as this might avail the development of this mechanistic PK model. Moreover, in order to provide evidence for the proposed mechanism of CL inhibition, further studies might aim at measuring the concentrations of the major hydroxyethyl glycine metabolite in plasma as well as other metabolites. In addition, linezolid as well as metabolite measurements in urine might be conducted. This way, the developed model might be extended to a complex parent-metabolite model, which would include the proposed inhibition of metabolite formation.

In the population PK analysis performed for this thesis ISF distribution was described using tissue partition coefficients. These can easily be interpreted, e.g. a PC of 1 would represent complete (100%) distribution, i.e. equal concentrations at steady state, whereas values lower and higher than 1 would indicate lower and higher concentrations at steady state than in plasma, respectively.

The tissue partition coefficient for subcutaneous ISF was estimated to be 1.05, indicating that overall linezolid displayed excellent penetration abilities into this matrix (i.e concentration values of 105% at steady state compared to plasma concentrations). This value was comparable to that obtained by Gee et al. who investigated linezolid penetration into skin by applying the skin blister technique. They estimated a skin penetration of 104% by comparing the AUC values of tissue and plasma after single dosing obtained from a noncompartmental analysis [91]. However, this

approach yields the following problem: as equilibration between plasma and tissue might not be complete at this stage plasma concentrations might over some time have exceeded those in the tissue even if in reality tissue penetration had been equal to 100%. In consequence, this would have resulted in higher AUC values for plasma and thus in an underestimation of tissue penetration. This underestimation might, however, have been compensated for the fact that skin blisters contain proteins, thus the investigation was based on total concentrations. So far it has not been proven that concentrations measured in blister fluid can be transferred to tissue concentrations [158].

With a value of 107% the penetration into muscular ISF was equally promising. Lovering et al. investigated linezolid penetration into muscular tissue after single dosing by applying the biopsy sampling technique [94]. They did not calculate an AUC but instead directly compared concentration values in muscle and plasma at different time points. Thirty minutes after the end of the infusion they estimated a muscle penetration of 93%. Firstly, is has to be stated that a single sample strategy seems to be inadequate in this setting. Secondly, the fact that penetration was determined after single dosing might on the one hand have led to an underestimation of tissue penetration. On the other hand, biopsy samples represent a mixture of different tissue types and, similar to the skin blister method, measure total concentrations. This might lead to an overestimation of tissue penetration. The influence of these two facts is hard to assess. However, they might explain the difference in the observed tissue penetrations. Rana et al. [93] administered 5 doses of linezolid bid and thus presumably attained steady state before taking one muscle biopsy sample. It was obtained 30 minutes after the end of the last linezolid infusion. Muscle penetration was reported to be 83.5%. This value was distinctly lower than the one estimated by the population PK approach in this thesis. In this case the low penetration cannot be explained by nonexisting equilibrium after single dosing as presumably steady state had been reached. One explanation might be, however, that the rate of tissue distribution was relatively small and the low distribution was thus an artefact of an ill chosen sampling time point. It might be possible that the tissue penetration estimate would have been higher if a later sampling time point had been chosen. Nevertheless, all studies investigating the tissue distribution of linezolid reported good penetration abilities. In general, this leads to the conclusion that on average concentrations in muscular and subcutaneous ISF will be sufficient for the treatment of gram-positive infections on the condition that adequate concentrations are reached in plasma. However, to assess if this also applies for all subject subgroups variability has to be taken into account as well. The variability for tissue partition coefficients was estimated to be 44% (IOV) for subcutaneous and 28% (IIV) for muscular ISF, respectively. The resulting individual parameter distribution is presented in figure 7.40. Translating these values into confidence intervals under the assumption of lognormal distribution reveals that in 68% of all occasions subcutaneous ISF penetration will lie between 68% and 163% whereas 16% will have lower ISF penetration estimates. Moreover, 2.5% of all individuals will have an ISF penetration below 44%. When applying the same method to ωPC24 16% of all

individuals will have an ISF penetration of less than 81% and 2.5% will be characterised by a penetration below 61%. These calculations are supported by the individual concentration-time profiles in which one patient had distinctly lower concentrations in both subcutaneous and muscular ISF. As expected, the estimates for PC23 and PC24 in this subject were all in the range of 0.25, yielding an ISF penetration of only 25%. The same variability as observed here was encountered by Rana et al. who observed individual muscle penetration of 45.1-161% [93]. It can therefore be concluded that for some individuals – despite the overall good penetration ability of linezolid – ISF penetration might not be sufficient to efficiently eradicate relevant bacteria.

4.3.3   Covariate influence

The covariate analyses performed for both the model describing unbound plasma concentrations and the joint model for unbound plasma and ISF concentrations revealed a statistically significant influence of WT, CLCR and THRO on the PK of linezolid. These influences will be discussed in the following.

WT was found to influence the parameters V3 and CL. With regard to the population parameter estimate V3 and CL increased by 1.52% and 1.13% per increasing kg of total body weight, respectively. In total, these influences resulted in decreased terminal elimination half-lives and decreased linezolid plasma concentrations with increasing WT (figure 7.28). Linezolid volume of distribution has been described to be dependent on ideal body weight (IBW) [100]. In obese patients IBW can significantly differ from total body weight. However, the authors stated that IBW and total body weight were considered independently and their influence did not differ significantly. Thus, their investigation yielded similar results to those presented here. The increase in V3 with increasing WT is in accordance with both the physicochemical properties of linezolid as well as physiological effects caused by increasing WT. Linezolid has been shown to distribute equally between the intracellular and extracellular space [311]. The extracellular space is known to increase with increasing WT [312]. Under the assumption that larger WT increased the extracellular space, the larger V3 in heavy subjects might be explained by differences in the volume of the extracellular space. Moreover, with an n-octanol-water partition coefficient of 0.55, linezolid displays at least some ability to penetrate into lipophilic tissues. As the proportion of fat will increase with higher WT, which can presumably be assigned to V3, obesity will also exert an influence on V3. Nevertheless, if all other covariates take median values, the influence of the changes in V3 can be regarded as negligible. Simulations were able to demonstrate that average concentrations were not influenced by a change in V3 (see section 3.3.5.4.2). The only difference was observed in minimum and maximum concentrations. The influence of WT on CL, however, was distinctly larger. Simulations were able to show that average concentrations increased by 108% when WT was reduced from 115 to 45.1 kg. These observations are in accordance with those of Meagher et al. [100] who included a linear relation between IBW and CL. Furthermore, other

investigations indicated a relation between WT and linezolid CL [313, 314]. This relation has also been reported for other drugs [315, 316]. A physiological explanation might be that the metabolic capacity of the body is raised with increasing WT [317]. For this reason it has even been recommended to include a relation between WT and CL in any model by default [317-319].

A statistically significant influence of CLCR was identified for the parameter CL. Compared to individuals with median CLCR values, CL was reduced by 31.9% in individuals with severe renal impairment (CLCR = 30 mL/min). This observation corresponded well to the reported fraction of linezolid which was renally eliminated, i.e. 30% [87]. Therefore, the relation identified between CLCR and CL may serve as a measure for the fraction of renal CL. Moreover, the same relation was found by Meagher et al. [100]. Own simulations investigating the influence of CLCR on plasma concentrations revealed that average concentrations increased by 129% when CLCR decreased from 99.0 to 18.4 mL/min. The reduction of CL opposed previous investigations that – despite observing an influence of CLCR on renal CL – did not find any differences in total CL and plasma concentrations [86]. The opposed findings might be explained by the way CL was modelled in this thesis. Every individual CL value was inhibitable to a certain extent over time. Therefore, although a correlation between VAR and CL could not be identified, it might be possible that an influence of e.g. low CLCR on total CL was compensated for a higher value of VAR. In the simulation, this relation would not have been accounted for as the population estimates of the final covariate model were used for all parameters. However, it might also be possible that the differences between healthy volunteers and renally impaired patients were not observed in the other investigations because of a limited data situation due to mere single drug administration. Brier et al. [86] reported that the reduced renal elimination was compensated for increased metabolism. However, they only investigated single dose data. In consequence, they would not have been able to observe the inhibition of metabolism over time, which can be assumed to be even more pronounced if the concentrations of the major metabolites increase. This leads to the conclusion that at the beginning of linezolid treatment the influence of renal function on linezolid PK can be regarded as minimal although it might become increasingly important in the longer course of treatment.

CLCR was also found to have a statistically significant influence on PC24. A direct influence of renal function on the extent to which linezolid penetrates into muscular ISF is hardly conceivable. However, one could imagine that CLCR serves as a surrogate for a covariate that was not investigated. As described in section 1.4 tissue perfusion might be impaired in septic patients due to a redistribution of cardiac output to vital organs such as heart and brain as well as to metabolic acidosis. Therefore, CLCR might serve as a function of illness severity. In this context, the covariate influence seems reasonable.

A similar approach might explain the observed covariate influence of THRO on CL and K40. Again, no reasonable explanation can be given for a direct relation between THRO and drug

elimination or rate of distribution into muscular ISF, respectively. However, THRO might again represent a surrogate for a covariate that was not measured. A reduction in platelet counts was observed in 38% of all subjects. It has been reported that linezolid induced thrombocytopenia over long-term treatment [320-323]. As the production of platelets depends on the energy reservoir of the body it seems to be possible that the underlying mechanism for thrombocytopenia is the same as the one for metabolic CL inhibition, namely the inhibition of the respiratory chain enzyme activity. THRO could therefore serve as an indicator for the extent of metabolic CL inhibition. To reflect this more closely, in future investigations one might aim at investigating a covariate model in which CL depends on thrombocyte changes from an initial baseline value instead of total thrombocyte values.

Moreover, not only is thrombocytopenia observed with linezolid treatment but it is also a common phenomenon during the state of sepsis [324, 325]. As described in section 1.4, sepsis is characterised by increased capillary permeability. In consequence, diffusion barriers might be reduced, which would lead to a faster equilibrium between blood and ISF. Therefore, the relation between THRO and K40 might be explained by platelets being a surrogate for the increased capillary permeability during sepsis.

The covariate analysis did not reveal any statistically significant difference between healthy volunteers and patients with sepsis or septic shock. This result might be unexpected. However, it can be explained by the covariates included in the model, as especially CLCR and THRO can be expected to differ between the investigated subgroups. Therefore, this result indicates that the difference between healthy volunteers and patients is not random but measurable, which might prove to be even more valuable than a mere unexplained difference between these subject subgroups if the covariate relations were used for dose selection purposes.

'Worst-case scenario' simulations of unbound plasma concentrations revealed that lightweight patients with high CLCR and thrombocyte values would potentially show the highest risk of having subinhibitory linezolid concentrations. This contradicted the results of the simulations that investigated the influence of WT alone, resulting in heavy subjects having the lowest concentrations. However, this can be explained by the increasing CL in the 'worst-case scenario' that is due to the additional influences of CLCR and THRO. In this setting, a heavy individual might profit from increased V3 as this would result in a lower amount of the drug being available for elimination in the central compartment. Thus, if CLCR and thrombocyte values are high the influence of WT is reversed. Accordingly, the same opposing observation was made when simulating the highest possible concentrations. In a heavy individual with low CLCR and thrombocyte values less drug would be available for elimination which would result in a higher risk of toxic linezolid concentrations. The clinical relevance of these findings was determined by investigating observed covariate combinations (see section 3.3.5.4.5). The results showed that some of the investigated subjects might potentially have been underdosed whereas the risk of toxic

concentrations seemed to be minimal. Dose selection based on covariate values might therefore mainly reduce the risk of subinhibitory concentrations. In this case it would, however, be advisable to always consider all found covariate relations.

When contemplating covariate influences on PK parameters one should bear in mind that the covariate analysis was performed with only 34 subjects. The case-deletion procedure performed for model evaluation (see section 3.3.5.3.3 and 3.3.6.3.3) revealed that some covariate relations were largely influenced by a single subject. It has been shown that, especially for highly correlated covariates, covariate selection bias can be quite high when a covariate analysis is based on datasets containing less than 50 subjects [326]. This does not necessarily mean that the relations found would not be observed when using a bigger dataset. Nevertheless, it might be possible that the significance of a weak covariate was increased by the low number of investigated subjects. Before using the covariate relations for the prediction of concentration-time profiles it would therefore be advisable to investigate the respective covariates in a larger patient population. Moreover, so far simulations did not take any parameter variability into account. Further simulations using e.g. Pharsight® Trial Simulator might help to investigate the significance of found covariate relations by comparing the 95% confidence intervals of simulated concentration-time profiles using different covariate values. If these demonstrated that the 95% confidence intervals obtained from differing covariate values did not overlap, it might provide evidence for a true influence of the respective covariate.

4.3.4   Model evaluation

The developed population PK model was evaluated in terms of its accuracy and precision, its ability to predict concentration-time profiles in plasma and ISF and the influence of single individuals on PK parameters.

In general, unbound plasma concentrations were better described than data obtained from microdialysis measurements. An explanation might be that microdialysis concentration-time profiles were not as smooth as the ones obtained for unbound plasma concentrations. This might be due to the larger intraindividual variability in microdialysate concentrations due to fluctations in relative recovery and perfusate flow rate. Therefore, this observation was expected.

PK parameters were estimated with acceptable accuracy and precision with the exception of parameters describing absorption after oral dosing. In addition, precision was initially estimated to be low for $\omega PC24$ and some covariate influences. The bias and imprecison of parameters connected with linezolid absorption – namely KA and ωKA – can be explained by the lack of data after oral dosing. Only 9 individuals provided oral data after one dosing occasion, which corresponds to only 15% of all available data. Nevertheless, the population value of KA with an estimate of 1.85 h^{-1} was in the same range as previously reported values. Previously, KA was estimated with values of

0.750 h^{-1} [98], 0.802 h^{-1} [99] and 5.73 h^{-1} [100]. However, large variability in KA estimates of previous reports could be observed, which might be due to differences in model structures.

The low initial precision of the other mentioned parameters was rebutted by performing a log-likelihood profiling. Using this approach the determined 95% confidence intervals did not include zero. It can therefore be concluded that the precision for these parameters was higher than originally predicted and therefore sufficient to legitimate their presence in the model.

Evaluation revealed that the parameter estimates KIC, θ_{CLCR_CL}, θ_{WT_CL}, $\omega PC24$ and θ_{THRO_K40} were extremely influenced by single individuals. While θ_{CLCR_CL} and θ_{WT_CL} should be reinvestigated with more individuals the influence of KIC, $\omega PC24$ and θ_{THRO_K40} on the concentration-time profiles could be regarded as rather small. Using a larger patient population might therefore result in slightly different nominal values for these parameters but would not influence overall model predictions. The largest influence on the prediction of concentration-time profiles was exerted by ωVAR. As soon as this variability was included the 90% prediction interval by far exceeded the range of observations. In order to be able to use the model for predicting concentrations one should therefore ignore variability of this parameter and assume that CL is inhibited to the same extent in every individual. Although this would represent a simplification of the results it could be demonstrated that this approach results in an accurate prediction of unbound plasma concentration-time profiles.

For ISF concentrations the simulations resulted in slight overpredictions and C_{max} values were lower than predicted and could be observed later than anticipated. Population PK models can be used as a means to determine optimal dosing strategies for a specific group of patients [327]. If the observed predictions were used in a clinical setting this might have the following consequences: actual concentrations would be slightly below those predicted by the model. Overall, this might result in less efficacy of linezolid than originally anticipated. In the worst case this could lead to treatment failure and the promotion of drug resistance. However, the trend to overprediction was not very pronounced. The estimation of C_{max} values in the ISF might be improved by introducing transit compartments [328, 329] between the central and the respective ISF compartment. This would lead to a delay in ISF distribution and would thus more closely resemble the observed profiles. However, as the implementation of transit compartments is connected with an exponential increase in CPU time it was not feasible to use this approach for further model improvement.

4.3.5 Optimised sampling design

An optimised sampling design for plasma as well as microdialysis in subcutaneous and muscle ISF was suggested to provide a basis for further clinical trials investigating the PK of linezolid. For plasma it could be demonstrated that the number of samples can be reduced from 40 to 6 per individual without loosing any information necessary for estimating all PK parameters. For microdialysis ISF measurements, the design could be reduced even further. By using only 4

samples per individual and matrix it was possible to obtain similar parameter estimates and parameter precision as with the original design.

Although this is the first optimal design application using a model for linezolid, this strategy has been applied for other drugs. Waterhouse et al. optimised a plasma sampling design for a study investigating itraconazole PK in cystic fibrosis patients [330]. As for the linezolid model they also assumed a study population of 30 individuals and divided this population into 3 groups. Some of the PK parameters had to be fixed due to long calculation times. The number of samples equated the number of estimated parameters which corresponded to the optimised design for linezolid. An advantage of their design was the estimation of sampling intervals and the consideration of two different competing models. The optimal sampling design has also been used in drug development. Here, optimal blood sampling time intervals were determined that would then be used in a prospective phase II study [331]. The developed design comprised different groups with differing sampling time points and dose amounts.

When applying the reduced sampling desing to the developed linezolid PK model, precision of ωK40 was impaired. However, this went along with increased precision for ωPC24. As ωPC24 can be regarded to be the more meaningful parameter – in the sense that a difference in PC24 will influence concentration-time profiles in muscle ISF more than a difference in K40 – it can be concluded that the impaired precision of ωK40 should be preferred to imprecision of ωPC24. Therefore, despite the low precision of one single parameter the reduced design for microdialysis sampling can be accepted. For microdialysis measurements, similar precision might even have been obtained with only 2 samples per matrix. However, in that case it would not have been possible to account for IOV as for this type of variability at least two samples have to be taken at different occasions. Therefore, in order to preserve the option of IOV estimation it was decided that 4 samples (2x2 at different occasions) should be taken instead.

The obtained sampling design was evaluated by simulating only one dataset and re-estimating the PK parameters of this single dataset. In order to obtain accurate information about the resulting PK parameters and their precision it would be preferable to simulate at least 100 datasets and estimate the parameters from each of them (compare to section 2.7.7.2). However, as this would have resulted in unacceptable run times this approach was not pursued. Nevertheless, the obtained results demonstrate the feasibility of the reduced sampling approach.

In further analyses the developed design might be advanced further in terms of improving its applicability in a clinical trial. One option, which is also available in POPT®, might be the estimation of sampling intervals as it would be quite probable in clinical routine that actual sampling time points might differ slightly from planned ones. This option would ensure that it would still be possible to estimate all PK parameters with sufficient precision. Moreover, after having fit one of the proposed mechanistic PK models (see section 4.3.1) to the data collected in this trial, it might be advisable to consider this model in a competing model approach also available

in POPT®. If two different models were considered in POPT® this would assure that the chosen sampling time points for further trials would support either of the two models.

4.3.6   Practical model implementation and perspectives

The performed clinical trial was a pilot project and was therefore only conducted with a small number of individuals. Because microdialysis is not yet accepted to be a standard procedure, which allows for measurements without highly harming the patient, its feasibility had to be demonstrated in a small setting. Using the thus obtained data, the PK of linezolid in a population of both healthy volunteers and septic patients was successfully described in plasma and ISF. In a further trial it would be desirable to investigate linezolid PK in a larger patient population. This way, covariate relations would be confirmed and influences of single individuals on some of the PK parameter estimates might be reduced. Moreover, the inclusion of further study subjects might help to successfully apply a more mechanistic indirect response model as suggested in section 4.3.2. Subsequent studies might profit from the developed optimised sampling design. Instead of having to take a total of 120 samples per patient this number might be reduced to 14 without any loss in information. The burden on the patients would be significantly reduced and the conduction of the clinical study would be facilitated. Moreover, a trial using minimal design would also interfere less with clinical routine. It would therefore contribute to a higher acceptance of the trial by hospital personnel. The developed model might then be used to estimate the PK parameters of linezolid based on data from more individuals. This way, covariate relations might be investigated more closely and thus be confirmed with a larger dataset. If samples were also taken after oral dosing, this would also contribute to minimise bias in the estimation of parameters related to gastrointestinal absorption.

It could be demonstrated that the model might also serve as a tool to predict concentration-time profiles of linezolid. Thus, based on demographic and laboratory data such as WT, CLCR and THRO it might be possible to identify subgroups of patients that are at higher risk of suffering from subinhibitory or toxic linezolid concentrations. Simulations using actual subject's covariate values (section 3.3.5.4.5) revealed that in the studied population highest concentrations were predicted for those individuals with CLCR and THRO values below the reference range and WT close to the median value. This corresponded to results from worst-case scenario simulations (section 3.3.5.4.4). Low concentrations were obtained for individuals with median WT, low CLCR and extremely high THRO values or higher WT, high CLCR values and low THRO values, i.e. no clear pattern was observable. However, none of the investigated subjects had a combination of covariate values as obtained in the worst-case scenario simulations. Therefore, the risk of subinhibitory concentrations might be assessable more closely using data from more individuals. After the covariate relations have been confirmed in further trials it would be possible to use the model and the found covariate relations for an individualised antimicrobial therapy. This might be especially

important in septic patients as it has been demonstrated that rational therapy from the beginning of treatment is a main predictor for the therapeutic outcome in this population [332].

The major goal of antimicrobial therapy is, of course, not to attain a certain drug concentration in the body but to successfully treat an infection. Thus, further investigations should aim at describing the relation between PK and PD of linezolid. The pharmacodynamics of an antimicrobial agent can be described by pharmacodynamic indices such as AUC/MIC_{90} [297]. Initial evaluations were conducted by calculating the AUC for a typical individual after single and multiple dosing and relating it to a MIC_{90} value of 2 µg/mL. The resulting AUC/MIC_{90} ratios were 26.1 and 46.0 for single and multiple dosing, respectively. For a MIC_{90} value of 4 µg/mL they would be even lower. This might indicate that the standard dosing regimen might not be sufficient to eradicate relevant bacteria. This should be investigated further, e.g. by applying time-kill curve methodology. In this setting, the PK of linezolid as described by the PK model would be simulated *in vitro* and the effect on bacterial growth would be assessed. It would then be possible to combine all available data in a model for the simultaneous description of both PK and PD. This model might then be used to predict therapeutical success in a given patient population for a given dose.

5   Conclusions

Antibiotics such as vancomycin and linezolid are used for the treatment of serious infections caused by problematic pathogens such as MRSA. However, in the last years bacterial resistance even to these reserve treatments has increased dramatically. One reason might be that only subinhibitory concentrations are reached in some individuals that lead to the promotion of drug resistance. In order to preserve the effectiveness of antiinfectives one should therefore aim to attain adequate concentrations at the site of action. In consequence, pharmacokinetics plays a fundamental role in the prevention of antibiotic resistance.

This thesis aimed at investigating three major projects, which are summarised in figure 5.1.
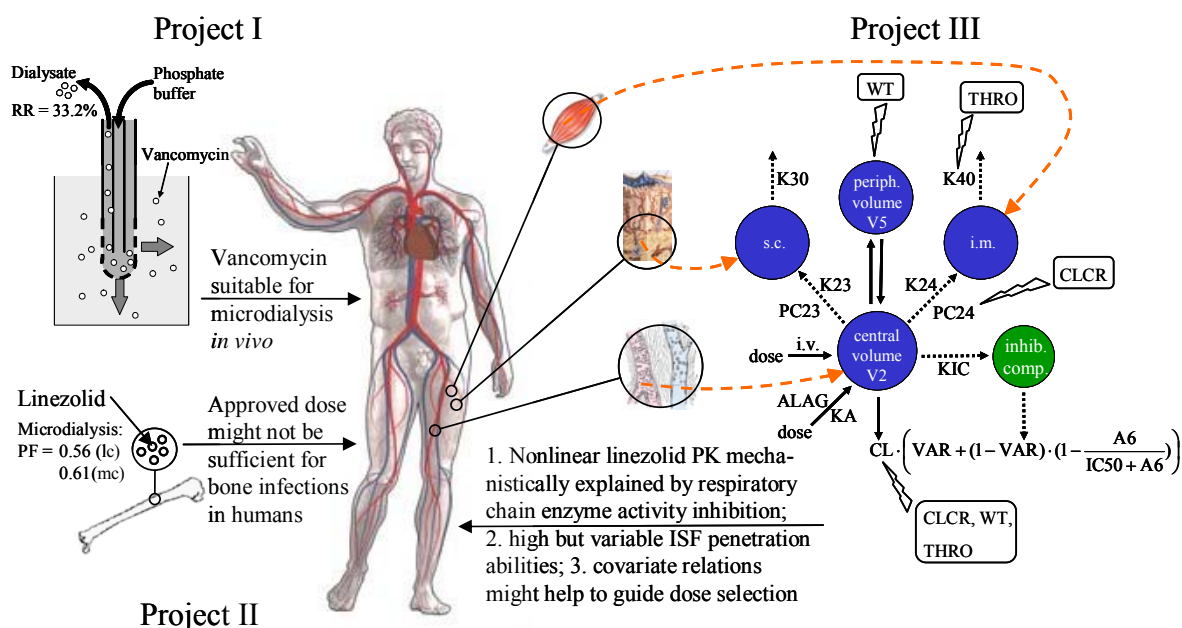
Figure 5.1: Summary of main results obtained in thesis

Firstly, an analytical assay for the determination of vancomycin in plasma and microdialysate was developed, which was characterised by fast and efficient quantification ability from small sample volumes like those obtained during microdialysis experiments. The developed method met the criteria for analytical method validation specified by the FDA. Subsequently, it was explored if vancomycin was suitable for being used in microdialysis studies, a prerequisite for studying unbound drug concentrations directly in the ISF of interest. Microdialysis investigations revealed an expected flow rate dependency. Further experiments showed that vancomycin microdialysis could not be applied using Ringer's solution as a perfusate. Vancomycin displayed an unwanted concentration dependency in microdialysis recovery experiments which, however, could be overcome by perfusing the probe with phosphate buffer. In summary, the presented results regarding both the analytical assay and the microdialysis experiments for vancomycin established the basis for investigating the ISF pharmacokinetics of vancomycin in an *in vivo* setting.

Secondly, an existing analytical assay for linezolid was extended to the matrices urine, bone marrow, bone biopsy samples and bone microdialysate. In the second project, the feasibility of microdialysis in bone tissue was assessed. It could be demonstrated that microdialysis is viable even in a hardly accessible matrix such as bone. Moreover, it is superior to the highly invasive biopsy sampling technique which only measures total drug concentrations and which, due to the resulting units, cannot be easily interpreted and compared to other matrices.

The pharmacokinetics of linezolid in bone tissue was determined in an *in vivo* setting using a noncompartmental analysis method in order to determine if adequate linezolid concentrations for the treatment of bone infections are reached in this matrix. The PK analysis revealed that plasma and bone marrow displayed similar kinetics. On the contrary, bone microdialysis measurements evinced that linezolid did not penetrate into bone to the extent that might have been expected from biopsy results. Although the study was only conducted over a time period of 6 h it indicated that the given dose might not be sufficient for the treatment of bone infections in both animals and humans. After having demonstrated the feasibility of the microdialysis technique in bone ISF further experiments should be conducted investigating this issue, preferably over a longer time period.

The main focus was placed on the conduction of a clinical trial that dealt with investigating the PK of unbound linezolid in plasma, subcutaneous and muscular ISF of healthy volunteers and septic patients after single and multiple dosing. Linezolid PK was described by means of a population PK model. Unbound plasma concentrations were characterised by a two-compartment model with linear absorption after oral administration. The observed nonlinearity, which presumably might be due to an inhibition of the respiratory chain enzyme activity in the course of linezolid treatment, was accounted for by introducing an empirical inhibition compartment. Linezolid CL, which was estimated to be 11.5 L/h, decreased over time to a value of 6.5 L/h, depending on the concentration in this empirical compartment. The developed model was shown to be superior to other previously published models describing linezolid PK in plasma. However, concentration predictions could only be attained if variability on the parameter VAR was ignored. This limitation might be overcome by applying a more mechanistic indirect response model as suggested in section 4.3.2. ISF concentrations were implemented by the use of two additional compartments that were coded using monodirectional rate-constants and partition coefficients. Overall, linezolid displayed good penetration abilities into both subcutaneous and muscular ISF. However, the analysis also revealed that due to the large variability in ISF penetration for some individuals concentrations reached in the ISF might not be sufficient to efficiently eradicate relevant bacteria. Model predictions for ISF C_{max} values were higher than observed. Better predictions might be obtained by introducing transit compartments. The covariate analysis identified CLCR, WT and THRO as having a significant influence on the parameters CL, V3, rate into the muscular compartment and on the partition coefficient into muscular ISF. While CLCR and WT could directly be linked to the respective PK

parameter it can be assumed that THRO represented a surrogate of a covariate that was not investigated in this study, e.g. other measures of illness severity or inhibition of NADPH production. Overall, the covariates were able to explain a part of the observed variability in the PK parameters. However, as the study population consisted of only 34 individuals it is recommended to investigate the found covariate influences in a larger setting before using them as a guidance for a more individualised antibiotic therapy. An investigation of linezolid PK in more individuals might also reduce the observed influence of single individuals on some of the PK parameter estimates and reduce the bias in PK parameters related to gastrointestinal absorption. A successive clinical trial might profit from the developed optimised study design, which was characterised by a reduction of total samples from 120 to 14 per individual without any loss of information. Based on the results from this subsequent study, the developed model might be used to predict linezolid concentrations at the site of infection and thus it might be used for a more targeted antimicrobial therapy. Not only would this help to improve individual therapy and outcome but it would also prevent further development of antimicrobial resistance – one of the most challenging problems in the ongoing combat against bacterial infections.

6 Bibliography

[1]   Berger-Bachi B: Resistance mechanisms of gram-positive bacteria. *Int J Med Microbiol*. **292**: 27-35 (2002).

[2]   Elsayed S, Laupland KB: Emerging gram-positive bacterial infections. *Clin Lab Med*. **24**: 587-603 (2004).

[3]   Schimpff SC, Gaya H, Klastersky J, Tattersall MH, Zinner SH: Three antibiotic regimens in the treatment of infection in febrile granulocytopenic patients with cancer. The EORTC international antimicrobial therapy project group. *J Infect Dis*. **137**: 14-29 (1978).

[4]   Cometta A, Calandra T, Gaya H, Zinner SH, de Bock R, Del Favero A, Bucaneve G, Crokaert F, Kern WV, Klastersky J, Langenaeken I, Micozzi A, Padmos A, Paesmans M, Viscoli C, Glauser MP: Monotherapy with meropenem versus combination therapy with ceftazidime plus amikacin as empiric therapy for fever in granulocytopenic patients with cancer. The International Antimicrobial Therapy Cooperative Group of the European Organization for Research and Treatment of Cancer and the Gruppo Italiano Malattie Ematologiche Maligne dell'Adulto Infection Program. *Antimicrob Agents Chemother*. **40**: 1108-1115 (1996).

[5]   Klastersky J: Treatment of neutropenic infection: trends towards monotherapy? *Support Care Cancer*. **5**: 365-370 (1997).

[6]   Ramphal R: Changes in the etiology of bacteremia in febrile neutropenic patients and the susceptibilities of the currently isolated pathogens. *Clin Infect Dis*. **39 Suppl 1**: S25-31 (2004).

[7]   Clark NM, Hershberger E, Zervosc MJ, Lynch JP, 3rd: Antimicrobial resistance among gram-positive organisms in the intensive care unit. *Curr Opin Crit Care*. **9**: 403-412 (2003).

[8]   Chaix C, Durand-Zaleski I, Alberti C, Brun-Buisson C: Control of endemic methicillin-resistant Staphylococcus aureus: a cost-benefit analysis in an intensive care unit. *J Am Med Assoc*. **282**: 1745-1751 (1999).

[9]   Carmeli Y, Eliopoulos G, Mozaffari E, Samore M: Health and economic outcomes of vancomycin-resistant enterococci. *Arch Intern Med*. **162**: 2223-2228 (2002).

[10]   Howard DH, Scott RD, 2nd, Packard R, Jones D: The global impact of drug resistance. *Clin Infect Dis*. **36**: S4-10 (2003).

[11]   Geffers C, Zuschneid I, Sohr D, Ruden H, Gastmeier P: Erreger nosokomialer Infektionen auf Intensivstationen: Daten des Krankenhaus-Infektions-Surveillance-Systems (KISS) aus 274 Intensivstationen. *Anasthesiol Intensivmed Notfallmed Schmerzther*. **39**: 15-19 (2004).

[12]   Jones RN: Resistance patterns among nosocomial pathogens: trends over the past few years. *Chest*. **119**: 397S-404S (2001).

[13]   Kyne L, Sougioultzis S, McFarland LV, Kelly CP: Underlying disease severity as a major risk factor for nosocomial Clostridium difficile diarrhea. *Infect Control Hosp Epidemiol*. **23**: 653-659 (2002).

[14]   Pingleton SK: Enteral nutrition as a risk factor for nosocomial pneumonia. *Eur J Clin Microbiol Infect Dis*. **8**: 51-55 (1989).

[15]   Drakulovic MB, Torres A, Bauer TT, Nicolas JM, Nogue S, Ferrer M: Supine body position as a risk factor for nosocomial pneumonia in mechanically ventilated patients: a randomised trial. *Lancet*. **354**: 1851-1858 (1999).

[16]   Craven DE, Goularte TA, Make BJ: Contaminated condensate in mechanical ventilator circuits. A risk factor for nosocomial pneumonia? *Am Rev Respir Dis*. **129**: 625-628 (1984).

[17]   Bueno Cavanillas A, Rodriguez-Contreras R, Delgado Rodriguez M, Moreno Abril O, Lopez Gigosos R, Guillen Solvas J, Galvez Vargas R: Preoperative stay as a risk factor for nosocomial infection. *Eur J Epidemiol*. **7**: 670-676 (1991).

[18]   White RL, Friedrich LV, Mihm LB, Bosso JA: Assessment of the relationship between antimicrobial usage and susceptibility: differences between the hospital and specific patient-care areas. *Clin Infect Dis*. **31**: 16-23 (2000).

[19]   Hauer T, Lacour M, Gastmeier P, Schulgen G, Schumacher M, Ruden H, Daschner F: Nosokomiale Infektionen auf Intensivstationen. Eine bundesweite Prävalenzstudie (NIDEP). *Anaesthesist*. **45**: 1184-1191 (1996).

[20]   Luzzati R, Antozzi L, Bellocco R, Del Bravo P, Mirandola M, Procaccio F, Cirillo FM, Romiti P, Sarti A, Manani G, Concia E: [Prevalence of nosocomial infections in Intensive Care Units in Triveneto area, Italy]. *Minerva Anestesiol*. **67**: 647-652 (2001).

[21]   Esen S, Leblebicioglu H: Prevalence of nosocomial infections at intensive care units in Turkey: a multicentre 1-day point prevalence study. *Scand J Infect Dis*. **36**: 144-148 (2004).

[22]   Gastmeier P, Meyer E, Schwab F, Geffers C, Ruden H, Daschner F: KISS und SARI: Benchmarking und Referenzdaten für Krankenhausinfektionen, Antibiotika-Verbrauch und Resistenz auf deutschen Intensivstationen. *Intensivmed*. **41**: 133-138 (2004).

[23]   Gerberding JL, McGowan JE, Jr., Tenover FC: Emerging nosocomial infections and antimicrobial resistance. *Curr Clin Top Infect Dis*. **19**: 83-98 (1999).

[24]   Jones RN: Global epidemiology of antimicrobial resistance among community-acquired and nosocomial pathogens: a five-year summary from the SENTRY Antimicrobial Surveillance Program (1997-2001). *Semin Respir Crit Care Med*. **24**: 121-134 (2003).

[25]   Diekema DJ, Pfaller MA, Schmitz FJ, Smayevsky J, Bell J, Jones RN, Beach M: Survey of infections due to Staphylococcus species: frequency of occurrence and antimicrobial susceptibility of isolates collected in the United States, Canada, Latin America, Europe, and the Western Pacific region for the SENTRY Antimicrobial Surveillance Program, 1997-1999. *Clin Infect Dis*. **32 Suppl 2**: S114-S132 (2001).

[26]   McGowan JE: The impact of changing pathogens of serious infections in hospitalized patients. *Clin Infect Dis*. **31 Suppl 4**: S124-S130 (2000).

[27]   Tiemersma EW, Bronzwaer SL, Lyytikainen O, Degener JE, Schrijnemakers P, Bruinsma N, Monen J, Witte W, Grundman H: Methicillin-resistant Staphylococcus aureus in Europe, 1999-2002. *Emerg Infect Dis*. **10**: 1627-1634 (2004).

[28]   National Nosocomial Infections Surveillance (NNIS) System Report, Data Summary from January 1992-June 2001, issued August 2001. *Am J Infect Control*. **29**: 404-421 (2001).

[29]   Vincent JL, Bihari DJ, Suter PM, Bruining HA, White J, Nicolas-Chanoin MH, Wolff M, Spencer RC, Hemmer M: The prevalence of nosocomial infection in intensive care units in Europe. Results of the European Prevalence of Infection in Intensive Care (EPIC) Study. EPIC International Advisory Committee. *J Am Med Assoc*. **274**: 639-644 (1995).

[30]   Romero-Vivas J, Rubio M, Fernandez C, Picazo JJ: Mortality associated with nosocomial bacteremia due to methicillin-resistant Staphylococcus aureus. *Clin Infect Dis*. **21**: 1417-1423 (1995).

[31]   Eguia JM, Chambers HF: Methicillin-resistant staphylococci and their treatment in the intensive care unit. *Semin Respir Crit Care Med*. **24**: 37-48 (2003).

[32]   Hiramatsu K, Hanaki H, Ino T, Yabuta K, Oguri T, Tenover FC: Methicillin-resistant Staphylococcus aureus clinical strain with reduced vancomycin susceptibility. *J Antimicrob Chemother*. **40**: 135-136 (1997).

[33]   Goldrick B: First reported case of VRSA in the United States. *Am J Nurs*. **102**: 17 (2002).

[34]   Apfalter P: MRSA/MRSE-VISA/GISA/VRSA-PRP-VRE: Aktuelle gram-positive Problemkeime und ihre Resistenzmechanismen, Pravalenz und klinische Konsequenz. *Wien Med Wochenschr*. **153**: 144-147 (2003).

[35]   Bartley J: First case of VRSA identified in Michigan. *Infect Control Hosp Epidemiol*. **23**: 480 (2002).

[36]   Spiers KM, Zervos MJ: Telithromycin. *Expert Rev Anti Infect Ther*. **2**: 685-693 (2004).

[37]   Shah PM: The need for new therapeutic agents: what is the pipeline? *Clin Microbiol Infect*. **11 Suppl 3**: 36-42 (2005).

[38]   Livermore DM: Tigecycline: what is it, and where should it be used? *J Antimicrob Chemother*. **56**: 611-614 (2005).

[39]   Nathwani D: Tigecycline: clinical evidence and formulary positioning. *Int J Antimicrob Agents*. **25**: 185-192 (2005).

[40]   Blondeau JM, Sanche SE: Quinupristin/dalfopristin. *Expert Opin Pharmacother*. **3**: 1341-1364 (2002).

[41]   Akins RL, Haase KK: Gram-positive resistance: pathogens, implications, and treatment options: insights from the Society of Infectious Diseases Pharmacists. *Pharmacotherapy*. **25**: 1001-1010 (2005).

[42]   Plouffe JF: Emerging therapies for serious gram-positive bacterial infections: a focus on linezolid. *Clin Infect Dis*. **31 Suppl 4**: S144-S149 (2000).

[43]   *Europäisches Arzneibuch*. 4 ed. Deutscher Apotheker Verlag, Stuttgart (2002).

[44]   Reynolds JEF: editor. *Martindale - The Extra Pharmacopoeia*. 30 ed. The Pharmaceutical Press, London (1993).

[45]   Pfeiffer RR: Structural features of vancomycin. *Clin Infect Dis*. **3 suppl**: S205-S209 (1981).

[46]   *United States Pharmacopeia*. 26 ed. United States Pharmacopeial Convention, Rockville (2003).

[47]   Lilly: Vancomycin product information for healthcare professionals. Gießen: Lilly Deutschland GmbH (2002).

[48]   Matzke GR, Zhanel GG, Guay DR: Clinical pharmacokinetics of vancomycin. *Clin Pharmacokinet*. **11**: 257-282. (1986).

[49]   Lamer C, de Beco V, Soler P, Calvat S, Fagon JY, Dombret MC, Farinotti R, Chastre J, Gibert C: Analysis of vancomycin entry into pulmonary lining fluid by bronchoalveolar lavage in critically ill patients. *Antimicrob Agents Chemother*. **37**: 281-286. (1993).

[50]   Georges H, Leroy O, Alfandari S, Guery B, Roussel-Delvallez M, Dhennain C, Beaucaire G: Pulmonary disposition of vancomycin in critically ill patients. *Eur J Clin Microbiol Infect Dis*. **16**: 385-388. (1997).

[51]   Kitzes-Cohen R, Farin D, Piva G, Ivry S, Sharony R, Amar R, Uretzky G: Pharmacokinetics of vancomycin administered as prophylaxis before cardiac surgery. *Ther Drug Monit*. **22**: 661-667. (2000).

[52]   Luzzati R, Sanna A, Allegranzi B, Nardi S, Berti M, Barisoni D, Concia E: Pharmacokinetics and tissue penetration of vancomycin in patients undergoing prosthetic mammary surgery. *J Antimicrob Chemother*. **45**: 243-245. (2000).

[53]   Krivoy N, Yanovsky B, Kophit A, Zaher A, Bar-El Y, Adler Z, Gaitini L, Milo S: Vancomycin sequestration during cardiopulmonary bypass surgery. *J Infect*. **45**: 90-95. (2002).

[54]   Sun H, Maderazo EG, Krusell AR: Serum protein-binding characteristics of vancomycin. *Antimicrob Agents Chemother*. **37**: 1132-1136. (1993).

[55]   Cutler NR, Narang PK, Lesko LJ, Ninos M, Power M: Vancomycin disposition: the importance of age. *Clin Pharmacol Ther*. **36**: 803-810. (1984).

[56]   Yasuhara M, Iga T, Zenda H, Okumura K, Oguma T, Yano Y, Hori R: Population pharmacokinetics of vancomycin in Japanese adult patients. *Ther Drug Monit*. **20**: 139-148 (1998).

[57]   Buelga DS, del Mar Fernandez de Gatta M, Herrera EV, Dominguez-Gil A, Garcia MJ: Population pharmacokinetic analysis of vancomycin in patients with hematological malignancies. *Antimicrob Agents Chemother*. **49**: 4934-4941 (2005).

[58]   Hammes WP, Neuhaus FC: On the mechanism of action of vancomycin: inhibition of peptidoglycan synthesis in Gaffkya homari. *Antimicrob Agents Chemother*. **6**: 722-728 (1974).

[59]   Perkins HR, Nieto M: The chemical basis for the action of the vancomycin group of antibiotics. *Ann New York Acad Sci*. **235**: 348-363 (1974).

[60] Kuzin AP, Sun T, Jorczak-Baillass J, Healy VL, Walsh CT, Knox JR: Enzymes of vancomycin resistance: the structure of D-alanine-D-lactate ligase of naturally resistant Leuconostoc mesenteroides. *Structure*. **8**: 463-470 (2000).

[61] Sakoulas G, Moise-Broder PA, Schentag J, Forrest A, Moellering RC, Jr., Eliopoulos GM: Relationship of MIC and bactericidal activity to efficacy of vancomycin for treatment of methicillin-resistant Staphylococcus aureus bacteremia. *J Clin Microbiol*. **42**: 2398-2402 (2004).

[62] Hammett-Stabler CA, Johns T: Laboratory guidelines for monitoring of antimicrobial drugs. National Academy of Clinical Biochemistry. *Clin Chem*. **44**: 1129-1140 (1998).

[63] Jacqueline C, Caillon J, Le Mabecque V, Miegeville AF, Donnio PY, Bugnon D, Potel G: In vitro activity of linezolid alone and in combination with gentamicin, vancomycin or rifampicin against methicillin-resistant Staphylococcus aureus by time-kill curve methods. *J Antimicrob Chemother*. **51**: 857-864 (2003).

[64] Jones RN: Microbiological features of vancomycin in the 21st century: minimum inhibitory concentration creep, bactericidal/static activity, and applied breakpoints to predict clinical outcomes or detect resistant strains. *Clin Infect Dis*. **42 Suppl 1**: S13-S24 (2006).

[65] Lundstrom TS, Sobel JD: Antibiotics for gram-positive bacterial infections: vancomycin, quinupristin-dalfopristin, linezolid, and daptomycin. *Infect Dis Clin North Am*. **18**: 651-668, x (2004).

[66] Launay-Vacher V, Izzedine H, Mercadal L, Deray G: Clinical review: use of vancomycin in haemodialysis patients. *Crit Care*. **6**: 313-316. Epub 2002 Jun 2010. (2002).

[67] EUCAST: Glycopeptides - EUCAST clinical MIC breakpoints. (2006); available from: *www.srga.org/eucastwt/MICTAB/MICglycopeptides.html* [accessed 03 November 2006].

[68] Kaplan SL, Deville JG, Yogev R, Morfin MR, Wu E, Adler S, Edge-Padbury B, Naberhuis-Stehouwer S, Bruss JB: Linezolid versus vancomycin for treatment of resistant Gram-positive infections in children. *Pediatr Infect Dis J*. **22**: 677-686 (2003).

[69] Weigelt J, Itani K, Stevens D, Lau W, Dryden M, Knirsch C: Linezolid versus vancomycin in treatment of complicated skin and soft tissue infections. *Antimicrob Agents Chemother*. **49**: 2260-2266 (2005).

[70] Begg EJ, Barclay ML, Kirkpatrick CM: The therapeutic monitoring of antimicrobial agents. *Br J Clin Pharmacol*. **52 Suppl 1**: 35S-43S (2001).

[71] Toyoguchi T, Nakagawa Y, Watanabe H: [Nephrotoxicity and drug interaction of vancomycin]. *Nippon Yakurigaku Zasshi*. **107**: 53-66 (1996).

[72] Toyoguchi T, Nakagawa Y: [Nephrotoxicity and drug interaction of vancomycin (2)]. *Nippon Yakurigaku Zasshi*. **107**: 225-235 (1996).

[73] Toyoguchi T, Takahashi S, Hosoya J, Nakagawa Y, Watanabe H: Nephrotoxicity of vancomycin and drug interaction study with cilastatin in rabbits. *Antimicrob Agents Chemother*. **41**: 1985-1990 (1997).

[74] Pharmacia: Zyvox[®] product information for healthcare professionals. Kalamazoo: Pharmacia & Upjohn Company, USA (2001).

[75] Pharmacia: Zyvoxid[®] - Standardinformation für Krankenhausapotheker. Erlangen: Pharmacia GmbH (2002).

[76] Slatter JG, Stalker DJ, Feenstra KL, Welshman IR, Bruss JB, Sams JP, Johnson MG, Sanders PE, Hauer MJ, Fagerness PE, Stryd RP, Peng GW, Shobe EM: Pharmacokinetics, metabolism, and excretion of linezolid following an oral dose of [(14)C]linezolid to healthy human subjects. *Drug Metab Dispos*. **29**: 1136-1145 (2001).

[77] Wynalda MA, Hauer MJ, Wienkers LC: Oxidation of the novel oxazolidinone antibiotic linezolid in human liver microsomes. *Drug Metab Dispos*. **28**: 1014-1017 (2000).

[78] Islinger F, Dehghanyar P, Sauermann R, Burger C, Kloft C, Muller M, Joukhadar C: The effect of food on plasma and tissue concentrations of linezolid after multiple doses. *Int J Antimicrob Agents*. **27**: 108-112 Epub 2006 Jan 2004 (2006).

[79] Stalker DJ, Jungbluth GL: Clinical pharmacokinetics of linezolid, a novel oxazolidinone antibacterial. *Clin Pharmacokinet*. **42**: 1129-1140 (2003).

[80] Welshman IR, Sisson TA, Jungbluth GL, Stalker DJ, Hopkins NK: Linezolid absolute bioavailability and the effect of food on oral bioavailability. *Biopharm Drug Dispos*. **22**: 91-97. (2001).

[81] Pharmacia: Zyvoxid® product information for healthcare professionals. Karlsruhe: Pharmacia GmbH Deutschland (2005).

[82] Ford C, Hamel J, Stapert D, Moerman J, Hutchinson H, Barbachyn M, Zurenko G: Oxazolidinones: a new class of antimicrobials. *Infect Med*. **16**: 435-445 (1999).

[83] Slatter JG, Adams LA, Bush EC, Chiba K, Daley-Yates PT, Feenstra KL, Koike S, Ozawa N, Peng GW, Sams JP, Schuette MR, Yamazaki S: Pharmacokinetics, toxicokinetics, distribution, metabolism and excretion of linezolid in mouse, rat and dog. *Xenobiotica*. **32**: 907-924 (2002).

[84] Diekema DJ, Jones RN: Oxazolidinone antibiotics. *Lancet*. **358**: 1975-1982 (2001).

[85] Perry CM, Jarvis B: Linezolid: a review of its use in the management of serious gram-positive infections. *Drugs*. **61**: 525-551 (2001).

[86] Brier ME, Stalker DJ, Aronoff GR, Batts DH, Ryan KK, O'Grady M, Hopkins NK, Jungbluth GL: Pharmacokinetics of linezolid in subjects with renal dysfunction. *Antimicrob Agents Chemother*. **47**: 2775-2780 (2003).

[87] Moellering RC: Linezolid: the first oxazolidinone antimicrobial. *Ann Intern Med*. **138**: 135-142 (2003).

[88] Fung HB, Kirschenbaum HL, Ojofeitimi BO: Linezolid: an oxazolidinone antimicrobial agent. *Clin Ther*. **23**: 356-391 (2001).

[89] Conte JE, Jr., Golden JA, Kipps J, Zurlinden E: Intrapulmonary pharmacokinetics of linezolid. *Antimicrob Agents Chemother*. **46**: 1475-1480 (2002).

[90] Honeybourne D, Tobin C, Jevons G, Andrews J, Wise R: Intrapulmonary penetration of linezolid. *J Antimicrob Chemother*. **51**: 1431-1434 (2003).

[91] Gee T, Ellis R, Marshall G, Andrews J, Ashby J, Wise R: Pharmacokinetics and tissue penetration of linezolid following multiple oral doses. *Antimicrob Agents Chemother*. **45**: 1843-1846 (2001).

[92] Dehghanyar P, Burger C, Zeitlinger M, Islinger F, Kovar F, Muller M, Kloft C, Joukhadar C: Penetration of linezolid into soft tissues of healthy volunteers after single and multiple doses. *Antimicrob Agents Chemother*. **49**: 2367-2371 (2005).

[93] Rana B, Butcher I, Grigoris P, Murnaghan C, Seaton RA, Tobin CM: Linezolid penetration into osteo-articular tissues. *J Antimicrob Chemother*. **50**: 747-750 (2002).

[94] Lovering AM, Zhang J, Bannister GC, Lankester BJ, Brown JH, Narendra G, MacGowan AP: Penetration of linezolid into bone, fat, muscle and haematoma of patients undergoing routine hip replacement. *J Antimicrob Chemother*. **50**: 73-77 (2002).

[95] Stolle LB, Plock N, Joukhadar C, Arpi M, Emmertsen KJ, Buerger C, Riegels-Nielsen P, Kloft C: Microdialysis in Bone Tissue - Pharmacokinetics of Linezolid *45th Interscience Conference on Antimicrobial Agents and Chemotherapy*; Washington D.C. (2005).

[96] Hachem R, Afif C, Gokaslan Z, Raad I: Successful treatment of vancomycin-resistant Enterococcus meningitis with linezolid. *Eur J Clin Microbiol Infect Dis*. **20**: 432-434 (2001).

[97] Whitehouse T, Cepeda JA, Shulman R, Aarons L, Nalda-Molina R, Tobin C, MacGowan A, Shaw S, Kibbler C, Singer M, Wilson APR: Pharmacokinetic studies of linezolid and teicoplanin in the critically ill. *J Antimicrob Chemother*. **55**: 333-340 (2005).

[98] Beringer P, Nguyen M, Hoem N, Louie S, Gill M, Gurevitch M, Wong-Beringer A: Absolute bioavailability and pharmacokinetics of linezolid in hospitalized patients given enteral feedings. *Antimicrob Agents Chemother*. **49**: 3676-3681 (2005).

[99]   Antal EJ, Grasela T, Bergstrom T, Bruss JB, Wong E: The Role of Population PK/PD Analysis During the Implementation of a Bridging Strategy for Linezolid. *Drug Information Association Meeting*; Hongkong. (2000).

[100]   Meagher AK, Forrest A, Rayner CR, Birmingham MC, Schentag JJ: Population pharmacokinetics of linezolid in patients treated in a compassionate-use program. *Antimicrob Agents Chemother*. **47**: 548-553 (2003).

[101]   Swaney SM, Aoki H, Ganoza MC, Shinabarger DL: The oxazolidinone linezolid inhibits initiation of protein synthesis in bacteria. *Antimicrob Agents Chemother*. **42**: 3251-3255 (1998).

[102]   Kloss P, Xiong L, Shinabarger DL, Mankin AS: Resistance mutations in 23 S rRNA identify the site of action of the protein synthesis inhibitor linezolid in the ribosomal peptidyl transferase center. *J Mol Biol*. **294**: 93-101 (1999).

[103]   Bozdogan B, Appelbaum PC: Oxazolidinones: activity, mode of action, and mechanism of resistance. *Int J Antimicrob Agents*. **23**: 113-119 (2004).

[104]   Aoki H, Ke L, Poppe SM, Poel TJ, Weaver EA, Gadwood RC, Thomas RC, Shinabarger DL, Ganoza MC: Oxazolidinone antibiotics target the P site on Escherichia coli ribosomes. *Antimicrob Agents Chemother*. **46**: 1080-1085 (2002).

[105]   Bowker KE, Wootton M, Holt HA, MacGowan AP: In vitro activity of linezolid against Gram-positive isolates causing infection in continuous ambulatory peritoneal dialysis patients. *J Antimicrob Chemother*. **49**: 578-580 (2002).

[106]   Zurenko GE, Yagi BH, Schaadt RD, Allison JW, Kilburn JO, Glickman SE, Hutchinson DK, Barbachyn MR, Brickner SJ: In vitro activities of U-100592 and U-100766, novel oxazolidinone antibacterial agents. *Antimicrob Agents Chemother*. **40**: 839-845 (1996).

[107]   Wise R, Andrews JM, Boswell FJ, Ashby JP: The in-vitro activity of linezolid (U-100766) and tentative breakpoints. *J Antimicrob Chemother*. **42**: 721-728 (1998).

[108]   Rybak MJ, Cappelletty DM, Moldovan T, Aeschlimann JR, Kaatz GW: Comparative in vitro activities and postantibiotic effects of the oxazolidinone compounds eperezolid (PNU-100592) and linezolid (PNU-100766) versus vancomycin against Staphylococcus aureus, coagulase-negative staphylococci, Enterococcus faecalis, and Enterococcus faecium. *Antimicrob Agents Chemother*. **42**: 721-724 (1998).

[109]   Brickner SJ, Hutchinson DK, Barbachyn MR, Manninen PR, Ulanowicz DA, Garmon SA, Grega KC, Hendges SK, Toops DS, Ford CW, Zurenko GE: Synthesis and antibacterial activity of U-100592 and U-100766, two oxazolidinone antibacterial agents for the potential treatment of multidrug-resistant gram-positive bacterial infections. *J Med Chem*. **39**: 673-679 (1996).

[110]   Alcaide F, Calatayud L, Santin M, Martin R: Comparative in vitro activities of linezolid, telithromycin, clarithromycin, levofloxacin, moxifloxacin, and four conventional antimycobacterial drugs against Mycobacterium kansasii. *Antimicrob Agents Chemother*. **48**: 4562-4565 (2004).

[111]   Erturan Z, Uzun M: In vitro activity of linezolid against multidrug-resistant Mycobacterium tuberculosis isolates. *Int J Antimicrob Agents*. **26**: 78-80 (2005).

[112]   Fortun J, Martin-Davila P, Navas E, Perez-Elias MJ, Cobo J, Tato M, De la Pedrosa EG, Gomez-Mampaso E, Moreno S: Linezolid for the treatment of multidrug-resistant tuberculosis. *J Antimicrob Chemother*. **56**: 180-185 (2005).

[113]   EUCAST: Oxazolidinones - EUCAST clinical MIC breakpoints. (2006); available from: *www.srga.org/eucastwt/MICTAB/MICoxazolidones.htm* [accessed 03 November 2006].

[114]   Livermore DM, Mushtaq S, Warner M: Susceptibility testing with linezolid by different methods, in relation to published 'general breakpoints'. *J Antimicrob Chemother*. **48**: 452-454 (2001).

[115]   French G: Safety and tolerability of linezolid. *J Antimicrob Chemother*. **51 Suppl 2**: ii45-ii53 (2003).

[116]   Chen YS, Lee SC, Kim WJ: Efficacy and tolerability of linezolid in treating severe skin and soft tissue infections caused by Gram-positive pathogens. *J Formos Med Assoc*. **103**: 349-354 (2004).

[117] Abena PA, Mathieux VG, Scheiff JM, Michaux LM, Vandercam BC: Linezolid and reversible myelosuppression. *J Am Med Assoc*. **286**: 1973; author reply 1974 (2001).

[118] Green SL, Maddox JC, Huttenbach ED: Linezolid and reversible myelosuppression. *J Am Med Assoc*. **285**: 1291 (2001).

[119] Gerson SL, Kaplan SL, Bruss JB, Le V, Arellano FM, Hafkin B, Kuter DJ: Hematologic effects of linezolid: summary of clinical experience. *Antimicrob Agents Chemother*. **46**: 2723-2726 (2002).

[120] Norrby R: Linezolid-a review of the first oxazolidinone. *Expert Opin Pharmacother*. **2**: 293-302 (2001).

[121] Antal EJ, Hendershot PE, Batts DH, Sheu WP, Hopkins NK, Donaldson KM: Linezolid, a novel oxazolidinone antibiotic: assessment of monoamine oxidase inhibition using pressor response to oral tyramine. *J Clin Pharmacol*. **41**: 552-562 (2001).

[122] Egle H, Trittler R, Kummerer K, Lemmen SW: Linezolid and rifampin: Drug interaction contrary to expectations? *Clin Pharmacol Ther*. **77**: 451-453 (2005).

[123] Wang LY, Tang ZQ, Feng FY: [Practical control methods for the dose individualization of anticancer drugs]. *Ai Zheng*. **21**: 1382-1385 (2002).

[124] Grochow LB, Baraldi C, Noe D: Is dose normalization to weight or body surface area useful in adults? *J Natl Cancer Inst*. **82**: 323-325 (1990).

[125] de Jongh FE, Verweij J, Loos WJ, de Wit R, de Jonge MJ, Planting AS, Nooter K, Stoter G, Sparreboom A: Body-surface area-based dosing does not increase accuracy of predicting cisplatin exposure. *J Clin Oncol*. **19**: 3733-3739 (2001).

[126] Veal GJ, Coulthard SA, Boddy AV: Chemotherapy individualization. *Invest New Drugs*. **21**: 149-156 (2003).

[127] Jelliffe RW, Schumitzky A, Van Guilder M, Liu M, Hu L, Maire P, Gomis P, Barbaut X, Tahani B: Individualizing drug dosage regimens: roles of population pharmacokinetic and dynamic models, Bayesian fitting, and adaptive control. *Ther Drug Monit*. **15**: 380-393 (1993).

[128] Proost JH: Adaptive control of drug dosage regimens using maximum a posteriori probability Bayesian fitting. *Int J Clin Pharmacol Ther*. **33**: 531-536 (1995).

[129] Rousseau A, Marquet P, Debord J, Sabot C, Lachatre G: Adaptive control methods for the dose individualisation of anticancer agents. *Clin Pharmacokinet*. **38**: 315-353 (2000).

[130] Sandstrom M, Karlsson MO, Ljungman P, Hassan Z, Jonsson EN, Nilsson C, Ringden O, Oberg G, Bekassy A, Hassan M: Population pharmacokinetic analysis resulting in a tool for dose individualization of busulphan in bone marrow transplantation recipients. *Bone Marrow Transplant*. **28**: 657-664 (2001).

[131] Duffull SB, Begg EJ, Robinson BA, Deely JJ: A sequential Bayesian algorithm for dose individualisation of carboplatin. *Cancer Chemother Pharmacol*. **39**: 317-326 (1997).

[132] Duffull SB, Kirkpatrick CM, Begg EJ: Comparison of two Bayesian approaches to dose-individualization for once-daily aminoglycoside regimens. *Br J Clin Pharmacol*. **43**: 125-135 (1997).

[133] Joukhadar C, Derendorf H, Muller M: Microdialysis. A novel tool for clinical studies of anti-infective agents. *Eur J Clin Pharmacol*. **57**: 211-219. (2001).

[134] Muller M, dela Pena A, Derendorf H: Issues in pharmacokinetics and pharmacodynamics of anti-infective agents: distribution in tissue. *Antimicrob Agents Chemother*. **48**: 1441-1453 (2004).

[135] Siegel RE: The significance of serum vs tissue levels of antibiotics in the treatment of penicillin-resistant Streptococcus pneumoniae and community-acquired pneumonia: are we looking in the wrong place? *Chest*. **116**: 535-538 (1999).

[136] Barza M: Anatomical barriers for antimicrobial agents. *Eur J Clin Microbiol Infect Dis*. **12 Suppl 1**: S31-S35 (1993).

[137] Barza M: Pharmacokinetics of antibiotics in shallow and deep compartments. *J Antimicrob Chemother*. **31 Suppl D**: 17-27 (1993).

[138] Bergan T, Engeset A: Penetration of antibiotics to tissues and infected foci. *Scand J Gastroenterol Suppl*. **90**: 29-34 (1984).

[139] Tegeder I, Schmidtko A, Brautigam L, Kirschbaum A, Geisslinger G, Lotsch J: Tissue distribution of imipenem in critically ill patients. *Clin Pharmacol Ther*. **71**: 325-333 (2002).

[140] Jynge P, Skjetne T, Gribbestad I, Kleinbloesem CH, Hoogkamer HF, Antonsen O, Krane J, Bakoy OE, Furuheim KM, Nilsen OG: In vivo tissue pharmacokinetics by fluorine magnetic resonance spectroscopy: a study of liver and muscle disposition of fleroxacin in humans. *Clin Pharmacol Ther*. **48**: 481-489 (1990).

[141] Fischman AJ, Livni E, Babich J, Alpert NM, Liu YY, Thom E, Cleeland R, Prosser BL, Correia JA, Strauss HW, et al.: Pharmacokinetics of [18F]fleroxacin in healthy human subjects studied by using positron emission tomography. *Antimicrob Agents Chemother*. **37**: 2144-2152 (1993).

[142] Muller M, Mader RM, Steiner B, Steger GG, Jansen B, Gnant M, Helbich T, Jakesz R, Eichler HG, Blochl-Daum B: 5-fluorouracil kinetics in the interstitial tumor space: clinical response in breast cancer patients. *Cancer Res*. **57**: 2598-2601 (1997).

[143] Fischman AJ, Babich JW, Bonab AA, Alpert NM, Vincent J, Callahan RJ, Correia JA, Rubin RH: Pharmacokinetics of [18F]trovafloxacin in healthy human subjects studied with positron emission tomography. *Antimicrob Agents Chemother*. **42**: 2048-2054 (1998).

[144] Brunner M, Pernerstorfer T, Mayer BX, Eichler HG, Muller M: Surgery and intensive care procedures affect the target site distribution of piperacillin. *Crit Care Med*. **28**: 1754-1759 (2000).

[145] Joukhadar C, Frossard M, Mayer BX, Brunner M, Klein N, Siostrzonek P, Eichler HG, Muller M: Impaired target site penetration of beta-lactams may account for therapeutic failure in patients with septic shock. *Crit Care Med*. **29**: 385-391 (2001).

[146] Kunin CM, Craig WA, Kornguth M, Monson R: Influence of binding on the pharmacologic activity of antibiotics. *Ann N Y Acad Sci*. **226**: 214-224 (1973).

[147] Craig WA, Ebert SC: Protein binding and its significance in antibacterial therapy. *Infect Dis Clin North Am*. **3**: 407-414 (1989).

[148] Merrikin DJ, Briant J, Rolinson GN: Effect of protein binding on antibiotic activity in vivo. *J Antimicrob Chemother*. **11**: 233-238 (1983).

[149] Ryan DM: Pharmacokinetics of antibiotics in natural and experimental superficial compartments in animals and humans. *J Antimicrob Chemother*. **31**: 1-16. (1993).

[150] Lambert HP: Clinical significance of tissue penetration of antibiotics in the respiratory tract. *Scand J Infect Dis Suppl*. 262-266 (1978).

[151] Hyatt JM, McKinnon PS, Zimmer GS, Schentag JJ: The importance of pharmacokinetic/pharmacodynamic surrogate markers to outcome. Focus on antibacterial agents. *Clin Pharmacokinet*. **28**: 143-160 (1995).

[152] Liu P, Muller M, Derendorf H: Rational dosing of antibiotics: the use of plasma concentrations versus tissue concentrations. *Int J Antimicrob Agents*. **19**: 285-290 (2002).

[153] Food and Drug Administration (FDA): Guidance for Industry. Developing antimicrobial drugs - general considerations for clinical trials. Draft guidance. (1998); available from: *www.fda.gov/cder/guidance/2580dft.pdf* [accessed 25 October 2006].

[154] Miller Reporting Company I: Anti-Infective Drugs Advisory Committee Meeting, 64th Meeting.: Department of Health and Human Services, Food and Drug Administration. (1998).

[155] Ungerstedt U, Pycock C: Functional correlates of dopamine neurotransmission. *Bull Schweiz Akad Med Wiss*. **30**: 44-55. (1974).

[156] Joukhadar C, Muller M: Microdialysis: current applications in clinical pharmacokinetic studies and its potential role in the future. *Clin Pharmacokinet*. **44**: 895-913 (2005).

[157] Garrison KE, Pasas SA, Cooper JD, Davies MI: A review of membrane sampling from biological tissues with applications in pharmacokinetics, metabolism and pharmacodynamics. *Eur J Pharm Sci*. **17**: 1-12. (2002).

[158]   Plock N, Kloft C: Microdialysis - theoretical background and recent implementation in applied life-sciences. *Eur J Pharm Sci*. **25**: 1-24 (2005).

[159]   Buerger C, Joukhadar C, Muller M, Kloft C: Development of a liquid chromatography method for the determination of linezolid and its application to in vitro and human microdialysis samples. *J Chromatogr B Analyt Technol Biomed Life Sci*. **796**: 155-164. (2003).

[160]   Jacobson I, Sandberg M, Hamberger A: Mass transfer in brain dialysis devices-a new method for the estimation of extracellular amino acids concentration. *J Neurosci Methods*. **15**: 263-268. (1985).

[161]   Chaurasia CS: In vivo microdialysis sampling: theory and applications. *Biomed Chromatogr*. **13**: 317-332. (1999).

[162]   Lonnroth P, Jansson PA, Smith U: A microdialysis method allowing characterization of intercellular water space in humans. *Am J Physiol*. **253**: E228-E231 (1987).

[163]   Olson RJ, Justice JB, Jr.: Quantitative microdialysis under transient conditions. *Anal Chem*. **65**: 1017-1022. (1993).

[164]   Stahle L, Arner P, Ungerstedt U: Drug distribution studies with microdialysis. III: Extracellular concentration of caffeine in adipose tissue in man. *Life Sci*. **49**: 1853-1858 (1991).

[165]   Bouw MR, Hammarlund-Udenaes M: Methodological aspects of the use of a calibrator in in vivo microdialysis-further development of the retrodialysis method. *Pharm Res*. **15**: 1673-1679. (1998).

[166]   Larsson CI: The use of an "internal standard" for control of the recovery in microdialysis. *Life Sci*. **49**: L73-L78. (1991).

[167]   Brunner M, Joukhadar C, Schmid R, Erovic B, Eichler HG, Muller M: Validation of urea as an endogenous reference compound for the in vivo calibration of microdialysis probes. *Life Sci*. **67**: 977-984. (2000).

[168]   Strindberg L, Lonnroth P: Validation of an endogenous reference technique for the calibration of microdialysis catheters. *Scand J Clin Lab Invest*. **60**: 205-211. (2000).

[169]   Schwalbe O, Buerger C, Plock N, Joukhadar C, Kloft C: Urea as an endogenous surrogate in human microdialysis to determine relative recovery of drugs: analytics and applications. *J Pharm Biomed Anal*. **41**: 233-239 (2006).

[170]   Voigt R: *Pharmazeutische Technologie*. 7 ed. Ullstein Mosby, Berlin (1993).

[171]   Bauer KH, Froemming K-H, Fuehrer C: *Lehrbuch der Pharmazeutischen Technologie*. 6 ed. Wissenschaftliche Verlagsgesellschaft mbH, Stuttgart (1999).

[172]   Mutschler E, Geisslinger G, Kroemer H, Schäfer-Korting M: *Arzneimittelwirkungen*. 8 ed. Wissenschaftliche Verlagsgesellschaft, Stuttgart (2001).

[173]   Michel CC: Filtration coefficients and osmotic reflexion coefficients of the walls of single frog mesenteric capillaries. *J Physiol*. **309**: 341-355 (1980).

[174]   Renkin EM: Multiple pathways of capillary permeability. *Circ Res*. **41**: 735-743 (1977).

[175]   Renkin EM: Capillary transport of macromolecules: pores and other endothelial pathways. *J Appl Physiol*. **58**: 315-325 (1985).

[176]   Beck RE, Schultz JS: Hindrance of solute diffusion within membranes as measured with microporous membranes of known pore geometry. *Biochim Biophys Acta*. **255**: 273-303 (1972).

[177]   Curry FE: Determinants of capillary permeability: a review of mechanisms based on single capillary studies in the frog. *Circ Res*. **59**: 367-380 (1986).

[178]   De Paepe P, Belpaire FM, Buylaert WA: Pharmacokinetic and pharmacodynamic considerations when treating patients with sepsis and septic shock. *Clin Pharmacokinet*. **41**: 1135-1151 (2002).

[179]   Bone RC, Sibbald WJ, Sprung CL: The ACCP-SCCM consensus conference on sepsis and organ failure. *Chest*. **101**: 1481-1483 (1992).

[180]   Clowes GH, Jr., Vucinic M, Weidner MG: Circulatory and metabolic alterations associated with survival or death in peritonitis: clinical analysis of 25 cases. *Ann Surg*. **163**: 866-885 (1966).

[181]   Siegel JH, Greenspan M, Del Guercio LR: Abnormal vascular tone, defective oxygen transport and myocardial failure in human septic shock. *Ann Surg*. **165**: 504-517 (1967).

[182]   Increase in National Hospital Discharge Survey rates for septicemia-United States, 1979-1987. *Morb Mortal Wkly Rep*. **39**: 31-34 (1990).

[183]   Kennedy JM, Riji AM: Effects of surgery on the pharmacokinetic parameters of drugs. *Clin Pharmacokinet*. **35**: 293-312 (1998).

[184]   Power BM, Forbes AM, van Heerden PV, Ilett KF: Pharmacokinetics of drugs used in critically ill adults. *Clin Pharmacokinet*. **34**: 25-56 (1998).

[185]   Kreuzer F, Cain SM: Regulation of the peripheral vasculature and tissue oxygenation in health and disease. *Crit Care Clin*. **1**: 453-470 (1985).

[186]   Ishihara H, Matsui A, Muraoka M, Tanabe T, Tsubo T, Matsuki A: Detection of capillary protein leakage by indocyanine green and glucose dilutions in septic patients. *Crit Care Med*. **28**: 620-626 (2000).

[187]   van Lambalgen AA, Bronsveld W, van den Bos GC, Thijs LG: Distribution of cardiac output, oxygen consumption and lactate production in canine endotoxin shock. *Cardiovasc Res*. **18**: 195-205 (1984).

[188]   Macnab MS, Macrae DJ, Guy E, Grant IS, Feely J: Profound reduction in morphine clearance and liver blood flow in shock. *Intensive Care Med*. **12**: 366-369 (1986).

[189]   Groeger JS, Inturrisi CE: High-dose naloxone: pharmacokinetics in patients in septic shock. *Crit Care Med*. **15**: 751-756 (1987).

[190]   Hinshaw LB: Sepsis/septic shock: participation of the microcirculation: an abbreviated review. *Crit Care Med*. **24**: 1072-1078 (1996).

[191]   Neugebauer E, Dietrich A, Lechleuthner A, Bouillon B, Eypasch E: Pharmacotherapy in shock syndromes: the neglected field of pharmacokinetics and pharmacodynamics. *Circ Shock*. **36**: 312-320 (1992).

[192]   Park GR: Pharmacokinetics and pharmacodynamics in the critically ill patient. *Xenobiotica*. **23**: 1195-1230 (1993).

[193]   Bodenham A, Shelly MP, Park GR: The altered pharmacokinetics and pharmacodynamics of drugs commonly used in critically ill patients. *Clin Pharmacokinet*. **14**: 347-373 (1988).

[194]   Verbeeck RK, Horsmans Y: Effect of hepatic insufficiency on pharmacokinetics and drug dosing. *Pharm World Sci*. **20**: 183-192 (1998).

[195]   McKindley DS, Hanes S, Boucher BA: Hepatic drug metabolism in critical illness. *Pharmacotherapy*. **18**: 759-778 (1998).

[196]   Gomez CM, Cordingly JJ, Palazzo MG: Altered pharmacokinetics of ceftazidime in critically ill patients. *Antimicrob Agents Chemother*. **43**: 1798-1802 (1999).

[197]   Hanes SD, Wood GC, Herring V, Croce MA, Fabian TC, Pritchard E, Boucher BA: Intermittent and continuous ceftazidime infusion for critically ill trauma patients. *Am J Surg*. **179**: 436-440 (2000).

[198]   Lugo G, Castaneda-Hernandez G: Relationship between hemodynamic and vital support measures and pharmacokinetic variability of amikacin in critically ill patients with sepsis. *Crit Care Med*. **25**: 806-811 (1997).

[199]   Joukhadar C, Klein N, Frossard M, Minar E, Stass H, Lackner E, Herrmann M, Riedmuller E, Muller M: Angioplasty increases target site concentrations of ciprofloxacin in patients with peripheral arterial occlusive disease. *Clin Pharmacol Ther*. **70**: 532-539. (2001).

[200]   Joukhadar C, Klein N, Mayer BX, Kreischitz N, Delle-Karth G, Palkovits P, Heinz G, Muller M: Plasma and tissue pharmacokinetics of cefpirome in patients with sepsis. *Crit Care Med*. **30**: 1478-1482 (2002).

[201]   Port RE: Populations-Pharmakokinetik und individuelle Dosisanpassung. *Onkologie - Grundlagen, Diagnostik, Therapie, Entwicklungen*. Section IV-8.1, 1-13. Landsberg (2003).

[202]   Sheiner LB: The population approach to pharmacokinetic data analysis: rationale and standard data analysis methods. *Drug Metab Rev*. **15**: 153-171 (1984).

[203]   Wahlby U, Jonsson EN, Karlsson MO: Comparison of stepwise covariate model building strategies in population pharmacokinetic-pharmacodynamic analysis. *AAPS PharmSci*. **4**: E27 (2002).

[204]   Jonsson S, Karlsson MO: A rational approach for selection of optimal covariate-based dosing strategies. *Clin Pharmacol Ther*. **73**: 7-19 (2003).

[205]   Food and Drug Administration (FDA): Guidance for Industry. Population Pharmacokinetics. (1999); available from: *www.fda.gov/cder/guidance/1852pk.htm* [accessed 25 October 2006].

[206]   Food and Drug Administration (FDA): Exposure-Response Relationships - Study Design, Data Analysis, and Regulatory Applications. (2003); available from: *www.fda.gov/cber/gdlns/exposure.htm* [accessed 25 October 2006].

[207]   International Conference on Harmonisation (ICH): Guideline for Industry. Dose-Response Information to Support Drug Registration. (1994); available from: *www.fda.gov/cder/guidance/iche4.pdf* [accessed 25 October 2006].

[208]   International Conference on Harmonisation (ICH): Guideline for Industry. Studies in Support of Special Populations: Geriatrics. (1994); available from: *www.fda.gov/cder/guidance/iche7.pdf* [accessed 25 October 2006].

[209]   Aarons L: Population pharmacokinetics: theory and practice. *Br J Clin Pharmacol*. **32**: 669-670 (1991).

[210]   Derendorf H, Gramatté T, Schaefer HG: *Pharmakokinetik*. 2 ed. Wissenschaftliche Verlagsgesellschaft mbH, Stuttgart (2002).

[211]   *WinNonlin help guide*. Pharsight Corporation (2002).

[212]   Sheiner LB, Beal SL: Evaluation of methods for estimating population pharmacokinetics parameters. I. Michaelis-Menten model: routine clinical pharmacokinetic data. *J Pharmacokinet Biopharm*. **8**: 553-571 (1980).

[213]   Sheiner BL, Beal SL: Evaluation of methods for estimating population pharmacokinetic parameters. II. Biexponential model and experimental pharmacokinetic data. *J Pharmacokinet Biopharm*. **9**: 635-651 (1981).

[214]   Sheiner LB, Beal SL: Some suggestions for measuring predictive performance. *J Pharmacokinet Biopharm*. **9**: 503-512 (1981).

[215]   Sheiner LB, Beal SL: Evaluation of methods for estimating population pharmacokinetic parameters. III. Monoexponential model: routine clinical pharmacokinetic data. *J Pharmacokinet Biopharm*. **11**: 303-319 (1983).

[216]   Steimer JL, Mallet A, Golmard JL, Boisvieux JF: Alternative approaches to estimation of population pharmacokinetic parameters: comparison with the nonlinear mixed-effect model. *Drug Metab Rev*. **15**: 265-292 (1984).

[217]   Sheiner LB, Beal SL: Bayesian individualization of pharmacokinetics: simple implementation and comparison with non-Bayesian methods. *J Pharm Sci*. **71**: 1344-1348 (1982).

[218]   Sun H, Fadiran EO, Jones CD, Lesko L, Huang SM, Higgins K, Hu C, Machado S, Maldonado S, Williams R, Hossain M, Ette EI: Population pharmacokinetics. A regulatory perspective. *Clin Pharmacokinet*. **37**: 41-58 (1999).

[219]   Sheiner LB, Beal S, Rosenberg B, Marathe VV: Forecasting individual pharmacokinetics. *Clin Pharmacol Ther*. **26**: 294-305 (1979).

[220]   Sheiner LB: Analysis of pharmacokinetic data using parametric models. I: Regression models. *J Pharmacokinet Biopharm*. **12**: 93-117 (1984).

[221]   Karlsson MO, Sheiner LB: The importance of modeling interoccasion variability in population pharmacokinetic analyses. *J Pharmacokinet Biopharm*. **21**: 735-750 (1993).

[222]   Mandema JW, Verotta D, Sheiner LB: Building population pharmacokinetic--pharmacodynamic models. I. Models for covariate effects. *J Pharmacokinet Biopharm*. **20**: 511-528 (1992).

[223]   Bonate PL: *Pharmacokinetic-Pharmacodynamic Modeling and Simulation*. 1 ed. Springer Science and Business Media, New York (2006).

[224] Wade JR, Beal SL, Sambol NC: Interaction between structural, statistical, and covariate models in population pharmacokinetic analysis. *J Pharmacokinet Biopharm*. **22**: 165-177 (1994).

[225] Jonsson N, Karlsson MO: *Xpose 2.0 User's Manual*. Department of Pharmacy, Uppsala University, Sweden (1998).

[226] Akaike H: Canonical correlation analysis of time series and the use of an information criterion. System identification: Advances and case studies. *Academic Press*. 27-96. Mehra, R.K., Lainiotis, D.G. New York (1976).

[227] Jonsson EN, Karlsson MO: Automated covariate model building within NONMEM. *Pharm Res*. **15**: 1463-1468 (1998).

[228] Maitre PO, Buhrer M, Thomson D, Stanski DR: A three-step approach combining Bayesian regression and NONMEM population analysis: application to midazolam. *J Pharmacokinet Biopharm*. **19**: 377-384 (1991).

[229] Kowalski KG, Hutmacher MM: Efficient screening of covariates in population models using Wald's approximation to the likelihood ratio test. *J Pharmacokinet Pharmacodyn*. **28**: 253-275 (2001).

[230] Aarons L, Balant LP, Mentre F, Morselli PL, Rowland M, Steimer JL, Vozeh S: Population approaches in drug development. Report on an expert meeting to discuss population pharmacokinetic/pharmacodynamic software. *Eur J Clin Pharmacol*. **46**: 389-391 (1994).

[231] Aarons L: Software for population pharmacokinetics and pharmacodynamics. *Clin Pharmacokinet*. **36**: 255-264 (1999).

[232] Beal S, Sheiner L: *NONMEM Users Guides*. University of California, San Francisco (1998).

[233] Meyer V: *Praxis der Hochleistungs-Flüssigkeitschromatographie*. Otto Salle Verlag, Frankfurt/M. (1999).

[234] Food and Drug Administration (FDA): Guidance for Industry. Bioanalytical Method Validation. (2001); available from: *www.fda.gov/cder/guidance/4252fnl.pdf* [accessed 25 October 2006].

[235] Stolle LB, Arpi M, Jorgensen PH, Riegels-Nielsen P, Keller J: In situ gentamicin concentrations in cortical bone: an experimental study using microdialysis in bone. *Acta Orthop Scand*. **74**: 611-616. (2003).

[236] Cockcroft DW, Gault MH: Prediction of creatinine clearance from serum creatinine. *Nephron*. **16**: 31-41 (1976).

[237] Holford NH, Sheiner LB: Understanding the dose-effect relationship: clinical application of pharmacokinetic-pharmacodynamic models. *Clin Pharmacokinet*. **6**: 429-453 (1981).

[238] Gabrielsson J, Weiner D: *Pharmacokinetic and Pharmacodynamic Data Analysis: Concepts and Applications*. Apotekarsocieteten (Swedish Pharmaceutical Society), Stockholm (2000).

[239] Sheiner LB: Analysis of pharmacokinetic data using parametric models. III. Hypothesis tests and confidence intervals. *J Pharmacokinet Biopharm*. **14**: 539-555 (1986).

[240] Holford NH, Peace KE: Results and validation of a population pharmacodynamic model for cognitive effects in Alzheimer patients treated with tacrine. *Proc Natl Acad Sci*. **89**: 11471-11475 (1992).

[241] Akins RB, Tolson H, Cole BR: Stability of response characteristics of a Delphi panel: application of bootstrap data expansion. *BMC Med Res Methodol*. **5**: 37 (2005).

[242] Gibiansky E, Struys MM, Gibiansky L, Vanluchene AL, Vornov J, Mortier EP, Burak E, Van Bortel L: AQUAVAN injection, a water-soluble prodrug of propofol, as a bolus injection: a phase I dose-escalation comparison with DIPRIVAN (part 1): pharmacokinetics. *Anesthesiology*. **103**: 718-729 (2005).

[243] Hooker AC, Foracchia M, Dodds MG, Vicini P: An evaluation of population D-optimal designs via pharmacokinetic simulations. *Ann Biomed Eng*. **31**: 98-111 (2003).

[244] D'Argenio DZ: Optimal sampling times for pharmacokinetic experiments. *J Pharmacokinet Biopharm*. **9**: 739-756 (1981).

[245] Duffull SB, Mentre F, Aarons L: Optimal design of a population pharmacodynamic experiment for ivabradine. *Pharm Res*. **18**: 83-89 (2001).

[246] Duffull S, Waterhouse T, Eccleston J: Some considerations on the design of population pharmacokinetic studies. *J Pharmacokinet Pharmacodyn*. **32**: 441-457 (2005).

[247] Almeida AM, Castel-Branco MM, Falcao AC: Linear regression for calibration lines revisited: weighting schemes for bioanalytical methods. *J Chromatogr B Analyt Technol Biomed Life Sci*. **774**: 215-222 (2002).

[248] Luer MS, Neill KK, Gurley BJ, Shannon ML, Killian AD, Rodvold KA: Fluctuations in vancomycin CNS tissue concentrations following intermittent and continuous infusions in the rat. *Neurol Res*. **26**: 312-315. (2004).

[249] Food and Drug Administration (FDA): Guidance for Industry. Pharmacokinetics in Patients with Impaired Renal Function - Study Design, Data Analysis, and Impact on Dosing and Labeling. (1998); available from: *www.fda.gov/CDER/GUIDANCE/1449fnl.pdf* [accessed 30 October 2006].

[250] Schwenzer KS, Wang CH, Anhalt JP: Automated fluorescence polarization immunoassay for monitoring vancomycin. *Ther Drug Monit*. **5**: 341-345 (1983).

[251] Demotes-Mainard F, Labat L, Vincon G, Bannwarth B: Column-switching high-performance liquid chromatographic determination of vancomycin in serum. *Ther Drug Monit*. **16**: 293-297. (1994).

[252] Farin D, Piva GA, Gozlan I, Kitzes-Cohen R: A modified HPLC method for the determination of vancomycin in plasma and tissues and comparison to FPIA (TDX). *J Pharm Biomed Anal*. **18**: 367-372. (1998).

[253] Backes DW, Aboleneen HI, Simpson JA: Quantitation of vancomycin and its crystalline degradation product (CDP-1) in human serum by high performance liquid chromatography. *J Pharm Biomed Anal*. **16**: 1281-1287. (1998).

[254] Greene SV, Abdalla T, Morgan SL, Bryan CS: High-performance liquid chromatographic analysis of vancomycin in plasma, bone, atrial appendage tissue and pericardial fluid. *J Chromatogr A*. **417**: 121-128. (1987).

[255] Hu MW, Anne L, Forni T, Gottwald K: Measurement of vancomycin in renally impaired patient samples using a new high-performance liquid chromatography method with vitamin B12 internal standard: comparison of high-performance liquid chromatography, emit, and fluorescence polarization immunoassay methods. *Ther Drug Monit*. **12**: 562-569. (1990).

[256] Furuta I, Kitahashi T, Kuroda T, Nishio H, Oka C, Morishima Y: Rapid serum vancomycin assay by high-performance liquid chromatography using a semipermeable surface packing material column. *Clin Chim Acta*. **301**: 31-39. (2000).

[257] Luksa J, Marusic A: Rapid high-performance liquid chromatographic determination of vancomycin in human plasma. *J Chromatogr B Analyt Technol Biomed Life Sci*. **667**: 277-281. (1995).

[258] Hosotsubo H: Rapid and specific method for the determination of vancomycin in plasma by high-performance liquid chromatography on an aminopropyl column. *J Chromatogr A*. **487**: 421-427 (1989).

[259] Li L, Miles MV, Hall W, Carson SW: An improved micromethod for vancomycin determination by high-performance liquid chromatography. *Ther Drug Monit*. **17**: 366-370. (1995).

[260] Favetta P, Guitto J, Bleyzac N, Dufresne C, Bureau J: New sensitive assay of vancomycin in human plasma using high-performance liquid chromatography and electrochemical detection. *J Chromatogr B Analyt Technol Biomed Life Sci*. **751**: 377-382 (2001).

[261] Cass RT, Villa JS, Karr DE, Schmidt DE, Jr.: Rapid bioanalysis of vancomycin in serum and urine by high-performance liquid chromatography tandem mass spectrometry using on-line sample extraction and parallel analytical columns. *Rapid Commun Mass Spectrom*. **15**: 406-412. (2001).

[262] Shibata N, Ishida M, Prasad YV, Gao W, Yoshikawa Y, Takada K: Highly sensitive quantification of vancomycin in plasma samples using liquid chromatography-tandem

mass spectrometry and oral bioavailability in rats. *J Chromatogr B Analyt Technol Biomed Life Sci*. **789**: 211-218. (2003).

[263]   Morishige H, Shuto H, Ieiri I, Otsubo K, Oishi R: Instability of standard calibrators may be involved in overestimating vancomycin concentrations determined by fluorescence polarization immunoassay. *Ther Drug Monit*. **18**: 80-85 (1996).

[264]   Anne L, Hu M, Chan K, Colin L, Gottwald K: Potential problem with fluorescence polarization immunoassay cross-reactivity to vancomycin degradation product CDP-1: its detection in sera of renally impaired patients. *Ther Drug Monit*. **11**: 585-591 (1989).

[265]   Morse GD, Nairn DK, Bertino JS, Jr., Walshe JJ: Overestimation of vancomycin concentrations utilizing fluorescence polarization immunoassay in patients on peritoneal dialysis. *Ther Drug Monit*. **9**: 212-215 (1987).

[266]   Najjar TA, al-Dhuwailie AA, Tekle A: Comparison of high-performance liquid chromatography with fluorescence polarization immunoassay for the analysis of vancomycin in patients with chronic renal failure. *J Chromatogr B Analyt Technol Biomed Life Sci*. **672**: 295-299 (1995).

[267]   Follin SL, Mueller BA, Scott MK, Carfagna MA, Kraus MA: Falsely elevated serum vancomycin concentrations in hemodialysis patients. *Am J Kidney Dis*. **27**: 67-74 (1996).

[268]   Saunders NJ, Want SV, Adams DJ: Assay of vancomycin by fluorescence polarisation immunoassay and EMIT in patients with renal failure. *J Antimicrob Chemother*. **36**: 411-415 (1995).

[269]   Smith PF, Petros WP, Soucie MP, Copeland KR: New modified fluorescence polarization immunoassay does not falsely elevate vancomycin concentrations in patients with end-stage renal disease. *Ther Drug Monit*. **20**: 231-235 (1998).

[270]   Sym D, Smith C, Meenan G, Lehrer M: Fluorescence polarization immunoassay: can it result in an overestimation of vancomycin in patients not suffering from renal failure? *Ther Drug Monit*. **23**: 441-444 (2001).

[271]   Adamczyk M, Brate EM, Chiappetta EG, Ginsburg S, Hoffman E, Klein C, Perkowitz MM, Rege SD, Chou PP, Costantino AG: Development of a quantitative vancomycin immunoassay for the Abbott AxSYM analyzer. *Ther Drug Monit*. **20**: 191-201 (1998).

[272]   Trujillo TN, Sowinski KM, Venezia RA, Scott MK, Mueller BA: Vancomycin assay performance in patients with acute renal failure. *Intensive Care Med*. **25**: 1291-1296 (1999).

[273]   Johnson JLH, Yalkowsky SH: Reformulation of a New Vancomycin Analog: An Example of the Importance of Buffer Species and Strength. *AAPS PharmSciTech*. **7**: E1-E5 (2006).

[274]   Hui F, Caude M: Enantioseparation in CE using macrocyclic antibiotics as chiral selectors. *Analusis*. **27**: 131-138 (1999).

[275]   Kralovic SM, Danko LH, Roselle GA: Laboratory reporting of Staphylococcus aureus with reduced susceptibility to vancomycin in United States Department of Veterans Affairs facilities. *Emerg Infect Dis*. **8**: 402-407. (2002).

[276]   Abrahamsson P, Winso O: An assessment of calibration and performance of the microdialysis system. *J Pharm Biomed Anal*. **39**: 730-734 (2005).

[277]   Bielecka-Grzela S, Klimowicz A: Application of cutaneous microdialysis to evaluate metronidazole and its main metabolite concentrations in the skin after a single oral dose. *J Clin Pharm Ther*. **28**: 465-469 (2003).

[278]   Mayer BX, Petsch M, Tschernko EM, Muller M: Strategies for the determination of cefazolin in plasma and microdialysis samples by short-end capillary zone electrophoresis. *Electrophoresis*. **24**: 1215-1220 (2003).

[279]   Petsch M, Mayer-Helm BX, Sauermann R, Joukhadar C, Kenndler E: Capillary electrophoresis analysis of fosfomycin in biological fluids for clinical pharmacokinetic studies. *Electrophoresis*. **25**: 2292-2298 (2004).

[280]   Bielecka-Grzela S, Klimowicz A: Penetration of ciprofloxacin and its desethylenemetabolite into skin in humans after a single oral dose of the parent drug assessed by cutaneous microdialysis. *J Clin Pharm Ther*. **30**: 383-390 (2005).

[281] Muller M: Science, medicine, and the future: Microdialysis. *Br Med J*. **324**: 588-591. (2002).

[282] EUCAST: Oxazolidinones - EUCAST clinical MIC breakpoints. (2004); available from: *www.srga.org/eucastwt/MICTAB/index.html* [accessed 20 January 2006].

[283] Stolle LB, Arpi M, Holmberg-Jorgensen P, Riegels-Nielsen P, Keller J: Application of microdialysis to cancellous bone tissue for measurement of gentamicin levels. *J Antimicrob Chemother*. **54**: 263-265 (2004).

[284] Thorsen K, Kristoffersson AO, Lerner UH, Lorentzon RP: In situ microdialysis in bone tissue. Stimulation of prostaglandin E2 release by weight-bearing mechanical loading. *J Clin Invest*. **98**: 2446-2449. (1996).

[285] Mathy FX, Denet AR, Vroman B, Clarys P, Barel A, Verbeeck RK, Preat V: In vivo tolerance assessment of skin after insertion of subcutaneous and cutaneous microdialysis probes in the rat. *Skin Pharmacol Physiol*. **16**: 18-27. (2003).

[286] Davies MI, Lunte CE: Microdialysis sampling for hepatic metabolism studies. Impact of microdialysis probe design and implantation technique on liver tissue. *Drug Metab Dispos*. **23**: 1072-1079. (1995).

[287] Ault JM, Riley CM, Meltzer NM, Lunte CE: Dermal microdialysis sampling in vivo. *Pharm Res*. **11**: 1631-1639. (1994).

[288] Nicholson C, Sykova E: Extracellular space structure revealed by diffusion analysis. *Trends Neurosci*. **21**: 207-215. (1998).

[289] Hoistad M, Chen KC, Nicholson C, Fuxe K, Kehr J: Quantitative dual-probe microdialysis: evaluation of [3H]mannitol diffusion in agar and rat striatum. *J Neurochem*. **81**: 80-93. (2002).

[290] Weiss M: Moments of physiological transit time distributions and the time course of drug disposition in the body. *J Math Biol*. **15**: 305-318 (1982).

[291] Prete MR, Hannan CJ, Jr., Burkle FM, Jr.: Plasma atropine concentrations via intravenous, endotracheal, and intraosseous administration. *Am J Emerg Med*. **5**: 101-104 (1987).

[292] Valdes MM: Intraosseous fluid administration in emergencies. *Lancet*. **1**: 1235-1236 (1977).

[293] Waisman M, Waisman D: Bone marrow infusion in adults. *J Trauma*. **42**: 288-293 (1997).

[294] Warren DW, Kissoon N, Mattar A, Morrissey G, Gravelle D, Rieder MJ: Pharmacokinetics from multiple intraosseous and peripheral intravenous site injections in normovolemic and hypovolemic pigs. *Crit Care Med*. **22**: 838-843 (1994).

[295] Food and Drug Administration (FDA): Guidance for Industry. Bioequivalence guidance. (2002); available from: *www.fda.gov/cvm/Guidance/bioequivalence_Oct02.pdf* [accessed 25 October 2006].

[296] Forrest A: Patient Studies Modeling Surrogates and Their Linkages: MIC, Clinical Scoring and PK/PD Indices of Effect. *15th ISAP International Symposium*; Washington, DC. (2005).

[297] Mouton JW: Pharmacodynamic Indices. *45th Interscience Conference on Antimicrobial Agents and Chemotherapy*; Washington, DC. (2005).

[298] Kutscha-Lissberg F, Hebler U, Muhr G, Koller M: Linezolid penetration into bone and joint tissues infected with methicillin-resistant staphylococci. *Antimicrob Agents Chemother*. **47**: 3964-3966 (2003).

[299] Zhang L, Beal SL, Sheiner LB: Simultaneous vs. sequential analysis for population PK/PD data I: best-case performance. *J Pharmacokinet Pharmacodyn*. **30**: 387-404 (2003).

[300] Schoerlin MP, Mayersohn M, Korn A, Eggers H: Disposition kinetics of moclobemide, a monoamine oxidase-A enzyme inhibitor: single and multiple dosing in normal subjects. *Clin Pharmacol Ther*. **42**: 395-404 (1987).

[301] Welker HA: Single- and multiple-dose mibefradil pharmacokinetics in normal and hypertensive subjects. *J Pharm Pharmacol*. **50**: 983-987 (1998).

[302] Terao N, Shen DD: Pharmacokinetics of l-propranolol during repetitive dosing in normal and uranyl nitrate-induced renal failure rats. *J Pharmacokinet Biopharm*. **12**: 479-493 (1984).

[303] Pfister CU, Martoni A, Zamagni C, Lelli G, De Braud F, Souppart C, Duval M, Hornberger U: Effect of age and single versus multiple dose pharmacokinetics of letrozole (Femara) in breast cancer patients. *Biopharm Drug Dispos*. **22**: 191-197 (2001).

[304] Daneshmend TK, Warnock DW: Clinical pharmacokinetics of ketoconazole. *Clin Pharmacokinet*. **14**: 13-34 (1988).

[305] Burkhardt O, Borner K, von der Hoh N, Koppe P, Pletz MW, Nord CE, Lode H: Single- and multiple-dose pharmacokinetics of linezolid and co-amoxiclav in healthy human volunteers. *J Antimicrob Chemother*. **50**: 707-712 (2002).

[306] Feenstra KL, Slatter JG, Stalker DJ, Welshman IR, Sams JP, Hauer MJ, Cathcart KS, Verburg MT, Johnson MG, Bothwell BE, Koets MD, Peng GW, Stryd RP, Fagerness PE: Metabolism and excretion of the oxazolidinone antibiotic linezolid (PNU-100766) following oral administration of [14C]PNU-100766 to healthy human volunteers. *38th Interscience Conference on Antimicrobial Agents and Chemotherapy*; San Diego, CA. (1998).

[307] Palenzuela L, Hahn NM, Nelson RP, Jr., Arno JN, Schobert C, Bethel R, Ostrowski LA, Sharma MR, Datta PP, Agrawal RK, Schwartz JE, Hirano M: Does linezolid cause lactic acidosis by inhibiting mitochondrial protein synthesis? *Clin Infect Dis*. **40**: e113-e116 (2005).

[308] De Vriese AS, Coster RV, Smet J, Seneca S, Lovering A, Van Haute LL, Vanopdenbosch LJ, Martin JJ, Groote CC, Vandecasteele S, Boelaert JR: Linezolid-induced inhibition of mitochondrial protein synthesis. *Clin Infect Dis*. **42**: 1111-1117 (2006).

[309] Berg JM, Tymoczko JL, Stryer L: *Biochemie*. 5 ed. Spektrum Akademischer Verlag GmbH, Heidelberg, Berlin (2003).

[310] Mager DE, Wyska E, Jusko WJ: Diversity of mechanism-based pharmacodynamic models. *Drug Metab Dispos*. **31**: 510-518 (2003).

[311] Pascual A, Ballesta S, Garcia I, Perea EJ: Uptake and intracellular activity of linezolid in human phagocytes and nonphagocytic cells. *Antimicrob Agents Chemother*. **46**: 4013-4015 (2002).

[312] Dvorchik B, Arbeit RD, Chung J, Liu S, Knebel W, Kastrissios H: Population pharmacokinetics of daptomycin. *Antimicrob Agents Chemother*. **48**: 2799-2807 (2004).

[313] Sisson TL, Jungbluth GL, Hopkins NK: Age and sex effects on the pharmacokinetics of linezolid. *Eur J Clin Pharmacol*. **57**: 793-797 (2002).

[314] Grunder G, Zysset-Aschmann Y, Vollenweider F, Maier T, Krahenbuhl S, Drewe J: Lack of pharmacokinetic interaction between linezolid and antacid in healthy volunteers. *Antimicrob Agents Chemother*. **50**: 68-72 (2006).

[315] Chetty M, Miller R, Moodley SV: Smoking and body weight influence the clearance of chlorpromazine. *Eur J Clin Pharmacol*. **46**: 523-526 (1994).

[316] Trenque T, Simon N, Villena I, Chemla C, Quereux C, Leroux B, Jaussaud R, Remy G, Dupouy D, Millart H, Pinon JM, Urien S: Population pharmacokinetics of pyrimethamine and sulfadoxine in children with congenital toxoplasmosis. *Br J Clin Pharmacol*. **57**: 735-741 (2004).

[317] Anderson BJ, McKee AD, Holford NH: Size, myths and the clinical pharmacokinetics of analgesia in paediatric patients. *Clin Pharmacokinet*. **33**: 313-327 (1997).

[318] Holford NH: A size standard for pharmacokinetics. *Clin Pharmacokinet*. **30**: 329-332 (1996).

[319] Matthews I, Kirkpatrick C, Holford N: Quantitative justification for target concentration intervention--parameter variability and predictive performance using population pharmacokinetic models for aminoglycosides. *Br J Clin Pharmacol*. **58**: 8-19 (2004).

[320] Waldrep TW, Skiest DJ: Linezolid-induced anemia and thrombocytopenia. *Pharmacotherapy*. **22**: 109-112 (2002).

[321] Attassi K, Hershberger E, Alam R, Zervos MJ: Thrombocytopenia associated with linezolid therapy. *Clin Infect Dis*. **34**: 695-698 (2002).

[322] Wu VC, Wang YT, Wang CY, Tsai IJ, Wu KD, Hwang JJ, Hsueh PR: High frequency of linezolid-associated thrombocytopenia and anemia among patients with end-stage renal disease. *Clin Infect Dis*. **42**: 66-72 (2006).

[323] Mateu de Antonio J, Grau S, Morales-Molina JA, Marin-Casino M: Thrombocytopenia and anemia associated with linezolid in patients with kidney failure. *Clin Infect Dis*. **42**: 1500; author reply 1501 (2006).

[324] Lee KH, Hui KP, Tan WC: Thrombocytopenia in sepsis: a predictor of mortality in the intensive care unit. *Singapore Med J*. **34**: 245-246 (1993).

[325] Francois B, Trimoreau F, Vignon P, Fixe P, Praloran V, Gastinne H: Thrombocytopenia in the sepsis syndrome: role of hemophagocytosis and macrophage colony-stimulating factor. *Am J Med*. **103**: 114-120 (1997).

[326] Ribbing J, Jonsson EN: Power, selection bias and predictive performance of the Population Pharmacokinetic Covariate Model. *J Pharmacokinet Pharmacodyn*. **31**: 109-134 (2004).

[327] Vozeh S, Steimer JL, Rowland M, Morselli P, Mentre F, Balant LP, Aarons L: The use of population pharmacokinetics in drug development. *Clin Pharmacokinet*. **30**: 81-93 (1996).

[328] Friberg LE, Freijs A, Sandstrom M, Karlsson MO: Semiphysiological model for the time course of leukocytes after varying schedules of 5-fluorouracil in rats. *J Pharmacol Exp Ther*. **295**: 734-740 (2000).

[329] Friberg LE, Henningsson A, Maas H, Nguyen L, Karlsson MO: Model of chemotherapy-induced myelosuppression with parameter consistency across drugs. *J Clin Oncol*. **20**: 4713-4721 (2002).

[330] Waterhouse TH, Redmann S, Duffull SB, Eccleston JA: Optimal design for model discrimination and parameter estimation for itraconazole population pharmacokinetics in cystic fibrosis patients. *J Pharmacokinet Pharmacodyn*. **32**: 521-545 (2005).

[331] Chenel M, Ogungbenro K, Duval V, Laveille C, Jochemsen R, Aarons L: Optimal blood sampling time windows for parameter estimation using a population approach: design of a phase II clinical trial. *J Pharmacokinet Pharmacodyn*. **32**: 737-756 (2005).

[332] Harbarth S, Garbino J, Pugin J, Romand JA, Lew D, Pittet D: Inappropriate initial antimicrobial therapy and its effect on survival in a clinical trial of immunomodulating therapy for severe sepsis. *Am J Med*. **115**: 529-535 (2003).

7   Appendix

7.1   Tables

Table 7.1 Sampling schedule for all investigated matrices of project II

Matrix	Sampling schedule [min after T_0]
Blood	0, 15, 30, 45, 60, 75, 90, 105, 120, 135, 150, 165, 180, 195, 210, 225, 240, 255, 270, 285, 300
Bone marrow	0, 30, 60, 90, 120, 150, 180, 210, 240, 270, 300
Bone microdialysate	0, 30, 60, 90, 120, 150, 180, 210, 240, 270, 300
Bone biopsy	0, 60, 120, 180, 240, 300

Table 7.2: Inclusion and exclusion criteria for healthy volunteers of project III

Inclusion criteria
- Female or male, aged between 40 and 80 years.
- No history of drug or alcohol abuse (40 g ethanol per day).
- No regular concomitant medication within the last 2 weeks prior to the start of trial (oral contraceptives excluded).
- Body mass index between 20 to 30 kg/m^2.
- Normal laboratory values unless the investigator considers an abnormality to be clinically irrelevant.
- Normotension defined as systolic blood pressure (BP) $\leq$ 150 mmHg or diastolic BP $\leq$ 90 mmHg after 5 min rest in supine position.
- Written informed consent.

Exclusion criteria
- Positive testing for HIV or Hepatitis B at the screening visit.
- Pregnancy or lactation.
- Allergy or hypersensitivity against study drugs.

Table 7.3: Sampling schedule for healthy volunteers and patients of project III

Matrix	Sampling schedule [min after drug administration]
Blood	0, 20, 40, 60, 80, 100, 120, 140, 160, 180, 210, 240, 270, 300, 330, 360, 390, 420, 450, 480
Microdialysate	0, 20, 40, 60, 80, 100, 120, 140, 160, 180, 210, 240, 270, 300, 330, 360, 390, 420, 450, 480

Table 7.4: Inclusion and exclusion criteria for patients of project III

Inclusion criteria
- Female or male, aged between 40 and 80 years.
- Indication to linezolid therapy made by an independent physician.
- Probable resistance of responsible pathogens against less toxic antiinfective agents[#].
- No linezolid therapy within the last 72 hours.

Severe sepsis and septic shock were diagnosed according to the criteria of the ACCP/SCCM Consensus Conference Committee [179] with at least two of the following criteria fulfilled:
- Tachycardia ($\geq$ 90 beats/min).
- Tachypnea ($\geq$ 20/min).
- Temperature $\geq$ 38.0 or < 36.0 °C.
- Leukocytosis ($\geq$ 12000/μL) or leukopenia ($\leq$ 4000/μL) or $\geq$ 10% immature (band) forms.

In addition at least one of the following criteria had to be fulfilled[#]:
- Lactic Acidosis (either elevated serum lactate concentration and an arterial pH $\leq$ 7.30 or elevated serum lactate concentration and a base deficit $\geq$ 5 mmol/L).
- Sustained oliguria (urine output $\leq$ 0.5 mL/kg/h for $\geq$ 2 hours, which persists despite objective evidence of adequate volume replacement unless contraindicated).
- Coagulation abnormality (either a prothrombin time, international normalisation ratio $\geq$ 1.5 or partial thromboplastin time $\geq$ 1.5 times the upper limit of normal for reporting laboratory in the absence of anticoagulants).
- Thrombocytopenia (platelet count $\leq$ 100 x 10³ cells/μL).
- Acute alteration in mental status (Glasgow Coma Scale score $\leq$ 11 in the absence of a head injury, other central nervous system (CNS) condition that would make it difficult to detect an acute alteration, or the administration of medications with CNS depressant effects).

To meet septic shock criteria the following had to be fulfilled as well:
- Sustained hypotension. Either of the following: Systolic BP $\leq$ 90 mmHg or evidence that vasopressors are required to maintain BP. These criteria must be met in the absence of other causes for hypotension and persist despite objective evidence of adequate volume replacement unless contraindicated.

Exclusion criteria
- Positive testing for HIV or Hepatitis B at the screening visit.
- Hemodialysis or hemofiltration 3 days prior to or within the first four days of study drug administration.
- Allergy against study drugs.
- Concomitant administration of MAO-inhibitors.
- Serum creatinine $\geq$ 5 mg/dL.
- Pregnancy or lactation.[#]

[#]only in effect for patients recruited in Berlin

Table 7.5: Variables included in the NONMEM dataset

Item description	Item name
Basic items	ID, TIME, AMT, RATE, EVID, CMT
Dependent variable	DV
Time related data items	TILD, DAY, VIST, OCC
Continuous covariates	AGE, WT, HT, SCRE, CLCR, AST, ALT, GGT, LDH, THRO, LEUC, CRP, APCH
Categorical covariates	SEX, CID, TYPE
Others	ADMA, FLMA

ID: individual subject record; TIME: relative time after start of first drug administration (h); AMT: amount of drug administered; RATE: (amount/infusion duration) normalised to 1 h; EVID: identification number of event; CMT: number of compartment in model; DV: dependent variable; TILD: relative time after start of last drug administration (h); DAY: study day; VIST: study visit; OCC: occasion (number of dose); AGE: age of subject; WT: body weight of subject; HT: body height of subject; SCRE: serum creatinine concentration; CLCR: creatinin clearance; AST: aspartate aminotransferase; ALT: alanine aminotransferase; GGT: gamma glutamyl transferase; LDH: lactate dehydrogenase; THRO: thrombocytes; LEUC: leucocytes; CRP: C-reactive protein; APCH: APACHE score; SEX: sex of subject; CID: identification number of study centre; TYPE: type of study subject (healthy, sepsis or septic shock); ADMA: administration matrix (oral, i.v.); FLMA: flag for matrix (plasma, s.c., i.m.)

Table 7.6: Mean stability of vancomycin in microdialysate

	Concentration [μg/mL]	n	Mean stability, %	Range[1], %
F-T-1[2]	1.379	3	100	95 – 109
	83.698	3	101	99 – 103
F-T-2[2]	1.379	3	102	101 – 104
	83.698	3	102	100 – 103
F-T-3[2]	1.379	3	101	97 – 105
	83.698	3	101	99 – 102
RT-4[3]	1.379	3	106	105 –107
	83.698	3	102	100 – 104
RT-24[3]	1.379	3	99	94 – 102
	83.698	3	101	100 – 103
AS-RT[4]	1.379	3	105	104 – 106
	83.698	3	101	97 – 104
AS-RF[5]	1.379	3	102	101 – 103
	83.698	3	104	102 – 106

[1] minimum – maximum

[2] freeze-thaw stability after 1, 2 or 3 cycles

[3] stability at room temperature over 4 or 24 h

[4] stability after sample preparation and storage at room temperature over 24 h

[5] stability after sample preparation and storage at -24°C over 24 h

Table 7.7: Mean stability of vancomycin in plasma

	Concentration [µg/mL]	n	Mean stability, %	Range[1], %
F-T-1[2]	1.037	3	106	93 – 119
	70.810	3	97	95 – 98
F-T-2[2]	1.037	3	108	93 – 116
	70.810	3	97	92 – 100
F-T-3[2]	1.037	3	108	94 – 116
	70.810	3	82	69 – 101
RT-4[3]	1.037	3	100	95 – 110
	70.810	3	88	82 –97
RT-24[3]	1.037	3	89	83 – 99
	70.810	3	90	79 – 97
AS-RT[4]	1.037	3	111	107 – 115
	70.810	3	91	85 – 95
AS-RF[5]	1.037	3	120	117 – 125
	70.810	3	100	94 – 104

[1] minimum – maximum
[2] freeze-thaw stability after 1, 2 and 3 cycles
[3] stability at room temperature over 4 or 24 h
[4] stability after sample preparation and storage at room temperature over 27 h
[5] stability after sample preparation and storage at -24°C over 24 h

Table 7.8: Within- and between-day imprecision (expressed as coefficient of variation, CV, %) and inaccuracy (expressed as mean percentage deviation, RE, %) of determined vancomycin concentrations in microdialysate

C_{nom} [µg/mL]	C [µg/mL] (mean $\pm$ SD)	CV, %	RE, %
Within-day variability (n = 5)			
0.416	0.38 $\pm$ 0.04	10.9	-9.1
1.042	1.06 $\pm$ 0.04	4.1	-5.2
26.43	27.85 $\pm$ 0.80	2.9	5.6
69.50	70.55 $\pm$ 6.55	9.3	3.5
Between-day variability (n = 15)			
0.416	0.40 $\pm$ 0.03	7.6	-3.7
1.042	1.01 $\pm$ 0.05	4.5	-3.0
26.43	27.82 $\pm$ 0.57	2.1	5.3
69.50	71.42 $\pm$ 4.08	5.7	2.8

Table 7.9: Within- and between-day imprecision (expressed as coefficient of variation, CV, %) and inaccuracy (expressed as mean percentage deviation, RE, %) of determined vancomycin concentrations in plasma

C_{nom} [µg/mL]	C [µg/mL] (mean $\pm$ SD)	CV, %	RE, %
Within-day variability (n = 5)			
0.305	0.29 ± 0.02	6.7	11.5
1.04	0.97 ± 0.04	4.2	-6.7
26.72	25.90 ± 2.44	9.4	9.8
70.81	74.73 ± 5.05	6.8	7.3
Between-day variability (n = 15)			
0.305	0.32 ± 0.03	8.0	4.8
1.04	1.00 ± 0.04	3.8	-3.3
26.72	27.63 ± 2.03	7.4	3.4
70.81	75.18 ± 3.63	4.8	6.2

Table 7.10: Mean regression parameters of the vancomycin calibration functions for plasma and microdialysate ($\overline{x} \pm$ SD)

Matrix	n	Slope [AU·mL/µg]	Intercept [AU]	Correlation coefficient
Plasma	3	0.247 ± 0.013	-0.006 ± 0.003	0.999 ± 3.6E-04
Microdialysate	3	0.209 ± 0.003	-0.026 ± 0.002	0.999 ± 6.9E-05

Table 7.11: Recovery of linezolid from bone marrow and bone using plasma calibration samples

C_{nom} [µg/mL]	C_{calc} [µg/mL]	Recovery, %	RE, %
Bone marrow (n = 1)			
20	20.680	103.4	3.4
10	10.322	103.2	3.2
5	4.856	97.1	-2.9
1	1.144	114.4	14.4
0.5	0.594	118.8	18.8
0.2	0.266	132.9	32.9
Bone (n = 1)			
2.05	2.257	110.1	10.1
1.02	0.963	94.4	-5.6
0.395	0.442	112.0	12.0

Table 7.12: Calculated pharmacokinetic parameters in the different matrices (n = 10). Data are presented as geometric mean (CV,%)

Parameter	Matrix	Geometric mean	CV,%
AUC_{0-6h} (µg·h/mL)	Plasma	75.7	27.2
	Bone marrow	72.8	28.8
	MD_{mc}	45.8	64.0
	MD_{lc}	42.5	61.1
	Bone biopsy	92.9	19.9
C_{max} (µg/mL)	Plasma	26.1	31.6
	Bone marrow	21.9	37.3
	MD_{mc}	13.2	65.4
	MD_{lc}	11.8	70.3
	Bone biopsy	21.9	20.8
Clearance (L/h)	Plasma	2.9	27.7
	Bone marrow	3.1	16.7
	MD_{mc}	4.8	83.2
	MD_{lc}	5.5	77.6
	Bone biopsy	3.5	35.1
Volume of distribution (L)	Plasma	37.9	26.7
	Bone marrow	38.1	32.7
	MD_{mc}	57.1	61.8
	MD_{lc}	61.0	57.9
	Bone biopsy	48.1	25.3

MD_{mc}: data from medial microdialysis catheter; MD_{lc}: data from lateral microdialysis catheter

Table 7.13: Distribution of observations for healthy volunteers and patients for the studied matrices and application routes

Type	Subjects		Number of samples					
			Plasma		s.c.[1]		i.m.[2]	
	n	%	s.d.[3]	m.d.[4]	s.d.[3]	m.d.[4]	s.d.[3]	m.d.[4]
Healthy volunteers	10	29.4	190	180	174	176	184	165
Patients with sepsis	8	23.5	153	131	160	137	155	133
Patients with septic shock	16	47.1	307	215	304	217	300	220
Subtotal	-	-	650	526	638	530	639	518
Total	34	100	1176		1168		1157	

green box: preliminary dataset; red box: dataset A; blue box: dataset B
[1] samples from subcutaneous ISF
[2] samples from muscular ISF
[3] samples obtained after single intravenous dosing
[4] samples obtained after multiple dosing; in healthy volunteers doses were given orally while patients received all doses as intravenous infusions

Table 7.14: Demographic statistics of the study population

Individuals		Healthy volunteers	Septic patients	Patients with septic shock	Total
Number	(male/ female)	10 (5/5)	8 (4/4)	16 (10/6)	34 (19/15)
Age (years)	median (min.-max.)	54 (41-76)	72 (53-80)	63 (51-78)	62 (41-80)
Height (cm)	median (min.-max.)	171 (157-178)	169 (156-180)	169 (149-192)	170 (149-192)
Weight (kg)	median (min.-max.)	65 (51-80)	60 (40-102)	85 (45-142)	67 (40-142)
CLCR (mL/min)	median (min.-max.)	79 (39-99)	59 (18-200)	61 (16-96)	65 (16-200)
THRO (1/nL)	median (min.-max.)	223 (160-296)	267 (115-637)	127 (59-524)	201 59-637)

CLCR: creatinine clearance; THRO: thrombocytes

Table 7.15: Renal status of study population

Renal impairment	CLCR [mL/min]	Number of subjects	% of population
Severe	< 30	5	15
Moderate	30 - 50	5	15
Mild	50 - 80	13	38
None	> 80	11	32

Table 7.16: Covariates selected by the GAM analysis and other covariates tested for reasons of plausibility on unbound plasma and ISF parameters

Parameter	GAM analysis	Additional covariates
CL	HT, CRP, LDH, TYPE, CID	CLCR, WT, THRO, SEX, AGE
V2	WT, LDH, TYPE	HT, TYPE, SEX, THRO, CLCR
V3	WT, CRP, THRO, SEX	CLCR, CID, HT, AGE
PC23	AGE, LDH	CLCR, SCRE, WT
PC24	SCRE, HT	CLCR, AGE, WT

Table 7.17: 95% confidence intervals obtained from the final model and after log-likelihood profiling

	95% confidence interval	
Parameter	final covariate model	log-likelihood profiling
Model for unbound plasma concentrations		
ωKA	-0.112 – 1.36	0.247 – 2.16
θ_{CL}	-0.003 – 0.025	0.005 – 0.017
Joint model for unbound ISF and plasma concentrations		
$\omega PC24$	-0.034 – 0.191	0.049 – 0.134
θ_{CLCR_PC24}	-0.002 – 0.010	0.002 – 0.006

Table 7.18: Results of the bootstrap analysis for the final plasma model

Model parameter		Final model estimate	Bootstrap mean[#]	Bias[#]	Relative Bias, %[#]
CL	[L/h]	11.5	12.8	-1.34	-11.6
V2	[L]	19.8	19.3	0.480	2.42
Q	[L/h]	76.8	79.6	-2.76	-3.59
V3	[L]	27.0	27.9	-0.935	-3.46
KA	[1/h]	1.85	0.916	0.934	50.5
VAR		0.567	0.561	-0.006	-0.988
KIC	[1/h]	0.0027	0.0021	0.0006	23.7
Covariate influence, %					
θ_{CLCR_CL}		0.911	0.736	0.176	19.3
θ_{WT_CL}		1.13	0.765	0.366	32.3
θ_{THRO_CL}		0.229	0.167	0.063	27.3
θ_{WT_V3}		1.52	1.55	-0.032	-2.07
Interindividual variability					
$\omega^2 CL$		0.248	0.269	-0.021	-8.53
$\omega^2 V2$		0.138	0.107	0.031	22.7
$\omega^2 V3$		0.042	0.025	0.017	40.6
$\omega^2 KA$		0.622	3.04	-2.42	-389
$\omega^2 VAR$		6.36	7.09	-0.727	-11.4
Residual Variability					
σ proportional		0.096	0.116	-0.021	-21.8
σ additive		0.042	0.029	0.013	30.6

[#] = obtained from 20 bootstrap runs

Table 7.19: Optimised sampling time points for the final plasma model

	Sampling time points [h] per dose number						
Group*	**1**	**2**	**3**	**4**	**5**	**6**	**7**
1	0.24 0.53 1.62	12.0	-	-	0[#]	-	12.0
2	-	0.24 0.53 1.62	12.0	0[#]	12.0	-	-
3	12.0	-	-	0[#]	0.24 0.53 1.62 12.0	-	-

*where 1 group consisted of 10 individuals; [#] corresponds to trough sample

Table 7.20: Parameters from final plasma model and from simulations using the optimised sampling design

		Final model		**Optimised design**	
Model parameter		Estimate	RSE %[#]	Estimate	RSE %[#]
CL	[L/h]	11.5	8.78	11.8	11.4
V2	[L]	19.8	8.38	20.9	9.28
Q	[L/h]	76.8	8.16	78.9	9.34
V3	[L]	27.0	6.26	30.3	5.74
VAR		0.567	19.9	0.595	4.82
KIC	[1/h]	0.0027	12.6	0.0015	41.6
IC50	[mg/L]	0.1 FIX	-	0.1	-
Interindividual variability					
ωCL	[CV%]	49.8	40.7[*]	58.0	21.7[*]
ωV2	[CV%]	37.1	25.1[*]	37.9	36.0[*]
ωV3	[CV%]	20.5	46.2[*]	17.5	41.5[*]
Residual Variability					
σ proportional	[CV%]	9.59	7.60	8.55	7.38
σ additive	[mg/L]	0.042	74.3	0.051	19.8

[*] = standard error given on the variance scale; [#] = relative standard error

Table 7.21: Results of the bootstrap analysis for the joint model describing plasma and ISF concentrations

Model parameter		Final model estimate	Bootstrap mean[#]	Bias[#]	Relative Bias, %[#]
PC23		1.05	1.04	0.011	1.02
PC24		1.07	1.05	0.018	1.64
K40	[1/h]	13.0	12.7	0.300	2.31
Covariate influence, %					
θ_{THRO_K40}		0.211	0.184	0.028	13.0
θ_{CLCR_PC24}		0.382	0.274	0.109	28.4
Interindividual and interoccasion variability					
$\pi^2 PC23$		0.190	0.184	0.006	3.07
$\omega^2 PC24$		0.078	0.085	-0.007	-8.90
$\omega^2 K40$		0.404	0.398	0.006	1.41
Residual Variability					
σ proportional		0.202	0.398	-0.004	-2.03

[#] = obtained from 20 bootstrap runs

Table 7.22: Tissue penetration parameter change of a model with linear elimination compared to inhibition compartment model

Parameter	Median model predicted value		Median change, %	Range of change, %
	Final model	**Linear model**		
PC23	1.23	1.24	2.96	-38.1 – 13.2
PC24	1.11	1.12	-0.04	-10.4 – 8.49

Table 7.23: Optimised sampling time points for s.c. and i.m. microdialysis

Group*	Sampling time points [h] per dose number						
	1	**2**	**3**	**4**	**5**	**6**	**7**
1	0[#] 0.69	-	-	-	0[#] 0.52	-	-
2	-	0[#] 0.50	-	1.0 3.0	-	-	-
3	-	-	-	0.70 0.80	2.0 6.0	-	-

*where 1 group consisted of 10 individuals; [#] corresponds to trough sample

Table 7.24: Parameters from final joint model and from simulations using the optimised sampling design

Model parameter		**Final model**		**Optimised design**	
		Estimate	RSE %[#]	Estimate	RSE %[#]
PC23		1.05	6.39	1.04	3.25
PC24		1.07	5.87	1.19	5.09
K40		13.0	14.5	8.71	26.5
Interindividual and interoccasion variability					
πPC23	[CV%]	43.6	41.0*	35.1	19.8*
ωPC24	[CV%]	28.0	71.9*	14.1	33.7*
ωK40	[CV%]	63.6	36.4*	69.9	89.6*
Residual Variability					
σ proportional	[CV%]	20.2	4.18	19.5[a] 19.6[b]	4.93[a] 5.15[b]

* = standard error given on the variance scale; [#] = relative standard error; [a] = optimisation for muscular ISF;
[b] = optimisation for subcutaneous ISF

7.2   Figures
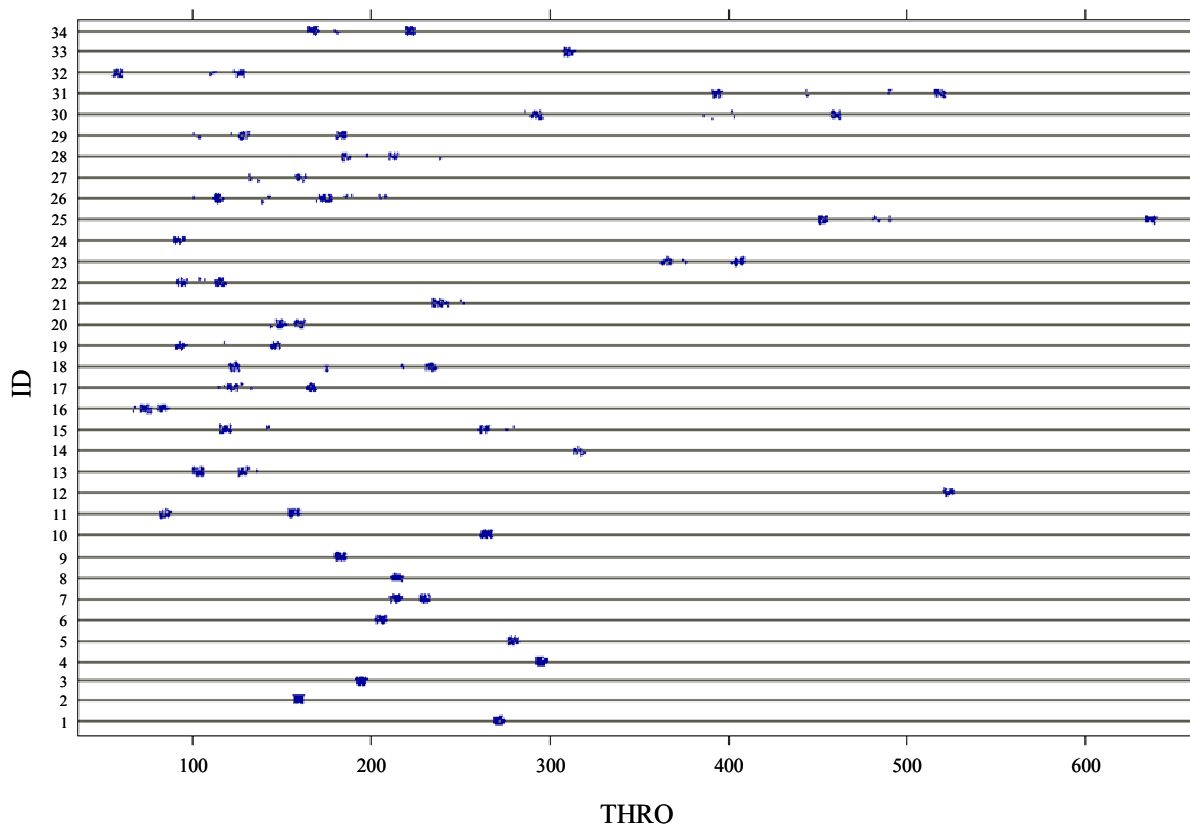
Figure 7.1: Example of an index plot showing individual subject records (ID) vs thrombocyte values (THRO)
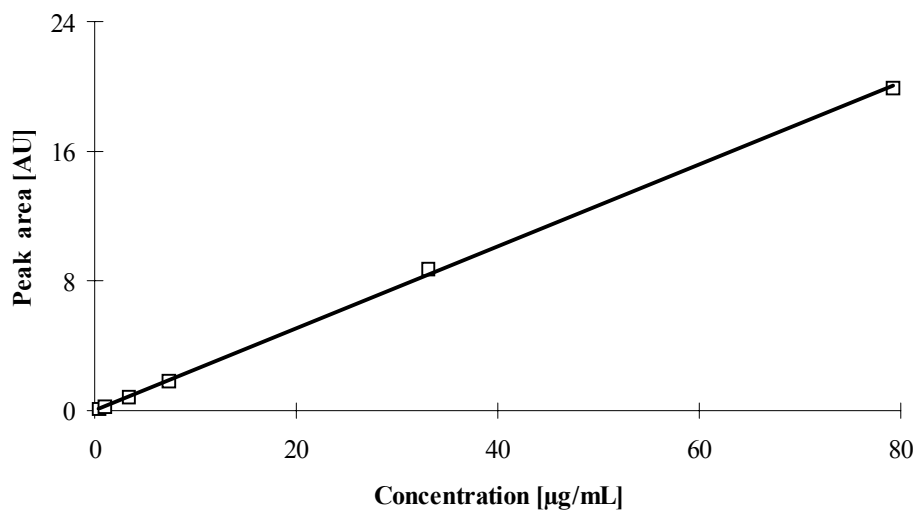
Figure 7.2: Representative calibration function of vancomycin in plasma (n = 1)
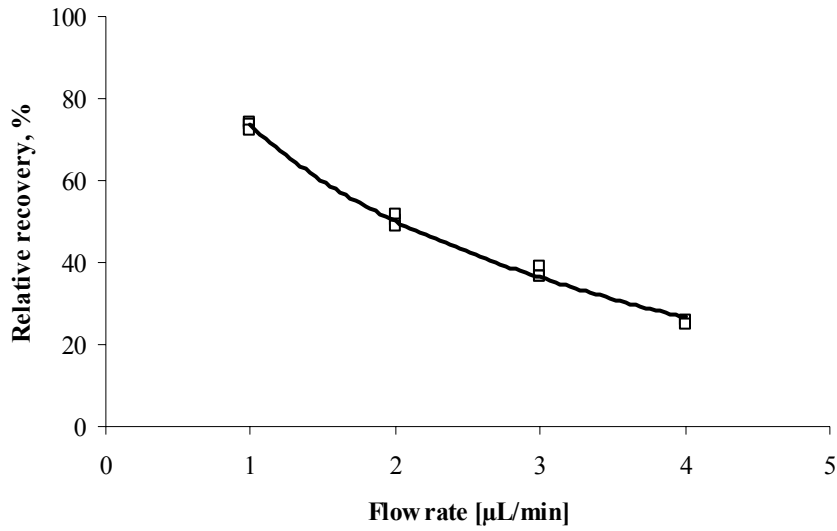
Figure 7.3: Dependence of relative recovery (RR, %) on flow rate (µL/min) of microdialysis perfusate (80 µg/mL vancomycin). The individual results ($n = 3$) are depicted as open squares.
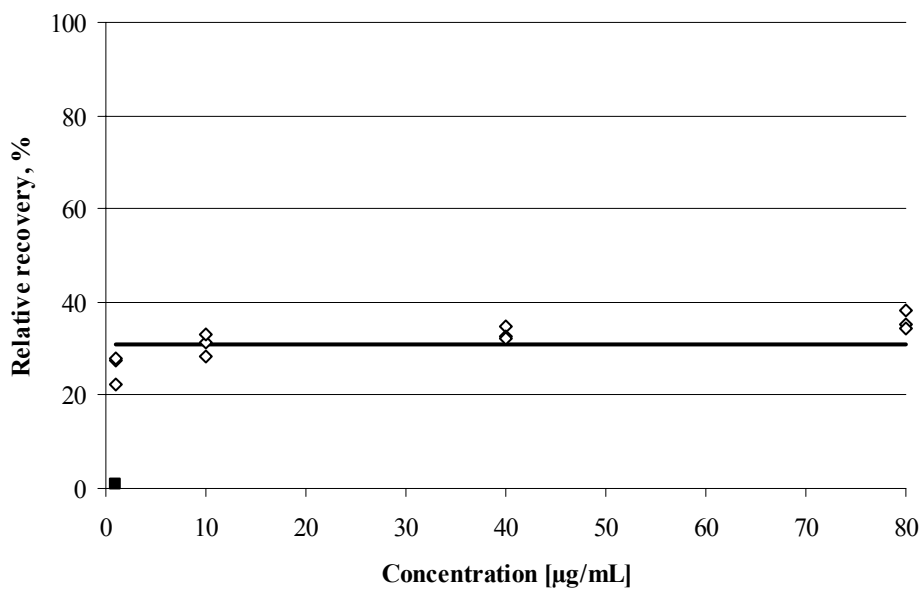
Figure 7.4: Dependence of relative recovery (RR, %) on vancomycin concentration (µg/mL) in the perfusate achieved in initial delivery experiments ($n = 3$, open diamonds). The black line corresponds to the arithmetic mean relative relcovery.
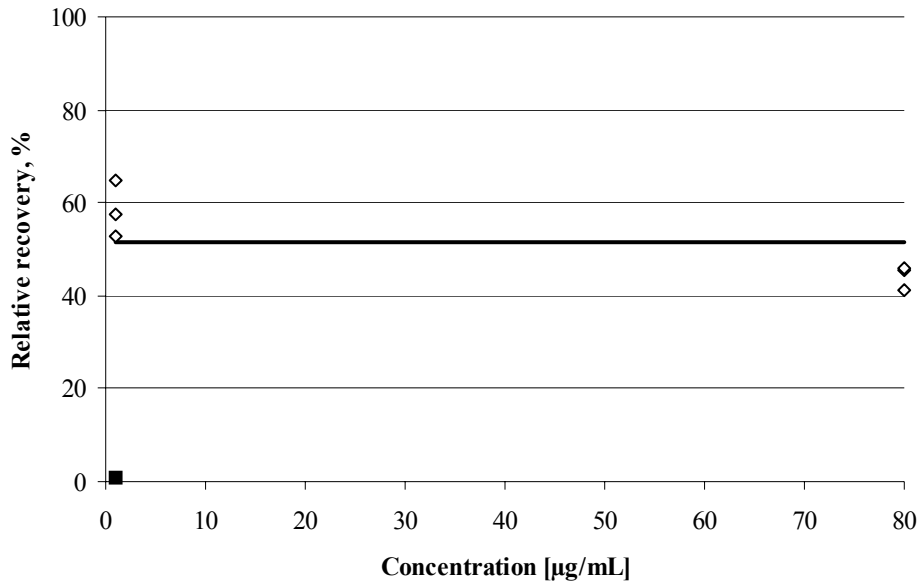
Figure 7.5: Dependence of relative recovery (RR, %) on vancomycin concentration (µg/mL) in the perfusate achieved in the experimental setup as performed by Luer et al. (*n* = 3, open diamonds). The black line corresponds to the arithmetic mean relative relcovery.
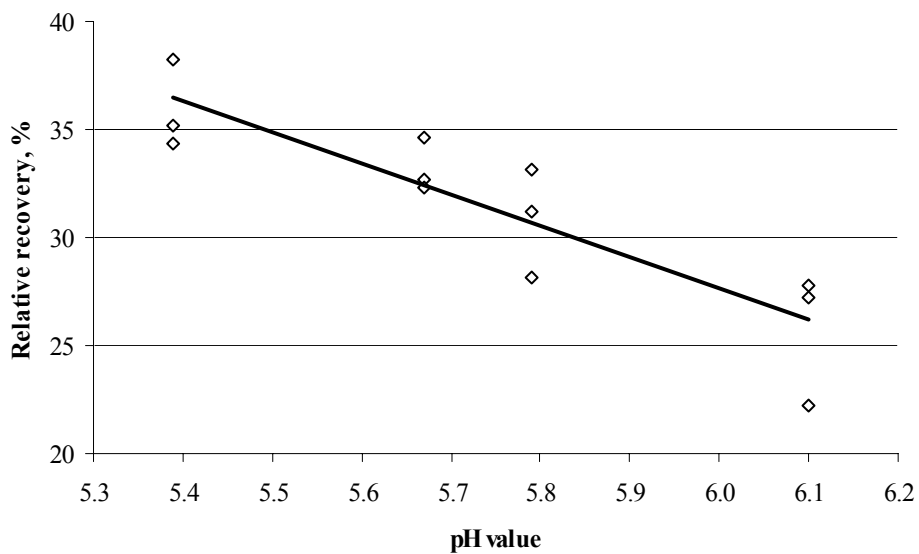
Figure 7.6: Dependence of relative recovery (RR, %) on pH value achieved in initial delivery experiments (*n* = 3, open diamonds). Lower pH values correspond to high concentrations and vice versa. The black line corresponds to the calculated regression line.
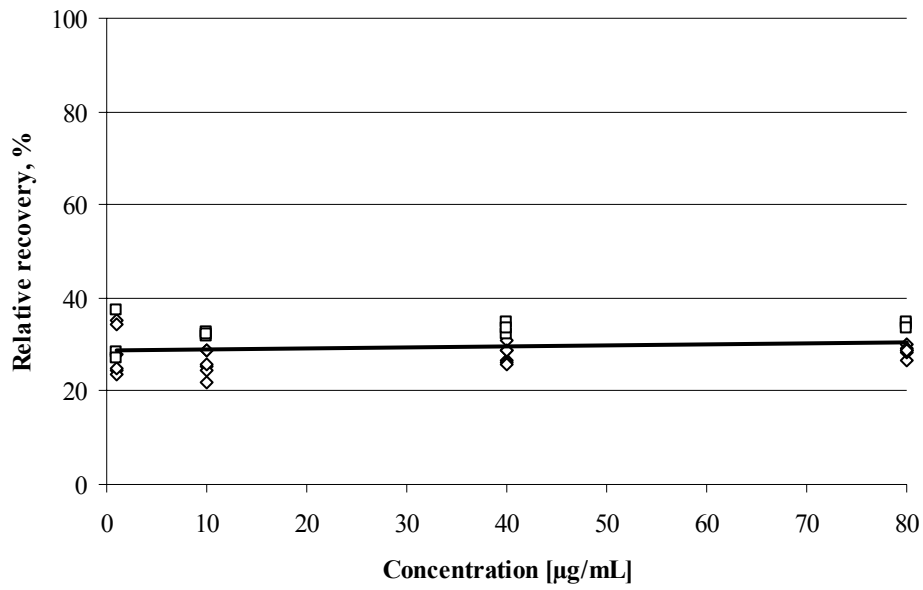
Figure 7.7: Independence of relative recovery (RR, %) on concentration (µg/mL) of perfusion or surrounding medium, respectively, achieved in final recovery ($n = 6$, open diamonds) and delivery ($n = 3$, open squares) experiments with phosphate buffer. The black line corresponds to the calculated regression line.
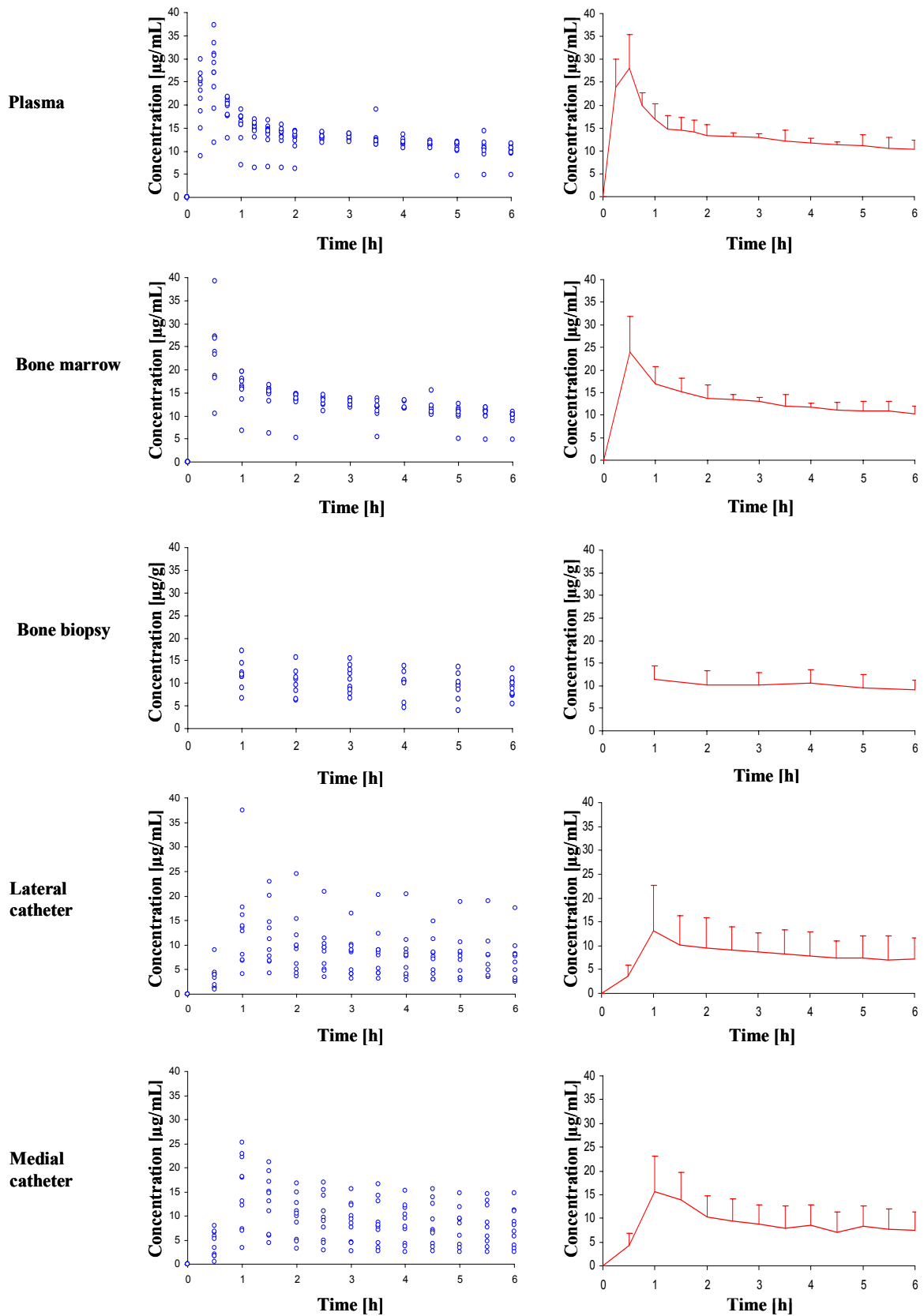
Figure 7.8: Concentration-time plots of different matrices; blue circles: observed concentrations, red lines: median concentration-time profiles (+ SD).
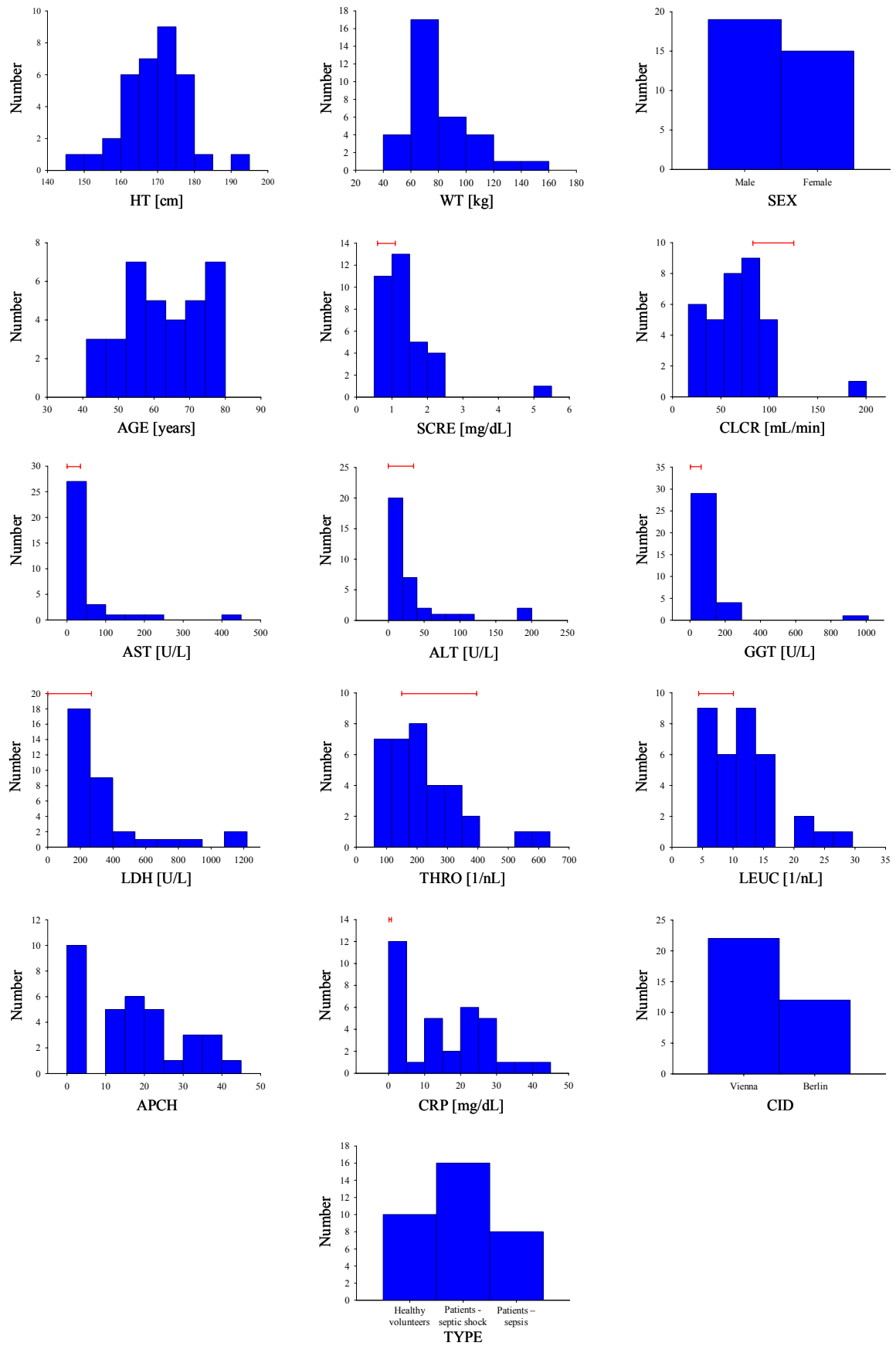
Figure 7.9: Covariate histograms of the study population. If applicable, reference ranges are presented as red bars.

Single dose   **Multiple dose**

Ultrafiltrate

s.c.

i.m.
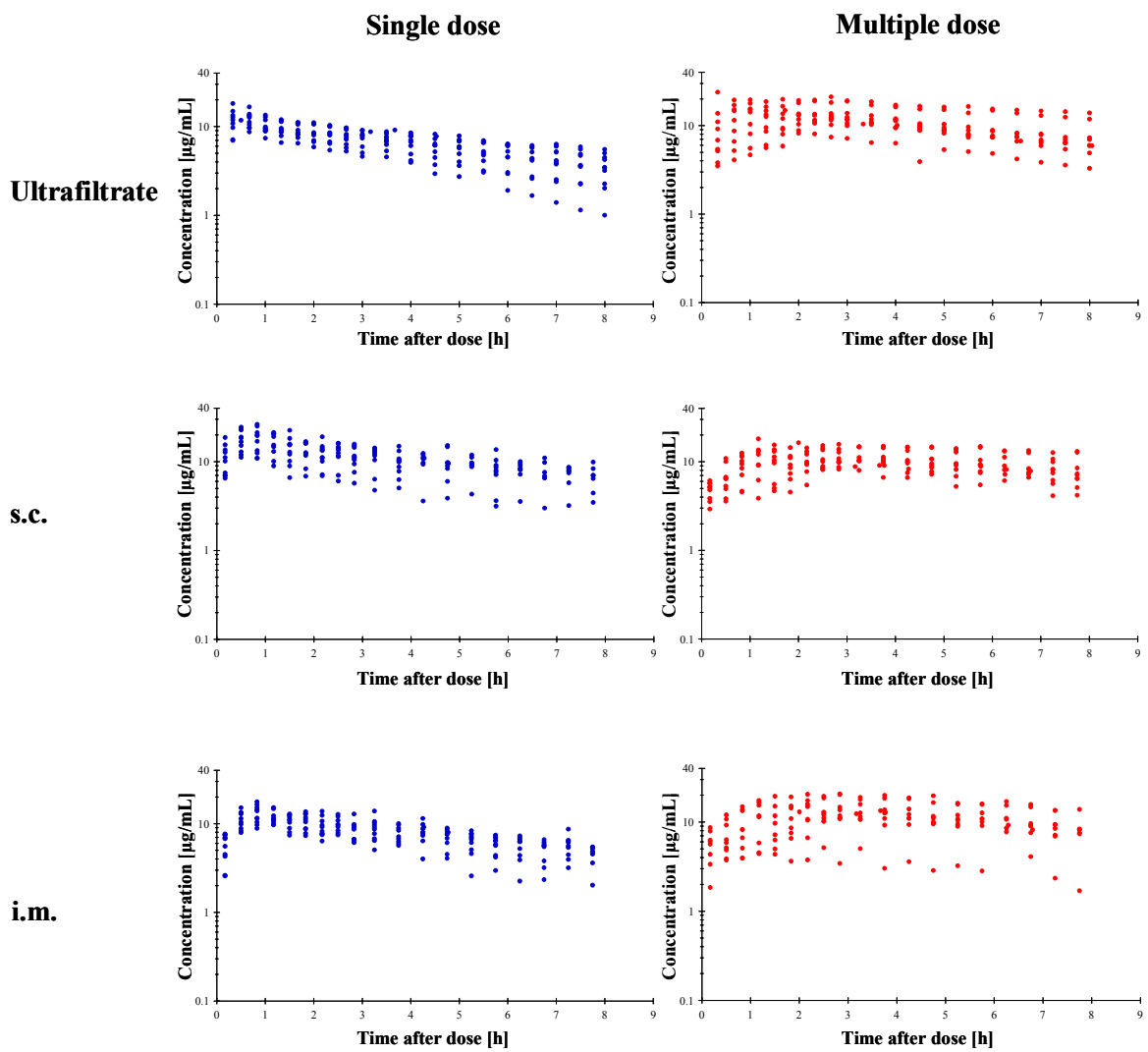
Figure 7.10: Concentration-time plots of healthy volunteers after single intravenous and multiple oral linezolid administration in different matrices; s.c.: subcutaneous ISF; i.m.: muscular ISF.

Single dose **Multiple dose**
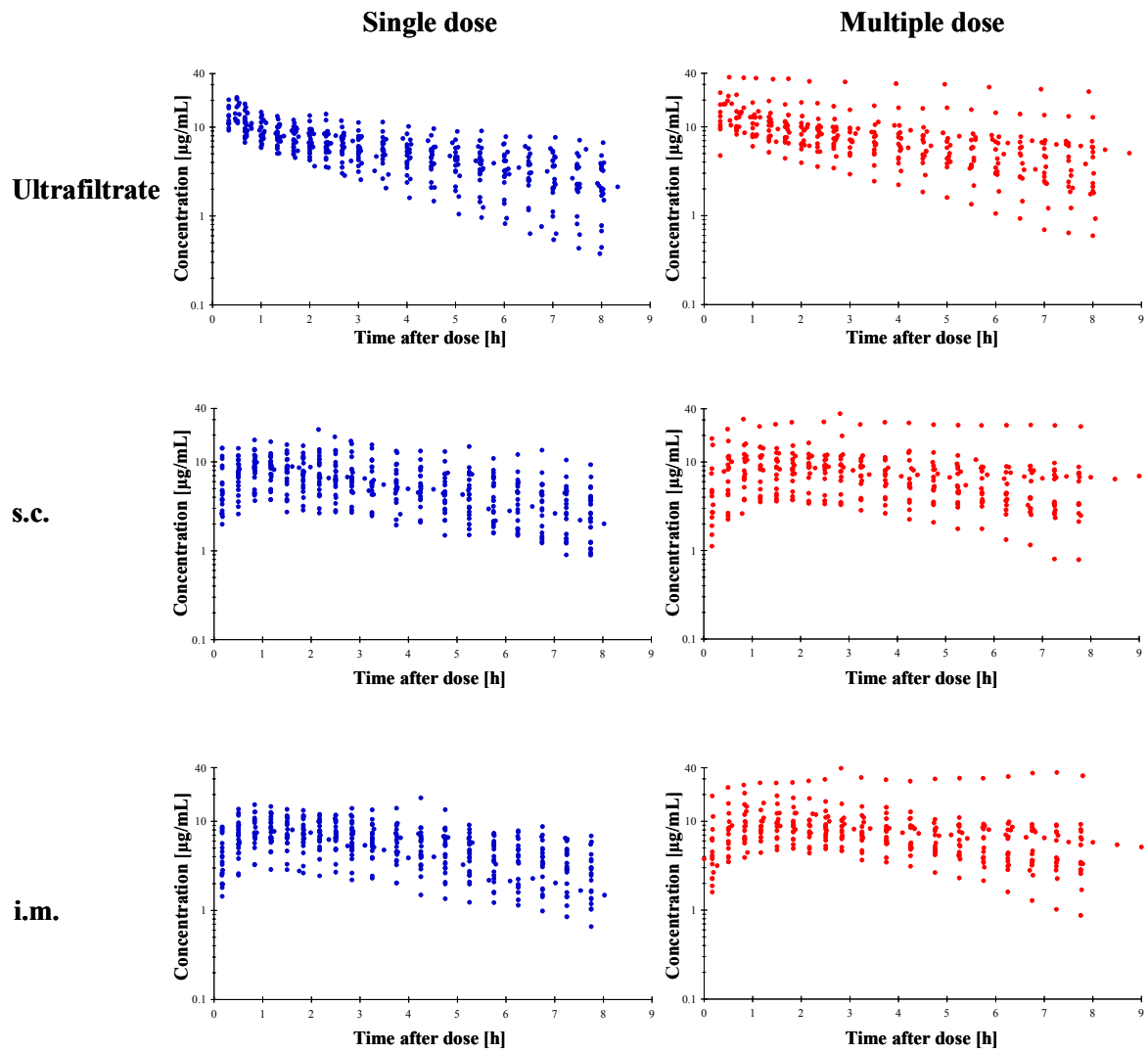
Figure 7.11: Concentration-time plots of patients after single and multiple intravenous linezolid administration in different matrices; s.c.: subcutaneous ISF; i.m.: muscular ISF.
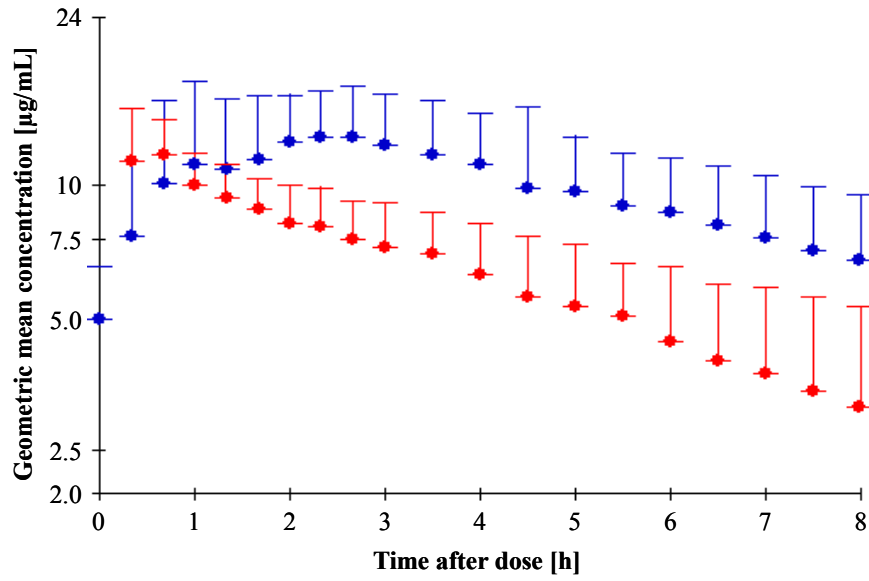
Figure 7.12: Geometric mean (+SD) unbound plasma concentrations observed in healthy volunteers (*n* = 10) after single intravenous (red filled circles) and multiple oral (blue filled circles) dosing.
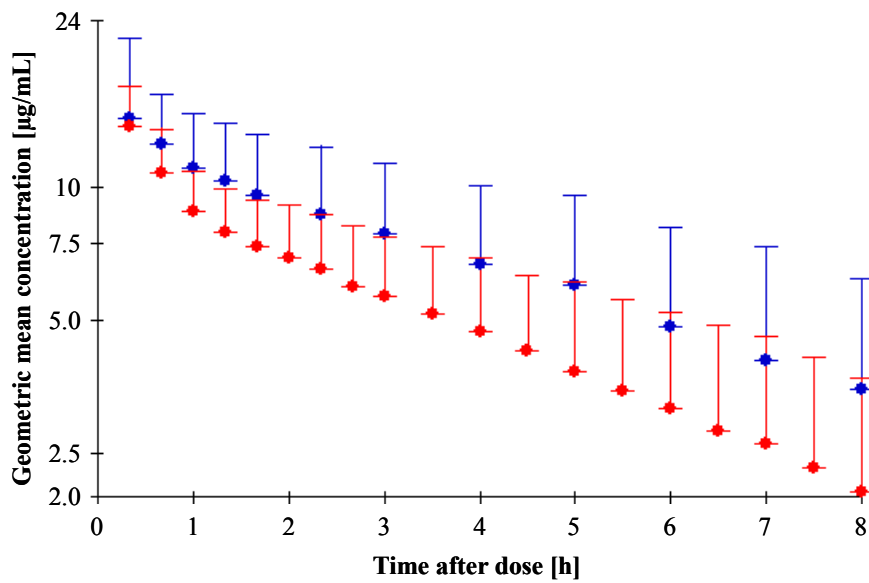
Figure 7.13: Geometric mean (+SD) unbound plasma concentrations observed in patients (*n* = 24) after single (red filled circles) and multiple (blue filled circles) intravenous dosing.
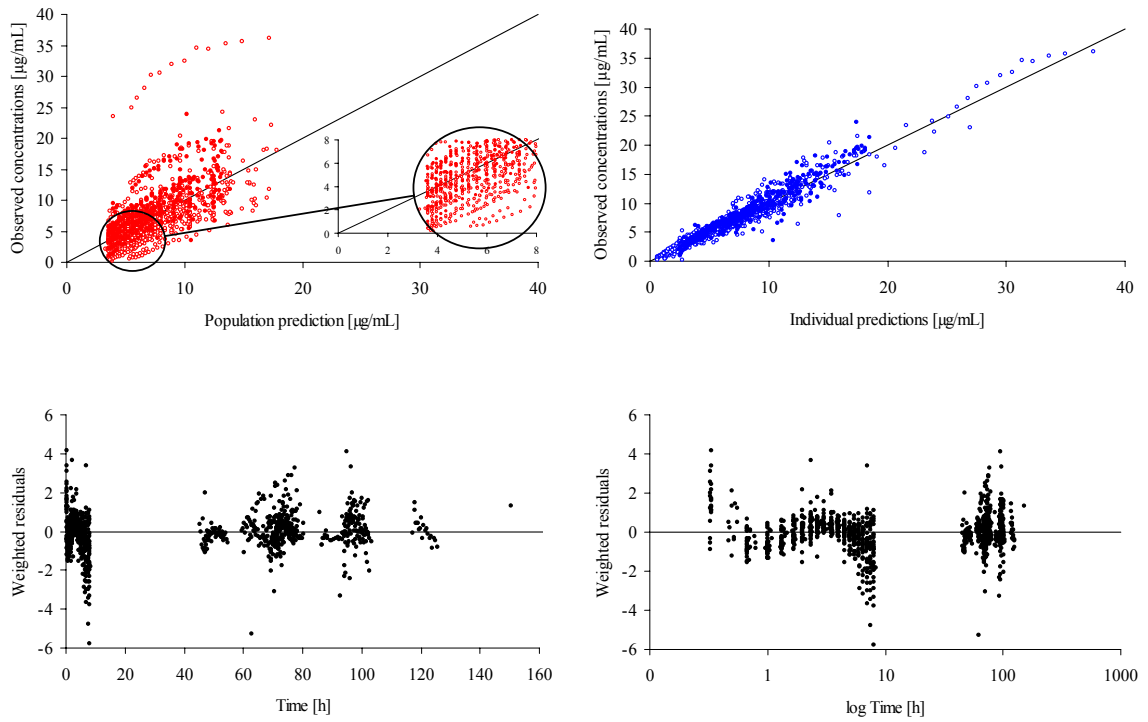
Figure 7.14: Goodness of fit plots for unbound plasma data using model DSA1 (linear elimination). The enlarged section reveals model misspecifications: low values were overestimated; upper panel: filled circles: healthy volunteers, empty circles: patients.
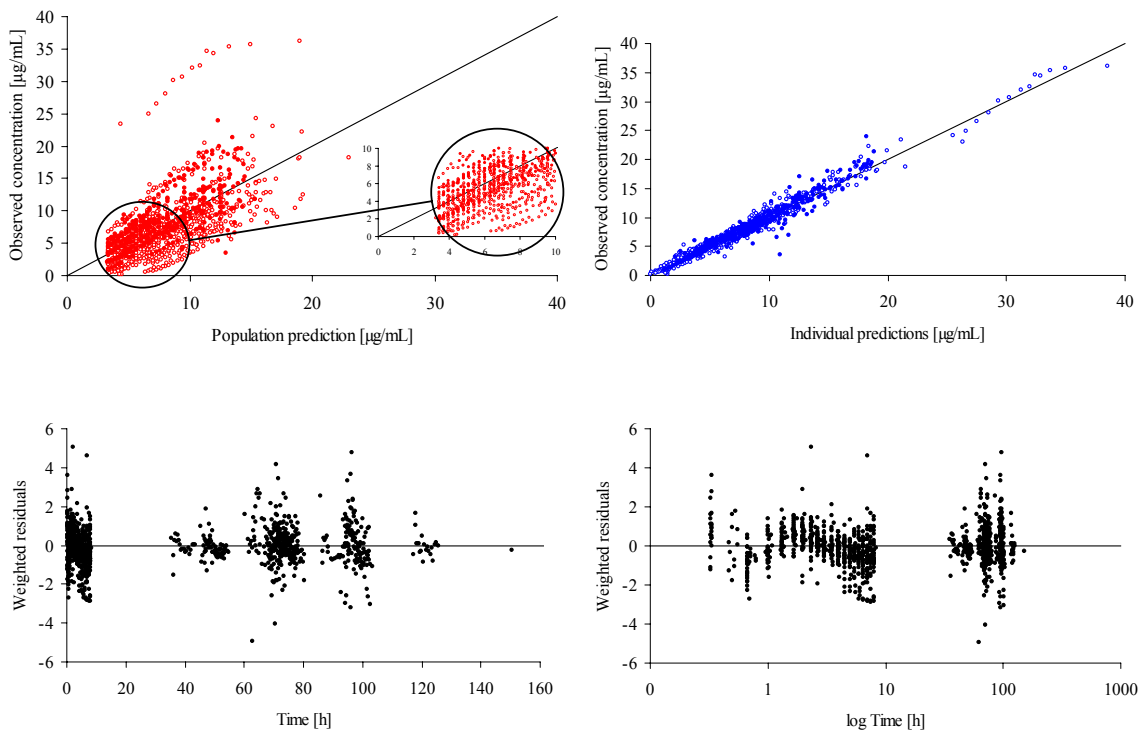
Figure 7.15: Goodness of fit plots for unbound plasma data using model DSA2 (parallel linear and Michaelis Menten elimination). The enlarged section reveals model misspecifications: low values were overestimated; upper panel: filled circles: healthy volunteers, empty circles: patients.
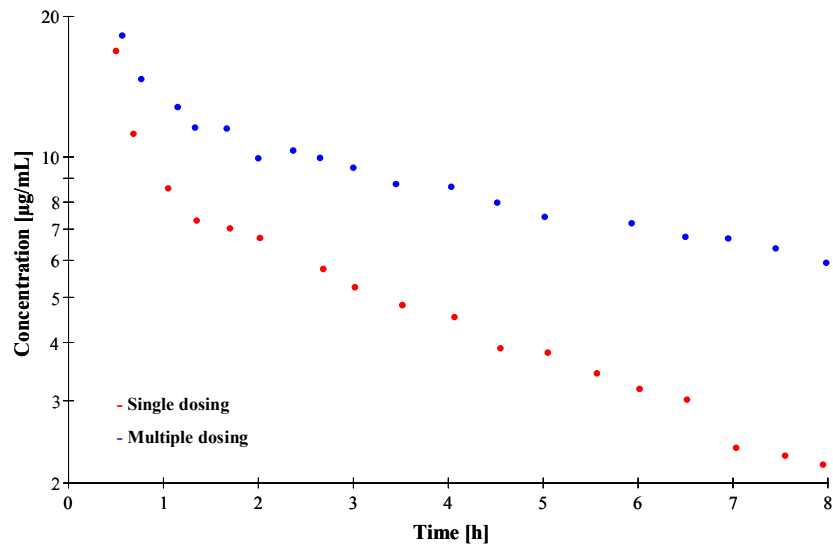
Figure 7.16: Individual concentration-time profile of a single individual having almost the same C_{max} after single and multiple dosing.
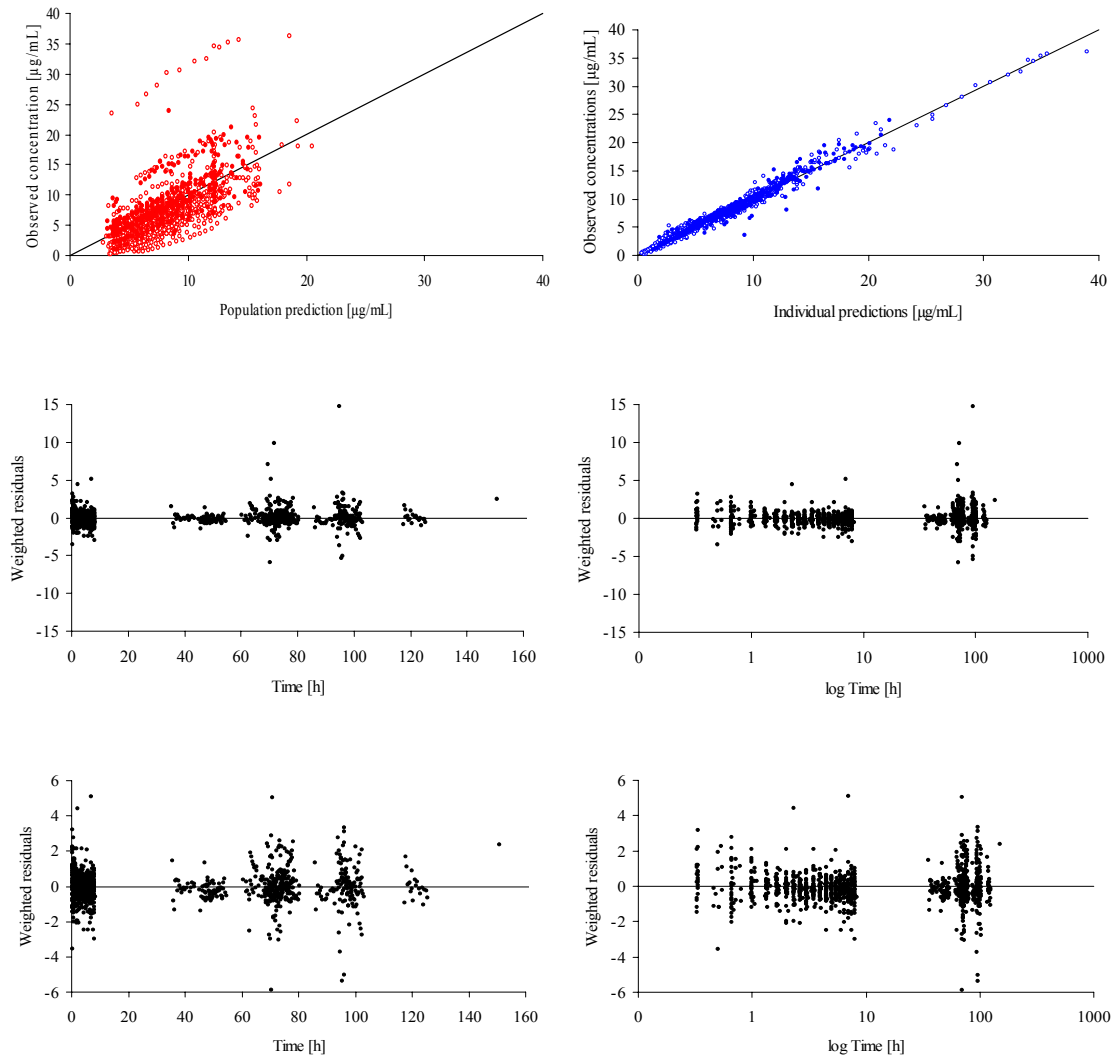
Figure 7.17: Goodness of fit plots for unbound plasma data using model DSA3 (effect compartmental approach); upper panel: filled circles: healthy volunteers, empty circles: patients. The lower panel represents an enlarged section of weighted residuals against time or logarithm of time.
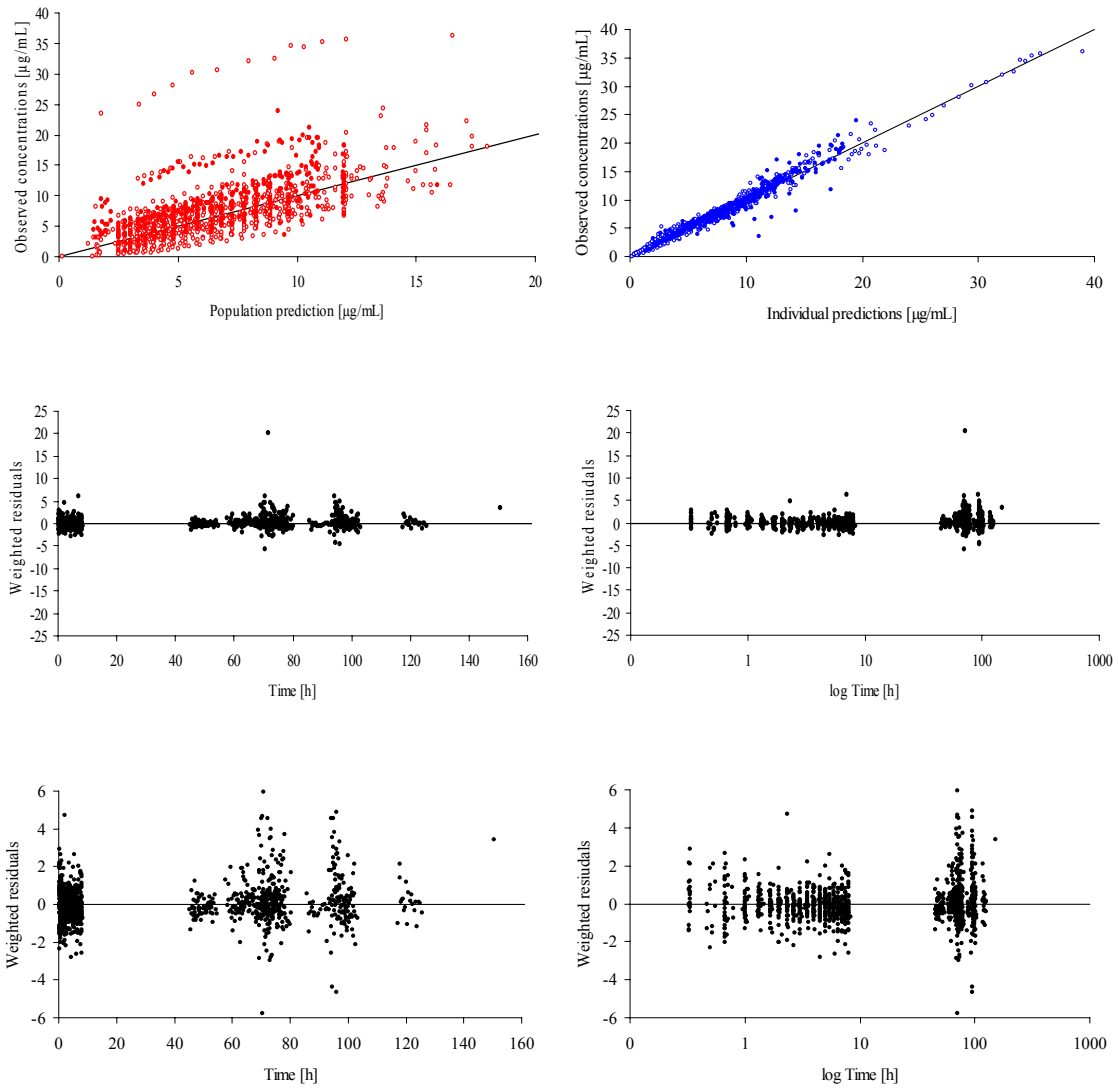
Figure 7.18: Goodness of fit plots for unbound plasma data using model DSA4; clearance was inhibited as a function of time, only one clearance estimated; upper panel: filled circles: healthy volunteers, empty circles: patients. The lower panel represents an enlarged section of weighted residuals against time or logarithm of time.
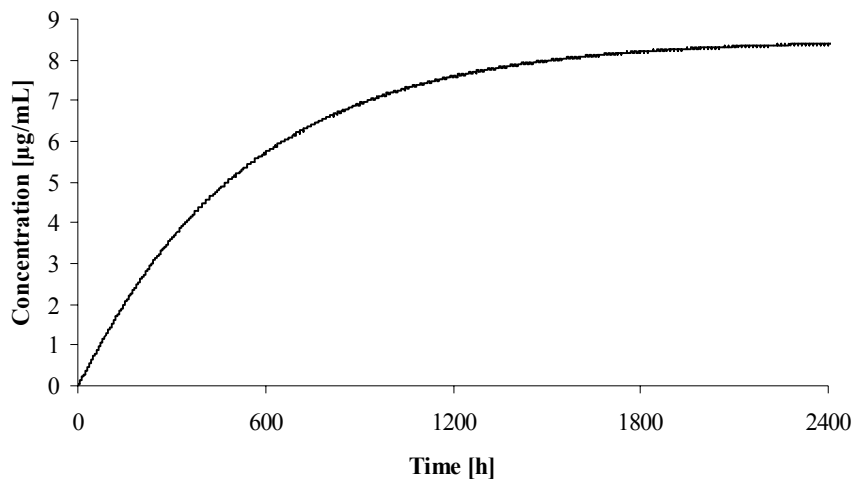
Figure 7.19: Simulated concentration-time course of linezolid in the empirical inhibiton compartment of model DSA5 over a 100-day period. Simulations were performed under the assumption of 600 mg dosing bid over the whole time period.
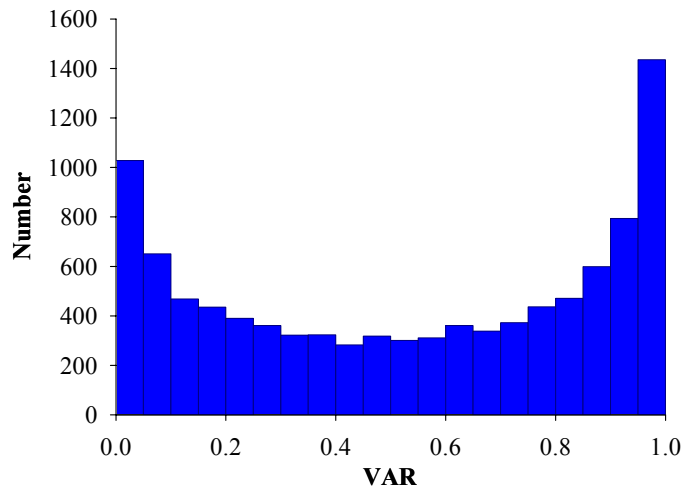
Figure 7.20: Distribution of individual values of VAR (simulation of 10000 values).
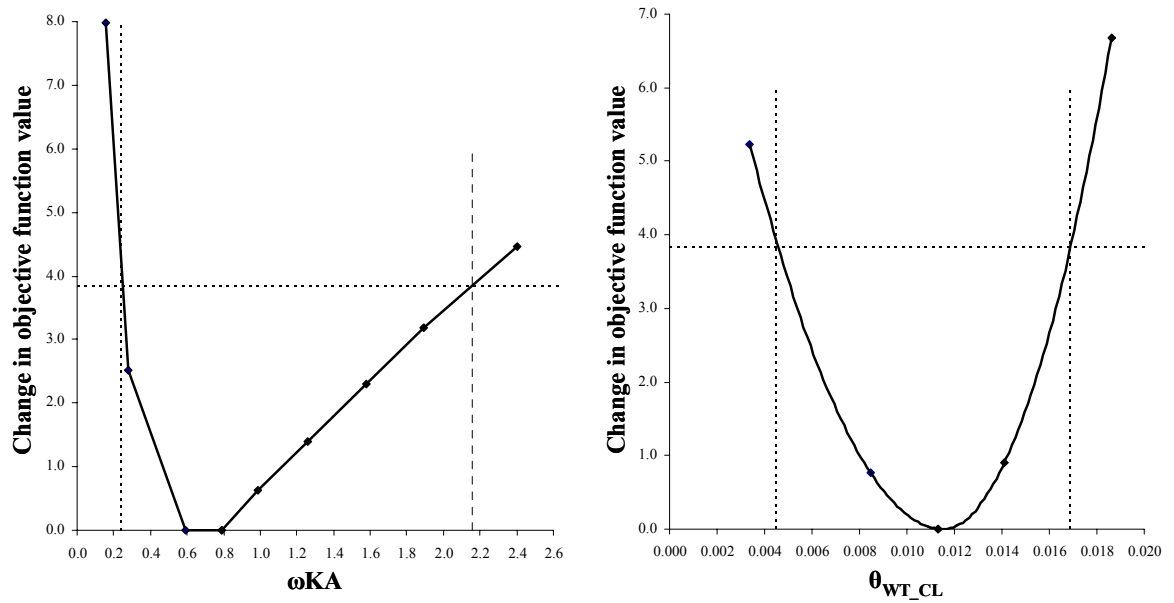
Figure 7.21: Log-likelihood profiles for the parameters ωKA and θ_{WT_CL}.
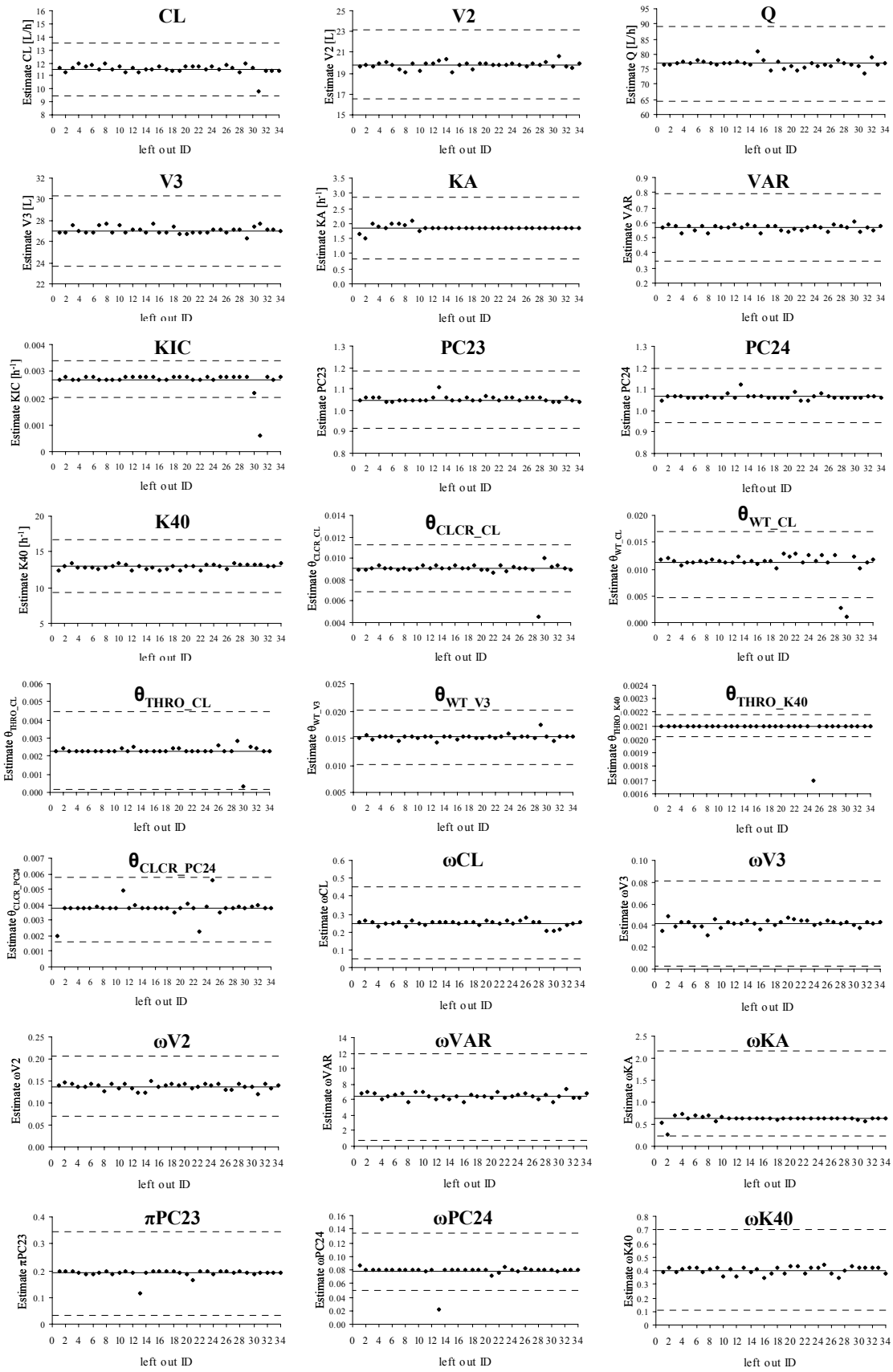
Figure 7.22: Results of case deletion diagnostics based on datasets in which only one individual was deleted. Black symbols: parameter estimate of the reduced dataset; black line: original parameter estimate obtained from the full dataset; dashed lines include the 95% confidence interval obtained from the full dataset.
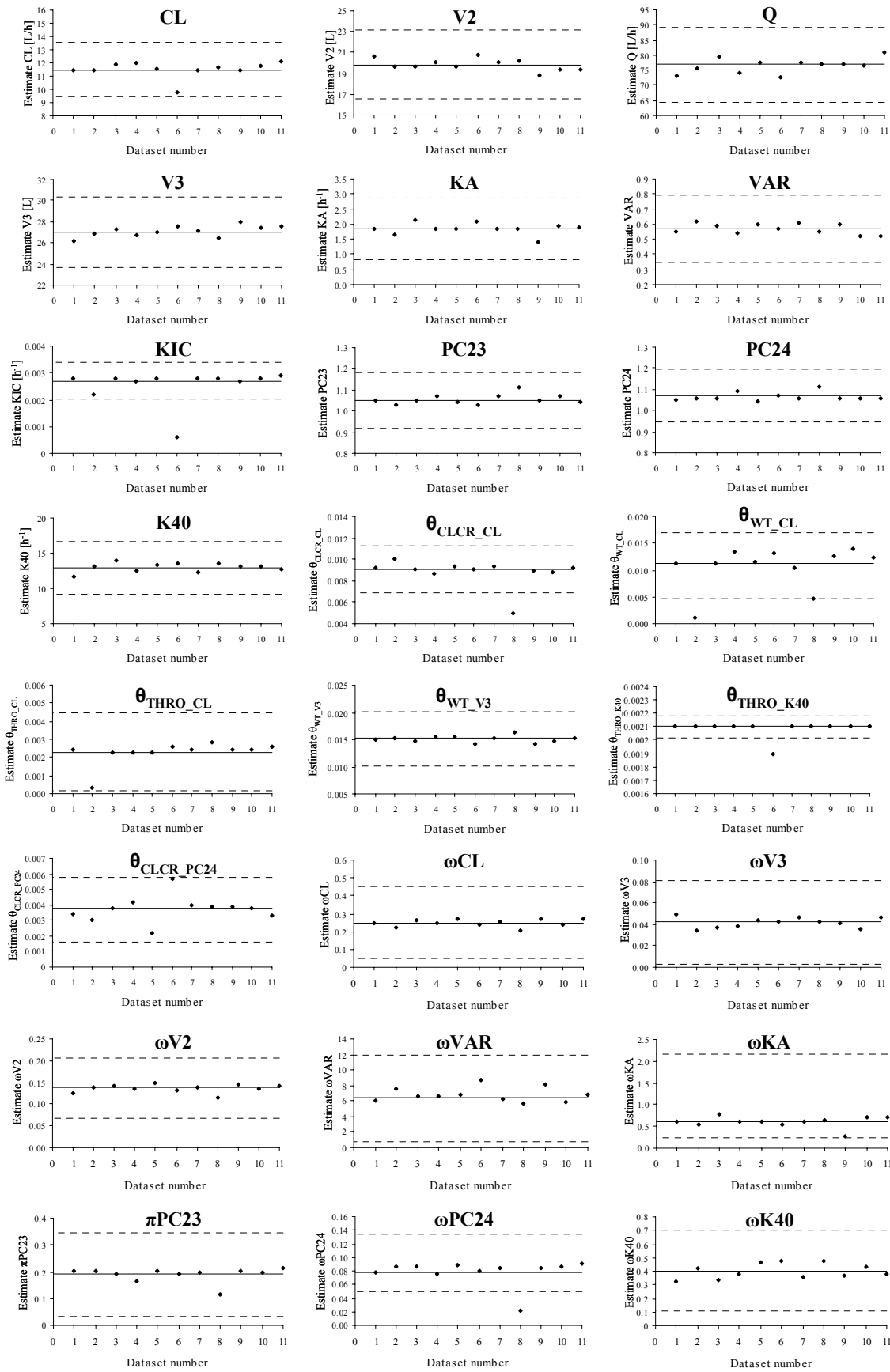
Figure 7.23: Results of case deletion diagnostics based on datasets in which 10% of the individuals were deleted. Black symbols: parameter estimate of the reduced dataset; black line: original parameter estimate obtained from the full dataset; dashed lines include the 95% confidence interval obtained from the full dataset.
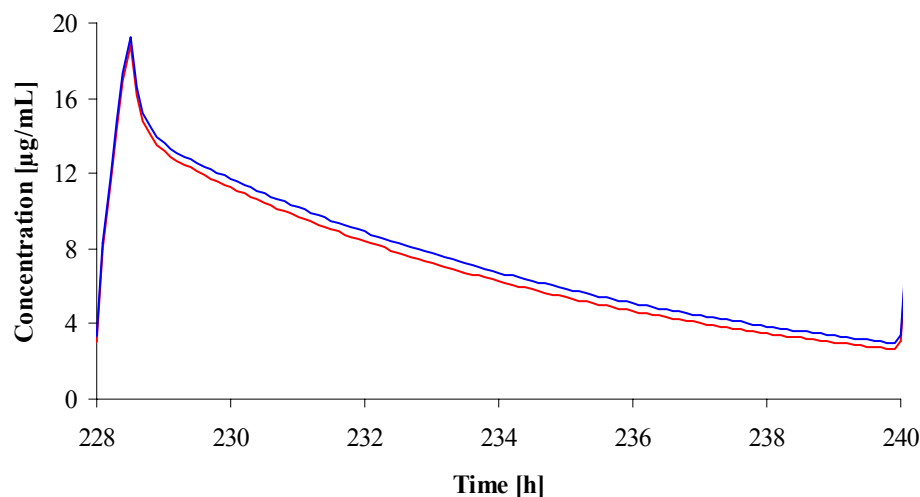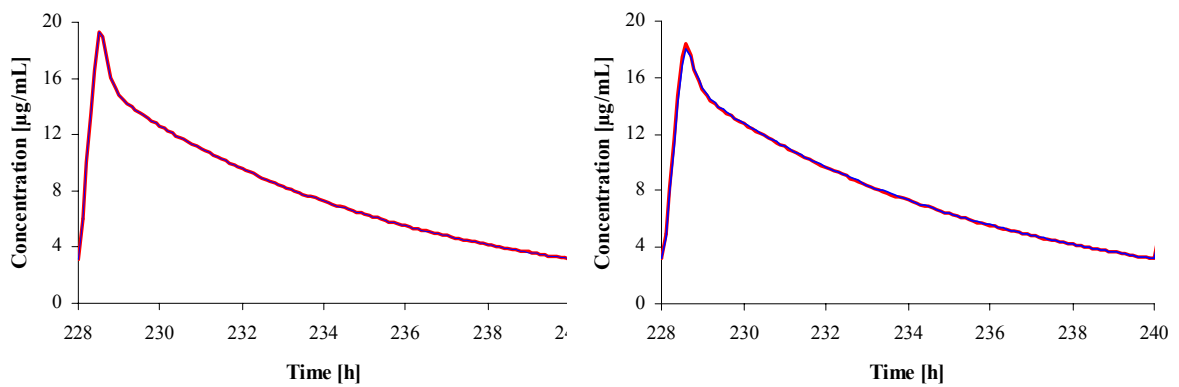
Figure 7.24: Simulated concentration-time profile over one dosing interval after multiple dosing using extreme KIC values obtained during case deletion diagnostics. Red line: KIC=0.0006 h^{-1}; Blue line: KIC=0.0029 h^{-1}.
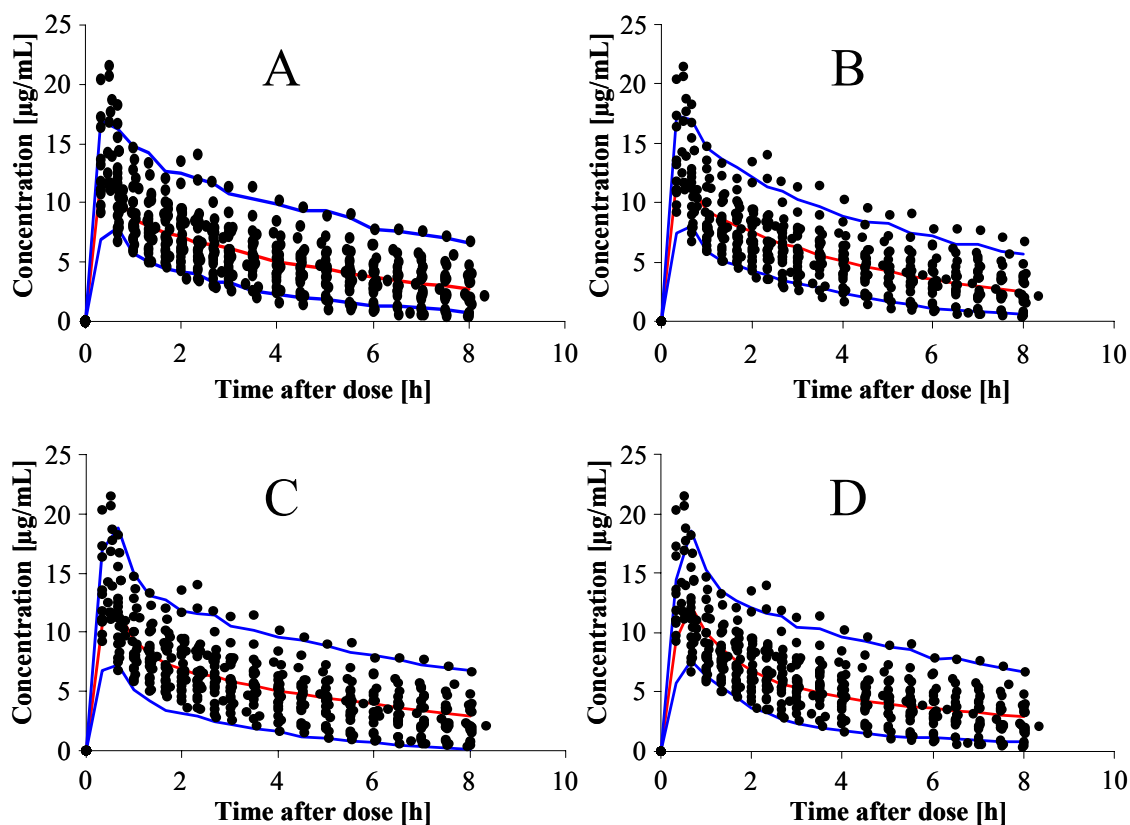
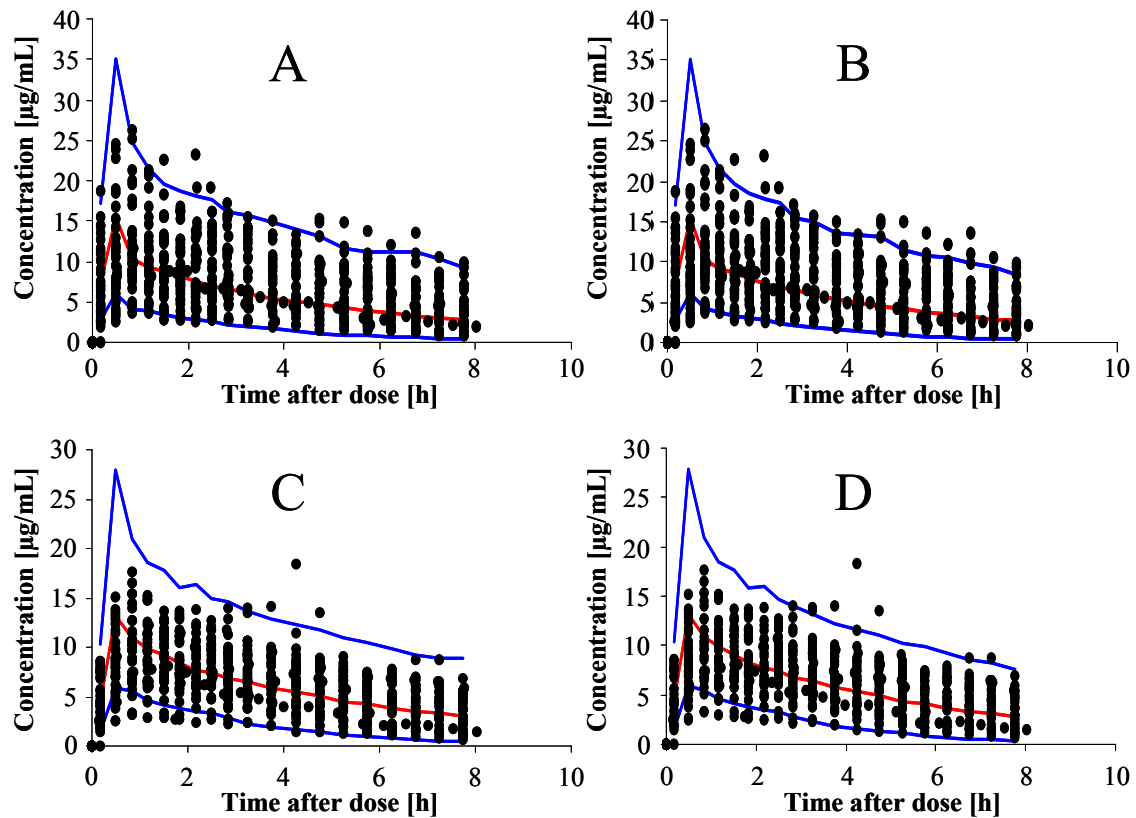Figure 7.25: Predictive check for the model describing unbound plasma concentrations after single dosing. Red lines represent the simulated median concentration-time profile whereas blue lines represent the 5% and 95% quantile and enclose the 90% prediction interval. Filled circles represent observed concentrations after single dosing. A: inhibition compartment model; B: inhibition compartment model, ωVAR set to zero; C: model with parallel linear and Michaelis Menten elimination; D: model with linear elimination.
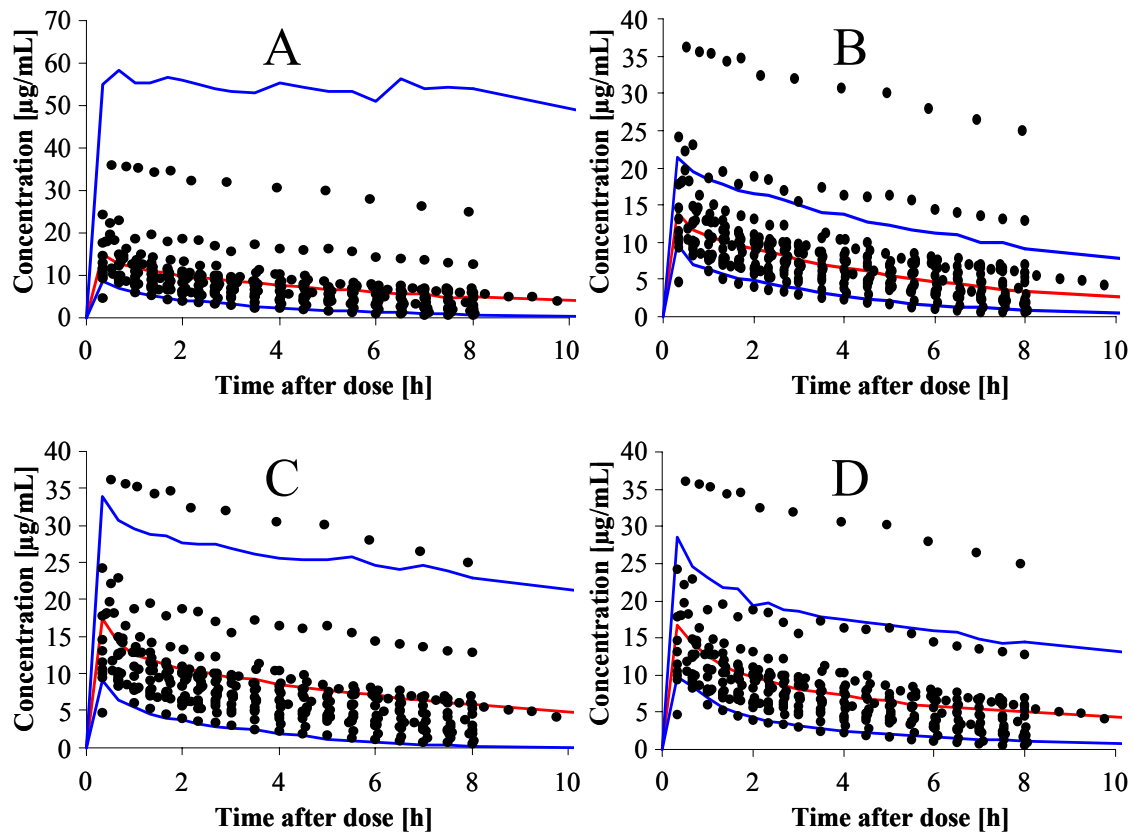
Figure 7.26: Predictive check for the model describing unbound plasma concentrations after multiple dosing. Red lines represent the simulated median concentration-time profile whereas blue lines represent the 5% and 95% quantile and enclose the 90% prediction interval. Filled circles represent observed concentrations after multiple dosing. A: inhibition compartment model; B: inhibition compartment model, ω VAR set to zero; C: model with parallel linear and Michaelis Menten elimination; D: model with linear elimination.
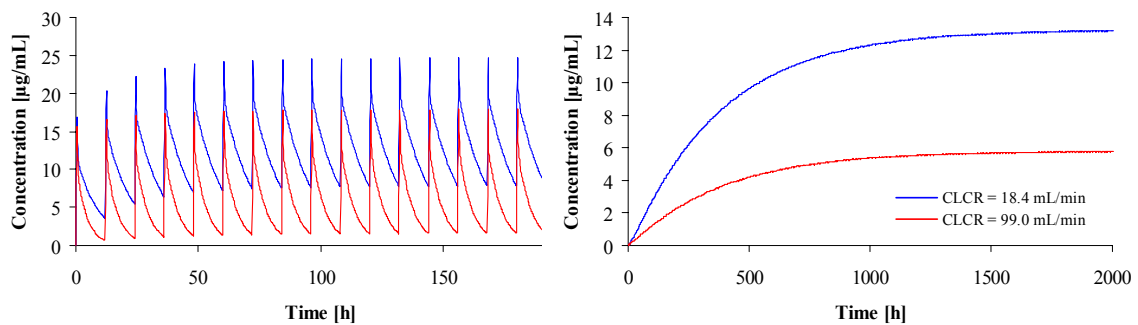
Figure 7.27: Influence of creatinine clearance on the concentration-time profiles in the central (left) and inhibition (right) compartment.
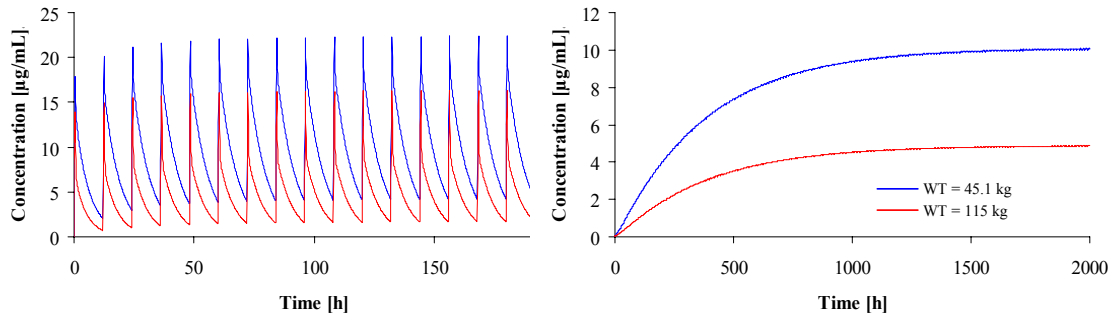
Figure 7.28: Influence of body weight on the concentration-time profiles in the central (left) and inhibition (right) compartment.
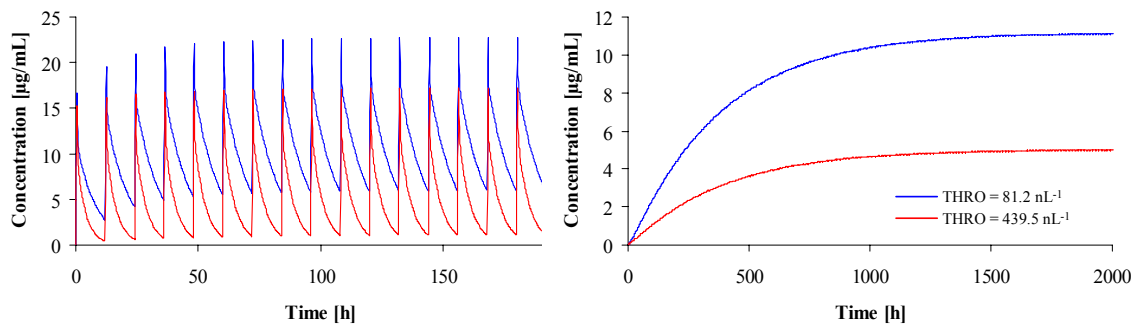
Figure 7.29: Influence of thrombocytes on the concentration-time profiles in the central (left) and inhibition (right) compartment.
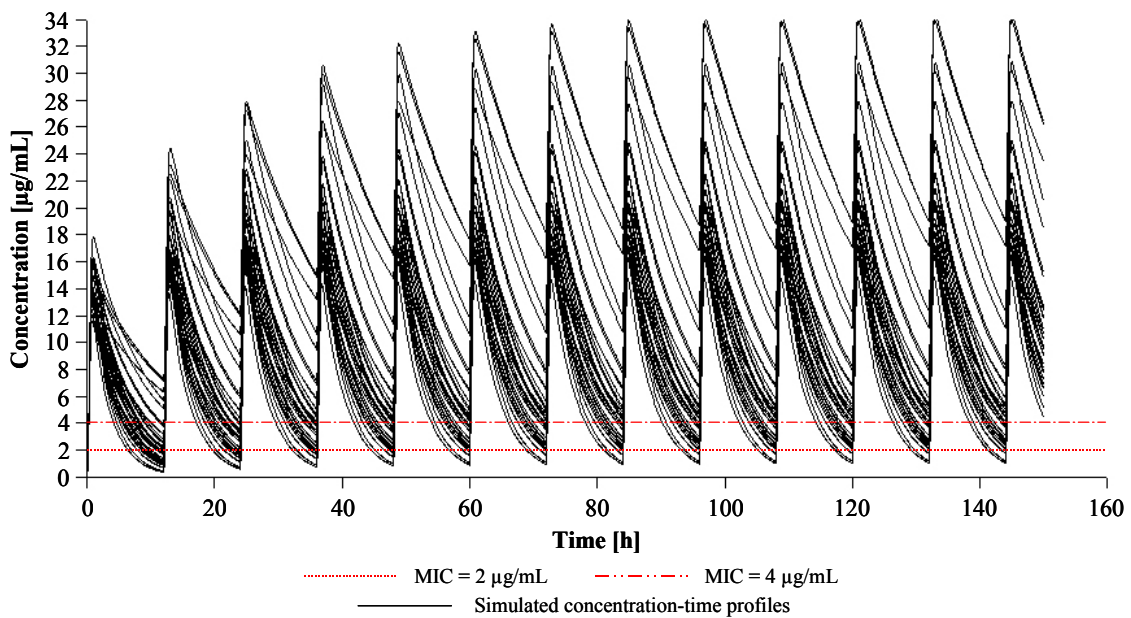
Figure 7.30: Simulated concentrations using observed combinations of covariate values.
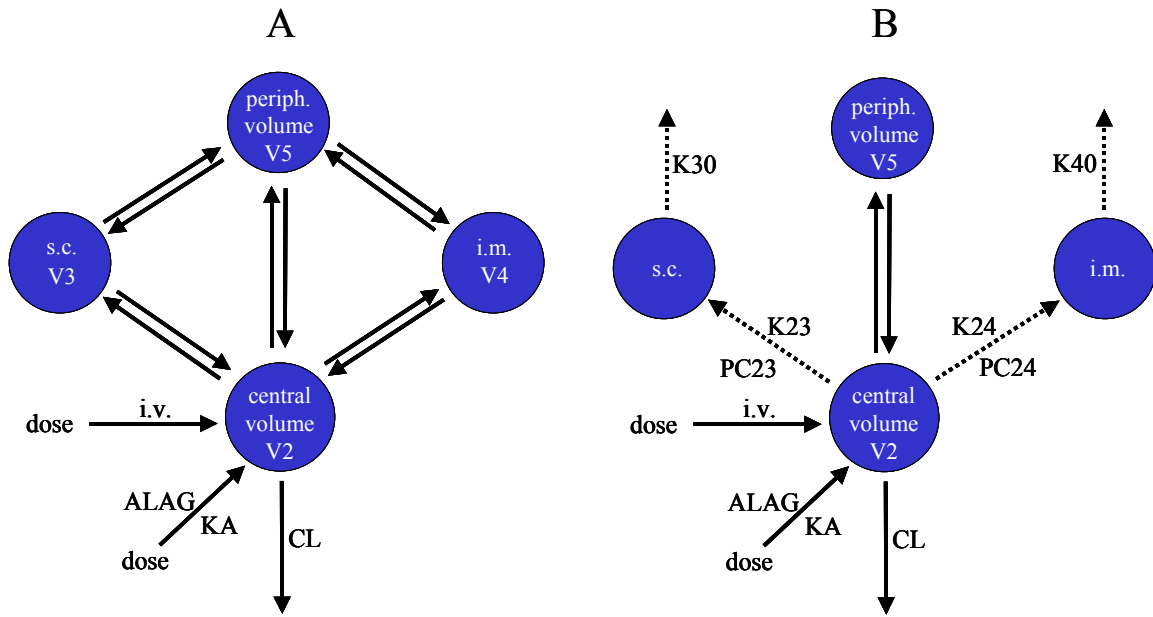
Figure 7.31: Model structures used for developing the model describing unbound plasma and ISF concentrations. A: model coded with intercompartmental clearances; B: model coded with monodirectional rate-constants and tissue partition coefficients.
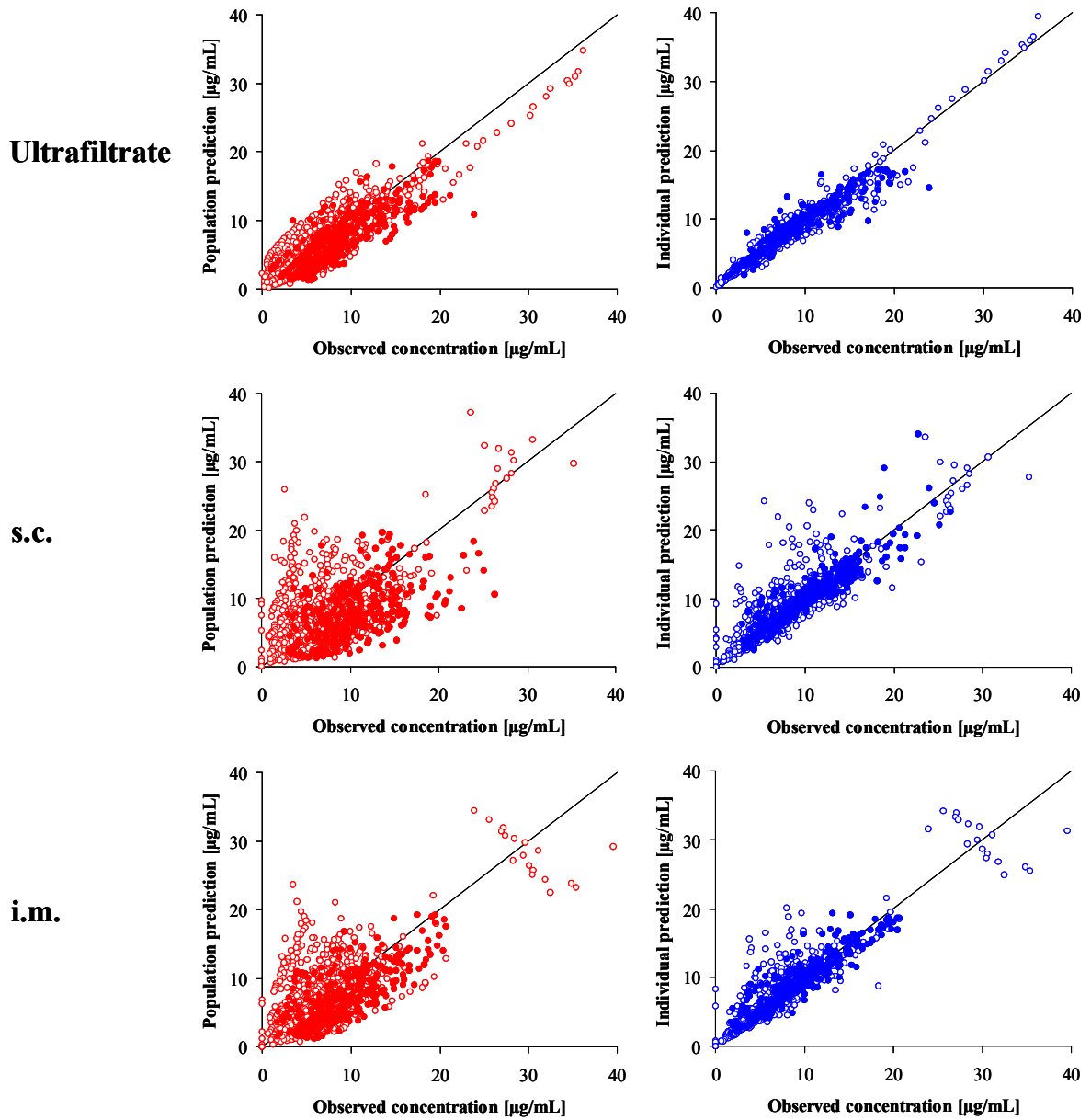
Figure 7.32: Goodness of fit plots of the base model describing ultrafiltrate, s.c. and i.m. concentrations; filled circles: healthy volunteers; empty circles: patients.
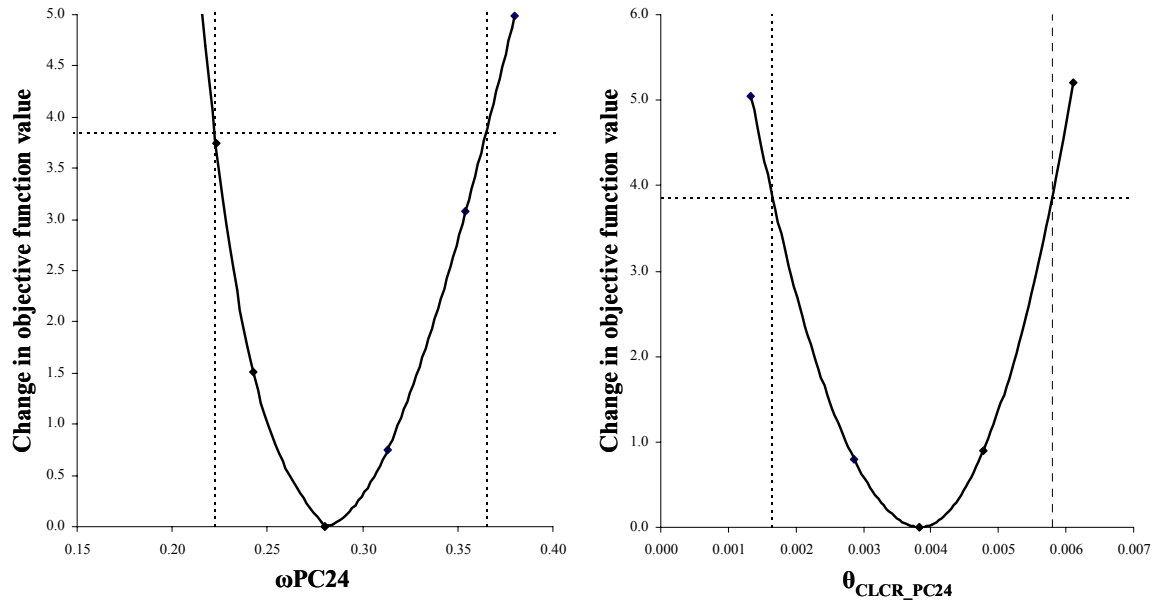
Figure 7.33: Log-likelihood profiles for the parameters $\omega PC24$ and θ_{CLCR_PC24}

Figure 7.34: Simulated concentration-time profile over one dosing interval after multiple dosing using extreme θ_{THRO_K40} values obtained during case deletion diagnostics. Left side: thrombocyte value of 81.2 nL^{-1}; Right side: thrombocyte value of 439.5 nL^{-1}; Red line: θ_{THRO_K40} =0.0017; Blue line: θ_{THRO_K40} =0.0021.

Figure 7.35: Predictive check for the model describing unbound concentrations in subcutaneous and muscle ISF after single dosing. Red lines represent the simulated median concentration-time profile whereas blue lines represent the 5% and 95% quantile and enclose the 90% prediction interval. Filled circles represent observed concentrations after single dosing. A: inhibition compartment model, subcutaneous data; B: inhibition compartment model, ω VAR set to zero, subcutaneous data; C: inhibition compartment model, muscle data; D: inhibition compartment model, ω VAR set to zero, muscle data.
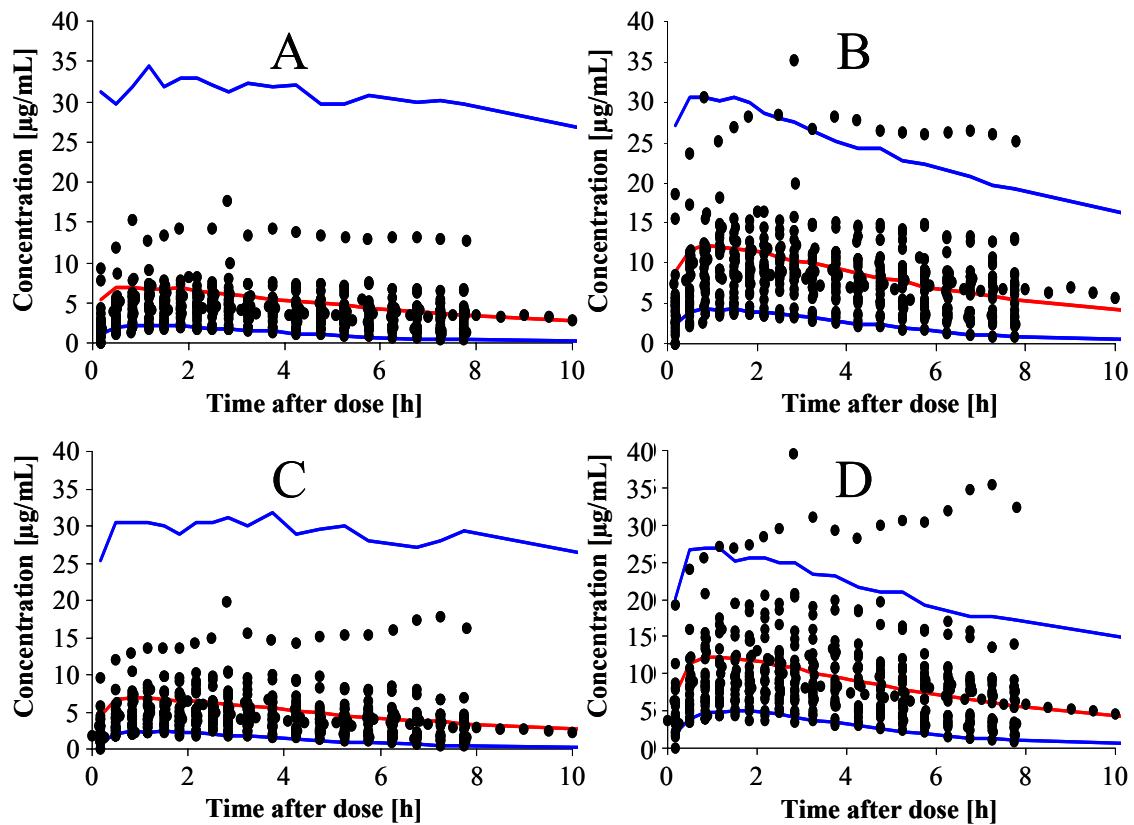
Figure 7.36: Predictive check for the model describing unbound concentrations in subcutaneous and muscle ISF after multiple dosing. Red lines represent the simulated median concentration-time profile whereas blue lines represent the 5% and 95% quantile and enclose the 90% prediction interval. Filled circles represent observed concentrations after multiple dosing. A: inhibition compartment model, subcutaneous data; B: inhibition compartment model, ωVAR set to zero, subcutaneous data; C: inhibition compartment model, muscle data; D: inhibition compartment model, ωVAR set to zero, muscle data.
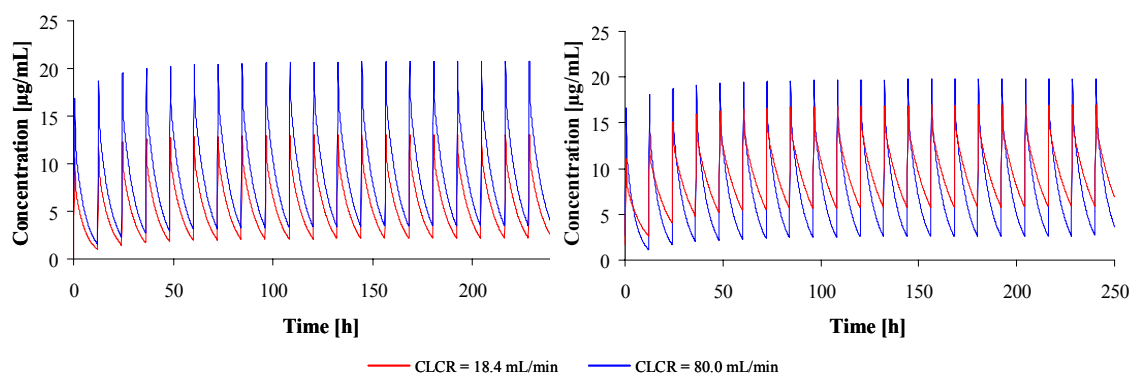
Figure 7.37: Influence of creatinine clearance on the concentration-time profiles in skeletal muscle. On the left the influence of creatinine clearance on PC24 is considered seperately whereas on the right the influence of creatinine clearance on PC24 as well as on clearance is taken into account.
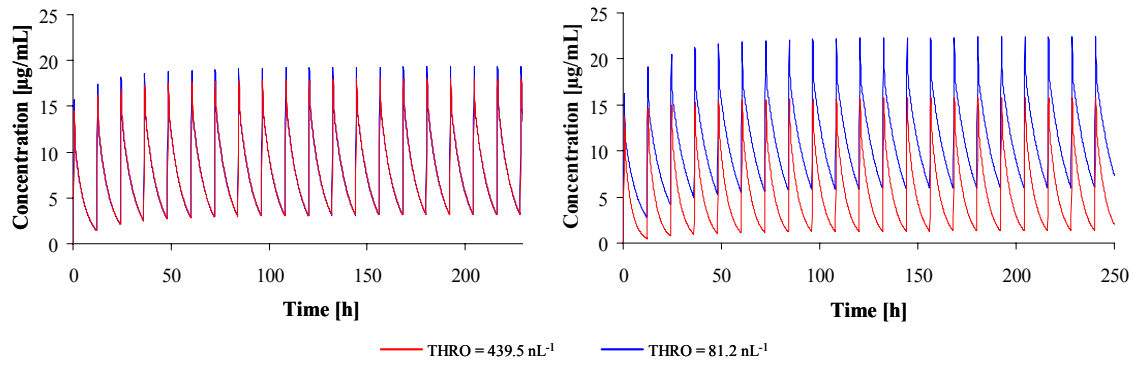
Figure 7.38: Influence of thrombocytes on the concentration-time profiles in skeletal muscle. On the left the influence of thrombocytes on K40 is considered seperately whereas on the right the influence of thrombocytes on K40 as well as on clearance is taken into account.
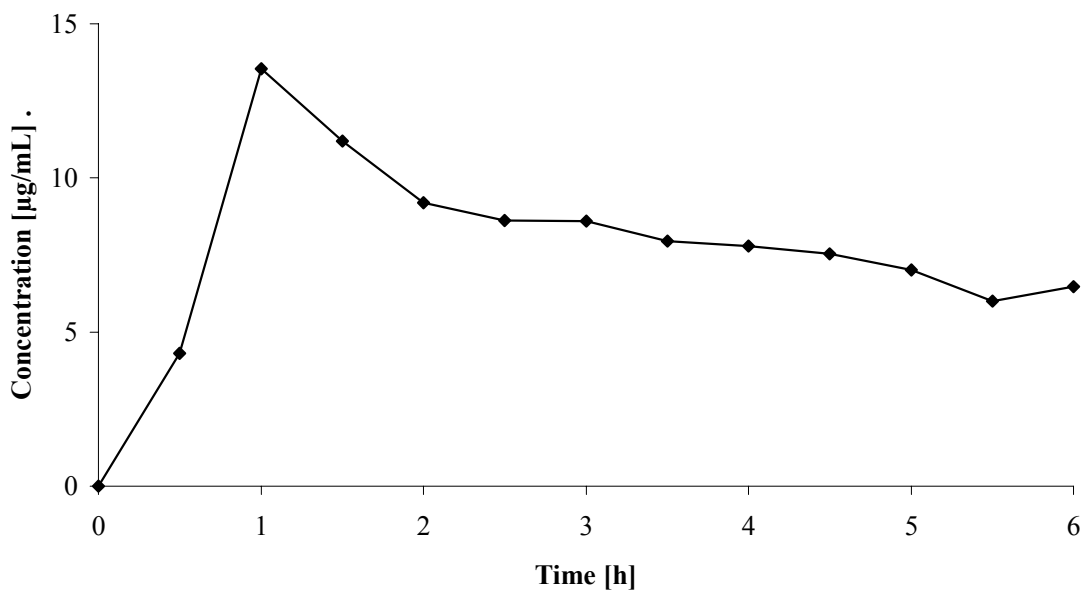
Figure 7.39: Concentration-time profile obtained from bone microdialysate from the lateral catheter of a representative pig.
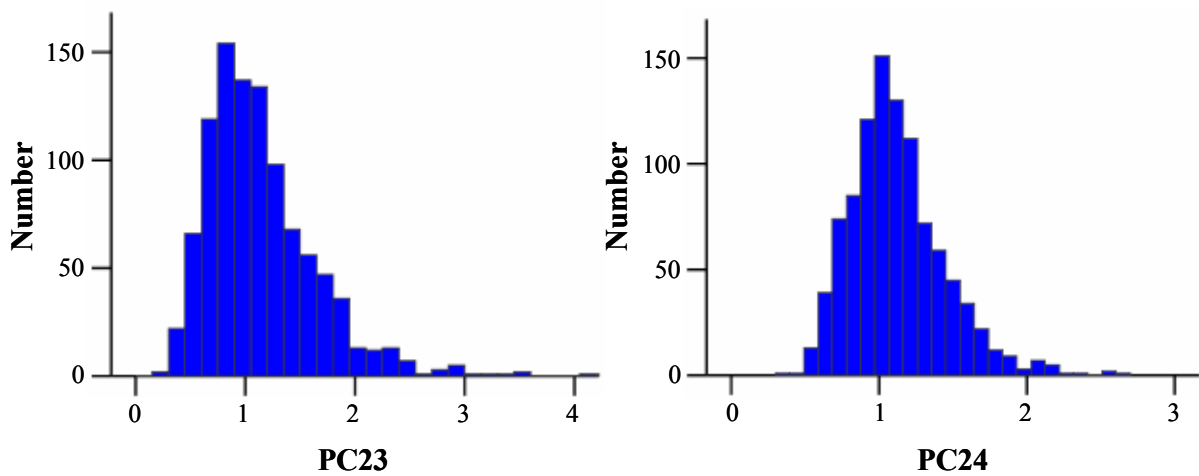

Figure 7.40: Individual parameter distributions of PC23 (left) and PC24 (right). Distributions were obtained by simulating 1000 individual parameters under the assumption of log-normal distribution.

7.3   NONMEM code

Code 7.1: Code for base model describing unbound plasma concentrations. Clearance is allowed to be inhibited depending on the concentration in an empirical inhibition compartment.

```
;PROJECT: KP-Lin01
;STUDY: 600 mg iv/po multiple dose
;RUN: 009
;KINETICIST: N. Plock
;NOTES: 2-COMP. MODEL, COMBINED ERROR MODEL, inhibition compartment included

$PROBLEM Linezolid iv/po healthy volunteers
$INPUT ID TIME TILD AMT RATE ADMA CMT DV FLMA EVID VIST OCC DAY AGE SEX HT
    CID=DROP TYPE=DROP FUPL FLAG

$DATA ivpo_151105_ID01-34 IGNORE=#

$SUBROUTINES ADVAN6 TRANS1 TOL5
$MODEL
 NCOMPS=4
 COMP=(ABS)
 COMP=(CENTRAL, DEFOBS)
 COMP=(PERIP1)
 COMP=(DELAY)

$PK

TVCL=THETA(1)
CL=TVCL*EXP(ETA(1))

TVV2=THETA(2)
V2=TVV2*EXP(ETA(3))

TVQ=THETA(3)
Q=TVQ

TVV3=THETA(4)
V3=TVV3*EXP(ETA(2))

TVKA=THETA(5)
KA=TVKA*EXP(ETA(5))

ALAG1=0
IF (ID.EQ.3.AND.OCC.GT.1) ALAG1=THETA(6)
IF (ID.EQ.6.AND.OCC.GT.1) ALAG1=THETA(6)
IF (ID.EQ.9.AND.OCC.GT.1) ALAG1=THETA(6)

PHI=LOG(THETA(7)/(1-THETA(7)))
VAR=EXP(PHI+ETA(4))/(1+EXP(PHI+ETA(4)))

TVKIC=THETA(8)
KIC=TVKIC

TVIC50=THETA(9)
IC50=TVIC50

S2=V2

K20=CL/V2
K23=Q/V2
K32=Q/V3
K12=KA
```

Code 7.1: continued

```
$DES

CLIN=A(2)/V2
INH=VAR+(1-VAR)*(1-A(4)/(IC50+A(4)))
DADT(1)= -KA*A(1)
DADT(2)= KA*A(1)-A(2)*K23+A(3)*K32-A(2)*K20*INH
DADT(3) =  A(2)*K23 -A(3)*K32
DADT(4) = KIC*(CLIN-A(4))
CL2=K20*INH*V2

$ERROR

IPRED=F

DEL=0
IF (IPRED.EQ.0) DEL=0.0001
W=F

IRES=DV-IPRED
IWRES=IRES/(W+DEL)
Y=F+SQRT(THETA(11)**2+THETA(10)**2*F**2)*EPS(1)

;----------------------------------INITIAL ESTIMATES--------------------------------
$THETA (0.1,10.5)        ; 1 CL
$THETA (0.1,20)          ; 2 V2
$THETA (0.1,75)          ; 3 Q
$THETA (0.1,30)          ; 4 V3
$THETA (0.001,2)         ; 5 KA
$THETA 1.27 FIX          ; 6 ALAG1
$THETA (0.001,0.8,1)     ; 7 VAR
$THETA (0.0001,0.002)    ; 8 KIC
$THETA 0.1 FIX           ; 9 IC50
$THETA 0.09              ; 9 prop.error
$THETA 0.3               ; 9 add.error

$OMEGA BLOCK(2) 0.1  ; 1 IIV_CL
0.01                 ; CORR_CL/V3
0.1                  ; 2 IIV_V3
$OMEGA BLOCK(2) 0.1  ; 3 IIV_V2
0.01                 ; CORR_V2/VAR
0.1                  ; 4 IIV_VAR
$OMEGA 1             ; 5 IIV_KA

$SIGMA 1 FIX             ; fixed sigma

$ESTIMATION PRINT=5 METHOD=1 INTERACTION MSFO=msf MAXEVAL=9999 NOABORT
$COV
```

Code 7.2: Code for final covariate model describing unbound plasma concentrations.

```
;PROJECT: KP-Lin01
;STUDY: 600 mg iv/po multiple dose
;RUN: 014
;KINETICIST: N. Plock
;NOTES: 2-COMP. MODEL, COMBINED ERROR MODEL, without correlation CL/V3

$PROBLEM Linezolid iv/po healthy volunteers
$INPUT ID TIME TILD AMT RATE ADMA CMT DV FLMA=DROP EVID VIST=DROP OCC DAY=DROP
AGE SEX WT HT SCRE=DROP CRCL AST=DROP ALT=DROP GGT=DROP LDH THRO LEUC=DROP
APCH=DROP CRP=DROP FLAP=DROP LAB=DROP CID=DROP TYPE FUPL=DROP FLAG

$DATA ivpo_151105_ID01-34_COV IGNORE=#

$SUBROUTINES ADVAN6 TRANS1 TOL5
$MODEL
 NCOMPS=4
 COMP=(ABS)
 COMP=(CENTRAL, DEFOBS)
 COMP=(PERIP1)
 COMP=(DELAY)

$PK

COVCL=1+THETA(10)*(CRCL-65)+THETA(11)*(WT-67)+THETA(12)*(THRO-220)
TVCL=THETA(1)*COVCL
CL=TVCL*EXP(ETA(1))

TVV2=THETA(2)
V2=TVV2*EXP(ETA(3))

TVQ=THETA(3)
Q=TVQ

TVV3=THETA(4)*(1+THETA(13)*(WT-67))
V3=TVV3*EXP(ETA(2))

TVKA=THETA(5)
KA=TVKA*EXP(ETA(5))

ALAG1=0
IF (ID.EQ.3.AND.OCC.GT.1) ALAG1=THETA(6)
IF (ID.EQ.6.AND.OCC.GT.1) ALAG1=THETA(6)
IF (ID.EQ.9.AND.OCC.GT.1) ALAG1=THETA(6)

PHI=LOG(THETA(7)/(1-THETA(7)))
VAR=EXP(PHI+ETA(4))/(1+EXP(PHI+ETA(4)))

TVKIC=THETA(8)
KIC=TVKIC

TVIC50=THETA(9)
IC50=TVIC50

S2=V2

K20=CL/V2
K23=Q/V2
K32=Q/V3
K12=KA
```

Code 7.2: continued

```
$DES

CLIN=A(2)/V2
INH=VAR+(1-VAR)*(1-A(4)/(IC50+A(4)))
DADT(1)= -KA*A(1)
DADT(2)= KA*A(1)-A(2)*K23+A(3)*K32-A(2)*K20*INH
DADT(3) =  A(2)*K23 -A(3)*K32
DADT(4) = KIC*(CLIN-A(4))
CL2=K20*INH*V2

$ERROR

IPRED=F

DEL=0
IF (IPRED.EQ.0) DEL=0.0001
W=F

IRES=DV-IPRED
IWRES=IRES/(W+DEL)
Y=F+SQRT(THETA(15)*THETA(15)+THETA(14)*THETA(14)*F**2)*EPS(1)

;----------------------------------INITIAL ESTIMATES--------------------------------
$THETA (0.1,8.5)         ; 1 CL
$THETA (0.1,21)          ; 2 V2
$THETA (0.1,75)          ; 3 Q
$THETA (0.1,27)          ; 4 V3
$THETA (0.001,1.8)       ; 5 KA
$THETA 1.27 FIX          ; 6 ALAG1
$THETA (0.001,0.6,1)     ; 7 VAR
$THETA (0.0001,0.003)    ; 8 KIC
$THETA 0.1 FIX           ; 9 IC50
$THETA (0.001,0.01)      ; CRCL_CL
$THETA (0.001,0.01)      ; WT_CL
$THETA (0.0001,0.002)    ; THRO_CL
$THETA (0.0001,0.015)    ; WT_V3
$THETA (0.001,0.09)      ; prop.error
$THETA (0.001,0.3)       ; add.error

$OMEGA 0.1               ; 1 IIV_CL
$OMEGA 0.1               ; 2 IIV_V3
$OMEGA BLOCK(2) 0.1      ; 3 IIV_V2
0.01                     ; CORR_V2/VAR
0.1                      ; 4 IIV_VAR
$OMEGA 1                 ; 5 IIV_KA

$SIGMA 1 FIX             ; fixed sigma

$ESTIMATION PRINT=5 METHOD=1 INTERACTION MSFO=msf MAXEVAL=9999 NOABORT
$COV
```

Code 7.3: Code for joint base model describing linezolid plasma and ISF pharmacokinetics.

```
$PROBLEM Linezolid iv/po in microdialysate and ultrafiltrate
$INPUT ID TIME TILD AMT RATE ADMA=DROP CMT DV FLMA EVID VIST OCC DAY=DROP
   AGE=DROP SEX=DROP HT=DROP WT SCRE=DROP CRCL AST=DROP ALT=DROP GGT=DROP
   LDH=DROP THRO LEUC=DROP APCH=DROP CRP=DROP FLAP=DROP LAB=DROP CID=DROP
   TYPE=DROP FUPL=DROP FLAG

$DATA KP-LIN01_01-34_UF_MD_ivpo_160106 IGNORE=#

$SUBROUTINES ADVAN6 TRANS1 TOL5
$MODEL
 NCOMPS=6
 COMP=(ABS)
 COMP=(CENTRAL, DEFOBS)
 COMP=(PERIP1)
 COMP=(SC)
 COMP=(IM)
 COMP=(DELAY)

$PK

COVCL=1+THETA(14)*(CRCL-65)+THETA(15)*(WT-67)+THETA(16)*(THRO-220)
TVCL=THETA(1)*COVCL
CL=TVCL*EXP(ETA(1))

TVV2=THETA(2)
V2=TVV2*EXP(ETA(3))

TVQ=THETA(3)
Q=TVQ

TVV5=THETA(4)*(1+THETA(17)*(WT-67))
V5=TVV5*EXP(ETA(2))

TVKA=THETA(5)
KA=TVKA*EXP(ETA(5))

ALAG1=0
IF (ID.EQ.3.AND.OCC.GT.1) ALAG1=THETA(6)
IF (ID.EQ.6.AND.OCC.GT.1) ALAG1=THETA(6)
IF (ID.EQ.9.AND.OCC.GT.1) ALAG1=THETA(6)

PHI=LOG(THETA(7)/(1-THETA(7)))
VAR=EXP(PHI+ETA(4))/(1+EXP(PHI+ETA(4)))

TVKIC=THETA(8)
KIC=TVKIC

TVIC50=THETA(9)
IC50=TVIC50

BOVP23=0
IF(VIST.EQ.1) BOVP23=ETA(6)
IF(VIST.EQ.2) BOVP23=ETA(7)

TVPC23=THETA(10)
PC23=TVPC23*EXP(BOVP23)

TVPC24=THETA(11)
PC24=TVPC24*EXP(ETA(8))

TVK30=THETA(12)
K30=TVK30

TVK40=THETA(13)
K40=TVK40*EXP(ETA(9))
```

Code 7.3: continued

```
S2=V2
K20=CL/V2
K25=Q/V2
K52=Q/V5
K12=KA
K23=K30
K24=K40

$DES

CLIN=A(2)/V2
INH=VAR+(1-VAR)*(1-A(6)/(IC50+A(6)))
DADT(1)= -KA*A(1)
DADT(2)= KA*A(1)-A(2)*K25+A(5)*K52-A(2)*K20*INH
DADT(3) = K23*PC23*CLIN-K30*A(3)
DADT(4) = K24*PC24*CLIN-K40*A(4)
DADT(5) = A(2)*K25 -A(5)*K52
DADT(6) = KIC*(CLIN-A(6))
CL2=K20*INH*V2

$ERROR

IPRED=F
DEL=0
IF (IPRED.EQ.0) DEL=0.0001
W=F
IRES=DV-IPRED
IWRES=IRES/(W+DEL)
Y=F+SQRT(THETA(19)*THETA(19)+THETA(18)*THETA(18)*F**2)*EPS(1)


;-------------------------------INITIAL ESTIMATES--------------------------------
$THETA 11.5 FIX          ; 1 CL
$THETA 19.8 FIX          ; 2 V2
$THETA 76.8 FIX          ; 3 Q
$THETA 27 FIX            ; 4 V5
$THETA 1.85 FIX          ; 5 KA
$THETA 1.27 FIX          ; 6 ALAG1
$THETA 0.567 FIX         ; 7 VAR
$THETA 0.00275 FIX       ; 8 KIC
$THETA 0.1 FIX           ; 9 IC50
$THETA (0.01,1.1)        ; 10 PC23
$THETA (0.01,1)          ; 11 PC24
$THETA 100 FIX           ; 12 K30
$THETA (0.1,13)          ; 13 K40
$THETA 0.00911 FIX       ; CRCL_CL
$THETA 0.0113 FIX        ; WT_CL
$THETA 0.00229 FIX       ; THRO_CL
$THETA 0.0152 FIX        ; WT_V5
$THETA (0.001,0.2)       ; prop.error
$THETA 0.01 FIX          ; add.error

$OMEGA 0.248 FIX              ; 1 IIV_CL
$OMEGA 0.042 FIX              ; 2 IIV_V5
$OMEGA BLOCK(2) 0.138 FIX     ; 3 IIV_V2
0.537                         ; CORR_V2/VAR
6.36                          ; 4 IIV_VAR
$OMEGA 0.622 FIX              ; 5 IIV_KA
$OMEGA BLOCK(1) 0.19          ; 6 BOV1_PC23
$OMEGA BLOCK(1) SAME          ; 6 BOV2_PC23
$OMEGA 0.09                   ; 7 IIV_PC24
$OMEGA 0.62                   ; 8 IIV_K40

$SIGMA 1 FIX            ; fixed sigma

$ESTIMATION PRINT=5 METHOD=1 INTERACTION MSFO=msf MAXEVAL=9999 NOABORT
$COV
```

Code 7.4: Code for joint covariate model describing linezolid plasma and ISF pharmacokinetics.

```
$PROBLEM Linezolid iv/po in microdialysate and ultrafiltrate
$INPUT ID TIME TILD AMT RATE ADMA=DROP CMT DV FLMA EVID VIST OCC DAY=DROP
AGE=DROP SEX=DROP HT WT SCRE=DROP CRCL AST=DROP ALT=DROP GGT=DROP
LDH THRO LEUC=DROP APCH=DROP CRP=DROP FLAP=DROP LAB=DROP CID=DROP
TYPE=DROP FUPL=DROP FLAG

$DATA KP-LIN01_01-34_UF_MD_ivpo_160106 IGNORE=#

$SUBROUTINES ADVAN6 TRANS1 TOL5
$MODEL
 NCOMPS=6
 COMP=(ABS)
 COMP=(CENTRAL, DEFOBS)
 COMP=(PERIP1)
 COMP=(SC)
 COMP=(IM)
 COMP=(DELAY)

$PK

COVCL=1+THETA(14)*(CRCL-65)+THETA(15)*(WT-67)+THETA(16)*(THRO-220)
TVCL=THETA(1)*COVCL
CL=TVCL*EXP(ETA(1))

TVV2=THETA(2)
V2=TVV2*EXP(ETA(3))

TVQ=THETA(3)
Q=TVQ

TVV5=THETA(4)*(1+THETA(17)*(WT-67))
V5=TVV5*EXP(ETA(2))

TVKA=THETA(5)
KA=TVKA*EXP(ETA(5))

ALAG1=0
IF (ID.EQ.3.AND.OCC.GT.1) ALAG1=THETA(6)
IF (ID.EQ.6.AND.OCC.GT.1) ALAG1=THETA(6)
IF (ID.EQ.9.AND.OCC.GT.1) ALAG1=THETA(6)

PHI=LOG(THETA(7)/(1-THETA(7)))
VAR=EXP(PHI+ETA(4))/(1+EXP(PHI+ETA(4)))

TVKIC=THETA(8)
KIC=TVKIC

TVIC50=THETA(9)
IC50=TVIC50

BOVP23=0
IF(VIST.EQ.1) BOVP23=ETA(6)
IF(VIST.EQ.2) BOVP23=ETA(7)

TVPC23=THETA(10)
PC23=TVPC23*EXP(BOVP23)

COCRCL=0
IF (CRCL.LT.80) COCRCL=THETA(19)*(CRCL-65)
TVPC24=THETA(11)*(1+COCRCL)
PC24=TVPC24*EXP(ETA(8))

TVK30=THETA(12)
K30=TVK30

TVK40=THETA(13)*(1+THETA(18)*(220-THRO))
K40=TVK40*EXP(ETA(9))
```

Code 7.4: continued

```
S2=V2
K20=CL/V2
K25=Q/V2
K52=Q/V5
K12=KA
K23=K30
K24=K40

$DES

CLIN=A(2)/V2
INH=VAR+(1-VAR)*(1-A(6)/(IC50+A(6)))
DADT(1)= -KA*A(1)
DADT(2)= KA*A(1)-A(2)*K25+A(5)*K52-A(2)*K20*INH
DADT(3) = K23*PC23*CLIN-K30*A(3)
DADT(4) = K24*PC24*CLIN-K40*A(4)
DADT(5) = A(2)*K25 -A(5)*K52
DADT(6) = KIC*(CLIN-A(6))
CL2=K20*INH*V2

$ERROR

IPRED=F
DEL=0
IF (IPRED.EQ.0) DEL=0.0001
W=F
IRES=DV-IPRED
IWRES=IRES/(W+DEL)
Y=F+SQRT(THETA(21)*THETA(21)+THETA(20)*THETA(20)*F**2)*EPS(1)


;-------------------------------INITIAL ESTIMATES--------------------------------
$THETA 11.5 FIX           ; 1 CL
$THETA 19.8 FIX           ; 2 V2
$THETA 76.8 FIX           ; 3 Q
$THETA 27 FIX             ; 4 V5
$THETA 1.85 FIX           ; 5 KA
$THETA 1.27 FIX           ; 6 ALAG1
$THETA 0.567 FIX          ; 7 VAR
$THETA 0.00275 FIX        ; 8 KIC
$THETA 0.1 FIX            ; 9 IC50
$THETA (0.01,1)           ; 10 PC23
$THETA (0.01,1)           ; 11 PC24
$THETA 100 FIX            ; 12 K30
$THETA (0.1,13)           ; 13 K40
$THETA 0.00911 FIX        ; CRCL_CL
$THETA 0.0113 FIX         ; WT_CL
$THETA 0.00229 FIX        ; THRO_CL
$THETA 0.0152 FIX         ; WT_V5
$THETA 0.002              ; THRO_K40
$THETA 0.004              ; CRCL_PC24
$THETA (0.001,0.2)        ; prop.error
$THETA 0.01 FIX           ; add.error


$OMEGA 0.248 FIX                  ; 1 IIV_CL
$OMEGA 0.042 FIX                  ; 2 IIV_V5
$OMEGA BLOCK(2) 0.138 FIX         ; 3 IIV_V2
0.537                             ; CORR_V2/VAR
6.36                              ; 4 IIV_VAR
$OMEGA 0.622 FIX                  ; 5 IIV_KA
$OMEGA BLOCK(1) 0.2               ; 6 BOV1_PC23
$OMEGA BLOCK(1) SAME              ; 7 IIV_PC24
$OMEGA 0.1                        ; 8 IIV_K40
$OMEGA 0.4                        ;

$SIGMA 1 FIX            ; fixed sigma

$ESTIMATION PRINT=5 METHOD=1 INTERACTION MSFO=msf MAXEVAL=9999 NOABORT
$COV
```

Curriculum vitae

Name	Nele Plock
Date of birth	17 August 1978
Place of birth	Oldenburg (Oldb)
Nationality	German

Education and Qualifications

03/2003 – 02/2007	Doctoral thesis under the supervision of Prof. Charlotte Kloft Department Clinical Pharmacy, Freie Universität Berlin and Martin-Luther-Universität Halle-Wittenberg *"Target Site Pharmacokinetics of Antiinfectives in the Treatment of Serious Gram-positive Infections"*
01/2003	Registration as a pharmacist in Germany
10/1997 – 10/2001	Degree in Pharmacy (2. Staatsexamen: 1.25) Westfaelische Wilhelms-Universitaet, Muenster, Germany
08/1990 – 06/1997	High school degree (Allgemeine Hochschulreife) Herbartgymnasium, Oldenburg, Germany
07/1994 – 12/1994	High school education Warrnambool College, Warrnambool, Australia

Professional Experience

Since 01/2007	Employment as pharmacometrician • Bayer Schering Pharma AG, Berlin, Germany
02/2006 – 04/2006	Industrial internship • Boehringer Ingelheim GmbH & Co. KG, Biberach, Germany Department Drug Metabolism and Pharmacokinetics
01/2003 – 07/2006	Employment as pharmacist • Apotheke im Ring-Center, Berlin, Germany
12/2001 – 11/2002	Pre-registration pharmacist • Apotheke des Klinikums Oldenburg, Hospital pharmacy Oldenburg, Germany • Fortunatus Apotheke Berlin, Germany
02/2000 - 04/2000	Industrial internship • Bayer Healthcare AG, Wuppertal, Germany Dept. of validation/qualification

Awards/Grants

06/2006	Travel award Population Approach Group Europe
04/2006	Funding by the 'Dr. August und Dr. Anni Lesmüller Stiftung'
03/2003 - 04/2006	Funding by the 'Berliner Programm zur Förderung der Chancengleichheit für Frauen in Forschung und Lehre'

Publications

Original papers

C. Buerger, N. Plock, P. Dehghanyar, C. Joukhadar, C. Kloft.
Pharmacokinetics of unbound linezolid in plasma and tissue interstitium of critically ill patients after multiple dosing using microdialysis.
Antimicrob Agents Chemother., 50(7):2455-63 (2006).

O. Schwalbe, C. Buerger, N. Plock, C. Joukhadar, C. Kloft.
Urea as an endogenous surrogate in human microdialysis to determine relative recovery of drugs: analytics and applications.
J. Pharm. Biomed. Anal., 41(1):233-9 (2006).

H. Stocker, C. Kloft, N. Plock, A. Breske, G. Kruse, C. Herzmann, H. Schulbin, P. Kreckel, C. Weber, F. Goebel, J. Roeling, S. Staszewski, A. Plettenberg, C. Moecklinghoff, K. Arastéh, M. Kurowski.
Pharmacokinetics of Enfuvirtide in Patients Treated in Typical Routine Clinical Settings.
Antimicrob. Agents Chemother., 50(2):667-73 (2006).

N. Plock, C. Buerger, C. Kloft.
Successful management of discovered pH dependence in vancomycin recovery studies: Novel HPLC method for microdialysis and plasma samples.
Biomed Chromatogr., 19(3): 237-244 (2005).

N. Plock, C. Kloft.
Microdialysis – Theoretical background and recent implementation in applied life-sciences.
Eur. J. Pharm. Sci., 25:1-24 (2005).

L.B. Stolle, N. Plock, C. Joukhadar, M. Arpi, K.J. Emmertsen, C. Buerger, P. Riegels Nielsen, C. Kloft.
Pharmacokinetics of Linezolid in Bone Tissue investigated by in situ Microdialysis.
Scand. J. Infect. Dis., submitted (2007).

N. Plock, C. Buerger, C. Joukhadar, S. Kljucar, C. Kloft.
Does linezolid inhibit its own metabolism? – Population pharmacokinetics as a tool to explain the observed nonlinearity in both healthy volunteers and septic patients.
Drug Metab. Dispos., submitted (2007).

N. Plock, C. Buerger, C. Joukhadar, S. Kljucar, C. Kloft.
Influence of creatinine clearance, weight and thrombocytes on the pharmacokinetics of linezolid in the critically ill.
In preparation.

N. Plock, C. Buerger, C. Joukhadar, S. Kljucar, C. Kloft.
Population pharmacokinetics of linezolid in healthy volunteers and septic patients – Analysis of microdialysis tissue data.
In preparation.

Conference Abstracts

N. Plock, C. Joukhadar, S. Kljucar, C. Kloft.
Population Pharmacokinetics of Linezolid in Tissue and Plasma of Healthy Subjects and Septic Patients – Managing Nonlinearity.
46th Interscience Conference on Antimicrobial Agents and Chemotherapy (ICAAC), San Francisco, USA, 27.-30.09.2006. Proceedings Journal 30 (2006).

N. Plock, C. Buerger, K. Kuester, C. Joukhadar, S. Kljucar, C. Kloft.
A Population Pharmacokinetic Model for the Simultaneous Description of Linezolid Tissue and Plasma Disposition in Healthy Volunteers and Septic Patients.
15th Annual Meeting Population Approach Group Europe (PAGE), Brugge, Belgium, 14.-16.06.2006. PAGE, 15: 886 (2006) [http://www.page-meeting.org/default.asp?abstract=886].

N. Plock, C. Buerger, C. Joukhadar, M. Mueller, S. Kljucar, C. Kloft.
Are we all the same? - Population Pharmacokinetics of Linezolid in Tissue and Plasma.
Annual meeting of the German Pharmaceutical Society (DPhG) 2005, Mainz, Germany, 05.-08.10.2005. Proceedings Journal 74 (2005).

L.B. Stolle, N. Plock, C. Joukhadar, M. Arpi, K.J. Emmertsen, C. Buerger, P. Riegels Nielsen, C. Kloft.
Microdialysis in Bone Tissue - Pharmacokinetics of Linezolid.
45th Interscience Conference on Antimicrobial Agents and Chemotherapy (ICAAC) 2005, Washington, USA, 16.-19.12.2005. Proceedings Journal 6 (2005).

N. Plock, C. Bürger, C. Joukhadar, M. Müller, S. Kljucar, C. Kloft.
Tissue and Plasma Pharmacokinetics of Linezolid - A Population Approach.
Annual meeting of the American Association of Pharmaceutical Scientists (AAPS), November 2005, Nashville, USA, 06.-10.11.2005. Proceedings AAPS Journal 6 (2005).

L.B. Stolle, N. Plock, C. Joukhadar, M. Muller, M. Arpi, C. Buerger, P. Riegels Nielsen, C. Kloft.
Pharmacokinetics of Linezolid in Bone Tissue investigated by in situ Microdialysis.
European Congress of Clinical Microbiology and Infectious Diseases 2005, Copenhagen, Denmark, 02.–05.04.2005. Proceedings Journal 30 (2005).

N. Plock, C. Kloft.
Special Characteristics of Microdialysis with Vancomycin – pH Dependence of Microdialysis Recovery.
World Conference on Dosing of Antiinfectives, 2004, Nuremberg, Germany, 09.-11.09.2004. Proceedings Journal 416 (2004).

C. Bürger, N. Plock, C. Kloft.
Tissue Pharmacokinetics of Linezolid Assessed by Microdialysis.
World Conference on Dosing of Antiinfectives, 2004, Nuremberg, Germany, 09.-11.09.2004. Proceedings Journal 417 (2004).

O. Schwalbe, C. Bürger, N. Plock, C. Scheerans, C. Kloft.
Human Microdialysis: Urea as an Endogenous Reference Compound to Determine Relative Recovery of Drugs.
World Conference on Dosing of Antiinfectives, 2004, Nuremberg, Germany, 09.-11.09.2004. Proceedings Journal 478 (2004).

Conference Abstracts (continued)

N. Plock, C. Kloft.
pH-dependency of microdialysis recovery – In vitro microdialysis of vancomycin.
Annual meeting of the German Pharmaceutical Society (DPhG) 2004, Regensburg, Germany, 07.-09.10.2004.
Proceedings Journal P K10 (2004).

N. Plock, C. Kloft.
Determination of vancomycin concentrations in tissue of critically ill patients: A combination of microdialysis and HPLC.
German Pharmaceutical Society (DPhG), Berlin-Brandenburg – presentation of young scientific candidates, Berlin, Germany, 05. July 2004. Proceedings Journal P20 (2004).

C. Bürger, N. Plock, C. Joukhadar, M. Müller, C. Kloft.
Pharmacokinetics of linezolid at the site of infection.
German Pharmaceutical Society (DPhG), Berlin-Brandenburg – presentation of young scientific candidates, Berlin, Germany, 05. July 2004. Proceedings Journal V2 (2004).

O. Schwalbe, C. Bürger, N. Plock, C. Kloft.
Urea as an endogenous reference compound fort he determination of the in vivo recovery in human microdialysis samples.
German Pharmaceutical Society (DPhG), Berlin-Brandenburg – presentation of young scientific candidates, Berlin, Germany, 05. July 2004. Proceedings Journal P24 (2004).

N. Plock, C. Kloft.
Tissue concentrations of vancomycin in critically ill patients: Microdialysis combined with a rapid and sensitive HPLC quantification.
Int. J. Clin. Pharmacol. Ther., 7: 398 (2004).

C. Buerger, N. Plock, C. Joukhadar, M. Mueller, C. Kloft.
Tissue pharmacokinetics of linezolid assessed by microdialysis.
Int. J. Clin. Pharmacol. Ther., 7: 399 (2004).

O. Schwalbe, C. Buerger, N. Plock, C. Kloft.
Determination of in vivo recovery in human microdialysis samples: Urea as a reference compound.
Int. J. Clin. Pharmacol. Ther., 7: 398 (2004).

N. Plock, C. Buerger, C. Kloft.
Rapid and sensitive HPLC quantification of vancomycin in critically ill patients.
Annual meeting of the German Pharmaceutical Society (DPhG) 2003, Würzburg, Germany, 08.-11.10.2003.
Proceedings Journal 61 (2003).

O. Schwalbe, C. Buerger, N. Plock, C. Kloft.
Urea as a reference compound to deterermine the in vivo recovery in human microdialysis samples.
Annual meeting of the German Pharmaceutical Society (DPhG) 2003, Würzburg, Germany, 08.-11.10.2003.
Proceedings Journal 111 (2003).

Presentations

N. Plock, C. Buerger, C. Joukhadar, M. Mueller, S. Kljucar, C. Kloft.
Are we all the same? - Population Pharmacokinetics of Linezolid in Tissue and Plasma.
Annual meeting of the German Pharmaceutical Society 2005, Mainz, Germany.

N. Plock, C. Bürger, S. Kljucar, C. Joukhadar, M. Müller, C. Kloft.
Clinical study on the pharmacokinetics (PK) and pharmacodynamics (PD) of linezolid at the site of infection.
Bad Honnef-Symposium 2005, Königswinter, Germany.

N. Plock, C. Buerger, C. Kloft.
Rapid and sensitive HPLC quantification of vancomycin in critically ill patients.
Annual meeting of the German Pharmaceutical Society 2003, Würzburg, Germany.

Acknowledgements

I would like to express my sincere gratitude to Prof. Dr. Charlotte Kloft who gave me the opportunity to work on such an exciting topic. She has always been an inspiration for my work and I thank her deeply for our numerous discussions, for the freedom she allowed me in my research and for her encouraging words and general understanding during both enjoyable and difficult times.

Also I am indebted to Prof. Dr. Hans-Hubert Borchert, who allowed me to officially become a PhD student in the first place.

For his cooperation during the clinical trial, I wish to acknowledge Dr. Christian Joukhadar. Dr. Sascha Kljucar was extremely supportive in the conduction of the clinical trial, and I am grateful to him also for sneaking me into a variety of outstanding dinners to which I had not been invited.

I would like to thank Karsten Röttger, Guido Finck and Dieter Lang for their commitment to the clinical trial and for all the extra hours they had to endure. A special word of thanks goes to Karsten for allowing only 4 hours of sleep before calling again. Moreover, the trial would not have been possible without the support of Dr. Anna Santarelli and Dr. Michael Toursarkissian, as well as the nursing staff in the intensive care unit of DRK Klinikum Westend, Berlin.

'Tusind tak' to Dr. Lars Stolle for a great cooperation in our pig study; especially his capacity for turning conferences and email exchanges into very enjoyable activities has been much appreciated.

A big thank you goes to a number of people without whom I would never have acquired the modelling experience I have: Dr. Nick Holford, Dr. Hans Günter Schäfer, Dr. Alexander Staab, Christiane Tillmann, Dr. Jürgen Bulitta and Dr. Stephen Duffull. Especially Stephen never tired of replying to every single email – which I sent day after day after day! Furthermore, thanks to Dirk Zeumer, who repeatedly helped with all those little things that I could never have done without.

Erklärung

Hiermit erkläre ich, dass ich mich mit der vorliegenden Dissertation erstmals um die Erlangung eines Doktorgrades bewerbe.

Ferner erkläre ich, dass ich die vorliegende Arbeit selbständig und ohne fremde Hilfe angefertigt, andere als die von mir angegebenen Quellen und Hilfsmittel nicht benutzt und die den verwendeten Werken wörtlich oder inhaltlich entnommenen Stellen als solche kenntlich gemacht habe.

Halle, 22.02.2007